2021

Lithium-ion Battery Recycling Using Mineral Processing Methods

Ruiting Zhan
Michigan Technological University, ruzhan@mtu.edu

LITHIUM-ION BATTERY RECYCLING USING MINERAL PROCESSING METHODS

By

Ruiting Zhan

A DISSERTATION

Submitted in partial fulfillment of the requirements for the degree of

DOCTOR OF PHILOSOPHY

In Chemical Engineering

MICHIGAN TECHNOLOGICAL UNIVERSITY

2021

This dissertation has been approved in partial fulfillment of the requirements for the Degree of DOCTOR OF PHILOSOPHY in Chemical Engineering.

Department of Chemical Engineering

Dissertation Advisor:	*Dr. Lei Pan*
Committee Member:	*Dr. Timothy C. Eisele*
Committee Member:	*Dr. Yixin Liu*
Committee Member:	*Dr. Kathryn A. Perrine*
Department Chair:	*Dr. Pradeep K. Agrawal*

Table of Contents

List of Figures

List of tables

Author Contribution Statement

Chapter 3 is investigation of froth flotation technique on separation of anode and cathode materials from spent and new lithium-ion batteries. Dr. Lei Pan proposed the experiment idea, helped to design the experiment, review, and improve the paperwork. I performed all experimental work, collected, analyzed, and presented all experimental data. Some preliminary testing was done by Zachary Oldenburg, but they are not used in this chapter. This chapter has been published in the peer-review journal, *Sustainable Materials and Technologies* (https://doi.org/10.1016/j.susmat.2018.e00062), this paper was highlighted by Sustainable Materials and Technologies journal (Rank: 99% under industrial and manufacturing engineering).

Chapter 4 is investigation of thermal treatment on removing hydrophilic layers from both anode and cathode electrode materials to facilitate their froth flotation separation performance. Dr. Lei Pan provided the experimental equipment, reviewed, and improved the paperwork. I have conducted most of experimental work except XPS and STEM, analyzed and interpreted all experiment data, written the draft paper. Dr. Zhenzhen Yang helped to conduct XPS experiments and explained the XPS result, both Dr. Zhenzhen Yang and Dr. Ira Bloom helped to improve paper writing. Dr. Pinaki Mukherjee conducted to STEM experiment and helped to understand its result. This chapter has been published in the peer-review journal, *ACS Sustainable Chemistry & Engineering* (https://doi.org/10.1021/acssuschemeng.0c07965).

Chapter 5 discussed de-agglomerate cathode materials from PVDF binding using high shear agitation, subsequent flotation carried out to separate and concentrate high purity cathode materials. Dr. Lei Pan helped to optimized and initiated the experimental equipment, revised and improved the paper writing. I conducted all the experiments except XPS, analyzed all the data, drawn all the figures, put together all the tables for data presentation, written the paper draft. Dr. Timothy Leftwich conducted XPS experiment and collected its data, Dr. Timothy Leftwich and Dr. Kathryn Perrine helped to analyze the XPS results. Trevyn Payne conducted some preliminary survey, his data is not shown in this work. This chapter has been published in the peer-review journal, *Waste Management* (https://doi.org/10.1016/j.wasman.2020.01.035).

Chapter 6 investigated enhanced gravity separation on pristine and collected from spent LIB anode and cathode materials. Dr. Lei Pan provided the experimental equipment and initiated its test run, reviewed and improved the writing. I have conducted all the experiments, collected, analyzed, and presented all the experimental data. This chapter is to be submitted to a peer-review journal.

Chapter 7 studied circuit design and multistage operations for enhanced gravity separation using pristine anode and cathode material. Dr. Lei Pan provided the experimental equipment, revised the draft. I have conducted all experiment, collected and analyzed all experimental data, and written the draft. This chapter is to be submitted to a peer-review journal.

Acknowledgements

First and foremost, I would like to express my deepest gratitude to my advisor, Dr. Lei Pan, for his relentless mentoring and generous support. He is an excellent advisor with creative mind, critical and logical thinking, great passion for scientific research. Those characteristics and his extraordinary self-discipline really inspire me along the way of exploring and researching. I am very grateful for Dr. Pan for giving me the opportunity to join his lab, carrying out research that I am interested in, funding me generously, and all of help on professional and personal development. I want to thank the Department of Chemical Engineering of Michigan Tech, Graduate School of Michigan Tech (Doctoral Finishing Fellowship Fall 2021), U. S. Environmental Protection Agency (SU839299, SV839485), Argonne National Laboratory (DE-AC02-06CH11357), National Science Foundation (1855197) for the generous support.

I would like to thank Dr. Timothy Eisele, Dr. Yixin Liu, and Dr. Kathryn Perrine for serving as my committee members, Dr. Andre Da Costa for serving as committee member for my proposal defense. They have provided meaning insights and professional guidance to my research and paperwork. I want to thank Jennifer Eikenberry for helping ICP experiments; Owen Mills, Dr. Timothy Leftwich, Dr. Edward Laitila, Dr. Pinaki Mukherjee, Gerald Anzalone, Elizabeth Miller for meaningful discussions and operation instructions on instruments in Applied Chemical and Morphological Analysis Laboratory. I also thank Dr. Agrawal, Dr. Co, Dr. Morrison, Dr. Ong, and Dr. Shonnard for their support and encouragement. I want to thank Taana, Jerry, Steve, and Alexis from Chemical Engineering for constant help and support.

I want to thank all my lab mates for their friendship and support, especially Yuesheng, Tinu, John, Zack, Trevyn, Michael, and Caroline. I want to thank Dr. Zhenzhen Yang and Dr. Ira Bloom for data advice and discussion on collaborated work. I want to thank Dr. Taehee Han, Dr. Hosop Shin, and Dr. Kulwinder Dhindsa for discussions, technical support, guidance on direct recycling method and collaborated research. I also thank Michigan Tech IT, Battery Solution, CEAR, and Northern Michigan University for supplying end-of-life batteries for this study.

Last but not the least, I want to appreciate all the support from my family, especially my mother Xiaobing Wang and father Xiaofeng Zhan for their endless love and unconditional support throughout my life, I will never be where I am without them. I want to express my deepest gratitude to my partner Ya'nan Xu for her continuous support and love along the way. I also want to thank my friends, especially Zhuohong Zhou, Wenjian Chen, Shaonan Liu, and Yihang Fang for their friendships and support.

Abstract

The surges in the volume of the retired Li-ion batteries (LIBs) in future motivate Li-ion battery recycling R&D activities worldwide. Within the Li-ion batteries, the most valuable component is cathode active materials that consist of critical minerals and materials such as lithium, cobalt, nickel, manganese. The LIB recycling has been investigated at both the lab scale and industrial scale. There are three existing recycling methods, namely physical separation, pyrometallurgy, and hydrometallurgy. Physical separation methods sort individual battery components without changing materials' physical properties, while both pyrometallurgical and hydrometallurgical recycling routes aim to recover valuable metals using a high-temperature process and a leaching process, respectively. The conventional pyrometallurgical and hydrometallurgical processes are targeted to a few metal elements only. The goal of this work is to take the physical recycling methods to the next level by separating and concentrating individual battery components to the highest purity in the solid phase while preserving the electrochemical integrity of individual battery components.

In this work, two physical separation methods were investigated to separate two electrode active materials from LIBs. They are froth flotation and enhanced gravity separation technology. First, separation of the black mass from spent and new LIBs by froth flotation have been investigated. Graphite is commonly used as the anode active material and it is naturally hydrophobic, while lithium transitional metal oxides are commonly used as the cathode active materials, and they are hydrophilic. By taking the advantage in the surface property between the two electrode active materials, froth flotation method separates the two electrode active materials from spent LIBs. Our result showed that all anode active materials from new and lightly degraded EV batteries were reported in the froth product in the presence of kerosene as the collector, while the sink (tailing) product contained over 87% purity of lithium transitional metal oxides. The cathode recovery was approximately 60-80%, which was attributed to the presence of PVDF binders in the cathode composite materials. The separation performance deteriorated for spent LIBs due to the formation of solid electrolyte interphase (SEI) layers on the anode surfaces. To restore the original surface properties of the electrode active materials, a heating process was applied to the black mass. Over 99% purity of graphite and lithium metal oxide was obtained by multistage stages of the froth flotation process. In addition, a high-shear blending process was developed to de-agglomerate cathode active particles from PVDF binders in cathode composites. Individual cathode active particles got liberated from binders. Froth flotation concentrated PVDF binders and carbon additives in the froth product, leaving high purity (98% purity or above) of lithium metal oxides in the tailing product.

Centrifugal gravity separation method was introduced for the first time to separate both the pristine and spent electrode active materials by taking the advantage of the difference in specific densities between the two electrode active materials. Graphite was flushed with the overflow slurry, while lithium metal oxides were retained at the inner wall of the concentrator bowl to achieve a separation between the two materials. Over 99% purity of lithium metal oxides from spent Li-ion batteries in the concentrate product was

demonstrated for the first time. Circuit design and locked-cycle experiments were conducted to validate the separation results. Compared with froth flotation process, the centrifugal gravity separation has an advantage for spent Li-ion batteries since the specific gravity of the electrode active materials remained unchanged after numerous charge-discharge cycles.

1 Background, Introduction and Overview

1.1 Background and Introduction

Lithium-ion batteries (LIBs) have been developed and commercialized since 1990s [1-4]. It has vast capabilities to be used for multiple portable electronic devices, including cell phones, laptops, and remote controllers. It also got largely applied in electric vehicles for its high energy density, light weight, low self-discharge, low maintenance, high cell voltage, low self-discharge rate, variable electrode materials, more charge/discharge cycles. In order to lower carbon emissions and provide better living environments [5, 6], sales of electric vehicles (EVs) have been surged in recent years in China, Europe, and United States. It is expected that global LIB demand will increase to 408 GWh in 2025 and 1,293 GWh in 2030 [7] to satisfies rising sales of EVs. However, lithium-ion batteries have average lifetime between 2 – 10 years before reaching end-of-life (EOL) state and entering waste stream [8]. Thermal runaways [9, 10], environmental contaminations and subsequent health impacts on civilians [5] cannot be avoided if proper management of retired LIBs are not in placed. For example, spent LIBs could have internal short circuits due to internal and structure damages, storing them as normal solid waste can easily led to fire hazards. Burning spent LIBs as normal solid waste can generate toxic gases such as hydrogen fluoride (HF) to contaminate the atmosphere. Other gaseous products like polymers and organic compounds are dependent on burning temperatures [11], making direct burning difficult to control. Similarly, cathode electrode materials contain heavy metal contents include cobalt, manganese, and nickel. If spent LIBs are land filled, those transition metals and toxic organics can infiltrate the soil and underground water system to cause severe environmental pollutions. It has been shown that with 4,000 t of spent LIBs collected, 200 t of toxic electrolyte solvents and 1,100 t of heavy metals are generated [12].

As a new type of solid waste with distinct characteristics, it is necessary to investigate methods to properly handle spent LIBs to minimize safety and environmental issues, while valuable materials inside can also be recovered and re-supply back into the market to make this recycling process more sustainable. Cathode electrode materials are the mainly targeted components from most research activities and industrial applications [13] for its high values. Cobalt price is as high as 50505 $/tonne, nickel price is 19365 $/tonne to the date of writing. For comparison, prices for copper and aluminum are 9347 and 2694 $/tonne, respectively [14]. Currently, there are three popular methods for recycling activities. Pyrometallurgy is feeding batteries to a high-temperature shaft furnace, plastics and electrolyte are burnt out to supply some energy for smelting, metals include nickel, cobalt, and copper are reduced to an alloy, lithium and manganese are lost in slag [15]. This process does not require excess pretreatment, yet the loss of metals, high energy consumptions, and exhausted gases challenge its application. Hydrometallurgy is usually started with pretreatment and leaching, leaching process is to dissolve valuable metals into leachate. Then a series of solvent extraction, chemical precipitation, and electrochemical deposition are applied to separate valuable metals from leachate [16]. Hydrometallurgy requires further pretreatments to concentrate cathode electrode materials first before leaching. The advantage of hydrometallurgy is less energy

consumption compared to pyrometallurgy, higher add-on values on products and high recoveries (over 99%) of valuable metals from cathode electrode materials can be achieved [17], lithium and manganese can also be recovered without losing to slag. However, the consumptions of leaching agents and other chemicals are non-negligible, long processing routes could incur higher operation cost. Physical recycling method mainly applies physical separation processes including gravity separation, magnetic separation, froth flotation, size separation, and other methods [18] to separate and concentrate electrode materials and potentially other components. It requires less energy and chemical consumptions than pyro- and hydro- processes, it also has the potential to provide valuable electrode materials that preserved structure and function integrities for cathode regeneration and reutilization purpose [19], which helps to associate physical separation with direct recycling process [20]. Physical method requires moderate level of pretreatment between pyro- and hydro- metallurgy, its feed mass is electrode material mixtures after classification.

In this dissertation, physical separation methods are chosen and applied for cathode and anode electrode material separation and purification. Froth flotation and centrifugal gravity separation, combined with other pretreatments such as thermal treatment and high shear blending, have been detailly investigated. High grade and high recovery of cathode electrode materials (over 99%) have been achieved, sample characterizations have conducted using Scanning Electron Microscope (SEM), Energy Dispersive X-Ray Analysis (EDX), Thermal Gravimetric Analysis (TGA), X-ray Diffraction Analysis (XRD), Inductively Coupled Plasma – Optical Emission Spectrometry (ICP-OES), Transmission Electron Microscopy (TEM), X-Ray Photoelectron Spectroscopy (XPS).

1.2 Overview

This dissertation begins with a background of lithium-ion battery and introduction of its recycling activity status as stated in chapter 1. In chapter 2, a detailed literature review has been shown to answer why and how the lithium-ion batteries are being recycled. Pretreatment methods are investigated to properly obtain inner materials of LIBs. Physical method, pyrometallurgy, and hydrometallurgy have been compared to remove impurities and recover valuable materials.

Chapter 3, 4, and 5 are discussing application of froth flotation to separate and concentrate anode and cathode electrode materials. Chapter 3 proves the possibility of froth flotation separation on black mass obtained from LIBs. MIBC is used to maintain the bubble form, while use of kerosene as collected showed an improved separation performance. Hydrophobic materials (anode) got floated while hydrophilic particles remained in the tailing product, entrained cathode materials found in froth might be attributed to surface coverage of binder and carbon additives. Flotability of anode from spent LIBs is slightly lower than that from new LIBs. Fine grinding was found to expose fresh surface of graphite to improve grade of cathode in concentrate. Chapter 4 discuss the impact of surface contamination of electrode particles on froth flotation performance. Thermal treatment conducted to remove PVDF binder on cathode surface and SEI layer on anode surface. Froth flotation conducted using release analysis method on black mass

with and without pyrolysis, it was shown that cathode grade in tailing has been improved significantly after surface layers removal. This chapter reveals the fundamental of flotation mechanism: by regaining the original surface hydrophobicity and hydrophilicity for anode and cathode particles, almost ideal flotation products can be achieved. Chapter 5 investigated mechanical method to remove binder and carbon additives from cathode composites, both its grade and recovery in tailing product improved after modified multistage froth flotation. Morphology and surface chemistry of cathode materials have been compared among raw material and high shear blending with different retention time. Individual cathode particles got liberated from composites and reported to tailing product, PVDF reported to froth product in flotation due to its surface hydrophobicity.

Chapter 6 and 7 discussed using enhanced gravity separator on anode and cathode electrode materials separation. Chapter 6 investigated the profile of material distribution of concentrate bed and tailing product with different G Forces, feed mass, and solid concentration to optimize working conditions. Separation index introduced to characterize separation performance; cut-off point selection generate potential to obtain high grade materials. Also, multistage operation carried out on both pristine materials and black mass obtained from spent LIBs with and without thermal treatment, they shared similar separation results with pristine black mass, especially for concentrate product that enriched with cathode materials. Chapter 7 focused on optimizing individual stages from multistage operation includes rougher, scavenger, and cleaner using pristine graphite and NMC111 powders. Detailed circuit analysis carried out to acquire operation routes for high purity material products. Multistage operation conducted with one pass and two passes of scavenger and cleaner with guidance from circuit design and operation optimizations, high purities of anode in tailing and cathode in concentrate achieved.

1.3 Reference

1. Huang, B., et al., *Recycling of lithium-ion batteries: Recent advances and perspectives.* Journal of Power Sources, 2018. **399**: p. 274-286.
2. Goodenough, J.B. and K.-S. Park, *The Li-Ion Rechargeable Battery: A Perspective.* Journal of the American Chemical Society, 2013. **135**(4): p. 1167-1176.
3. Huang, B., et al., *Novel carbon-encapsulated porous SnO2 anode for lithium-ion batteries with much improved cyclic stability.* Small, 2016. **12**(14): p. 1945-1955.
4. Kim, T.H., et al., *The current move of lithium ion batteries towards the next phase.* Advanced Energy Materials, 2012. **2**(7): p. 860-872.
5. Kang, D.H.P., M. Chen, and O.A. Ogunseitan, *Potential Environmental and Human Health Impacts of Rechargeable Lithium Batteries in Electronic Waste.* Environmental Science & Technology, 2013. **47**(10): p. 5495-5503.
6. Dunn, J.B., et al., *Impact of Recycling on Cradle-to-Gate Energy Consumption and Greenhouse Gas Emissions of Automotive Lithium-Ion Batteries.* Environmental Science & Technology, 2012. **46**(22): p. 12704-12710.
7. Curry, C., *Lithium-ion battery costs and market.* Bloomberg New Energy Finance, 2017. **5**: p. 4-6.

8. Bied-Charreton, B., *Closed loop recycling of lead/acid batteries.* Journal of Power Sources, 1993. **42**(1): p. 331-334.
9. Feng, X., et al., *Thermal runaway mechanism of lithium ion battery for electric vehicles: A review.* Energy Storage Materials, 2018. **10**: p. 246-267.
10. Harper, G., et al., *Recycling lithium-ion batteries from electric vehicles.* Nature, 2019. **575**(7781): p. 75-86.
11. Chen, Y., et al., *Toxicity Identification and Evolution Mechanism of Thermolysis-Driven Gas Emissions from Cathodes of Spent Lithium-Ion Batteries.* ACS Sustainable Chemistry & Engineering, 2019. **7**(22): p. 18228-18235.
12. Ordoñez, J., E.J. Gago, and A. Girard, *Processes and technologies for the recycling and recovery of spent lithium-ion batteries.* Renewable and Sustainable Energy Reviews, 2016. **60**: p. 195-205.
13. Li, L., et al., *The Recycling of Spent Lithium-Ion Batteries: a Review of Current Processes and Technologies.* Electrochemical Energy Reviews, 2018. **1**(4): p. 461-482.
14. *LME COBALT*. 2021; Available from: https://www.lme.com/metals/minor-metals/cobalt/#tabIndex=0.
15. Gaines, L., *The future of automotive lithium-ion battery recycling: Charting a sustainable course.* Sustainable Materials and Technologies, 2014. **1-2**: p. 2-7.
16. Yao, Y., et al., *Hydrometallurgical Processes for Recycling Spent Lithium-Ion Batteries: A Critical Review.* ACS Sustainable Chemistry & Engineering, 2018. **6**(11): p. 13611-13627.
17. Joulié, M., R. Laucournet, and E. Billy, *Hydrometallurgical process for the recovery of high value metals from spent lithium nickel cobalt aluminum oxide based lithium-ion batteries.* Journal of Power Sources, 2014. **247**: p. 551-555.
18. Sommerville, R., et al., *A review of physical processes used in the safe recycling of lithium ion batteries.* Sustainable Materials and Technologies, 2020. **25**: p. e00197.
19. Zhao, Y., et al., *Regeneration and reutilization of cathode materials from spent lithium-ion batteries.* Chemical Engineering Journal, 2020. **383**: p. 123089.
20. Larouche, F., et al., *Progress and Status of Hydrometallurgical and Direct Recycling of Li-Ion Batteries and Beyond.* Materials, 2020. **13**(3).

2 Literature Review

2.1 Construction of Lithium-ion batteries

2.1.1 Structure of Li-ion Battery

There are four popular LIB shapes have been developed for consumer electronics, they are coin cell, cylinder cell, prismatic cell, and pouch cell as shown in figure 2-1 [1]. Despite the different outer shape of LIBs, five major components are generally found inside the casing as inner materials, which are cathode, anode, electrolyte, separator, and current collectors.

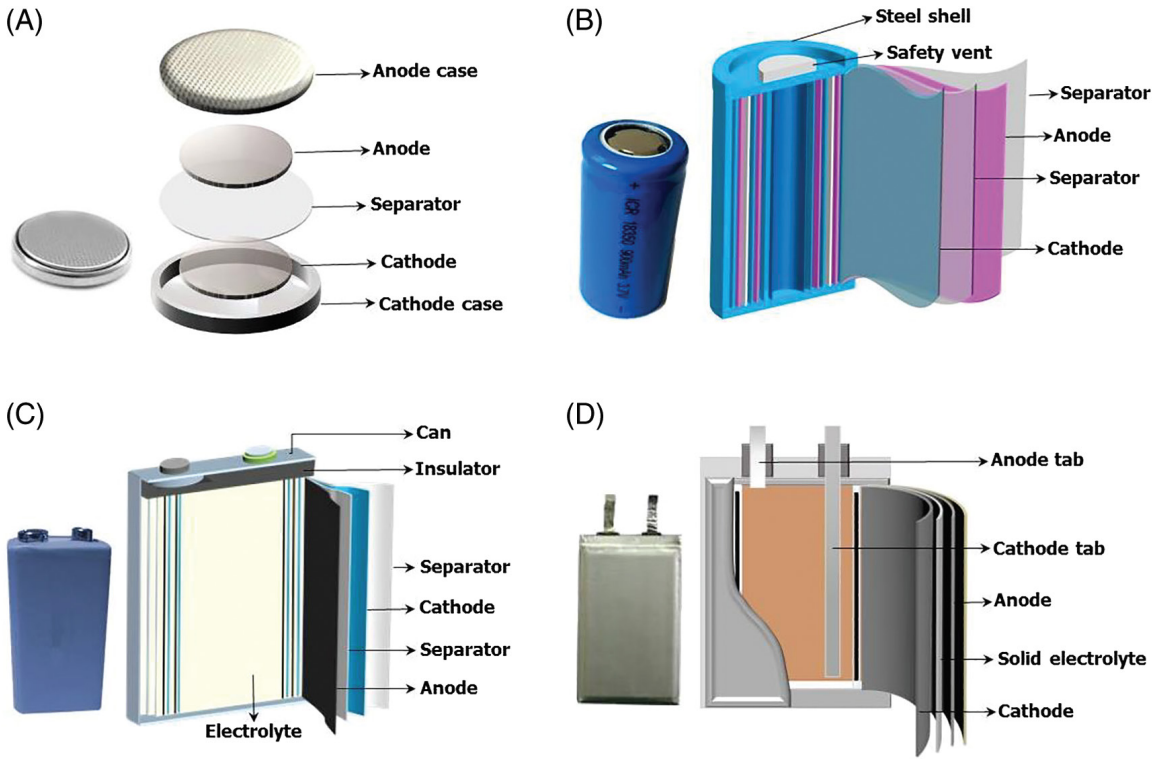

The cathode/positive electrode is constructed of aluminum foil with cathode active materials coatings [2], cathode active material is normally made of lithium metal oxides such as $LiNi_xMn_yCo_zO_2$, $LiCoO_2$, $LiFePO_4$, $LiMn_2O_4$ [3, 4]. The anode/negative electrode is composited of copper foil coated with graphite powder, graphite is selected due to its low cost, long cycle life, high coulombic efficiency, and abundant availability [5-7]. Binder are commonly used to adhere electrode materials onto current collector, polyvinylidene fluoride (PVDF) and polytetrafluoroethylene (PTFE) are normally used for cathode electrode [8, 9], carboxymethyl cellulose (CMC) is used for anode electrode [10]. Electrolyte ($LiPF_6$) is to facilitate the lithium ions movement and exchanges between anode and cathode layers during charging and discharging process [11].

Electrolyte solution composed of mixtures of alkyl carbonates: ethylene carbonate (EC), dimethyl carbonate (DMC), diethyl carbonate (DEC), and ethyl-methyl carbonate (EMC) [12-14]. They are chosen due to their acceptable anodic stability for 4V cathodes, high polarity, low toxicity, acceptable safety features, and reasonable temperature range between boiling and freezing points [15]. Separator membrane: 1) separate cathode and anode electrode sheets to avoid direct contact; 2) serves as medium for lithium ion transportation as well as controlling their numbers and mobility. It is normally made of polyethylene (PE) and polypropylene (PP) [16].

2.2 Pretreatments of Lithium-Ion Battery Recycling

2.2.1 Pretreatment Steps Arrangements

Generally, a series of pretreatment process is required before recycling activity happens. Although some of them have been reported in groups, pretreatment process has rarely been well classified and systematically established in previous studies. For example, mechanical separation [17-19], mechanochemical process [20], thermal treatment [21], and dissolution process [22] have been commonly investigated, all four processes are targeted on inner materials after cell dismantled. Mechanical separation are carried out using rough crushing, sieving, magnetic separation, fine crushing and classification to enrich and concentrate valuable cathode composites from battery scraps [23]. Mechanochemical process involves co-grinding of cathode composites with other materials to disorder the agglomerated structures and enable easier leaching extraction for lithium and other transition metals at room temperature [24, 25]. Thermal process utilizes muffle furnace at 100 - 500℃ to burn off insoluble carbon, graphite, organic additives and adhesives at a controlled atmosphere [21, 26, 27]. Dissolution process involves using organic solvent to dissolve PVDF (polyvinylidene fluoride) which serve as adhesive substrate for most cathode and some anode electrodes [28]. This process helps cathode and anode electrode powders to be separated easily from their support substrates and improve material recovery in subsequent recycling.

To move forward, Yao et al. [2] categorized pretreatment processes into three sections as discharging (discharger, NaCl solution), dismantling and separation (manual process, mechanical process), and separation of cathode active materials (dissolution, thermal treatment, vacuum pyrolysis). Garvin et al. have designated three pretreatment sections: stabilization (brine or ohmic discharge), opening (shredding or crushing cells with or without inert gas environment), and separation [29]. Zhang et al. have classified pretreatment processes into crushing, screening/sieving, and separation for industrial-scale; discharging, manual dismantle, and separation for lab-scale [30]. To systematically categorized all pretreatment processes, Kim et al. [31] have demonstrated them into six consecutive sections as: discharge, dismantling, comminution, classification and separation, solvent treatment, and thermal treatment. This structure is adopted in here.

2.2.2 Discharge

To recover the valuable metal contents within spent LIBs, stainless steel casing should be dismantled and removed. However, for spent LIBs, direct contact of anode and cathode

electrodes with remained capacities will easily cause short-circuit current flow, which generated heat and ignited flammable organic solvents to cause combustion of battery cells [32, 33]. Hence, it is necessary to discharge them first before opening to prevent self-ignition and other potential hazards. Kang et al. [34] proposed using a roll presser to treat prismatic spent LIB to achieve short-circuit between anode and cathode electrodes. Then they directly fell into distilled water to discharge for 1day. Instead of discharge at cell level, Kim et al. [35] manually dissembled cell first, stacked layers (separators, anode and cathode electrode sheets) were discharged in distilled water. Both methods mentioned above are dangerous and difficult to control at larger scale level. Lu et al. [36] and Li et al. [37] have investigated full discharge of spent LIBs in NaCl solution with 1 wt.% and 5 wt.%. Wang et al. [38] also reported discharge with dilute NaCl solution can remove excess capability. Li et al. [39] compared discharge efficiency versus time and water contamination during discharging with pure water, 5, 10, and 20 wt.% NaCl solutions. Discharge efficiencies increased quickly for NaCl solution samples in first 100 mins as 50%, 55%, and 65% for 5, 10, and 20 wt.% respectively, pure water sample's discharge efficiency reached at ~15% after 100 mins, then they slowly rose to ~70% for NaCl solution samples and ~ 40% for pure water sample after 24 hrs. Liquids with different conditions after fully discharge are compared on metal concentrations, indicated NaCl solutions yield much severe corrosion on stainless case than pure water condition. The 10 wt.% NaCl solution seemed to be the best for discharging for high discharge efficiency, less potential environmental damage and less valuable metals (Li, Cu, and Co) found in discharging solution.

Ojanen et al. [40] evaluated the behavior of spent LIBs during electrochemical discharge in different salt solutions, LIB discharged ex-situ with battery poles connected to Pt wires and the other end of wires submerged into electrolyte solutions: NaCl, $NaSO_4$, $FeSO_4$, and $ZnSO_4$ to measure evolution of voltage. Figure 2.2 (a) shows the discharge performances between these four electrolyte solutions, NaCl is most effective for fully discharge, enhance its concentration can also lower discharge time. While chloric gas formed from NaCl usage, solid salt precipitated on Pt wire found under use of sulfate solutions, which cause the impedance on subsequent discharge. Also, immersion of cell into NaCl solution could incur corrosion on battery connectors, which would lead to incomplete discharge and potential leakage of inner chemicals. Xiao et al. [41] investigated discharging performance of LIBs using electrolyte solutions with chloride ions, sulfate radical, and nitrate radical. Remained electricity versus discharge time with 1 mol/L solution concentrations were compared, after 25 hrs of discharge, remained electricity for spent LIBs discharged in NaCl and KCl, $MnSO_4$ and $MgSO_4$, $NaNO_3$ reached 0%, ~ 20%, and 60%, respectively. While other solutions could lead to obvious galvanic corrosions on iron shells during discharging, it was not found in $MnSO_4$ solution. It is possibly due to formation of isolation layer (manganese hydrogen peroxide) that inhibited direct contact between hydroxyl radical and positive connector (Fe or Al) to prevent corrosion on electrode. Hence, $MnSO_4$ is chosen to achieve mild discharge on spent LIBs without worrying serious galvanic reaction and organic leakage. Detailed schematic is shown in figure 2.2 (b). Yao et al. [42] investigated discharging using electrolyte solutions and solid medium (copper and graphite). Final voltages of three solutions decreases in sequence of $MnSO_4$>$FeSO_4$>NaCl, while $FeSO_4$ and NaCl

required less time to reach 1V. Copper and graphite powder have similar discharge capacities compared with NaCl and $FeSO_4$, yet their instabilities on voltage, potential explosion hazard from too fine of graphite powder, and reduced conductivities by easily oxidized copper powders make physical discharge not applicable. $FeSO_4$ solutions is considered most environmentally friendly discharge method for low levels of LIB components detected in both supernatant and sediment.

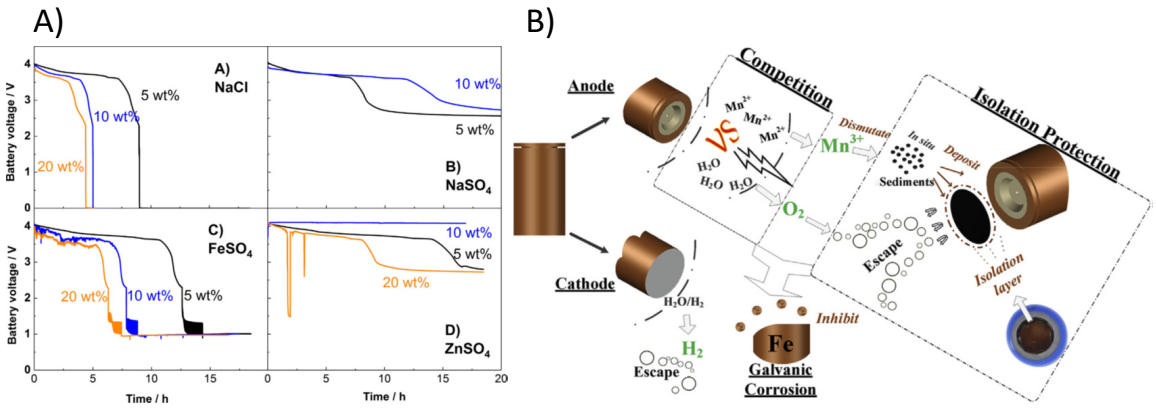

Figure 2-2 (a) [40] LIB discharging curves in aqueous solutions with various concentrations of (A) NaCl, (B) NaSO4, (C) FeSO4, and (D) ZnSO4. (b) [41] Proposed reaction mechanism for the batteries discharge in $MnSO_4$ solution. Reprinted with permission.

2.2.3 Dismantling

Manual dismantling processing on individual cell are commonly conducted using sharp-nose pliers, knife, screwdriver, and cutting saw. For cylinder cells, Aurbach et al. have proposed a dismantled design using a glove box, battery holders, an electrical circular curved tip saw, and remote-controlled X-Y moving stages. The cap of cylinder cell was cut first, then case was cut vertically and the battery core was released [43]. Due to small scale operation, remote control, and fume hood protection, potential thermal runaway and fire hazard caused by short circuit during opening presented minimal hazard to the operator. Compared to cylinder cell, pouch cell disassemble is easier, because pouch case can be cut through by knife or scissors [44]. A shallow cut on side of the cell was recommended before peeling off the remaining pouch foil by pliers. A comparison on opening processes for cylinder cell and pouch cell is shown in figure 2-3.

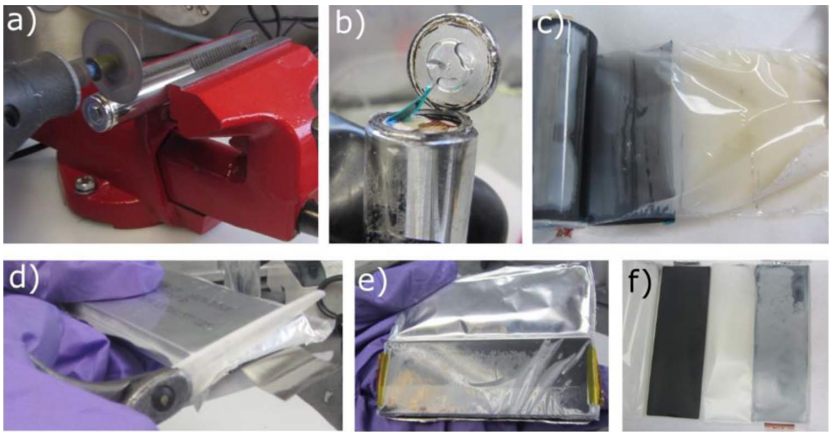

Figure 2-3. Cell opening process. a–c) Opening of a cylindrical cell using a Dremel tool. d–f) Opening of a pouch cell using ceramic scissors. Reprinted with permission. [44]

For most cases, fume hood, protective gloves and safety glasses were utilized for personal protection [19, 23, 45]. Li et al. [39] investigated the VOCs (volatile organic compounds) from dismantle process, detail compounds are listed in table 2-1. Dimethyl carbonate and tert-amylbenzene are two dominant VOCs, their emission per spent LIB were 4.298 mg/h and 0.749 mg/h, separately. Hardly any research have been focused on human exposure risk of tert-alkylbenzen, while DMC is a flammable liquid with a flash point of 170 ℃, it also has a recommended industrial exposure limit of 100 mg/L by inhalation over an 8 h work day [46]. Beside the VOCs, LiPF6 can easily reacts with water to form hydrogen fluoride gas, which can incur severe health issue [47, 48]. Thus, powerful air pump with adequate ventilation should be installed to pump organic vapor compounds out of the workspace.

Retention time (min)	Compounds	Molecular formula	Relative content (%)
3.20	Dimethyl carbonate	C3H6O3	65.10
4.22	Ethyl methyl carbonate	C4H8O3	3.29
5.01	Trifluoromethanesulfonic anhydride	C2F6O5S2	0.68
9.42	Ethylene carbonate	C3H4O3	9.50
9.89	Propylene carbonate	C4H6O3	5.45
11.55	Tert-Amylbenzene	C11H16	10.15
14.77	1H-Indene, 1-methylene	C10H8	0.92
17.02	2-Methylnaphthalene	C11H10	1.64
17.42	Diethyl Phthalate	C12H12O4	2.97

Table 2-1. Volatile organic compounds emissions from dismantled LIB cells [39].

2.2.4 Comminution

After cell dismantle, inner materials are obtained, crushing and grinding are normally applied to delamination and detachment of electrode materials. A series of established comminution processes have been developed for industrial-scale process: Retriev Inc. (previous, Toxco) proposed protective environment (brine solution and liquid nitrogen)

for spent LIB submersion during shredding, brine solution immersion can deactivate the batteries as well as prevent fire caused by Li oxidation. Liquid nitrogen can bring down LIB temperature to -200℃ for several hours, lithium reactivity lowered by 5 or 6 orders of magnitude compared to that at room temperature [49, 50]. Spent LIBs were crushed in a shredder and sieved by screen. Recupyl has proposed a two-step comminution for spent LIBs [51]. Battery cells were first fed to a low-speed rotary shear (11 rpm) under Ar or CO_2 atmosphere to expose inner materials, inert gases were to prevent thermal runaway from potentially charged cells. The second grinding was conducted in an impact mill with 90 rpm to downsize materials into – 3 mm particles. Akkuser process contained two continuous cutting mills [52, 53], first one operated at temperature of 40 to 50℃, at 100 – 400 rpm to reduce spent LIBs to size of 1.25 to 2.5 cm pieces. No inert gas environment mentioned during the crushing process for safety protection, gases occurred from crushing were extracted and filtered using a cyclonic system. Using an air-tight cooling tube, shredded materials fed to the second mill operating at 1000 – 1200 rpm, materials reduced to size – 6 mm. Batrec [54] proposed shredding of spent LIBs under protective atmosphere using CO_2 to prevent potential fire hazard, then scrapped materials were neutralized by moist air. Waste gases were collected with releasing of protective atmosphere, materials then sent for leaching process.

Beyond already established ones, emerging comminution industrial scale processes are shown as follow: Accurec proposed autothermal pyrolysis at 250℃ for cell level to safely evaporate electrolyte, solvents, and volatile hydrocarbons [55] to prevent thermal runaway, electrolyte was collected in a downstream condenser [56]. Then comminution and multistep mechanical treatment conducted to separate ferromagnetic steel, aluminum cases, copper and aluminum electrode foils, and anode and cathode active electrode materials [57]. LithoRec process included two non-continuous crushing steps [58], discharged and dismantled spent LIBs were crushed with a 20 mm rotary shear crusher between 100 – 140 ℃ under protective nitrogen atmosphere. After electrolyte extractions, shredded materials fed to air classification to remove materials of Al, Fe, Cu, and plastics. Fine particles contained most anode and cathode electrode materials fed to secondary crushing stage and sieved with 500 micrometers opening. Detailed flow sheet is shown in figure 2-4 (b) [59].

Lab scale studies have been carried out to understand more detailed information during comminution activities of spent LIBs. Wang et al. [60] have investigated commercial granulator (i.e., Econo Grind 180/180) on comminution of spent LIBs and material distributions afterwards. This granulator has a 200rpm roto speed with max. of 50 kg of material throughput per hour and 3 Kw drive capacity, shear force is assumed to be the dominant acting force. Battery cells first immersed in liquid nitrogen to minimize risk of thermal runaway, then they were fed into granulator and shredded into small pieces (-7.5 mm). Shredding process conducting in fume hood to minimize risk of exposure to electrolyte, shredded materials left in fume hood for a week to fully vaporize volatile chemicals. Then shredded pieces separated into five size fractions and shown in figure 2-4 (a): -0.5 mm, -1 mm +0.5 mm, -2.5 mm +1 mm, -6 mm +0.5 mm, +6 mm. Its result showed that most of electrode materials can be separated from the rest of components after shredding using size separation despite of battery brands and cathode types, most

electrode materials can be concentrated in smaller size fractions. Zhang et al. [61] have investigated wet and dry impact crushing methods on spent LIBs with LCO cathode using a blade crusher with water as medium, equipment schematic is shown in figure 2-4 (c). Wet impact crusher was used for wet crushing for 20 s with 500 L/h water consumption, water was fed into crusher from the top to form slurry and carry particles go through sieving plate. Dry crushing carried out by a two-stage method, spent LIBs were first cut into pieces by shear crusher and then crushed in impact crusher for 20 s. Wet crushing lead to enrichment of every component in spent LIB to fine fractions because of scouring action of water flow, fine products contained too many impurities. Selective crushing was achieved on drying crushing, where both cathode and anode electrode materials can be delaminated from aluminum and copper foils without over crushing of other components in spent LIBs. Barik et al. [62] also studied wet crushing using a single shaft shredder using shear cutting on spent LIBs, water used as scrubbing agent as well as temperature controller. After shredding, materials obtained at -10 mm size range, plastic/Teflon matrix floats on water and got removed manually, other parts (electrode materials, copper and aluminum foils, aluminum casing, and PCBs) got separated by size sieving.

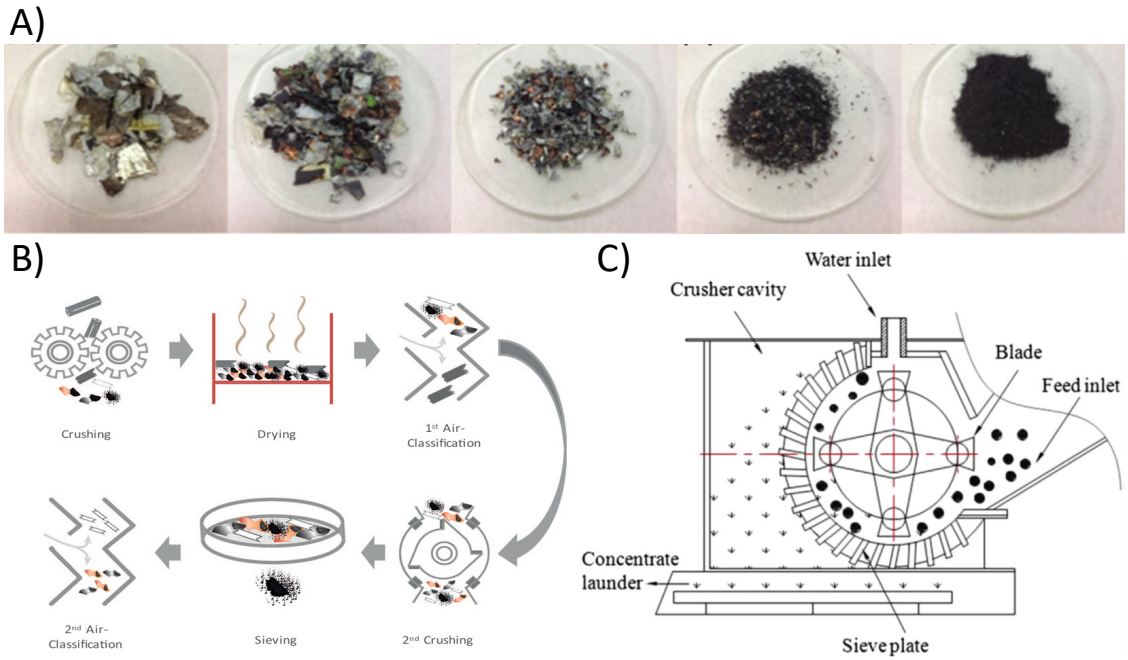

Figure 2-4. (a) Samples of five size fractions after granulator process for spent LIBs [60] (from left to right): (+6 mm), (-6 mm +2.5 mm), (-2.5 mm +1mm), (-1 mm +0.5 mm), (-0.5 mm). (b) Process step of two crushing steps delamination. [59]. (c)Sketch of wet impact crusher [61]. Reprinted with permission.

In addition to crushing on whole battery cell, some efforts have been devoted mainly on delamination of cathode electrode materials from aluminum foils. Spent LIBs were fully discharged and then dismantled, cathode electrode sheets were selected out manually and fed to a small high-speed universal pulverizer to delaminate $LiCoO_2$ powders from

aluminum foils [63]. Alternatively, delamination process of cathode electrode sheets carried out using a wet agitation process in a high shear blender, individual cathode sheet was agitated with water for 5 -10 s. Slurry contained agitated materials separated through a wet sieving process to remove aluminum from delaminated cathode composites [64]. At least 85% of cathode electrode materials got recovered with aluminum contamination less than 0.3%. Cryogenic grinding was applied on cathode delamination as an temperature-assisted mechanical method [65]. After cell dismantling, cathode sheets were cut into 1 cm^2 pieces manually, then ground with cryogenic ball mill using liquid nitrogen to provide low-temperature condition. Sample were ground at room temperature (298 K) and at low temperature (77 K) for the same amount of time. PVDF has glass transition temperature of 235 K to cause cathode composite microstructure damage, while Al foil remained form of large chips. Thus, delaminated cathode ground into powders and separated from Al by size screening.

Rather than cell level comminution, planetary ball milling mainly applied on electrode materials to decrease particle size and increase particles' specific surface area. Cathode active materials were ground with a planetary mill for 2 h [19, 66-68] to obtain smaller, higher-surface-area particles to increase leaching efficiency, which helped to obtain over 90% of cobalt recovery and almost 100% of lithium recovery after leaching process. Yu et al. have shown that ball milling on mixed electrode materials from spent LIBs can benefit subsequent flotation performance [69]. Spent LIBs first short-circuited and dismantled manually, cathode and anode sheets placed in an impact crusher with number ratio of 1:1. After crushing and sieving, -74 μm powders were mixed with graphite and $LiCoO_2$ collected for grinding, optimum condition is 5 min with 40 g of feed. Grades for cathode and anode electrode materials after flotation were 97.19% and 82.57%, with recoveries of 49.32% and 73.56%, respectively. Under horizontal shear force by grinding media, lamellar structures of graphite are sliding and flaking, new hydrophobic surfaces got exposed. On the other hand, organic film coating cathode electrode powders were worn down to restore their original hydrophilicity. Liu et al. [70] have proposed cryogenic ball mill (Retsch Cryomill, Germany) on mixed electrode materials obtained from spent LIBs to improve their flotation performance. The volume of the grinding chamber is 50 ml, the diameter of grinding ball is 26 mm, and its mass is 63 g. Grinding chamber was cooled by liquid nitrogen during processing, ratio of ball mass to sample mass is 10.5:1. Cryogenic temperature is lower than organic binder's transition temperature (~235 K), the organic binder became glassy and broke off from both anode and cathode electrode powders' surface under external force. While cathode particles remained in spherical shape, graphite particles became lamellar structures to expose more hydrophobic surface. Grade of cathode improved from 55.36% to 91.75% in tailing with recovery improved from 72.8% to 89.93% from subsequent flotation.

2.2.5 Classification

After LIB comminution and electrode sheet delamination, a classification process is required to separate and concentrate electrode materials from other components. Shin et al. [17] used sieving sizes of 106 μm, 200 μm, and 800 μm to separate materials after primary and fine crushing of spent LIBs. Undersized products that obtained at -850 μm

fraction mainly consisted of lithium cobalt oxide and graphite particles with less than 1 wt.% of Al or Cu as contamination, where oversized products were aluminum foil, copper foil, stainless steel casing, separator, and plastic packaging. Similarly, Kang et al. [71] have safely discharged, dismantled, crushed, and segmented spent LIBs into three size fractions: +8 mesh, -8 +16 mesh, and -16 mesh. Fraction of -1190 μm collected for reductive leaching. Granata et al. [72] separated crushed battery materials with more cut-off screen sizes: 2 mm, 1 mm, 0.5 mm, 0.25 mm, 0.2 mm, and 0.125 mm. Most of metal contents were concentrated in the fraction with -1 mm size range: 82% of Li, 88% of Mn, 81% of Co, and 62% of Ni. While copper and aluminum mainly concentrated at +1 mm range with 67% of Cu and 79% of Al. Wang et al. [60] have investigated the distributions of elements after crushing and sieving, crushed materials were separated into following size fractions: -0.5 mm, 0.5-1 mm, 1-2.5 mm, 2.5-6 mm, +6 mm using a Vibration Machine Test System. Cobalt content increased from 35 wt. % in the metal portion before crushing to 82 wt. % at -0.5 mm fraction and to 68 wt. % at 0.5-1 mm fraction, it was not found in +6 mm fraction. Zhang et al. [73] have divided crushing samples into three size fractions: +2 mm, -2 +0.25 mm, and -0.25 mm as Al-enriched, Al and Cu-enriched, Co and graphite-enriched, respectively. 76.3% of aluminum recovered at +2 mm fraction, 94.14% of aluminum collected above 0.25 mm, and total recovery of Cu was 90.44% for -2 +0.25 mm and 94.14% for +0.25 mm. Co recovery was 94.39% for -0.045 mm and 57.23% for -0.075 mm. Detailed recovery rate data shown in table 2-2.

Size fraction/mm	Cu	Co	Al
2	3.70	1.98	76.03
−2 + 1	33.49	1.62	10.84
−1 + 0.5	39.17	1.28	6.00
−0.5 + 0.25	17.78	0.77	1.27
−0.25 + 0.1	1.87	16.00	1.07
−0.1 + 0.075	0.98	21.16	1.08
−0.075 + 0.045	1.93	37.90	2.52
−0.045	1.06	19.33	1.17

Table 2-2. Distribution of copper, cobalt, and aluminum after crushing in each size range (wt. %) [73].

Pyrolysis-assisted delamination of anode and cathode electrode sheets and subsequent size sieving have been analyzed [74], electrode sheets were thermally treated to 500℃ and stayed for 10 mins under nitrogen atmosphere. Predominant pyrolysis products were fluorine-containing benzene and ester electrolyte that were collected by condensation process, organic binders were removed after pyrolysis. Both raw and pyrolyzed electrode sheets were crushed using pulverizer to obtain fine fractions, coarse fractions fed back to crushing process. Delamination efficiencies for anode and cathode have been improved from 88.08% and 82.88% to 99.60% and 99.78%, respectively. Pyrolytic electrode materials are mainly concentrated in -45 μm size fraction. Peng et al. [75] investigated the acid leaching efficiencies on -2 mm and +2 mm fractions of spent LIB scraps, underflow products (-2 mm) fraction was rich in cathode materials (~4 wt.% Li and ~21 wt.% Co) while overflow product (+2 mm) mainly composed of current conductor pieces

(~12 wt.% Cu and ~17 wt. % Al). -2 mm product were separated into five size fractions: -0.125 mm, 0.125-0.25 mm, 0.25-0.5 mm, 0.5-1.0 mm, 1.0-2.0 mm, where cathode electrode contents (Li, Co, Mn, Ni) were evenly distributed, while Cu, Al, and Fe were low (< 2 wt.%) in -0.25 mm but increased dramatically (5-20 wt.%) in +0.25 mm range. Acid leaching result showed leaching efficiencies of lithium and cobalt improved with increased impurity amount of copper and aluminum served as reductants during leaching process. Widijatmoko et al. [76] studied material distributions of crushed spent LIBs on different size fractions with and without subsequent attrition scrubbing process. Batteries were shredded using a cutting mill (Retsch SM2000) with 8mm grind, samples dried to vaporize the volatile organic electrolytes followed by optional attrition scrubbing, materials were separated into size ranges: +4750 µm, 4750-2360 µm, 2360-850 µm, 850-212 µm, 212-38 µm, and -38 µm. Figure 2-5 (a) shows the cumulative distribution of shredded materials, ~20 % of materials recovered at -100 µm range, ~20 % of material captured between 100 and 1000 µm, ~60 % materials remained at +1000 µm. Figure 2-5 (b) and 2-5 (c) compares the recoveries of copper, cobalt, and aluminum with and without attrition scrubbing after shredding, respectively. Without attrition, over 50 % of Al and Cu found at 4750-2380 µm, more than 80 %of each are above 212 µm, while only 30 % of Co found at -212 µm. After attrition, recovery of Co significantly improved from ~10 % to 80 % in -38 µm, Cu and Al got reduced and distributed more evenly at +212 µm, no significant increase of impurities found at -212 µm.

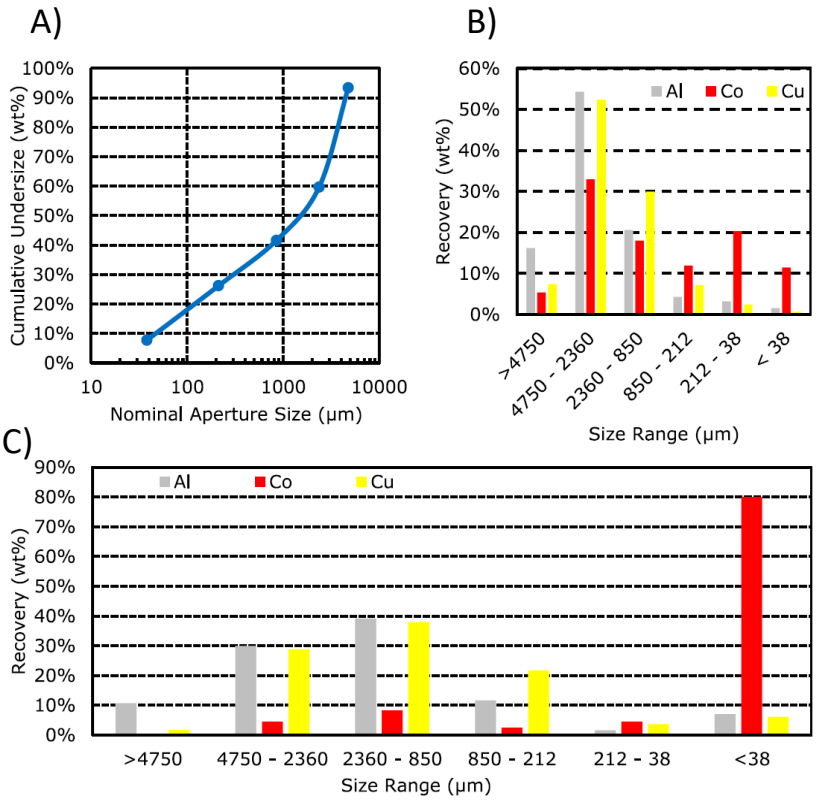

Figure 2-5. (a) Cumulative undersize semi-logarithmic pot of shredded spent LIBs. (b) Size-recovery rate of shredded spent LIBs for respective size range. (c) Recovery rates for different size fractions upon size attrition and reduction. Reprinted with permission. [76]

Delamination of cathode electrode materials from new and spent LIBs using ball milling and subsequent size separation have also been investigated [77]. Four size ranges have been used for separation of milled samples: +2360 μm, 2360-850 μm, 850-38 μm, -38 μm, their morphology characterizations have been carried out, schematic diagram and individual size-based recovery rates have been shown in figure 2-6. Largest particles (+2360 μm) are mainly electrode pieces under partially delamination, about 38 % of cathode electrode materials still adhered onto the metal surfaces. For 2360-850 μm range, materials are mainly composited of size reduced electrode pieces, recovery of cobalt is ~20 %. For 850-38 μm, delaminated but not yet fully down sized cathode composites are presented, recovery for cobalt is ~35 % with 5-10 % each of Al and Cu. For the finest fraction (-38 μm), particles are primarily composited of small cathode agglomerates, no impurities presented for new cells, 4-11 % of cobalt recovered at this fraction for new and spent batteries.

Characteristics	Schematic Diagram	Size-Based Recovery Rate
Category 1: Include the majority of particles that have experience reduction in size, accompanied by some detachment of its active materials such as particles in the range of >2360 µm.		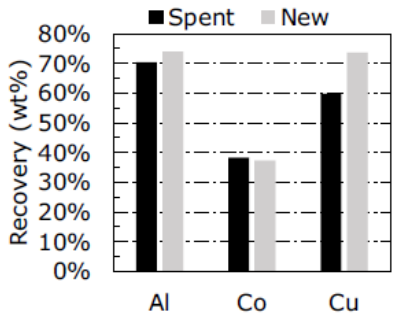
Category 2: Include particles that have a reduction in size with active materials lamination, such as in the range of 2360 µm – 850 µm. (only true for positive electrode)	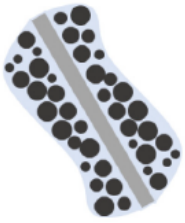	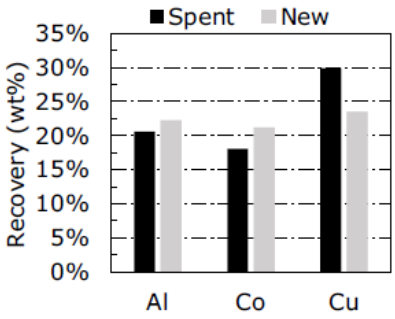
Category 3: Active materials laminate that have been detached from its current collector and still held together by the binder. This type of particles comes as aggregates for the particle size of 850 µm – 38 µm.	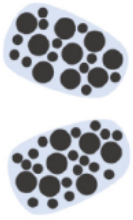	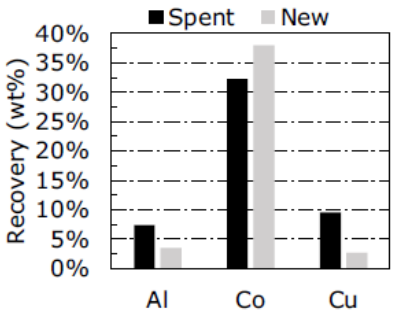
Category 4: Active materials laminate that have been detached from current collector and accompanied with minimum aggregation for the particle size of < 38 µm.	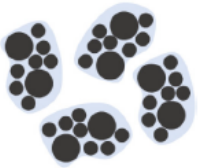	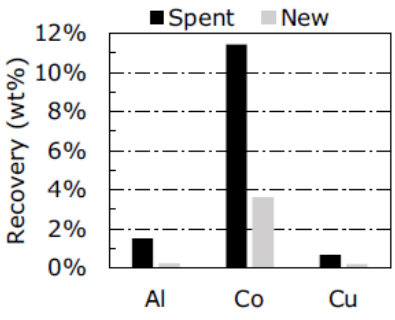

Figure 2-6. Characterization of classified cathode materials from ball-milled LIBs, reprinted with permission. [77].

2.2.6 Solvent Treatment

After classification and segmentation of crushed/milled spent LIBs, existence of binder still agglomerates cathode active materials together at smaller size fractions, which hinder the leaching efficiency and possibility for re-purpose/rejuvenation process towards direct recycling purpose. Moreover, certain amount of cathode active materials still adhered onto aluminum foils through PVDF binding after crushing, which results in lower delamination ratio. In order to remove binder, dissolution process has been widely adapted. Contestabile et al. [28] have proposed using N-methyl-2-pyrrolidone (NMP) to treat cathode electrode sheet at 100 ℃ for 1 h to dissolve PVDF binder, this is inspired by the fact that NMP is a good solvent (solubility around 200g/kg of solvent) for PVDF, with boiling point of ~200 ℃. Aluminum and copper foils recovered by filtration after both anode and cathode active materials successfully delaminated. Liu et al. [78] proposed using dimethyl acetamide (DMAC) treatment on cathode sheets to achieve cathode composites delamination, DMAC was chosen for economic consideration. Solid-liquid ratio was controlled between 1:4 and 1:5 to avoid viscous liquid from PVDF dissolution, cathode sheet immersed into DMAC for several hours until cathode composites delaminated. Obtained slurry filtered and dried at 120 ℃ for 12 h to vaporize excess DMAC, powders were heated for 450 ℃ and 600 ℃ to burn off PVDF and carbon additive, respectively. N, N-Dimetbylformamide (DMF) have also been investigated to dissolve PVDF binder [79]. Xu et al. [80] proposed fierce stirring on cathode sheets with organic DMF at room temperature to achieve delamination, obtained sediment were filtered with ethanol and dried in vacuum atmosphere at 80 ℃ to vaporize excess organics. Smashing and subsequent screening with 300 mesh applied to remove residual aluminum contents. Similarly, cathode sheets were cut into 4 cm^2 pieces and immersed into DMF at 70 ℃ for 2 h [81], sediments also washed with ethanol after aluminum removal. DMF process benefited from low cost and low temperature operation.

Dissolution combined with ultrasonic treatment have been combined to facilitate cathode delamination [82]. Yang et al. [83] sonicated small cathode pieces from spent LIBs in NMP for 3 mins to separate cathode composites from aluminum foils, NMP was recycled through subsequent filtration. The delamination mechanism of cathode composites from the aluminum foil can be ascribed to the ultrasonic waves that accelerate the convective motion with large amount of energy provided, as well as increased contact area of solid materials to accelerate the binder dissolution speed. He et al. [84] found that dissolution of PVDF binder and ultrasound caused cavitation contributed to cathode delamination, the peel-off efficiency reached about 99 % under optimal conditions of NMP solvent, treatment temperature of 70 ℃, 90 mins of ultrasonication time with power of 240 W. With the assistance of the ultrasound, the liberation efficiency increased in order: ethanol<DMSO<DMF<DMAC<NMP.

Molten salt systems have been compared for cathode delamination by melting PVDF [85]. Four combinations have been investigated: medium-free as blank group, NaOH/KOH, KNO_3/$NaNO_3$, and $AlCl_3$/NaCl. Cathode sheets obtained from dismantled spent LIBs treated with individual molten salt system for 20 mins at 160 ℃, salt/cathode sheet mass ratio was 10:1. As can be seen from figure 2-7(a), heating electrode at 160 ℃

did not melt binder, PVDF still bonded cathode electrode materials onto aluminum foils. Figure 2-7(b) shows the Al foil got corroded by Alkali solution, yet cathode material was not fully delaminated. Figure 2-7(c) shows $NaNO_3$-KNO_3 molten salt have no significant effect on peel-off of cathode materials at 160 ℃. Figure 2-7(d) shows that cathode materials and aluminum were well separated by $AlCl_3$-NaCl molten salt system at relatively low temperature.

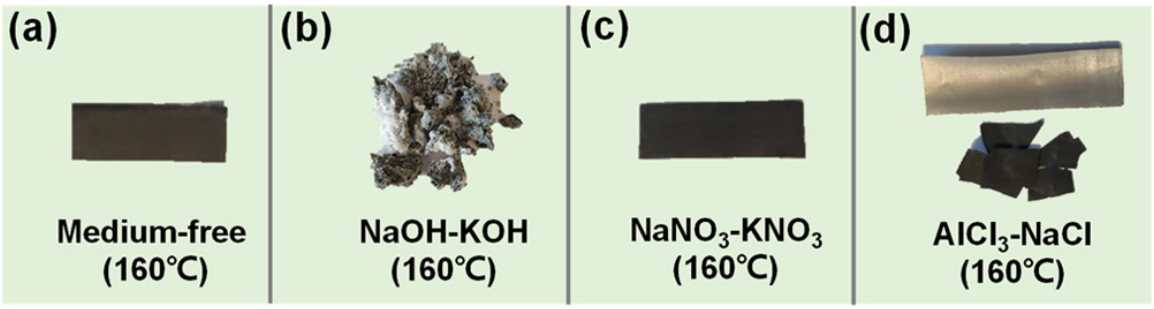

Figure 2-7. Effect of different molten salt systems on the peeling of cathode materials: (a) medium-free, (b) NaOH-KOH, (c) $NaNO_3$-KNO_3, and (d) $AlCl_3$-NaCl. Reprinted with permission. [85]

Bai et al. [86] has introduced using Ethylene glycol (EG) as a sustainable solvent to achieve cathode delamination by competitive inhibition mechanism. Cathode sheets obtained from spent cell was washed with dimethyl carbonate to remove electrolyte, then cut into small pieces and placed into EG solvent. Solid-liquid ratio was 1:10 by weight, heating temperature was 160 ℃ under stirring. Cathode active materials were adhered onto aluminum through PVDF binding, while PVDF can form hydrogen bonding with the aluminum surface, which typically has a thin layer of aluminum oxide. EG has a high boiling point due to the strong hydrogen bonding originating from the two hydroxyl groups in one molecule. When cathode electrode immersed into EG, solvent molecules immediately diffuse to wet the interface between electrode composites and the aluminum surface through interconnected pores in electrodes, then EG can form strong hydrogen bonds with Al oxide and competitively replacing the hydrogen bonds between PVDF and aluminum foil.

Nan et al. [32] used alkaline solution to dissolve aluminum out to liberate cathode active materials. Over 98 % of Al was dissolved under 10 wt.% NaOH solution at ambient temperature with a solid-liquid weight ratio of 1:10 for 5 hours. Copper and cathode materials were hardly dissolved in alkaline solution, filtered materials sent for acid leaching process. Gratz et al. [87] have also used NaOH to dissolve aluminum from battery scraps for 2 h, hydrogen gas and $NaAl(OH)_4$ were reaction products.

Ionic liquid was applied for cathode separation [88], 1-Butyl-3-methyl-imidazolium-tetrafluoroborate ([BMIm][BF_4]) agitated with cathode layers obtained from spent LIB. Over 99 % of cathode material detached from Al foil with 25 min agitation time, temperature of 180 ℃, and 300 rpm agitation speed. After cooling, cathode materials and

aluminum foils got separated by DI water washing and filtration. This ionic liquid can be reused.

2.2.7 Thermal Treatment

Thermal treatment is another efficient way to remove binder and fully liberate active electrode powders from current collectors and concentrated into small size fractions. Chen et al. [89] heated cathode sheets obtained from spent LIBs in air atmosphere for 1 h to achieve delamination of cathode composites with help of crushing and sieving. Further calcination at 550 ℃ in muffle furnace for 0.5 h conducted on under size powders to eliminate PVDF and acetylene black. However, the crystalline phase characterization showed synthesis of Co_3O_4 appeared in cathode concentrate after 550 ℃ calcination, also valence of Mn increased to form $Li_4Mn_5O_{12}$. Yang et al. [90] applied 550 ℃ of thermal treatment on cut cathode sheet pieces in a tube furnace, purity nitrogen purged in continuously to get rid of air, temperature controlled below 650 ℃ as aluminum melting point. Both anode and cathode delamination were conducted through controlled thermal treatment, recovery of substrates in metallic form achieved by separating fine powders, schematic results are shown in figure 2-8. It was also found that thermal treatment process changed the molecular structure of the cathode materials and reduced the charges of transition metal ions in the cathode materials, which is shown to be beneficial to the recovery of the transition metals by leaching. Hence, pyrolysis can help to prepare samples for metal recoveries through leaching but not suitable for direct recycling process, which requires feed materials maintained their function integrity and distinct structure.

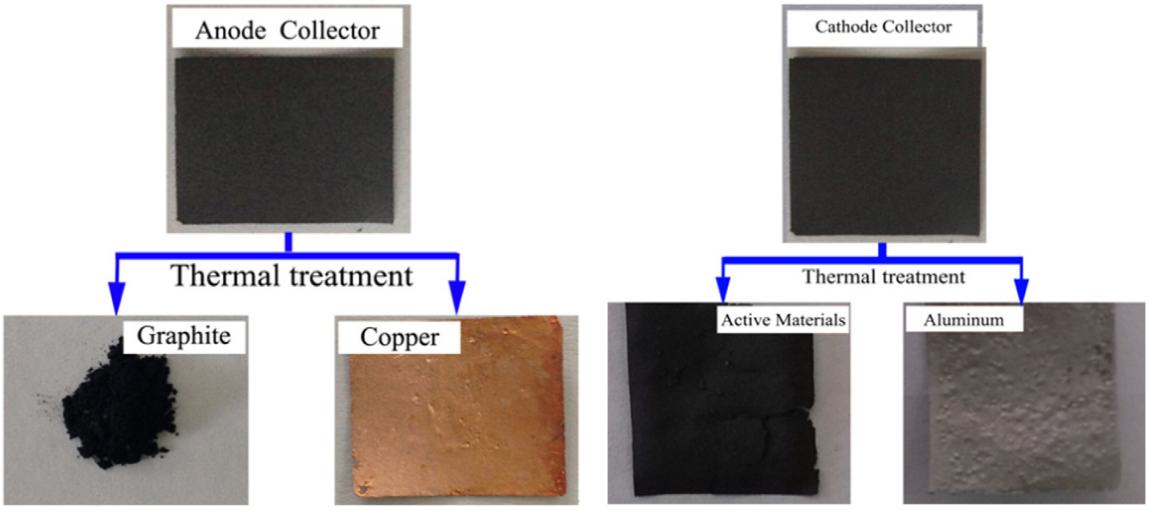

Figure 2-8. Segmentation of anode and cathode materials from Copper and Aluminum foils under nitrogen pyrolysis. Reprinted with permission. [90]

Sun et al. [91] used vacuum pyrolysis to delaminate cathode powders from aluminum. Cathode plates were placed into the reactor before vacuumed, pressure maintained lower than 1.0 kPa, temperature heated to 600 ℃ and held for 30 mins with heating rate of 10 ℃/min, peel-off materials mainly composited of $LiCoO_2$ and CoO. Volatiles were

condensed, vacuum pump and gas collector used to collect non-condensable. Effect of thermal treatment temperature from 450-700 ℃ have also been studied; experimental results are shown in figure 2-9. No significant change has been observed for 450 ℃ treatment, cathode materials still bonded onto aluminum foil, it is due to binder was not fully decomposed at this temperature. With temperature rises to 500-600 ℃ that shown in figure 2-9 (c)-(e), aluminum foil surface becomes more and more clear, meaning delamination efficiency increases correspondingly. Beyond 600 ℃, aluminum foil started to become fragile and even decomposed into smaller pieces before any cathode delaminated, making the separation impossible to occur. Also, thermal treatment in air atmosphere would render the delamination efficiency as well even temperature is controlled at 600 ℃. To improve recovery of cathode in subsequent leaching process, acid washing on thermal treated aluminum foil is viable, remained foil is shown in figure 2-9 (i) with much clear surface. Vacuum pyrolysis have also been applied for in situ recovery of lithium carbonate [92] and manganese oxide [93] from spent lithium ion batteries. Spent LIB scraps were prepared by shear crushing and screen sieving (-120 μm) to obtain cathode composites ($LiMn_2O_4$ and PVDF) and graphite, mixed materials thermally treated at 1073 K for 45 mins in oxygen free atmosphere supported by continuous vacuum pumping. It was found that graphite and cathode materials were in situ converted into Li_2CO_3 and MnO.

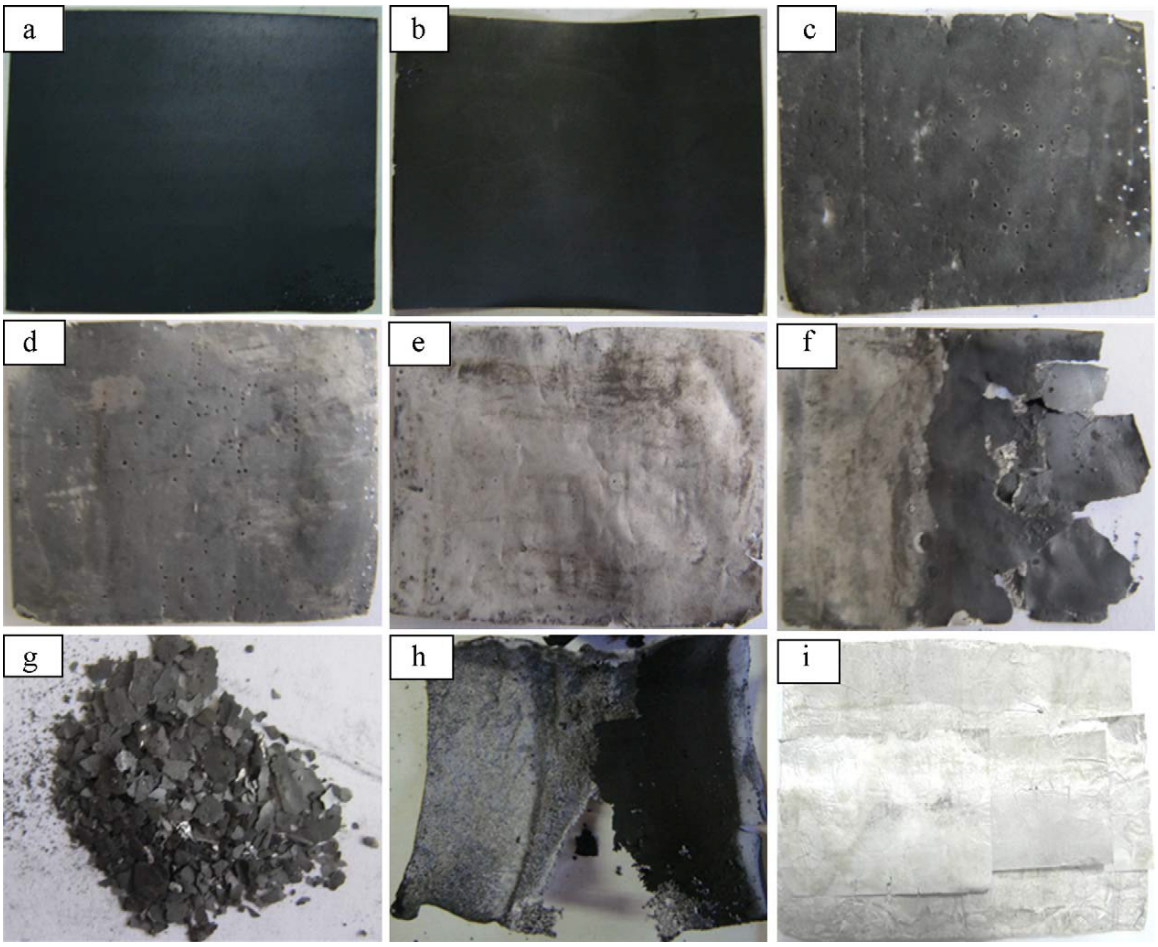

Figure 2-9. Cathode electrode sheets after different cheating process(es): (a) cathode electrode obtained from spent LIB after dismantling and cutting, cathode sheet pyrolyzed (b) at 450 ℃, (c) at 500 ℃, (d) at 550 ℃, (e) at 600 ℃, (f) at 650 ℃, (g) at 700 ℃, (h) cathode sheet heated at 600 ℃ in air atmosphere, (i) aluminum foil after acid washing. Reprinted with permission [91].

2.3 Physical Method

2.3.1 Density Separation

Density separation is generally used to separate low density materials include plastics, papers, metal pieces, and delaminated electrode materials from each other as a part of recycling routes, which is conducted using shaking tables, vibrating screens, intermedium of fluid or air [51, 52, 94]. Barik et al. [95] have proposed density separation with water to carried plastic to overflow product and concentrated Cu, Fe, Al, and PCBs with feed obtained from oversize product after spent LIBs shredded and sieved. Gratz et al. [87] have proposed density separation using diiodomethane with density of 3.3 g/cm^3 as separating medium, feed material was copper (8.96 g/cm^3) and plastic (polyethylene) (~0.9 g/cm^3) from +250 μm fraction after spent LIBs got crushed and sieved. Materials put into medium and were allowed to settle for 30 mins, then material on the surface was skimmed off and separated from the other components. A schematic of density separation by fluid medium is shown in figure 2-10 (a) [94].

Density separation using air as intermedium have been studied on separating separators from metal pieces after dismantling and crushing of spent LIBs [96], a calculation based design is shown in figure 2-10 (b). Experiments with hand cut samples shown efficiency of pneumatic separation is ~100 % with feed size of 3-4 cm*cm and airflow velocity of 6.96-7.8 m/s. From the industrial process, recoveries of separators and electrode pieces were 98.64 % and 99.23 %, respectively. Computer simulation has been developed and shown the turbulence and changes in high-speed zones in separator improved the separation efficiency. Then separation of aluminum and copper foils with and without electrode coatings using pneumatic separation has been studied [97]. Dynamic analysis has been carried out based on built separator, maximum separation happened for size of particle at -9 mm fraction. Without electrode materials coated, optimum airflow velocity was 1.7 m/s to separate Al and Cu pieces with 96 % and 97 % grade; optimal airflow velocity for electrode material coated pieces was 3.3 m/s with 97 % of grade for both products. Multiple stages of pneumatic separation have been proposed to detailly separate materials in spent LIBs scraps [98]. First separation occurred with feed of crushed cells to remove separators to low density fraction and metallic shells to high density fraction, remained materials fed for crushing and size sieving. Both undersize and oversize products sent to two pneumatic separators to remove aluminum and copper foil while concentrating electrode powders for subsequent thermal treatment and flotation. Detailed flowsheet and materials distribution is shown in figure 2-10 (c).

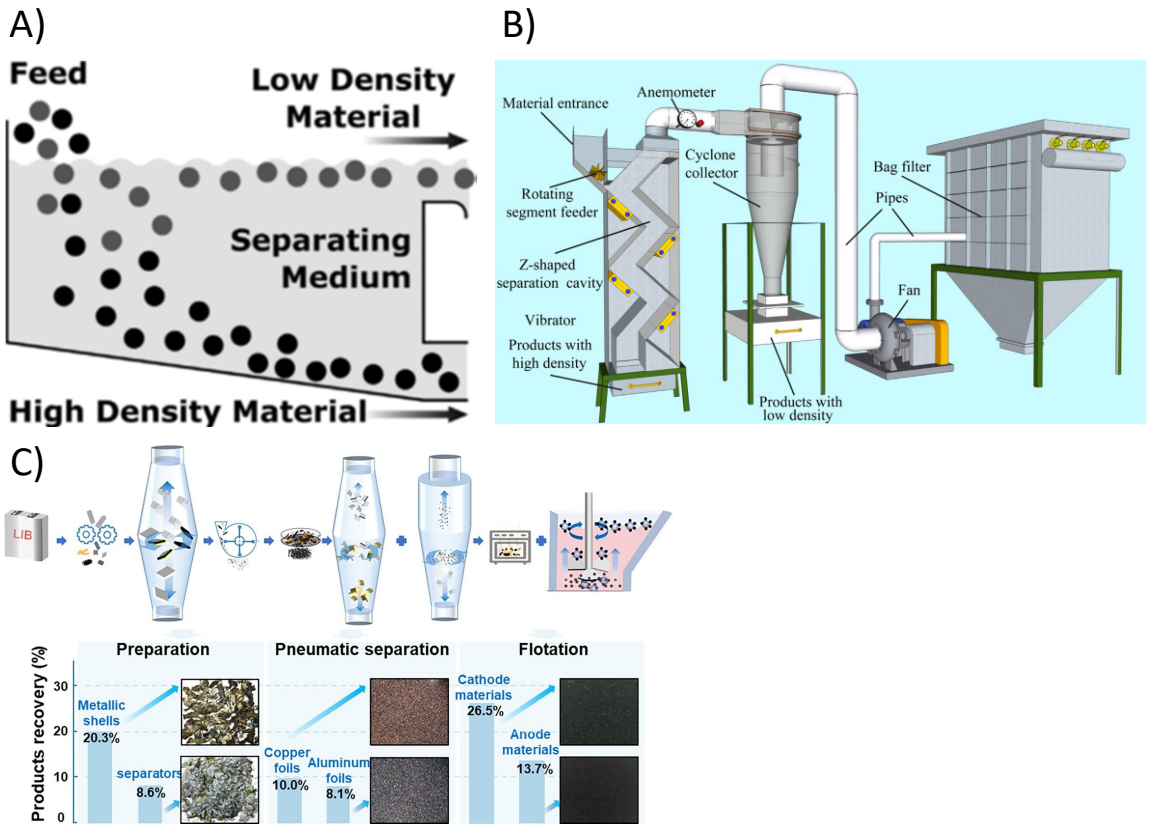

Figure 2-10. (a) A schematic diagram showing simple density separation using fluid as medium [94]. (b) Schematic of pneumatic separator comprised of zigzag classifier and cyclone collector [96]. (c) Multiple pneumatic separation [98]. Reprinted with permission.

2.3.2 Magnetic Separation

One of popular application of magnetic separation is to remove stainless steel after dismantling and crushing of spent LIBs, usually coupled with vibrating screening and air classification, then inner materials are obtained for further processes [56, 87, 99, 100]. Barik et al. [95] used magnetic separation to separate copper and aluminum foils from stainless steel cases and PCBs after screening and density separation, then Fe and PCBs fed for gold recovery. It was also applied to remove impurities include magnetic components from electrode material concentrates [101]. Li et al. [37] coupled wet magnetic separation and oxygen-free roasting for in situ recycle of cobalt, lithium carbonate, and graphite. Lithium cobalt oxide and graphite obtained from spent LIBs after dismantling, crushing, and size sieving, then -120 μm fraction was thermally treated in oxygen-free atmosphere at 1000 ℃, 30 mins to generate mixture of cobalt, lithium carbonate, and graphite. Graphite was used as reducing agent in smelting process. Wet magnetic separation conducted in lab scale using magnetic stirrer in water at 20 ℃, solid-liquid ratio was 1:200. 48 h agitation time required to fully dissolve lithium carbonate, ferromagnetic Co was magnetized and attached onto stirrer, graphite was precipitated in

the bottom of beaker and collected by filtration. Recoveries of graphite, lithium, and cobalt were 91.05 %, 98.93 %, and 95.72 %, respectively.

2.3.3 Eddy Current Separation

Eddy current separation (ECS) works best for separating nonferrous metallic particles with size range of 2-20 mm from feed materials, a case study has been conducted on spent Lithium iron phosphate (LFP) battery after dismantling and crushing [102], its separation diagram is shown in figure 2-12. Crushed products contained cathode materials, anode materials (graphite), copper, plastic membrane, and aluminum. In the feed materials for eddy current separation, graphite powders and separators were not mentioned. Copper and aluminum foils have good electrical conductivities, high-intensity eddy current generated by them in magnetic field, while LFP materials have lower conductivity than other popular cathode materials due to higher specific resistance, cycle performance, and resistivity. In the desired material range (2-20 mm), test results were consistent with results from simulation proposed by author. Maximum particle size ratio of copper and aluminum could reach 1.72 under magnetic roller speed of 800 r/min. Corresponded force and kinetic models have been proposed in study. Application of eddy current to separate LFP powders from cathode sheets after thermal treatment and crushing have been investigated by the same research group [103], the dissociation rate of cathode sheet reached 100 % after thermal treatment at 300 ℃ and 120 mins followed by high speed pulverization with 20 s. With optimized eddy current separation condition: feeding speed of 1 m/s, magnetic field rotation of 4 m/s, the separation rate of LFP powder and Al foils was 100 %.

Granate et al. have used eddy current separator on recycling of primary lithium, lithium-ion, and nickel metal hydride batteries [104]. After crushing and sieving, powders -1 mm were separated by an ECS to concentrate ferrous metals and non-metals separately, also concurrent combustion helped to eliminate lighter fractions like papers and dielectric materials which can cause problems during the ECS separation. Eddy current separation showed excellent separation between lithium and cobalt in non-electromagnetic fraction as well as copper and aluminum in electromagnetic fraction [105].

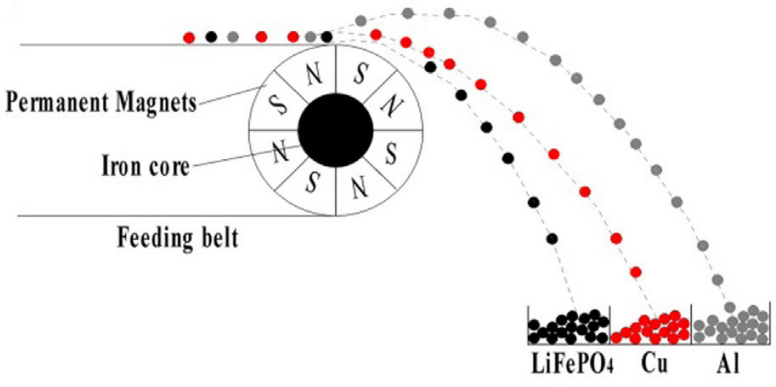

Figure 2-11. Eddy current separation diagram [102]. Reprinted with permission.

2.3.4 Electrostatic Separation

Electrostatic separation separate materials based on difference of surface conductivity, separation also happened by the favorable attraction or charging of materials to electric field of opposed charging potential [76, 106], a schematic diagram of electrode static separator has been shown in figure 2-11. It has been used to separate nonconductive attrition medium (silica sand) from separator and metal fractions after attrition milling [76]. Nonconductive fraction contained 95 v.% battery separator films; main contamination was silica sand. Conductive fraction was of 97.65 wt. % metals, contamination was silica sand. Middling contained 99.01 wt. % of silica sand with small amounts of Al and Cu. Silveira et al. [107] investigated using electrostatic separation on larger fraction (+212 µm) of milled spent LIBs after removing delaminated electrode materials (anode and cathode). Conductive material contained 98.98 wt. % of metallic materials while nonconductive fraction contained 99.6 wt. % of polymers, results showed that electrostatic process is promising and efficient method to recovery other materials beyond electrode materials. Zhang et al. [73] have used electrostatic separation to concentrate aluminum and copper as conductive materials from separator which is non-conductive materials. Spent LIBs discharged, crushed, and sieved into +2 mm, -2 +0.5 mm, -0.5 +0.075 mm, and -0.075 mm fractions. -0.5 +0.075 mm fraction got ground and sieved again to delaminate electrode materials from Al and Cu, +0.075 mm combined with materials from -2 +0.5 mm fraction and fed to electrostatic separator. Recovery rate of aluminum and copper were up to 94 % and 90 %, respectively.

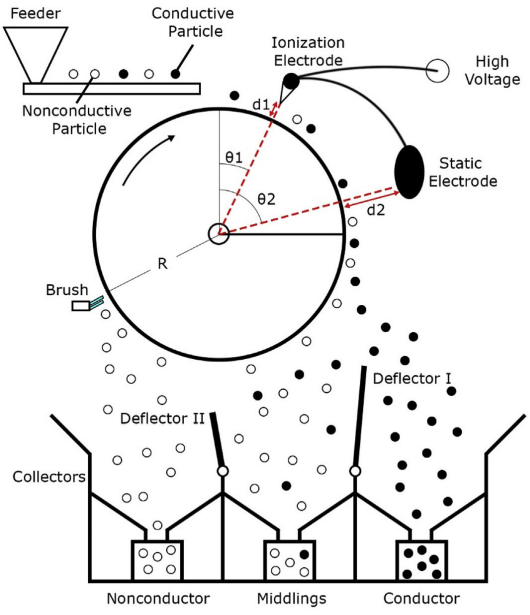

Figure 2-12. Schematic of electrostatic separation [76]. Reprinted with permission.

2.3.5 Froth Flotation and Surface Chemistry

2.3.5.1 Froth Flotation Separation

Froth flotation operates by exploiting the difference of particles' surface hydrophobicity, its desired particle size range is 10-100 μm. Fine air bubbles introduced into a vessel with slurries under agitation, frother chemicals added to obtained stabilized bubble form, general reagents include various alcohols, pine oils, and cyclical carbonates [94]. Collectors are used to selectively increase surface hydrophobicity of targeted minerals to improve separation efficiency. Hydrophobic materials are attached and carried to the top by rising air bubbles, floated materials are collected as froth products by overflow. Hydrophilic materials are maintained in the bottom of flotation tank and collected as tailing product. In the case of electrode materials from LIB, graphite (anode electrode material) is hydrophobic, while lithium metal oxide (cathode electrode material) is generally hydrophilic, hence froth flotation is widely used in black mass separation after classification pretreatments. Zhan et al. [108] have proposed a schematic drawing for flotation and separation process of anode and cathode materials as shown in figure 2-13 (a), its flotation product is shown in figure 2-13 (b).

However, impurities such as PVDF and surface organic layers can hinder the flotation performance. For example, in early times, KIM et al. [109] have conducted froth flotation on black mass obtained from spent LIBs screen below 65 mesh, poor separation performance was obtained, this is due to the cathode materials were covered by PVDF binder and their surface hydrophobicity changed. Thermal treatment of 773 K for 2 h was applied to burn off PVDF, subsequent flotation showed recoveries of 98 % were achieved for both graphite and cathode materials. 93 % grade of cathode was recovered with recovery of over 92 % using 0.2 kg/t kerosene as collector, 0.14 kg/t MIBC as frother, 10 % pulp density, and 10 mins flotation time. Zhong et al. [110] have proposed thermal treatment of 550 ℃ for 2 h at cell scraps to burn off binder. Pyrolytic gas and tar were collected and used for pyrolysis energy. After crushing and classification, -25 μm product collected and fed for froth flotation, while 99.34 % of aluminum and 96.25 % of copper were recovered through screening and color sorting. Flotation conducted under conditions: pH 10, 100 g/t of amylum dosage, 30 mg/L MIBC, about 50 % of cathode materials recovered.

As mentioned before, cryogenic grinding coupled with froth flotation was proposed [70]. Cryogenic grinding can effectively remove binder because its temperature is lower than binder's glass transition temperature, with effective removal of binder, agglomeration of electrode materials was eliminated, particle size was suitable for flotation. Also, cathode materials' new hydrophilic surface got exposed, while graphite materials were laminated to create more hydrophobic surface. Both recoveries and grades were improved significantly improved from flotation after cryogenic grinding, a schematic is shown in figure 2-13 (a). Fenton reagent has been applied to modify particle surface and improve flotation performance [111]. It was found that Fe^{2+}/H_2O_2 ratio as 1:120 with liquid-solid ratio of 75:1 was effective to remove outer organic layers of electrode materials. Macromolecule material such as PVDF was broken down into small molecules, organic materials were oxidized into CO_2 and H_2O afterwards. Classification of crushed spent

LIBs conducted, -25 μm materials sent for flotation, recovery of 98.99 % of Co obtained with content ratio of 39.91 wt. %, meaning grade of cathode is still far from satisfying. Flotation performance might be rendered by remained Fenton reagent and broken-down molecules that attached on particles' surface.

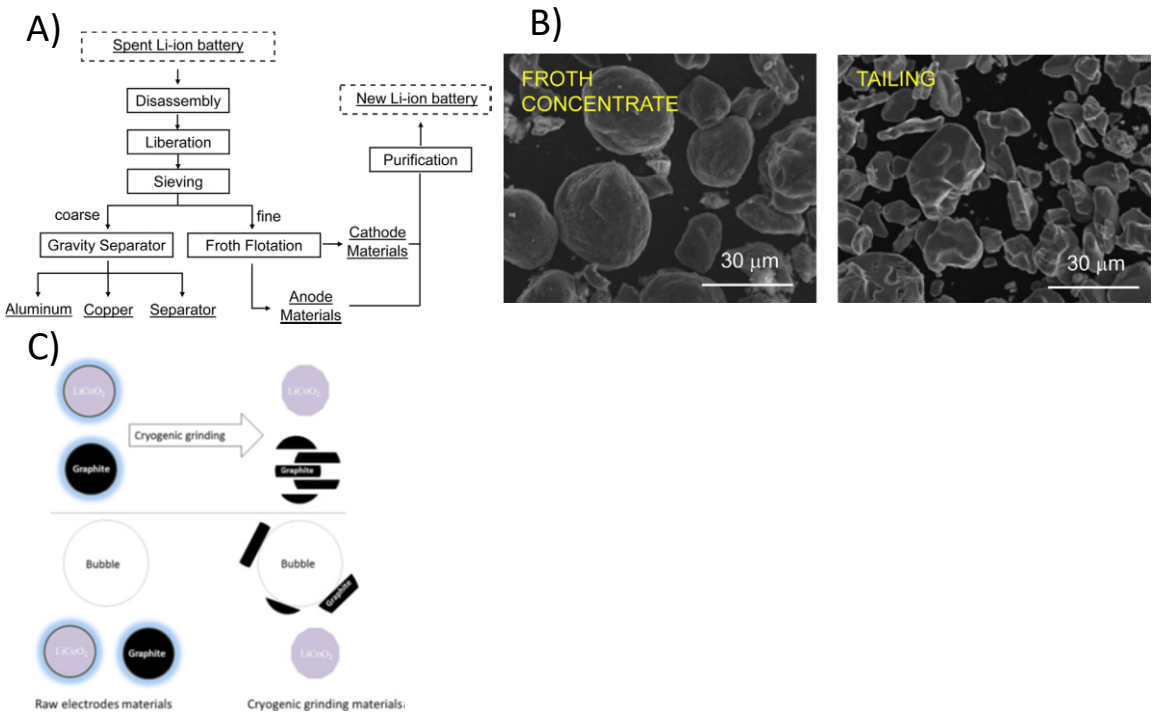

Figure 2-13. (a) Schematic of direct recycling using froth flotation; (b) Sem images of froth and tailing products after flotation; [108] (c) Mechanism of improved flotation separation of anode and cathode powders by cryogenic grinding [70]. Reprinted with permission.

2.3.5.2 Surface Chemistry of Physically Recycled Cathode Electrode Materials using XPS Scanning

To understand the surface chemistry of physically recovered materials, X-ray photoelectron spectroscopy (XPS) scanning have been widely used for characterization. Its scan on pristine cathode particles have been conducted since early 90s. Elp et al. [112] have reported that compared with CoO, $LiCoO_2$ has a strongly reduced interatomic distance of Co-O, which induced a strong ligand field to stabilize a Co^{3+} low-spin ground state. Madhavi et al. [113] have shown the binding energies of $LiCoO_2$ for different element:528.9 eV for O1s; 53.3 eV for Li1s; 779.5 eV for $Co2p_{3/2}$. For the cathode materials obtained from spent cells, Fan et al. [114] reported the spectra of C1s, O1s, and Ni 2p of recovered NMC532 cathode materials from spent LIB. Four peaks were fitted to C1s spectrum as: Co_3^{2-} (289.1 eV), O-C=O (287.8 eV), C-O (286.0 eV), and C-C (284.6 eV). Result showed the existence of lithium carbonate impurity on the particle surface. For the spectrum of O1s, three peaks found as: O impurity (532.0 eV), O lattice (529.2 eV), and oxygen vacancies (530.9 eV), where the impurity is also denoted for lithium

carbonate. For the Ni spectrum, Ni 2p showed the mixed valence of Ni^{2+} and Ni^{3+} co-existed, quantitative analysis conducted to show the amount of Ni^{3+} (26%) is much low than of Ni^{2+} (74%). Besides, Fu et al. [115] conducted XPS on recovered cathode materials (LCO) to show low atomic ratios of 3.55% cobalt and 2.79% lithium on the cathode surface, while high ratio of fluorine and carbon with 22.43% and 45.56% found on the surface. This result suggested the existence of organic layer attributed to PVDF deposited on the cathode materials after physical recovery, which hinder the performance of subsequent physical separation and acid leaching. Surface analyses have also been compared between NMC cathode materials obtained from spent LIBs with and without healing process. Sloop et al. [116] proposed healing method of harvested cathode materials by hydrothermal reaction: particles sealed with saturated lithium solution in pressure vessel. XPS analysis showed that healing achieved by oxidation of Ni^{2+} to Ni^{3+} with weaker Ni 3p signal at 67.5 eV after healing. However, the lithium peak at 55 eV decreased after healing, indicating minimal or no lithium-salt presented on the surface of healed particles.

2.4 Pyrometallurgy

Pyrometallurgy utilizes thermal treatment to decompose the components from spent LIBs, valuable materials are recovered and concentrated through physical and chemical transformations [5, 117]. Changes of structure and phase transitions occurred at lower temperatures, with increased temperatures, chemical reactions are involved [7]. Similar to physical treatments, thermal processes that have been discussed above as pretreatment methods such as binder removal and thermal assisted delamination will not be repeated, concentrated electrode materials obtained from spent LIBs after proper pretreatment are the main focus of thermal treatment presented as follow.

2.4.1 Calcination and Roasting

Calcination in LIB recycling is a thermal process of cathode electrode materials, it involves thermal decomposition and phase transition to decompose targeted materials and generate a desirable compound [118]. Carbothermic reduction (CTR) roasting is applied to process recovered cathode electrode materials. Maroufi et al. [119] have proposed using activated carbon to conduct CTR on lithium cobalt oxide obtained from spent LIBs to recover lithium and cobalt. Cathode sheet was manually removed from dismantled LIB first and then pulverized into fine powder using 30 s ring milling, aluminum contamination was removed using alkaline leaching and suspension stage. Cathode materials mixed with activated carbon and thermally treated at 600, 700, and 800 ℃ for 30 mins in argon atmosphere. At 600 ℃, no dissociation of $LiCoO_2$ was observed. At 800 ℃, lithium got totally liberated and escaped in form of gas from the sample, cobalt oxide was fully reduced to metallic cobalt. Only at 700 ℃, lithium got totally separated from sample in form of solid lithium carbonate, cobalt oxide was partially reduced to metallic cobalt. After water dissolution and filtration, recovery of cobalt was over 99 %, recovery of lithium was 36 %, which was relatively high considering using water as solvent. Graphite was used as reduction agent to conduct carbothermic reduction on cathode scraps coupled with NaOH catalyst [120]. Weight ratio for

graphite:$LiCoO_2$:NaOH was 2:10:1, material was mixed in glove box with motor to avoid moisture, then catalytic CTR conducted at 520 ℃ for 3 h followed three-stage cross-current water leaching and filtration to obtain lithium carbonate, NaOH, CoO, and graphite. Cobalt was recovered as metal oxide; lithium recovery rate was higher than 93 % with lithium concentration up to 14.99 g/L in lixivium of leaching. A detailed flowsheet is shown in figure 2-14 (a).

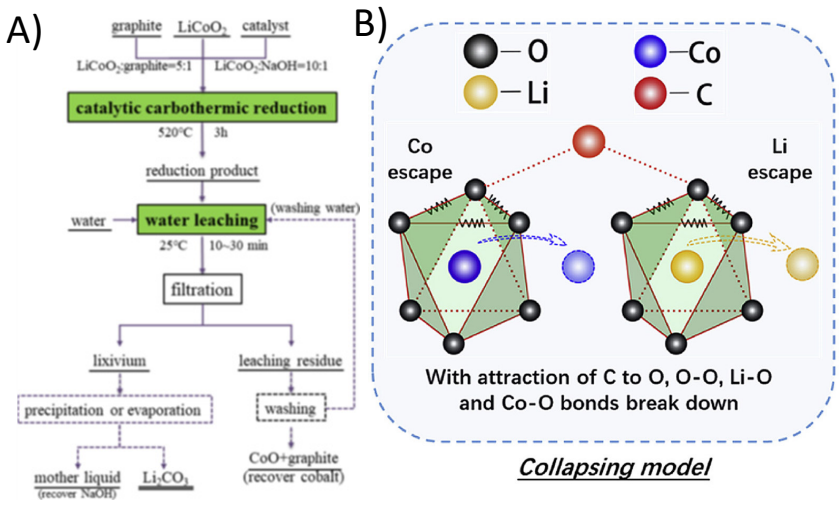

Figure 2-14. (a) Flowsheet of catalytic carbothermic reduction process for recovery of metals from $LiCoO_2$ cathode [120]. (b) Collapse model of lithium cobalt oxide during carbothermic reduction [121]. Reprinted with permission.

To deeper understand the carbothermic reaction, Mao et al. [121] have investigated its thermodynamics and proposed a collapse model of lithium cobalt oxide. Pure lithium cobalt oxide, CoO, and graphite were used to represent cathode electrode material, CTR product, and anode electrode material, respectively. Considering the reducing property of graphite and reducing property of lithium cobalt oxide, overall carbothermic reaction should be:

$$4LiCoO_2 + 3C \rightarrow 2Li_2CO_3 + 4Co + CO_2 \quad (1)$$

However, it was found that graphite does not reduce $LiCoO_2$, $LiCoO_2$ broke down first and followed by oxidation reduction of CoO and graphite, then Li_2O reacts with CO_2 to form Li_2CO_3 [37].

1) Decomposition of lithium cobalt oxide:

$$4LiCoO_2 \rightarrow 2Li_2O + O_2 + 4CoO \quad (2)$$

2) Incomplete and complete combustions of carbon:

$$2C + O_2 \rightarrow 2CO \quad (3)$$

$$C + O_2 \rightarrow CO_2 \quad (4)$$

3) Carbothermic reduction:

$$2CoO + C \rightarrow 2Co + CO_2 \quad (5)$$

$$CoO + Co \rightarrow Co + CO_2 \quad (6)$$

4) Lithium carbonate formation:

$$Li_2O + CO_2 \rightarrow Li_2CO_3 \quad (7)$$

As shown in figure 2-14 (b) for the collapse model for lithium cobalt oxide with graphite at 1173 K, both Co-O and Li-O octahedrons broke down due to the attraction of C to O, meaning both Co-O covalent bond and Li-O electrovalent bond became more unstable with the existence of graphite. As O octahedron collapses, lithium and cobalt can escape more easily and lower the required reaction temperature. Detailed thermodynamics were discussed in this research as well.

Similarly, carbothermic reduction have been investigated on other cathode electrode materials: $LiNi_{1/3}Co_{1/3}Mn_{1/3}O_2$, $LiNiO_2$, and $LiMn_2O_4$ [122, 123], where thermal decomposition of cathode happened first to lower transition metal to lower valence, then carbothermic reduction of metal oxide by carbon to obtain pure metal. Detailed reaction equations [7] are shown as follow:

5) Decomposition of lithium manganese oxide:

$$3LiMn_2O_4 \rightarrow 3LiMnO_2 + Mn_3O_4 + O_2 \quad (8)$$

$$4LiMn_2O_4 \rightarrow 8MnO + 2Li_2O + 3O_2 \quad (9)$$

$$4LiMnO_2 \rightarrow 4MnO + 2Li_2O + O_2 \quad (10)$$

6) Carbothermic reduction of manganese oxide:

$$Mn_3O_4 + C \rightarrow 3MnO + CO \quad (11)$$

$$Mn_3O_4 + CO \rightarrow 3MnO + CO_2 \quad (12)$$

7) Decomposition of lithium nickel oxide:

$$4LiNiO_2 \rightarrow 2Li_2O + 4NiO + O_2 \quad (13)$$

8) Carbothermic reduction of lithium nickel oxide:

$$4LiNiO_2 + C \rightarrow 2Li_2O + 4NiO + CO_2 \quad (14)$$

$$2LiNiO_2 + 3C \rightarrow Li_2O + 2Ni + 3CO \quad (15)$$

$$4LiNiO_2 + 3C \rightarrow 2Li_2CO_3 + 4Ni + CO_2 \quad (16)$$

9) Carbothermic reduction of nickel oxide by carbon and carbon monoxide:

$$2NiO + C \rightarrow 2Ni + CO_2 \quad (17)$$

$$NiO + C \rightarrow Ni + CO \quad (18)$$

$$NiO + CO \rightarrow Ni + CO_2 \quad (19)$$

Liu et al. have investigated the CTR of $LiNi_{1/3}Co_{1/3}Mn_{1/3}O_2$ [122] with carbon, optimal roasting temperature range was 650 ℃ for 30 min, coke with 10 wt. % used as reducing agent, the spent NMC cathode was decomposed and/or reduced into Li_2CO_3, NiO, Ni, MnO, and Co. Corresponding equation is shown:

$$12LiNi_{1/3}Co_{1/3}Mn_{1/3}O_2 + 7C \rightarrow 6Li_2CO_3 + 4Ni + 4Co + 4MnO + CO_2 \quad (20)$$

Leaching process was conducted on roasted products to recover valuable components, leaching efficiencies of lithium, nickel, cobalt, and manganese were 93.67 %, 93.33 %, 98.08 %, and 98.68 %, respectively. Lithium carbonate was captured by water leaching, vaporization was carried out to remove water and obtain it in solid form. Divalent acid was used for acid leaching of transition metal and their oxides, nickel, cobalt, and manganese were co-precipitated into ternary precursor while remained acid was collected and recycled. CTR on LCO powder and subsequent leaching has been discussed before [37], lithium cobalt oxide thermally treated with graphite at 1000 ℃ for 30 min, LCO got fully decomposed and reduced to Co and Li_2CO_3 with remained graphite as residue. Mixed materials were separated by wet magnetic separation, recovery rate of cobalt, lithium, and graphite were 96 %, 99 %, and 91 %, separately. CTR of LMO and follow-up leaching has also been studied [30, 92], lithium manganese oxide thermally treated with graphite at 800 ℃ for 45 min under oxygen-free atmosphere to in situ recover MnO and Li_2CO_3, recovery of lithium reached 91.3 % through water leaching process. Filtration residue from water leaching was burned in air to remove excess graphite, remained product contained 95.11 % of Mn_3O_4.

2.4.2 Smelting

Smelting is another pyrometallurgy method to recycle metal components from spent LIBs, all materials are heated over their melting points to form a slag with slag-forming agent (slag, sand, and limestone). Subsequent leaching is required to recover copper, nickel, cobalt, and iron, while lithium and manganese if contained in the cathode are lost [124]. Smelting usually included two steps: first is to carry out low temperature thermal treatment of spent LIBs to reduce danger of thermal runaway and evaporate the electrolyte. Secondly, all materials are burnt at higher temperature to reduce Co, Ni, Cu,

and Fe into alloys [5, 125]. During which, burning of electrolytes and plastics could provide energy for high temperature process to lower energy consumption [29]. With the presences of aluminum and carbon, nickel and cobalt can be reduced to metallic form and captured in metal, detailed reactions are shown as [126]:

$$2LiCoO_2 + 2Al \rightarrow Li_2O + 2Co + Al_2O_3 \quad (21)$$

$$2LiCo_{1-x}Ni_xO_2 + 3C \rightarrow Li_2O + {}^{(1-x)}/_2\, Co + {}^{x}/_2\, Ni + 3CO \quad (22)$$

$$4LiCo_{1-x}Ni_xO_2 + Al \rightarrow 2Li_2O + {}^{(1-x)}/_4\, Co + {}^{x}/_4\, Ni + 2Al_2O_3 \quad (23)$$

Slag system is essential for improving recovery efficiencies of valuable metals from smelting process, most popular slag systems is CaO-SiO_2-Al_2O_3, whose recovery of manganese and lithium are low. Both CaO and SiO2 are chosen as slag former for their fluidity and effective ability on temperature control [118], while aluminum oxide usually comes from batteries inside. Lithium is formed as compound in slag, its high melting and boiling point makes its smelting difficult and not economically feasible [126]. Amount of aluminum oxide in slag cannot be too high, otherwise slag system's viscosity and melting point would increase, resulted in alloy droplets trapped in the slag phase during separation of metal layers and slag to low metal recovery [7].

In order to achieve higher recovery of lithium from slag after smelting, Li et al. [127] have propose sodium roasting and water leaching on simulated slag. Optimal experimental condition was found at 800 ℃ for 60 min with molar ratio of 3:1 for Na_2SO_4/Li, subsequent water leaching conducted at 70 ℃ for 80 mins with liquid-solid mass ratio of 30:1, with 93.62 % of lithium recovered. This was achieved by transforming insoluble lithium from slag into soluble $LiNaSO_4$. However, due to lower price of lithium, this method is neither economical nor energy efficient. Another method was proposed by Ren et al. [128] to use slag system of FeO-SiO_2-Al_2O_3 to produce Co-Cu-Ni-Fe alloy, and manganese-high and lithium slag. They suggested that MnO/SiO_2 ratio need to be controlled between 2.05-3.23 (w/w) with Al_2O_3 in range of 19.23-26.32 wt. %. The slag contained 47.03 wt. % of MnO and 2.63 wt. % of LiO, further sulfuric acid leaching conducted on slag to achieved recovery of 94.85 % for lithium and of 79.86 % for manganese.

2.5 Hydrometallurgy

Hydrometallurgy method to process and recycle spent LIBs is the most essential approach since over 57 % of recycling activities accounted to this method [129]. Compared to pyrometallurgy which usually taken under high temperatures, hydrometallurgy embraces more advantages including high recovery efficiencies of valuable metal (lithium and manganese) [56], environmental friendly process, gentle reaction conditions, less hazardous gas emissions [53]. Different from physical method and pyrometallurgy, hydrometallurgy solely focus on treating electrode material rather than cell and pack level. Hydrometallurgy usually consisted of leaching (acid leaching,

alkaline leaching, etc.), separation and recovery (i.e., solvent extraction, chemical precipitation), detailed information will be discussed in this section.

2.5.1 Leaching Processes

Leaching process is the key step for recovering valuable metals from spent LIB scraps in hydrometallurgy method, materials are usually obtained through a series of pretreatment includes cell discharge and dismantle, crushing and material classification to concentrate electrode material, especially cathode electrode materials. In general, it dissolves metals from solid phase into liquid state for further processing. Both classification and leaching can highly affect the recovery rates. Leaching process usually conducted using inorganic acid, organic acid, alkali, and bacteria solution as leaching agents, while other physical and mechanochemical methods are coupled to improve leaching efficiencies [2, 118].

2.5.1.1 Inorganic Acid Leaching

Inorganic acids include HCl, HNO_3, and H_2SO_4 are widely used as leaching media. It was found that HCl has the higher leaching efficiency compared to the others [130], both cobalt and nickel reached over 99.99 % recoveries under optimal conditions. However, it was also pointed out that chloric gas was generated during the oxidation of HCl [118]:

$$22LiCoO_2 + 8HCl \rightarrow 2CoCl_2 + Cl_2 + 2LiCl + 4H_2O \quad (24)$$

With the generation of Cl_2, special antisepticising and gas collecting equipment are required to mitigate the environmental problem, which could increase the process cost. With lower reducing abilities, sulfuric acid and nitric acid normally companied with reducing agents: sodium hydrogen sulfite (sodium bisulfite) [131, 132], hydrogen peroxide [91, 133], and glucose [134, 135]. Reducing agents can reduce the metals from cathode materials to their divalent states, making them more soluble in acid. For example, Co (III) and Mn(IV) got reduced to Co(II) and Mn(II), respectively. With addition of hydrogen peroxide, leaching of lithium cobalt oxide with acid can be explained as [118]:

$$2LiCoO_2 + 6H^+ + H_2O_2 \rightarrow 2Co^{2+} + O_2 + 2Li^+ + 4H_2O \quad (25)$$

Lee et al. [133] obtained the cathode materials after two steps of thermal treatments to 1) Reduce binding energy between electrode powders and current collector (at 150 ℃) followed by high-speed shredding and sieving; 2) Burn off binder and carbon at 800 ℃ for 1 h, remained materials ball milled to obtain mean particle size of 15 μm. With addition of hydrogen peroxide as reducing agent, leaching ratios of lithium and cobalt increased by 10 % and 45 % separately, compared with leaching performance by nitric acid only. Optimal condition was 1 M HNO_3, S/L ratio of 10-20 g/L, temperature of 75 ℃, and 1.7 vol. % hydrogen peroxide.

Kinetics of inorganic leaching have been widely studied [132, 136, 137]. Both sulfuric acid and hydrochloric acid leaching of lithium cobalt without reducing agent were investigated [138], under optimal condition of 2 M HCl, 60-80 ℃ for 90 min, almost 100 % of Co and Li were leached. There were two time periods for cobalt and lithium

leaching, in time period 1, extraction of cobalt was controlled by chemical reaction in both leaching agents. Cobalt extraction in time period 2: diffusion is rate limiting step for sulfuric acid; diffusion of chlorine from solution to interphase boundary and chemical reaction of chlorides formation were controlling the process for HCl. Lithium extraction occurred in mixed mode for the time period 1, diffusion occurred in time period 2. It was also found that vacation of lithium directly affects cobalt extraction during leaching.

Other inorganic acid leaching results include: Zhu et al. dissolved 96.3 % of cobalt and 87.5 % of lithium (mass fractions) with solution of 2 mol/L H_2SO_4 and 2 vol.% of H_2O_2 [139]. Chen et al. presented that under optimal leaching conditions (slurry density: 25 g/L, reaction time 120 min, reaction temperature: 95 ℃, acid concentration: 3.0 mol/L, reductant dosage: 0.4 g/g), about 100 %, 100 %, and 96 % of lithium, 54 %, 96 %, and 98 % of cobalt were leached out in H_2SO_4 + cellulose, H_2SO_4 + sucrose, and H_2SO_4 + glucose, respectively [140]. Li et al. [141] leached 99 % of cobalt and 97 % of lithium with 4.0 M HCl for 2 h concurrent agitation at 80 ℃. Chen et al. leached over 99 % of Li and Co with mild conditions: 0.7 M H_3PO_4 + 4 vol. % H_2O_2 at 40 ℃ [142]. Zheng et al. [143] Leached 97 % Li and 98 % Fe from LFP powder under 2.5 M H_2SO_4 with 4 h reaction time. Tang et al. [144] obtained over 97 % leaching efficiency of both Li and Ti from lithium titanate cathode, 20 vol. % H_2O_2 added into 4 M of sulfuric acid solution with 4 h retention time and temperature of 80 ℃. Chen et al. [145] used 4 M H_2SO_4 + 10 vol. % H_2O_2 to leached over 95 % Co and 96 % Li from LIB scraps.

2.5.1.2 Organic Acid Leaching

With high recovery (>99 %) of valuable metals obtained by inorganic leaching, some disadvantages are concerning its sustainability. First, generation of hazardous gases such as NO_x, SO_3, and Cl_2 can bring huge burden on environment and human health [146], additional investment is required for proper handling. Secondly, low pH of leachate after leaching makes the recovering of metal more difficult. For example, to precipitate Al, Cu, and Fe as contamination removal or to precipitate nickel, manganese, and cobalt as metal recovery, more alkali is required to neutralize the solution, which significantly increase the operation cost. Thirdly, waste water needs to be properly treated due to its low pH, otherwise secondary pollution could happen [118].

Comparing with inorganic leaching, organic leaching is gaining more and more attention in recent years for its merits of easy degradation, recyclability, and little environmental pollution. Zheng et al. [147] have applied citric acid for leaching of LCO from spent LIB, at optimal condition: molar ratio of LCO/citric acid is 1:4, S/L ratio was 15 g/L, 90 ℃ of temperature, 5 h reaction time, 1.0 vol. % hydrogen peroxide, cobalt leaching efficiency reached 99.07 %. Leaching kinetic is shown as $1 - 3(1 - X)^{2/3} + 2(1 - X) = k_c t$, the apparent activation energy of the reaction was 45.73 KJ/mol, chemical reaction procedure controlling the leaching process. Sun et al. [146] have investigated oxalate leaching of $LiCoO_2$, Li2C2O3 was soluble while CoC2O4 was precipitated, the reaction was described as:

$$4H_2C_2O_4 + 2LiCoO_2(s) \rightarrow Li_2C_2O_4 + 2CoC_2O_4(s) + 4H_2O + 2CO_2(g) \quad (26)$$

Under optimal condition: 1.0 M oxalate solution, temperature of 80 ℃, S/L ratio of 50 g/L, 120 min, over 98 % reaction rate on LCO was achieved, lithium got removed from cobalt by dissolution after reaction.

Li et al. [67] have used environmental-friendly DL-malic acid as leaching agent to leach spent LCO powders with hydrogen peroxide as reducing agent. Optimized condition was 1.5 M DL-malic acid, 2 vol. % of H_2O_2, S/L ratio of 20 g/L, 90 ℃ for 40 min, then nearly 100 % of lithium and over 90 5 of cobalt were leached out. Formic acid coupled with hydrogen peroxide used to leach $LiNi_{1/3}Co_{1/3}Mn_{1/3}O_2$ from spent cell [148], overall recovery of Li, Ni, Co, Mn, and Al were found to be 98.22 %, 99.96 %, 99.96 %, 99.95 %, and 95.46 %. Rather using hydrogen peroxide, ascorbic acid was introduced as reducing agent in tartaric acid leaching of LCO powders. With 0.02 M of ascorbic acid and 0.4 M of tartaric acid, over 95 % of both lithium and cobalt were leached out with 5 h leaching at 80 ℃, cobalt was separated as cobalt oxalate from leachate.

Other organic acid leaching results include: Zheng et al. [149] leached over 99.90 % of lithium and 99.96 % of cobalt with molar ratio of formic acid and $LiCoO_2$ as 10:1, temperature of 60 ℃, reaction time of 20 min, solid/liquid ratio of 20 g/L. Sun et al. [150] achieved leaching efficiency from NMC111 of lithium, cobalt, nickel, and manganese as 98.9 %, 94.3 %, 95.1 %, and 96.4 %, respectively with 1.2 M DL-malic acid + 1.5 vol. % H_2O_2. 2 M maleic acid and 4 vol. % H_2O_2 used to leached over 98.24 %, 98.05 %, 98.41 %, and 98.06 % for lithium, nickel, cobalt, and manganese, respectively [151]. More than 98 % of each element leached out from NMC111 with 1 M citric acid +12 vol. % H_2O_2 with 40 min reaction time and temperature of 60 ℃ [152]. Over 95 % [153], 92 % [154], and 94 % [155] of metals leached from NMC mixtures with leaching systems of 0.5 M citric acid + 1.5 vol. % H_2O_2, 3.5 M acetic acid + 4 vol. % H_2O_2, and 2.0 M citric acid + 2.0 vol. % H_2O_2, respectively.

For scale-up and industrial processes, organic acid leaching has some disadvantages when comparing with inorganic acid. Firstly, organic acids are expansive than inorganic acid, which could yield higher operational cost. Secondly, reaction speed of organic acid are relatively slower, resulted in lower operation efficiency.

2.5.1.3 Bioleaching

Comparing with organic and inorganic leaching, bioleaching has merits as no emission of harmful gas, less energy intensive, and eco-friendly process. Thus, more and more research adopting this method recently. Bio-metallurgical method utilizes metabolites from microorganisms (i.e. fungi and bacteria) to dissolve and extract valuable metals from cathode materials, which shares similarity with traditional hydrometallurgy [118]. Mishra et al. [156] have proposed using chemolithotrophic and acidophilic bacteria Acidithiobacillus ferrooxidans that produce metabolites like ferric ion and sulfuric acids using ferrous iron and elemental sulfur as energy source. Leaching rate of Co was found to be faster than Li. Similarly, Li et al. [157] investigated experimental condition on leaching performance of LCO powder using Acidithiobacillus ferrooxidans. Maximum cobalt leaching efficiency was found at initial pH of 1.5 and initial Fe^{2+} concentration of 35 g/L, cobalt leaching lightly related with pH of solution.

Xin et al. [158] have applied a mixture of sulfur-oxidizing and iron-oxidizing bacteria to leach cobalt and lithium from LCO powder in a S + FeS_2 system. Acidithiobacillus ferrooxidans were used to generate acid. It was shown that acid dissolution as main mechanism for lithium bioleaching, while Co^{2+} was produced after insoluble Co^{3+} reduced to soluble Co^{2+} by Fe^{2+} from both FeS_2 and S + FeS_2 systems. Detailed reactions are described as below:

$$FeS_2 + 5O_2 + 4H^+ \rightarrow Fe^{3+} + 2SO_4^{2-} + 2H_2O \ (microbial\ action) \quad (27)$$

$$FeS_2 + Fe_2(SO_4)_3 \rightarrow 3FeSO_4 + 2S \ (chemical\ reaction) \quad (28)$$

$$FeS_2 + 7Fe_2(SO_4)_3 + 8H_2O \rightarrow 15FeSO_4 + 8H_2SO_4 \ (chemical\ reaction) \quad (29)$$

$$2S + 3O_2 + 2H_2O \rightarrow 2H_2SO_4 \ (microbial\ action) \quad (30)$$

$$4Fe^{2+} + O_2 + 4H^+ \rightarrow 4Fe^{3+} + 2H_2O \ (microbial\ action) \quad (31)$$

$$S + 3Fe_2(SO_4)_3 + 4H_2O \rightarrow 4H_2SO_4 + 6FeSO_4 \ (chemical\ action) \quad (32)$$

$$2FeSO_4 + 2LiCoO_2 + 4H_2SO_4 \rightarrow Fe_2(SO_4)_3 + 2CoSO_4 + Li_2SO_4 + 4H_2O \ (chemical\ action) \quad (33)$$

Besides bacteria bioleaching, fungal leaching was studied using Aspergillus niger [159]. Result suggested that 100 % Cu, 95 % Li, 38 % Ni, 70 % Mn, 45 % Co, 65 % Al were recovered with 1 % pulp density of spent medium bioleaching, while citric acid dominating other organic acid produced by fungus. Similarly, bioleaching has disadvantages of long processing time and low metal processing volume, increased pulp density from 2 % to 4 % significantly lower the recovery of cobalt from 89 % to 10 % and recovery of lithium from 72 % to 37 % [160].

2.5.1.4 Alkaline Leaching

Alkaline leaching of cathode materials is rarely mentioned comparing with acid leaching, ammonia-based system with relative selectivity due to the formation of stable complexes for specific elements (Ni, Li, and Co) is more preferable. Reactions are described as [118]:

$$Ni^{2+} + nNH_3 \rightarrow Ni(NH_3)n^{2+} \quad (34)$$

$$Co^{2+} + nNH_3 \rightarrow Co(NH_3)n^{2+} \quad (35)$$

As discussed by Meng et al. [161] on Eh-pH diagrams of Ni-NH_3-H_2O system and Co-NH_3-H_2O system, $Ni(NH_3)_6^{3+}$ is the dominant species in the solution with pH among 8.5 and 10.5, while $Co(NH_3)_6^{3+}$, $Co(NH_3)_5^{2+}$, and $Co(NH_3)_4^{3+}$ are major soluble components with solution pH of 9-11. Zheng et al. [162] have applied solidum sulphite as reducing agent and ammonia sulphate as leaching solution to selectively leach NMC powder. While only 1.36 % of Mn leached out, more than 98.6 % of Co and Ni were recovered.

2.5.1.5 Leaching with Assistance

To further improve the leaching efficiencies, physical methods have been applied. It has been reported that application of ultrasonic treatment helps to improve the leaching rates of targeted metals from various materials [163, 164]. Li et al. [165] have applied ultrasonic treatment on inorganic acid and organic acid leaching of LCO powder. Under optimal conditions: 0.5 M citric acid with 0.55 M hydrogen peroxide, S/L ratio was 25 g/L, temperature of 60 ℃ for 5 h, and ultrasonic power of 90 W, ~ 100 % lithium and ~ 96 % cobalt were leached out. The high leaching efficiency was mainly attributed by unique cavitation action from ultrasonic waves.

Guan et al. [166] applied ball milling of cathode powder from spent cells with Fe powders to improve leaching efficiencies of valuable metals. Yields of Co, Mn, and Ni were increased from 20.43 %, 33.19 %, and 38.67 % to 91.25 %, 100 %, and 99.9 %, respectively. Over 77 % of Li got leached out as well. The mechanism is explained by increase of specific surface area, reduction of particle sizes, and changes of crystal structures of particles. Moreover, reduction of Co (III) to Co(II) by Fe contributed to high leaching efficiency as well. Bertuol et al. [167] have proposed using supercritical carbon dioxide to achieve 95.5 wt. % cobalt recovery with only 5 min reaction time and smaller hydrogen peroxide amount of 4 vol. %. Liu et al. [168] co-treated LCO powder with waste polyvinyl chloride (PVC) in subcritical water, HCl was produced by dichlorination of PVC, more than 98 % Li and 95 % Co got leached out.

2.5.2 Metal Recovery and Extraction from Leachate

After leaching process, valuable metals such as Li, Ni, Mn, Co, Cu, Al, Fe are dissolved in solutions, proper extraction methods are required to separate them out. Due to the complexity of the solution, two or more methods are necessary to achieve separation.

2.5.2.1 Solvent Extraction

Using a two-liquid phase system, solvent extraction is realized by the different solubilities of compounds, which is generally composed of aqueous and organic phases. When reaching equilibrium, different concentration of metal ions recovered at each liquid to achieve the separation. For example, Wang et al. [169] used extraction characteristics of PC-88A (2-ethylhexyl phosphonic acid mono-2-ethylhexyl ester) and D2EHPA (di-(2-ethylhexyl) phosphoric acid) to leach specific metals at different pH condition, previous leaching carried out with NMC powder using sulfuric acid and hydrogen peroxide system. Optimal conditions for extraction were PC-88A and D2EHPA with saponification rate of 30 % and 20 %, respectively, sulfonated kerosene of 70 vol. %, O/A ratio of 1:1, process time of 10 min. Two extractions conducted first with D2EHPA with pH 2.7 and pH 2.6 to remove Cu and Mn. Then PC-88A extraction applied to recover cobalt and nickel ions at pH of 4.25, subsequent precipitation using oxalic acid to produce 99.5 % purity of cobalt.

After single solvent used for extraction, synergistic extractions have been studied using two or more solvents [170-172]. Cyanex272 (bis-2,4,4-trimethylpentyl phosphinic acid and PC-88A were mixed for extractant system [170] to separate Li (I), Co (II), and Mn

(II) from simulated sulfuric acid leachate of cathode materials. Distinct system synergistic effect has been reported, maximum synergistic enhancement coefficients, R_{max}, were 4.12 for Mn^{2+} and 3.48 for Co^{2+} at the mole fraction ~ 0.6 of $X_{Cyanex272}$ at pH of 4.95. Increased pH yielded higher R number, synergistic effect of Co^{2+} was weaker than that of Mn^{2+} when pH is above 5. Independent on using single or mixed extractant, orders of recoverability of metal ions as Mn > Co >> Li. With addition of equimolar EDTA (ethylenediaminetetra-acetic acid) into system, separation factors between Mn and Co got significantly improve, especially for mixed extractant system, the separation factor improved to two orders of magnitude than before adding EDTA.

Besides synergistic extraction, antagonistic extraction have been investigated to selectively recover individual metals from leachate [173, 174]. For example, Joo et al. [174] have proposed system of Versatic 10 acid (monocarboxylic acid) / D2EHPA on leaching solution contained Mn and Co. Addition of Versatic 10 acid to the system decreased solubilities of both Mn and Co in organic phase below pH 6. However, separation factor value of Mn over Co increased from 14 to 34, meaning solubility decrease in organic phase of cobalt is much larger than the one of manganese. With the mixture of 0.7 M Versatic 10 acid and 0.43 M D2EHPA under countercurrent batch simulation extraction, 98.3 % of manganese got extracted with 0.25 % lithium, 1.06 % nickel, and 4.11 % cobalt. Other metals were removed by 0.1 M EDTA solution at an oil-water ratio of 4, over 99.8 % of manganese obtained with stripping by 0.5 M sulfuric acid at an oil-water ratio of 2.

Other solvent extraction results include: Joo et al. [172] used 0.23 M LIX 84-I and 1.41 M Versatic 10 acid, with an oil-water ratio of 1, reaction pH of 5 at temperature of 25 °C to achieve extraction efficiency of 93% of Ni, and 0.23%, 0.15%, and 0.19% for Co, Mn and Li, respectively. With process time of 5 min, pH = 5, water-oil ratio of 0.5 and 20 vol % D2EHPA, about 97 % of manganese was extracted [175]. With optimal condition: Extraction time of 5 min, 4.5 as equilibrium pH, 20 vol % Mextral272P and water-oil ratio of 1/1, 97.8 % of cobalt was extracted [176]. Chen et al. [177] extracted 97.1 % of manganese with optimized condition: 300 s extraction time, equilibrium pH of 3.5, O/A ratio of 2:1. With MaCabe-Thiele diagram study, two theoretical counter-current extraction stages are needed to achieve 99 % manganese extraction rate from a raffinate contained less than 40 mg/L Mn.

2.5.2.2 Chemical Precipitation

To recycle and recover valuable metals from solutions after solvent extractions, chemical precipitation is viable by adding precipitants containing anions including CO_3^{2-}, $C_2O_4^{2-}$, and OH^- into leaching solutions, different metal compounds with different solubilities are precipitated at certain pH values [178]. For example, Pegoretti et al. [179] used KOH (1 mol/L) to neutralize the solution produced by sulfuric acid and hydrogen peroxide leaching on LCO powder, $Co(OH)_2$ was precipitated after pH reached 8.9. Wang et al. [63] used NaOH and Na_2CO_3 to separately recycle cobalt and lithium, cobalt oxide was obtained after calcination of precipitate at 500 °C for 2 h, then lithium carbonate got recovered with addition of sodium carbonate by crystallization and drying. Zhu et al.

[139] used sulfuric acid combined with hydrogen peroxide to dissolve spent LCO first, then $(NH_4)_2C_2O_4$ added to precipitate cobalt as $CoC_2O_4{\cdot}H_2O$. After collection of cobalt compound and filtration, lithium carbonate got recovered by addition of sodium carbonate. 96.3 wt. % of Co and 87.5 % of Li got dissolved by acid leaching while 94.7 % Co and 71.0 % Li got recovered from leachate.

When facing solutions containing multiple metal ions (Co, Ni, Mn, Cu, etc.), multistep precipitation/selective precipitation is required to separate different metal compounds. Kang et al. [34] proposed using Na_2S to first precipitate copper and removed it (99.9 %) as CuS after acid leaching, remained solution was treated with oxalic acid to precipitate $CoC_2O_4{\cdot}H_2O$. Chen et al. [180] conducted selective precipitation on MNC powder after acid leaching. First, about 100 % of Mn was precipitated and removed as MnO_2 or Mn2O3 by adding potassium permanganate (0.5 mol/L) [181]. Then the solution were processed by dimethylglyoxime (DMG, 0.2 mol/L), oxalic acid ($H_2C_2O_4$, 0.5 mol/L), and phosphoric acid (H_3PO_4, 0.5 mol/L) consecutively to precipitate Ni, Co, and Li in their precipitation forms with 96 %, 97 %, and 93 % recovery, respectively.

Rather than individual precipitation, co-precipitation was proposed to shorten process time and produce specific compound to re-synthesis electrode materials. For example, He et al. [182] have proposed a co-precipitation method: NMC111 powders obtained from spent LIB were leached through sulfuric acid and hydrogen peroxide first, then molar ratio between Ni, Co, and Mn were adjusted to 1:1:1 by adding analytically pure $NiSO_4{\cdot}6H_2O$, $CoSO_4{\cdot}7H_2O$, and $MnSO_4{\cdot}H_2O$. Na_2CO_3 and $NH_3{\cdot}H_2O$ pumped into solution to maintained pH at 7.5 for 12 h agitation at 60 ℃, $Ni_{1/3}Co_{1/3}Mn_{1/3}CO_3$ were obtained through carbonate co-precipitation process. NMC powders were obtained after mixing with Li_2CO_3 at lithium/metal molar ratio of 1.06:1 followed by preheat of 500 ℃ for 5 h and sintering in air at 900 ℃ for 12 h. Similarly, Yang et al. [183] conducted co-precipitation to obtain NMC precursor using alkaline solution. $LiCoO_2$ obtained from spent LIB and MnO_2 obtained from Zn-Mn cells were leached with nitric acid and hydrogen peroxide coupled with nickel nitrate, cobalt nitrate, and manganese nitrate to balance molar ratio of transition metals in solution to be 1:1:1. Then sodium hydroxide solution added into system to maintained pH of 8 with continuous stirring until suspension formed as: $Ni_{1/3}Co_{1/3}Mn_{1/3}(OH)_2$. Subsequent calcination and lithium salt addition carried out to form NMC111 powder.

2.5.2.3 Electrodeposition

Electrodeposition applies a voltage in the solution between two electrodes to introduce redox reactions between metal ions from spent LIB scraps. For example, Myoung et al. [184] have proposed electrochemical deposition of cobalt as cobalt hydroxide onto titanium cathode electrode after nitric acid leaching of spent LCO powders, detailed reactions can be described as:

$$2H_2O + O_2 + 4e^- \rightarrow 4OH^- \quad (36)$$

$$NO^{3-} + H_2O + 2e^- \rightarrow NO_2 + 2OH^- \quad (37)$$

$$Co^{3+} + e^{-} \rightarrow Co^{2+} \quad (38)$$

$$Co^{2+} + 2OH_{ad}^{-}/Ti \rightarrow Co(OH)_2/Ti \quad (39)$$

In electrodeposition, pH value is critical factor that heavily impacting charge efficiency. Freitas et al. [185] have conducted electrochemical deposition on solution from LCO powder after hydrochloric acid and hydrogen peroxide leaching, it was found that charge efficiency increased with increasing pH during the process [186]. Largest charge efficiency found as 96.90 % at pH 5.4, where the nuclei grew progressively. However, at pH of 2.7, nucleation process became instantaneous. Lupi et al. [187] found that during electrodeposition of nickel-cobalt alloy, addition of H_3BO_3 to catholyte gave higher current efficiencies by limiting the pH variations.

Cobalt recovery and cobalt oxide product application as supercapacitor material has been heavily investigated [188-190]. Garcia et al. [189] found that reversibility of both redox process in KOH 6 mol/L were high and promising for capacitive applications. Li et al. [191] proposed a method to directly generate LCO films through electrodeposition. After nitric acid leaching on spent LCO powder, with current density 1 mA/cm^2 and 20 h reaction time, new lithium cobalt oxide obtained as preferred (104) orientation deposited electronically on the nickel substrate. Regenerated crystalline layer powder had particle size of 0.5 μm and thickness of 2000 μm. Its initial charge and discharge capacities were 131 and 127 mAh/g, separately. Only 4 % decreased on capacity was found after first 30 cycles.

2.6 Reference

1. Liang, Y., et al., *A review of rechargeable batteries for portable electronic devices.* InfoMat, 2019. **1**(1): p. 6-32.
2. Yao, Y., et al., *Hydrometallurgical Processes for Recycling Spent Lithium-Ion Batteries: A Critical Review.* ACS Sustainable Chemistry & Engineering, 2018. **6**(11): p. 13611-13627.
3. Yuan, L.-X., et al., *Development and challenges of LiFePO4 cathode material for lithium-ion batteries.* Energy & Environmental Science, 2011. **4**(2): p. 269-284.
4. Goodenough, J.B., *How we made the Li-ion rechargeable battery.* Nature Electronics, 2018. **1**(3): p. 204-204.
5. Yun, L., et al., *Metallurgical and mechanical methods for recycling of lithium-ion battery pack for electric vehicles.* Resources, Conservation and Recycling, 2018. **136**: p. 198-208.
6. Zhang, W., et al., *A review on management of spent lithium ion batteries and strategy for resource recycling of all components from them.* Waste Management & Research, 2018. **36**(2): p. 99-112.
7. Makuza, B., et al., *Pyrometallurgical options for recycling spent lithium-ion batteries: A comprehensive review.* Journal of Power Sources, 2021. **491**: p. 229622.

8. Huang, Y.-H. and J.B. Goodenough, *High-Rate LiFePO4 Lithium Rechargeable Battery Promoted by Electrochemically Active Polymers.* Chemistry of Materials, 2008. **20**(23): p. 7237-7241.
9. Zheng, H., et al., *Cooperation between Active Material, Polymeric Binder and Conductive Carbon Additive in Lithium Ion Battery Cathode.* The Journal of Physical Chemistry C, 2012. **116**(7): p. 4875-4882.
10. Shi, Y., X. Zhou, and G. Yu, *Material and Structural Design of Novel Binder Systems for High-Energy, High-Power Lithium-Ion Batteries.* Accounts of Chemical Research, 2017. **50**(11): p. 2642-2652.
11. Goodenough, J.B. and K.-S. Park, *The Li-Ion Rechargeable Battery: A Perspective.* Journal of the American Chemical Society, 2013. **135**(4): p. 1167-1176.
12. Tarascon, J.M. and M. Armand, *Issues and challenges facing rechargeable lithium batteries.* Nature, 2001. **414**: p. 359-367.
13. Tanaka, T., K. Ohta, and N. Arai, *Year 2000 R&D status of large-scale lithium ion secondary batteries in the national project of Japan.* Journal of Power Sources, 2001. **97-98**: p. 2-6.
14. Chu, A. and P. Braatz, *Comparison of commercial supercapacitors and high-power lithium-ion batteries for power-assist applications in hybrid electric vehicles: I. Initial characterization.* Journal of Power Sources, 2002. **112**(1): p. 236-246.
15. Aurbach, D., et al., *Design of electrolyte solutions for Li and Li-ion batteries: a review.* Electrochimica Acta, 2004. **50**(2): p. 247-254.
16. Deimede, V. and C. Elmasides, *Separators for lithium-ion batteries: a review on the production processes and recent developments.* Energy technology, 2015. **3**(5): p. 453-468.
17. Shin, S.M., et al., *Development of a metal recovery process from Li-ion battery wastes.* Hydrometallurgy, 2005. **79**(3): p. 172-181.
18. Castillo, S., et al., *Advances in the recovering of spent lithium battery compounds.* Journal of Power Sources, 2002. **112**(1): p. 247-254.
19. Li, L., et al., *Recovery of cobalt and lithium from spent lithium ion batteries using organic citric acid as leachant.* Journal of Hazardous Materials, 2010. **176**(1): p. 288-293.
20. Ordoñez, J., E.J. Gago, and A. Girard, *Processes and technologies for the recycling and recovery of spent lithium-ion batteries.* Renewable and Sustainable Energy Reviews, 2016. **60**: p. 195-205.
21. Bahgat, M., et al., *Synthesis, characterization and magnetic properties of microcrystalline lithium cobalt ferrite from spent lithium-ion batteries.* Journal of Materials Processing Technology, 2007. **183**(1): p. 117-121.
22. Zhou, X., et al. *Recycling of electrode materials from spent lithium-ion batteries*. in *2010 4th International Conference on Bioinformatics and Biomedical Engineering*. 2010. IEEE.
23. Xu, J., et al., *A review of processes and technologies for the recycling of lithium-ion secondary batteries.* Journal of Power Sources, 2008. **177**(2): p. 512-527.

24. Zhang, Q., et al., *Room temperature acid extraction of Co from LiCo0.2Ni0.8O2 scrap by a mechanochemical treatment.* Advanced Powder Technology, 2000. **11**(3): p. 353-359.
25. Saeki, S., et al., *Co-grinding LiCoO2 with PVC and water leaching of metal chlorides formed in ground product.* International Journal of Mineral Processing, 2004. **74**: p. S373-S378.
26. Lee, C.K. and K.-I. Rhee, *Preparation of LiCoO2 from spent lithium-ion batteries.* Journal of Power Sources, 2002. **109**(1): p. 17-21.
27. Zhan, R., et al., *Significance of a Solid Electrolyte Interphase on Separation of Anode and Cathode Materials from Spent Li-Ion Batteries by Froth Flotation.* ACS Sustainable Chemistry & Engineering, 2021. **9**(1): p. 531-540.
28. Contestabile, M., S. Panero, and B. Scrosati, *A laboratory-scale lithium-ion battery recycling process.* Journal of Power Sources, 2001. **92**(1): p. 65-69.
29. Harper, G., et al., *Recycling lithium-ion batteries from electric vehicles.* Nature, 2019. **575**(7781): p. 75-86.
30. Zhang, X., et al., *Toward sustainable and systematic recycling of spent rechargeable batteries.* Chemical Society Reviews, 2018. **47**(19): p. 7239-7302.
31. Kim, S., et al., *A comprehensive review on the pretreatment process in lithium-ion battery recycling.* Journal of Cleaner Production, 2021. **294**: p. 126329.
32. Nan, J., D. Han, and X. Zuo, *Recovery of metal values from spent lithium-ion batteries with chemical deposition and solvent extraction.* Journal of Power Sources, 2005. **152**: p. 278-284.
33. Ku, H., et al., *Recycling of spent lithium-ion battery cathode materials by ammoniacal leaching.* Journal of Hazardous Materials, 2016. **313**: p. 138-146.
34. Kang, J., et al., *Preparation of cobalt oxide from concentrated cathode material of spent lithium ion batteries by hydrometallurgical method.* Advanced Powder Technology, 2010. **21**(2): p. 175-179.
35. Kim, S., et al., *Recycling process of spent battery modules in used hybrid electric vehicles using physical/chemical treatments.* Research on Chemical Intermediates, 2014. **40**(7): p. 2447-2456.
36. Lu, M., et al., *The re-synthesis of LiCoO2 from spent lithium ion batteries separated by vacuum-assisted heat-treating method.* Int. J. Electrochem. Sci, 2013. **8**(6): p. 8201-8209.
37. Li, J., G. Wang, and Z. Xu, *Environmentally-friendly oxygen-free roasting/wet magnetic separation technology for in situ recycling cobalt, lithium carbonate and graphite from spent LiCoO2/graphite lithium batteries.* Journal of Hazardous Materials, 2016. **302**: p. 97-104.
38. Wang, J., et al., *Leaching Study of Spent Li-ion Batteries.* Procedia Environmental Sciences, 2012. **16**: p. 443-450.
39. Li, J., G. Wang, and Z. Xu, *Generation and detection of metal ions and volatile organic compounds (VOCs) emissions from the pretreatment processes for recycling spent lithium-ion batteries.* Waste Management, 2016. **52**: p. 221-227.
40. Ojanen, S., et al., *Challenging the concept of electrochemical discharge using salt solutions for lithium-ion batteries recycling.* Waste Management, 2018. **76**: p. 242-249.

41. Xiao, J., et al., *A cleaner approach to the discharge process of spent lithium ion batteries in different solutions.* Journal of Cleaner Production, 2020. **255**: p. 120064.
42. Yao, L.P., et al., *An environmentally friendly discharge technology to pretreat spent lithium-ion batteries.* Journal of Cleaner Production, 2020. **245**: p. 118820.
43. Aurbach, D., et al., *An analysis of rechargeable lithium-ion batteries after prolonged cycling.* Electrochimica Acta, 2002. **47**(12): p. 1899-1911.
44. Waldmann, T., et al., *Review—Post-Mortem Analysis of Aged Lithium-Ion Batteries: Disassembly Methodology and Physico-Chemical Analysis Techniques.* Journal of The Electrochemical Society, 2016. **163**(10): p. A2149-A2164.
45. Dorella, G. and M.B. Mansur, *A study of the separation of cobalt from spent Li-ion battery residues.* Journal of Power Sources, 2007. **170**(1): p. 210-215.
46. CDC-NIOSH. *Pocket Guide to Chemical Hazards*. National Institute for Occupational Safety and Health (NIOSH), Washington, DC (2003) 2003; Available from: http://www.cdc.gov/niosh/npg/npgd0619.html.
47. Williard, N., et al., *Disassembly methodology for conducting failure analysis on lithium–ion batteries.* Journal of Materials Science: Materials in Electronics, 2011. **22**(10): p. 1616.
48. Kawamura, T., S. Okada, and J.-i. Yamaki, *Decomposition reaction of LiPF6-based electrolytes for lithium ion cells.* Journal of Power Sources, 2006. **156**(2): p. 547-554.
49. McLaughlin, W. and T.S. Adams, *Li reclamation process*. 1999, Google Patents.
50. Velázquez-Martínez, O., et al., *A Critical Review of Lithium-Ion Battery Recycling Processes from a Circular Economy Perspective.* Batteries, 2019. **5**(4): p. 68.
51. Tedjar, F. and J.-C. Foudraz, *Method for the mixed recycling of lithium-based anode batteries and cells*. 2010, Google Patents.
52. Pudas, J., A. Erkkila, and J. Viljamaa, *Battery recycling method*. 2015, Google Patents.
53. Lv, W., et al., *A Critical Review and Analysis on the Recycling of Spent Lithium-Ion Batteries.* ACS Sustainable Chemistry & Engineering, 2018. **6**(2): p. 1504-1521.
54. Vadenbo, C., *Prospective environmental assessment of lithium recovery in battery recycling.* Institute of Environmental Decisions: Zurich, Switzerland, 2009.
55. Meshram, P., B.D. Pandey, and T.R. Mankhand, *Extraction of lithium from primary and secondary sources by pre-treatment, leaching and separation: A comprehensive review.* Hydrometallurgy, 2014. **150**: p. 192-208.
56. Georgi-Maschler, T., et al., *Development of a recycling process for Li-ion batteries.* Journal of Power Sources, 2012. **207**: p. 173-182.
57. Pinegar, H. and Y.R. Smith, *Recycling of End-of-Life Lithium Ion Batteries, Part I: Commercial Processes.* Journal of Sustainable Metallurgy, 2019. **5**(3): p. 402-416.
58. Diekmann, J., et al., *(Invited) Ecologically Friendly Recycling of Lithium-Ion Batteries - the LithoRec Process.* ECS Transactions, 2016. **73**(1): p. 1-9.

59. Diekmann, J., et al., *Ecological Recycling of Lithium-Ion Batteries from Electric Vehicles with Focus on Mechanical Processes.* Journal of The Electrochemical Society, 2016. **164**(1): p. A6184-A6191.
60. Wang, X., G. Gaustad, and C.W. Babbitt, *Targeting high value metals in lithium-ion battery recycling via shredding and size-based separation.* Waste Management, 2016. **51**: p. 204-213.
61. Zhang, T., et al., *Characteristics of wet and dry crushing methods in the recycling process of spent lithium-ion batteries.* Journal of Power Sources, 2013. **240**: p. 766-771.
62. Barik, S.P., G. Prabaharan, and L. Kumar, *Leaching and separation of Co and Mn from electrode materials of spent lithium-ion batteries using hydrochloric acid: Laboratory and pilot scale study.* Journal of Cleaner Production, 2017. **147**: p. 37-43.
63. Wang, M.-M., C.-C. Zhang, and F.-S. Zhang, *An environmental benign process for cobalt and lithium recovery from spent lithium-ion batteries by mechanochemical approach.* Waste Management, 2016. **51**: p. 239-244.
64. Zhan, R., et al., *De-agglomeration of cathode composites for direct recycling of Li-ion batteries.* Waste Management, 2020. **105**: p. 39-48.
65. Wang, H., et al., *Separation of the cathode materials from the Al foil in spent lithium-ion batteries by cryogenic grinding.* Waste Management, 2019. **91**: p. 89-98.
66. Li, L., et al., *Recovery of metals from spent lithium-ion batteries with organic acids as leaching reagents and environmental assessment.* Journal of Power Sources, 2013. **233**: p. 180-189.
67. Li, L., et al., *Environmental friendly leaching reagent for cobalt and lithium recovery from spent lithium-ion batteries.* Waste Management, 2010. **30**(12): p. 2615-2621.
68. Guo, Y., et al., *Improved extraction of cobalt and lithium by reductive acid from spent lithium-ion batteries via mechanical activation process.* Journal of Materials Science, 2018. **53**(19): p. 13790-13800.
69. Yu, J., et al., *A promising physical method for recovery of LiCoO2 and graphite from spent lithium-ion batteries: Grinding flotation.* Separation and Purification Technology, 2018. **190**: p. 45-52.
70. Liu, J., et al., *Recovery of LiCoO2 and graphite from spent lithium-ion batteries by cryogenic grinding and froth flotation.* Minerals Engineering, 2020. **148**: p. 106223.
71. Kang, J., et al., *Recovery of cobalt sulfate from spent lithium ion batteries by reductive leaching and solvent extraction with Cyanex 272.* Hydrometallurgy, 2010. **100**(3): p. 168-171.
72. Granata, G., et al., *Product recovery from Li-ion battery wastes coming from an industrial pre-treatment plant: Lab scale tests and process simulations.* Journal of Power Sources, 2012. **206**: p. 393-401.
73. Zhang, T., et al., *Chemical and process mineralogical characterizations of spent lithium-ion batteries: An approach by multi-analytical techniques.* Waste Management, 2014. **34**(6): p. 1051-1058.

74. Zhang, G., et al., *Enhancement in liberation of electrode materials derived from spent lithium-ion battery by pyrolysis.* Journal of Cleaner Production, 2018. **199**: p. 62-68.
75. Peng, C., et al., *Extraction of Li and Co from industrially produced Li-ion battery waste – Using the reductive power of waste itself.* Waste Management, 2019. **95**: p. 604-611.
76. Widijatmoko, S.D., et al., *Recovering lithium cobalt oxide, aluminium, and copper from spent lithium-ion battery via attrition scrubbing.* Journal of Cleaner Production, 2020. **260**: p. 120869.
77. Widijatmoko, S.D., et al., *Selective liberation in dry milled spent lithium-ion batteries.* Sustainable Materials and Technologies, 2020. **23**: p. e00134.
78. Liu, Y.-j., et al., *Recycle and synthesis of LiCoO2 from incisors bound of Li-ion batteries.* Transactions of Nonferrous Metals Society of China, 2006. **16**(4): p. 956-959.
79. Song, D., et al., *Heat treatment of LiCoO2 recovered from cathode scraps with solvent method.* Journal of Power Sources, 2014. **249**: p. 137-141.
80. Xu, Y., et al., *A simple solvent method for the recovery of LixCoO2 and its applications in alkaline rechargeable batteries.* Journal of Power Sources, 2014. **252**: p. 286-291.
81. Song, D., et al., *Recovery and heat treatment of the Li(Ni1/3Co1/3Mn1/3)O2 cathode scrap material for lithium ion battery.* Journal of Power Sources, 2013. **232**: p. 348-352.
82. Nayaka, G.P., et al., *Effective and environmentally friendly recycling process designed for LiCoO2 cathode powders of spent Li-ion batteries using mixture of mild organic acids.* Waste Management, 2018. **78**: p. 51-57.
83. Yang, L., G. Xi, and Y. Xi, *Recovery of Co, Mn, Ni, and Li from spent lithium ion batteries for the preparation of LiNixCoyMnzO2 cathode materials.* Ceramics International, 2015. **41**(9, Part A): p. 11498-11503.
84. He, L.-P., et al., *Recovery of cathode materials and Al from spent lithium-ion batteries by ultrasonic cleaning.* Waste Management, 2015. **46**: p. 523-528.
85. Wang, M., et al., *Efficient Separation of Aluminum Foil and Cathode Materials from Spent Lithium-Ion Batteries Using a Low-Temperature Molten Salt.* ACS Sustainable Chemistry & Engineering, 2019. **7**(9): p. 8287-8294.
86. Bai, Y., et al., *Sustainable direct recycling of lithium-ion batteries via solvent recovery of electrode materials*. 2020, Oak Ridge National Lab.(ORNL), Oak Ridge, TN (United States).
87. Gratz, E., et al., *A closed loop process for recycling spent lithium ion batteries.* Journal of Power Sources, 2014. **262**: p. 255-262.
88. Zeng, X. and J. Li, *Innovative application of ionic liquid to separate Al and cathode materials from spent high-power lithium-ion batteries.* Journal of Hazardous Materials, 2014. **271**: p. 50-56.
89. Chen, Y., et al., *Thermal treatment and ammoniacal leaching for the recovery of valuable metals from spent lithium-ion batteries.* Waste Management, 2018. **75**: p. 469-476.

90. Yang, Y., et al., *Thermal treatment process for the recovery of valuable metals from spent lithium-ion batteries.* Hydrometallurgy, 2016. **165**: p. 390-396.
91. Sun, L. and K. Qiu, *Vacuum pyrolysis and hydrometallurgical process for the recovery of valuable metals from spent lithium-ion batteries.* Journal of Hazardous Materials, 2011. **194**: p. 378-384.
92. Xiao, J., J. Li, and Z. Xu, *Novel Approach for in Situ Recovery of Lithium Carbonate from Spent Lithium Ion Batteries Using Vacuum Metallurgy.* Environmental Science & Technology, 2017. **51**(20): p. 11960-11966.
93. Xiao, J., J. Li, and Z. Xu, *Recycling metals from lithium ion battery by mechanical separation and vacuum metallurgy.* Journal of Hazardous Materials, 2017. **338**: p. 124-131.
94. Sommerville, R., et al., *A review of physical processes used in the safe recycling of lithium ion batteries.* Sustainable Materials and Technologies, 2020. **25**: p. e00197.
95. Barik, S.P., G. Prabaharan, and B. Kumar, *An innovative approach to recover the metal values from spent lithium-ion batteries.* Waste Management, 2016. **51**: p. 222-226.
96. Zhong, X., et al., *Pneumatic separation for crushed spent lithium-ion batteries.* Waste Management, 2020. **118**: p. 331-340.
97. Bi, H., et al., *Pneumatic separation and recycling of anode and cathode materials from spent lithium iron phosphate batteries.* Waste Management & Research, 2019. **37**(4): p. 374-385.
98. Zhu, X., et al., *A novel pulsated pneumatic separation with variable-diameter structure and its application in the recycling spent lithium-ion batteries.* Waste Management, 2021. **131**: p. 20-30.
99. Hanisch, C., et al., *Recycling of lithium-ion batteries: a novel method to separate coating and foil of electrodes.* Journal of Cleaner Production, 2015. **108**: p. 301-311.
100. Sa, Q., et al., *Synthesis of high performance LiNi1/3Mn1/3Co1/3O2 from lithium ion battery recovery stream.* Journal of Power Sources, 2015. **282**: p. 140-145.
101. Al-Thyabat, S., et al., *Adaptation of minerals processing operations for lithium-ion (LiBs) and nickel metal hydride (NiMH) batteries recycling: Critical review.* Minerals Engineering, 2013. **45**: p. 4-17.
102. Bi, H., et al., *A new model of trajectory in eddy current separation for recovering spent lithium iron phosphate batteries.* Waste Management, 2019. **100**: p. 1-9.
103. Bi, H., et al., *Eddy current separation for recovering aluminium and lithium-iron phosphate components of spent lithium-iron phosphate batteries.* Waste Management & Research, 2019. **37**(12): p. 1217-1228.
104. Granata, G., et al., *Simultaneous recycling of nickel metal hydride, lithium ion and primary lithium batteries: Accomplishment of European Guidelines by optimizing mechanical pre-treatment and solvent extraction operations.* Journal of Power Sources, 2012. **212**: p. 205-211.
105. Marinos, D. and B. Mishra, *An Approach to Processing of Lithium-Ion Batteries for the Zero-Waste Recovery of Materials.* Journal of Sustainable Metallurgy, 2015. **1**(4): p. 263-274.

106. Kelly, E.G. and D.J. Spottiswood, *The theory of electrostatic separations: A review Part I. Fundamentals.* Minerals Engineering, 1989. **2**(1): p. 33-46.
107. Silveira, A.V.M., et al., *Recovery of valuable materials from spent lithium ion batteries using electrostatic separation.* International Journal of Mineral Processing, 2017. **169**: p. 91-98.
108. Zhan, R., Z. Oldenburg, and L. Pan, *Recovery of active cathode materials from lithium-ion batteries using froth flotation.* Sustainable Materials and Technologies, 2018. **17**: p. e00062.
109. Kim, Y., et al., *Recovery of LiCoO₂ from Wasted Lithium Ion Batteries by using Mineral Processing Technology.* Resources Processing, 2004. **51**(1): p. 3-7.
110. Zhong, X., et al., *Pyrolysis and physical separation for the recovery of spent LiFePO4 batteries.* Waste Management, 2019. **89**: p. 83-93.
111. He, Y., et al., *Recovery of LiCoO2 and graphite from spent lithium-ion batteries by Fenton reagent-assisted flotation.* Journal of Cleaner Production, 2017. **143**: p. 319-325.
112. Van Elp, J., et al., *Electronic structure of coo, li-doped coo, and licoo 2.* Physical Review B, 1991. **44**(12): p. 6090.
113. Madhavi, S., et al., *Synthesis and Cathodic Properties of LiCo[sub 1−y]Rh[sub y]O[sub 2] (0≤y≤0.2) and LiRhO[sub 2].* Journal of The Electrochemical Society, 2001. **148**(11): p. A1279.
114. Fan, X., et al., *A green, efficient, closed-loop direct regeneration technology for reconstructing of the LiNi0.5Co0.2Mn0.3O2 cathode material from spent lithium-ion batteries.* Journal of Hazardous Materials, 2021. **410**: p. 124610.
115. Fu, Y., et al., *Enhancement in leaching process of lithium and cobalt from spent lithium-ion batteries using benzenesulfonic acid system.* Waste Management, 2019. **88**: p. 191-199.
116. Sloop, S.E., et al., *Cathode healing methods for recycling of lithium-ion batteries.* Sustainable Materials and Technologies, 2019. **22**: p. e00113.
117. Liu, C., et al., *Recycling of spent lithium-ion batteries in view of lithium recovery: A critical review.* Journal of Cleaner Production, 2019. **228**: p. 801-813.
118. An, L., *Recycling of Spent Lithium-Ion Batteries.* Processing Methods and Environmental Impacts, 2019.
119. Maroufi, S., et al., *Recovery of lithium and cobalt from waste lithium-ion batteries through a selective isolation-suspension approach.* Sustainable Materials and Technologies, 2020. **23**: p. e00139.
120. Wang, W., et al., *Alkali Metal Salt Catalyzed Carbothermic Reduction for Sustainable Recovery of LiCoO2: Accurately Controlled Reduction and Efficient Water Leaching.* ACS Sustainable Chemistry & Engineering, 2019. **7**(19): p. 16729-16737.
121. Mao, J., J. Li, and Z. Xu, *Coupling reactions and collapsing model in the roasting process of recycling metals from LiCoO2 batteries.* Journal of Cleaner Production, 2018. **205**: p. 923-929.

122. Liu, P., et al., *Study on the reduction roasting of spent LiNixCoyMnzO2 lithium-ion battery cathode materials.* Journal of Thermal Analysis and Calorimetry, 2019. **136**(3): p. 1323-1332.
123. Lombardo, G., et al., *Chemical Transformations in Li-Ion Battery Electrode Materials by Carbothermic Reduction.* ACS Sustainable Chemistry & Engineering, 2019. **7**(16): p. 13668-13679.
124. Gaines, L., *The future of automotive lithium-ion battery recycling: Charting a sustainable course.* Sustainable Materials and Technologies, 2014. **1-2**: p. 2-7.
125. Chen, M., et al., *Recycling End-of-Life Electric Vehicle Lithium-Ion Batteries.* Joule, 2019. **3**(11): p. 2622-2646.
126. Ren, G.-x., et al., *Recovery of valuable metals from spent lithium ion batteries by smelting reduction process based on FeO–SiO2–Al2O3 slag system.* Transactions of Nonferrous Metals Society of China, 2017. **27**(2): p. 450-456.
127. Li, N., et al., *Aqueous leaching of lithium from simulated pyrometallurgical slag by sodium sulfate roasting.* RSC Advances, 2019. **9**(41): p. 23908-23915.
128. Guoxing, R., et al. *Recovery of Valuable Metals from Spent Lithium-Ion Batteries by Smelting Reduction Process Based on MnO-SiO2-Al2O3 Slag System*. in *Advances in Molten Slags, Fluxes, and Salts: Proceedings of the 10th International Conference on Molten Slags, Fluxes and Salts 2016*. 2016. Cham: Springer International Publishing.
129. Zeng, X., J. Li, and N. Singh, *Recycling of Spent Lithium-Ion Battery: A Critical Review.* Critical Reviews in Environmental Science and Technology, 2014. **44**(10): p. 1129-1165.
130. Joulié, M., R. Laucournet, and E. Billy, *Hydrometallurgical process for the recovery of high value metals from spent lithium nickel cobalt aluminum oxide based lithium-ion batteries.* Journal of Power Sources, 2014. **247**: p. 551-555.
131. Meshram, P., et al., *Comparision of Different Reductants in Leaching of Spent Lithium Ion Batteries.* JOM, 2016. **68**(10): p. 2613-2623.
132. Meshram, P., B.D. Pandey, and T.R. Mankhand, *Hydrometallurgical processing of spent lithium ion batteries (LIBs) in the presence of a reducing agent with emphasis on kinetics of leaching.* Chemical Engineering Journal, 2015. **281**: p. 418-427.
133. Lee, C.K. and K.-I. Rhee, *Reductive leaching of cathodic active materials from lithium ion battery wastes.* Hydrometallurgy, 2003. **68**(1): p. 5-10.
134. Meshram, P., et al., *Acid baking of spent lithium ion batteries for selective recovery of major metals: A two-step process.* Journal of Industrial and Engineering Chemistry, 2016. **43**: p. 117-126.
135. Pagnanelli, F., et al., *Acid reducing leaching of cathodic powder from spent lithium ion batteries: Glucose oxidative pathways and particle area evolution.* Journal of Industrial and Engineering Chemistry, 2014. **20**(5): p. 3201-3207.
136. Jha, M.K., et al., *Recovery of lithium and cobalt from waste lithium ion batteries of mobile phone.* Waste Management, 2013. **33**(9): p. 1890-1897.
137. Meshram, P., B.D. Pandey, and T.R. Mankhand, *Recovery of valuable metals from cathodic active material of spent lithium ion batteries: Leaching and kinetic aspects.* Waste Management, 2015. **45**: p. 306-313.

138. Takacova, Z., et al., *Cobalt and lithium recovery from active mass of spent Li-ion batteries: Theoretical and experimental approach.* 2016. **163**: p. 9-17.
139. Zhu, S.-g., et al., *Recovery of Co and Li from spent lithium-ion batteries by combination method of acid leaching and chemical precipitation.* Transactions of Nonferrous Metals Society of China, 2012. **22**(9): p. 2274-2281.
140. Chen, X., et al., *Organic reductants based leaching: A sustainable process for the recovery of valuable metals from spent lithium ion batteries.* Waste Management, 2018. **75**: p. 459-468.
141. Li, J., et al., *A combined recovery process of metals in spent lithium-ion batteries.* Chemosphere, 2009. **77**(8): p. 1132-1136.
142. Chen, X., et al., *Recovery of valuable metals from waste cathode materials of spent lithium-ion batteries using mild phosphoric acid.* Journal of Hazardous Materials, 2017. **326**: p. 77-86.
143. Zheng, R., et al., *Optimized Li and Fe recovery from spent lithium-ion batteries via a solution-precipitation method.* RSC Advances, 2016. **6**(49): p. 43613-43625.
144. Tang, W., et al., *Recovery of Ti and Li from spent lithium titanate cathodes by a hydrometallurgical process.* Hydrometallurgy, 2014. **147-148**: p. 210-216.
145. Chen, L., et al., *Process for the recovery of cobalt oxalate from spent lithium-ion batteries.* Hydrometallurgy, 2011. **108**(1): p. 80-86.
146. Sun, L. and K.J.W.m. Qiu, *Organic oxalate as leachant and precipitant for the recovery of valuable metals from spent lithium-ion batteries.* 2012. **32**(8): p. 1575-1582.
147. Zheng, Y., et al., *Leaching Procedure and Kinetic Studies of Cobalt in Cathode Materials from Spent Lithium Ion Batteries using Organic Citric acid as Leachant.* International Journal of Environmental Research, 2016. **10**(1): p. 159-168.
148. Gao, W., et al., *Lithium Carbonate Recovery from Cathode Scrap of Spent Lithium-Ion Battery: A Closed-Loop Process.* Environmental Science & Technology, 2017. **51**(3): p. 1662-1669.
149. Zheng, Y., et al., *Lithium fluoride recovery from cathode material of spent lithium-ion battery.* RSC Advances, 2018. **8**(16): p. 8990-8998.
150. Sun, C., et al., *Sustainable recovery of valuable metals from spent lithium-ion batteries using DL-malic acid: Leaching and kinetics aspect.* Waste Management & Research, 2018. **36**(2): p. 113-120.
151. Li, L., et al., *Economical recycling process for spent lithium-ion batteries and macro- and micro-scale mechanistic study.* Journal of Power Sources, 2018. **377**: p. 70-79.
152. Yao, L., Y. Feng, and G. Xi, *A new method for the synthesis of LiNi1/3Co1/3Mn1/3O2 from waste lithium ion batteries.* RSC Advances, 2015. **5**(55): p. 44107-44114.
153. Li, L., et al., *Process for recycling mixed-cathode materials from spent lithium-ion batteries and kinetics of leaching.* Waste Management, 2018. **71**: p. 362-371.
154. Gao, W., et al., *Selective recovery of valuable metals from spent lithium-ion batteries – Process development and kinetics evaluation.* Journal of Cleaner Production, 2018. **178**: p. 833-845.

155. Chen, X. and T. Zhou, *Hydrometallurgical process for the recovery of metal values from spent lithium-ion batteries in citric acid media.* Waste Management & Research, 2014. **32**(11): p. 1083-1093.
156. Mishra, D., et al., *Bioleaching of metals from spent lithium ion secondary batteries using Acidithiobacillus ferrooxidans.* Waste Management, 2008. **28**(2): p. 333-338.
157. Li, L., et al., *Influences of solution pH and redox potential on the bioleaching of LiCoO2 from spent lithium-ion batteries.* Journal of the Korean Society for Applied Biological Chemistry, 2013. **56**(2): p. 187-192.
158. Xin, B., et al., *Bioleaching mechanism of Co and Li from spent lithium-ion battery by the mixed culture of acidophilic sulfur-oxidizing and iron-oxidizing bacteria.* Bioresource Technology, 2009. **100**(24): p. 6163-6169.
159. Horeh, N.B., S.M. Mousavi, and S.A. Shojaosadati, *Bioleaching of valuable metals from spent lithium-ion mobile phone batteries using Aspergillus niger.* Journal of Power Sources, 2016. **320**: p. 257-266.
160. Niu, Z., et al., *Process controls for improving bioleaching performance of both Li and Co from spent lithium ion batteries at high pulp density and its thermodynamics and kinetics exploration.* Chemosphere, 2014. **109**: p. 92-98.
161. Meng, X. and K.N. Han, *The Principles and Applications of Ammonia Leaching of Metals—A Review.* Mineral Processing and Extractive Metallurgy Review, 1996. **16**(1): p. 23-61.
162. Zheng, X., et al., *Spent lithium-ion battery recycling – Reductive ammonia leaching of metals from cathode scrap by sodium sulphite.* Waste Management, 2017. **60**: p. 680-688.
163. Zhang, K., et al., *Recycling of indium from waste LCD: A promising non-crushing leaching with the aid of ultrasonic wave.* Waste Management, 2017. **64**: p. 236-243.
164. Zhang, L., et al., *Comparison of ultrasonic-assisted and regular leaching of germanium from by-product of zinc metallurgy.* Ultrasonics Sonochemistry, 2016. **31**: p. 143-149.
165. Li, L., et al., *Recovery of valuable metals from spent lithium-ion batteries by ultrasonic-assisted leaching process.* Journal of Power Sources, 2014. **262**: p. 380-385.
166. Guan, J., et al., *Mechanochemical Process Enhanced Cobalt and Lithium Recycling from Wasted Lithium-Ion Batteries.* ACS Sustainable Chemistry & Engineering, 2017. **5**(1): p. 1026-1032.
167. Bertuol, D.A., et al., *Recovery of cobalt from spent lithium-ion batteries using supercritical carbon dioxide extraction.* Waste Management, 2016. **51**: p. 245-251.
168. Liu, K. and F.-S. Zhang, *Innovative leaching of cobalt and lithium from spent lithium-ion batteries and simultaneous dechlorination of polyvinyl chloride in subcritical water.* Journal of Hazardous Materials, 2016. **316**: p. 19-25.
169. Wang, F., et al., *Recovery of cobalt from spent lithium ion batteries using sulphuric acid leaching followed by solid–liquid separation and solvent extraction.* RSC Advances, 2016. **6**(88): p. 85303-85311.

170. Zhao, J.M., et al., *Synergistic extraction and separation of valuable metals from waste cathodic material of lithium ion batteries using Cyanex272 and PC-88A.* Separation and Purification Technology, 2011. **78**(3): p. 345-351.
171. Pranolo, Y., W. Zhang, and C.Y. Cheng, *Recovery of metals from spent lithium-ion battery leach solutions with a mixed solvent extractant system.* Hydrometallurgy, 2010. **102**(1): p. 37-42.
172. Joo, S.-H., et al., *Selective extraction and separation of nickel from cobalt, manganese and lithium in pre-treated leach liquors of ternary cathode material of spent lithium-ion batteries using synergism caused by Versatic 10 acid and LIX 84-I.* Hydrometallurgy, 2016. **159**: p. 65-74.
173. Joo, S.-H., et al., *Extractive separation studies of manganese from spent lithium battery leachate using mixture of PC88A and Versatic 10 acid in kerosene.* Hydrometallurgy, 2015. **156**: p. 136-141.
174. Joo, S.-H., et al., *Extraction of manganese by alkyl monocarboxylic acid in a mixed extractant from a leaching solution of spent lithium-ion battery ternary cathodic material.* Journal of Power Sources, 2016. **305**: p. 175-181.
175. Chen, X., et al., *Separation and recovery of metal values from leach liquor of waste lithium nickel cobalt manganese oxide based cathodes.* Separation and Purification Technology, 2015. **141**: p. 76-83.
176. Chen, X., et al., *Separation and recovery of metal values from leaching liquor of mixed-type of spent lithium-ion batteries.* Separation and Purification Technology, 2015. **144**: p. 197-205.
177. Chen, X., et al., *Hydrometallurgical recovery of metal values from sulfuric acid leaching liquor of spent lithium-ion batteries.* Waste Management, 2015. **38**: p. 349-356.
178. Cai, G., et al., *Process Development for the Recycle of Spent Lithium Ion Batteries by Chemical Precipitation.* Industrial & Engineering Chemistry Research, 2014. **53**(47): p. 18245-18259.
179. Pegoretti, V.C.B., et al., *Thermal synthesis, characterization and electrochemical study of high-temperature (HT) LiCoO2 obtained from Co(OH)2 recycled of spent lithium ion batteries.* Materials Research Bulletin, 2017. **86**: p. 5-9.
180. Chen, X., et al., *An atom-economic process for the recovery of high value-added metals from spent lithium-ion batteries.* Journal of Cleaner Production, 2016. **112**: p. 3562-3570.
181. Wang, R.-C., Y.-C. Lin, and S.-H. Wu, *A novel recovery process of metal values from the cathode active materials of the lithium-ion secondary batteries.* Hydrometallurgy, 2009. **99**(3): p. 194-201.
182. He, L.-P., S.-Y. Sun, and J.-G. Yu, *Performance of LiNi1/3Co1/3Mn1/3O2 prepared from spent lithium-ion batteries by a carbonate co-precipitation method.* Ceramics International, 2018. **44**(1): p. 351-357.
183. Yang, L. and G. Xi, *Preparation and Electrochemical Performance of LiNi 1/3 Co 1/3 Mn 1/3 O 2 Cathode Materials for Lithium-ion Batteries from Spent Mixed Alkaline Batteries.* Journal of Electronic Materials, 2016. **45**(1): p. 301-306.

184. Myoung, J., et al., *Cobalt oxide preparation from waste LiCoO2 by electrochemical–hydrothermal method.* Journal of Power Sources, 2002. **112**(2): p. 639-642.
185. Freitas, M.B.J.G. and E.M. Garcia, *Electrochemical recycling of cobalt from cathodes of spent lithium-ion batteries.* Journal of Power Sources, 2007. **171**(2): p. 953-959.
186. Garcia, E.M., et al., *Electrodeposition of cobalt from spent Li-ion battery cathodes by the electrochemistry quartz crystal microbalance technique.* Journal of Power Sources, 2008. **185**(1): p. 549-553.
187. Lupi, C. and D. Pilone, *Electrodeposition of nickel□cobalt alloys: the effect of process parameters on energy consumption.* Minerals Engineering, 2001. **14**(11): p. 1403-1410.
188. Garcia, E.M., et al., *Electrochemical recycling of cobalt from spent cathodes of lithium–ion batteries: its application as coating on SOFC interconnects.* Journal of Applied Electrochemistry, 2011. **41**(11): p. 1373.
189. Garcia, E.M., et al., *Electrochemical recycling of cobalt from spent cathodes of lithium-ion batteries: its application as supercapacitor.* Journal of Applied Electrochemistry, 2012. **42**(6): p. 361-366.
190. Barbieri, E.M.S., et al., *Recycling of spent ion-lithium batteries as cobalt hydroxide, and cobalt oxide films formed under a conductive glass substrate, and their electrochemical properties.* Journal of Power Sources, 2014. **269**: p. 158-163.
191. Li, L., et al., *Preparation of LiCoO2 films from spent lithium-ion batteries by a combined recycling process.* Hydrometallurgy, 2011. **108**(3): p. 220-225.

3 Flotation of Composite Electrode Materials

3.1 Introduction

Lithium-ion battery (LIB) has become a dominating energy storage solution for consumer electronics, electric vehicles (EVs), and renewable energy systems such as wind and solar [1, 2]. Because these batteries are expected to last 2-10 years, they will enter the waste stream after reaching their useful life cycles [3]. It is estimated about as high as 340,000 t/y of lithium-ion batteries from EVs are available for recycling by 2040 [4]. Lithium-ion batteries are classified as a hazardous material under federal regulation. One reason is that lithium-ion battery is nothing more than a package of chemical energy, and it can catch a fire or an explosion if the battery is short circuited [5]. Another reason is that the disposal of end-of-life LIBs can have negative impacts on the environments and human health due to toxic materials that potentially release into the environment [6]. To date, many articles have been devoted to the environmental and life-cycle impacts of battery recycling [7-9].

Battery recycling is a norm in the United States, when it comes to lead-acid and nickel-cadmium batteries [10-12]. However, recycling of lithium-ion batteries is much less mature compared to lead-acid batteries, since both the recycling network and technology have not yet been established [3, 13]. As a result, recycling rate of spent lithium-ion battery is much lower compared to other types of batteries in the United States. Cylinder lithium-ion batteries, used for computer laptops and EVs, are constructed by rolling anode layers, separator layers, and cathode layers in a steel casing. In contrast to simple chemistry used in lead-acid batteries, components used in lithium-ion batteries are much more complex. In addition, battery manufactures have their own proprietary, non-standard chemistry, further complicating the recycling process. Current research has been directed towards the extraction of high-value metals from cathode materials using pyrometallurgical and hydrometallurgical processes [14-16]. Before being fed into metal extraction processes, separation of mixed materials from lithium-ion batteries using low-cost and energy-efficient methods is critical to lower processing cost, minimize secondary waste, and increase product values [17].

Various separation technologies have been studied to sort battery materials by size, specific gravity, magnetism and electrostatic conductivity [18]. For instance, magnetic components (*e.g.* steel casings) can be sorted by means of dry and wet magnetic separators [19]. One of most simple methods is sieving by means of a screen. In this process, coarse particles are retained above the screen while fine materials pass through. Separation by sieving can be operated in both dry and wet conditions. In lithium-ion batteries, fines materials rich in cobalt and nickel metals can be separated from coarse pieces such as copper and aluminum using a sieve [20, 21]. For particles of similar sizes, components can be separated individually based on differences in specific gravity (SG). For instance, among all coarse components (+200 μm) in lithium-ion batteries, plastic pieces can be separated from aluminum and copper pieces using a table [22] or an air classifier [20]. Such separation equipment have been widely used in the minerals industry, and includes devices such as jigs, spiral, sluice, shaking table, and etc [23]. Al-Thyabat introduced a Li-ion battery recycling system based on a combination of mechanical, pyrometallurgical and hydrometallurgical processes [17].

Chen *et al*. recently reported a recycling method that effectively physically recover and regenerate valuable cathode materials for the spent $LiFePO_4$ batteries [24]. In this process, cathode materials were manually removed by cathode layers. One benefit of this method is that recovered cathode powders can be regenerated and reused in new lithium-ion batteries [24-26]. To scale up the cathode regeneration process, it is requisite to have a scalable separation and purification process that segments pure cathode materials from other components in spent batteries while preserving functional integrity.

In lithium-ion batteries, anode and cathode materials are graphite and lithium metal oxide, respectively. After lithium-ion batteries are shredded and crushed, a fine fraction (-200 μm) mainly consists of anode and cathode materials. Previously, purification of cathode materials can be achieved using 1) thermal method, 2) physical separation method, and 3) chemical method. The first method burns off volatile materials, such as binders, carbon blacks, and graphite, from a mixture of fine battery materials at a temperature of 500-800 ^oC [27, 28]. The second method involves a separation of anode materials from cathode materials by a physical separation method. The separation of fine particles has been studied using a dense liquid separation, such as bromoform [29]. This process might become very difficult to scale up due to environmental toxicity of those heavy liquids. The chemical method involves a dissolution of cathode materials in corrosive acids while retaining anode powders as solids [30]. This process is followed by a solid-liquid separation, whereby metal-rich filtrate can be processed to precipitate metal hydroxide [30-32], be synthesized to active cathode materials [33, 34], or a new type of cathode material by controlling solution chemistry [35, 36]. It is more desirable to have a physical or physiochemical separation system that separates mixed fine materials since as they are much more cost efficient.

Froth flotation is a physicochemical separation process that separates fine materials based on the differences in surface hydrophobicity. In this process, only hydrophobic particles are attached on surfaces of air bubbles. The particle-laden air bubbles rise to form a froth layer, and exits into a launder, while leaving hydrophilic particles behinds. A key in froth flotation is the control of particle hydrophobicity [37, 38]. Graphite is naturally hydrophobic, while cathode material such as $LiCoO_2$ is hydrophilic. Thus, one can separate two materials. For example, naturally hydrophobic materials, e.g., molybendum, graphite, coal, and talc, can be readily separated from hydrophilic fine materials by froth flotation in water [39]. To increase the hydrophobicity of naturally hydrophobic minerals, a small amount of kerosene might be used [40]. Due to recent emerging research on lithium-ion battery recycling, studies on froth flotation for the separation of anode and cathode materials are very rare [41, 42]. In one patent, a froth flotation process is integrated in a recycling system to separate carbon black from cathode powders [42]. In this process, slurries were filtered and treated at a temperature of 500 ^oC for an hour to burn off binders. Particles were then mixed with water and subjected to froth flotation. However, no experimental results in details have been released, and the effects of heat treatment on surface hydrophobicities were not studied. In addition, it is not clear how binders and conducting additives used in cathode electrode sheets affect the separation performance of anode and cathode materials.

The objective of the present work is to study the performance of froth flotation in separating cathode and anode materials from new and spent lithium-ion batteries. A series of laboratory-scale froth flotation experiments were conducted with individual anode and cathode materials as well as mixed materials. The results show that the froth flotation process enables a separation of fine battery materials efficiently. The recovered powder samples were examined using thermogravimetric (TGA) and chemical analyses.

3.2 Materials and Experiments

3.2.1 Materials and Chemicals

New lithium-ion batteries were obtained from vendors, and they come in different sizes and configurations. Used lithium-ion batteries were provided from Michigan Tech's Information Technology Department, Marquette County Solid Waste Management Authority, and other sources. Used battery packs were removed from old working laptops and consumer electronics. These were opened by manually removing plastic casings to obtain 18650 cylinder cells. A fraction of lithium-ion batteries surveyed in this study are of a pouch cell design, which were manufactured by stacking layers of electrodes in a foil envelope. Pure graphite flake (>99%) and lithium cobalt oxide (97%) were obtained from Alfa Ester. The top sizes of graphite and lithium cobalt oxide are 44 and 30 μm, respectively.

Lithium-ion batteries were first discharged to 1.0-2.0 V by connecting with a load (a 10W – 35W halogen bulb) in a circuit to prevent explosion and fire during disassembly process. The discharged lithium-ion battery cells were manually disassembled to remove stainless steel casing using a rotary tool (Proxxon). Lithium-ion battery cores were unfolded to sort anode electrode layers, cathode electrode layers, plastic separators, and other components individually. The unfolding process was performed under a fume hood to evaporate toxic organic solvents (ethylene carbonate and/or ethyl methyl carbonate). A fraction of the samples were used for single-component flotation tests. Samples were prepared by scraping off coatings from either anode or cathode conducting layers. The fine materials were dry grinded using a pestle and mortar until all fine powders passed through a 70-mesh screen (-210 μm). This ensured that flotation experiments were performed at an optimum size range. Fine materials were rinsed with distilled water at least five (5) times to remove excess electrolytes and additional distilled water was added to obtain a 1-2% w/w solid slurry for flotation tests. Kerosene and methyl isobutyl carbinol (MIBC) were used as the collector and frother, respectively, except where otherwise specified.

For multi-stage flotation tests, a mixture of anode and cathode layers were shredded into micro-cut pieces (5 mm x 12mm) using a heavy-duty paper shredder. The shredded metal foils were mixed with distilled water for at least five (5) times to rinse off electrolyte and other soluble organic components. A slurry of shredded metal foils with electrode materials was transferred into a 3hp blender (CleanBlend) at a speed of approximately 12000 rpm. The agitation time was controlled to ensure that active battery materials were liberated from current conducting layers while the size of current conducting foils

remained significantly larger than that of active battery materials. Liberated active battery materials were separated from metal foils by wet sieving using a 70 mesh screen (-210 μm). The battery materials were filtered using a laboratory-scale pressure filter, and fine battery materials retained above the filter were mixed with distilled water for flotation experiments.

3.2.2 Froth Flotation

Flotation experiments were carried out in a 2-liter batch cell using a Denver D-12 laboratory flotation machine. In a single-material flotation experiment, a slurry was fed to a flotation cell and allowed to condition for five (5) minutes at an impeller speed of 1500 rpm. Collector was then added, and the slurry conditioned for three (3) minutes. This was followed by adding frother and conditioning the slurry for two (2) more minutes prior to flotation. Flotation commenced after the air inlet valve was open. Froth products were collected in collection pans every 30-60 seconds. The obtained products were dried in an oven at a temperature of 105 ℃ overnight and weighed. Froth height was kept at approximately 40 mm throughout the course of experiments by adding water periodically. Froth products from a batch flotation cell in a series of timed fractions were collected, dried and weighed.

Separation performance of a mixture of anode and cathode electrode materials was evaluated using a modified experimental procedure which was originally developed by Dell [43]. The original test procedure, also known as “release analysis”, provides a measure of materials’ separability by froth flotation. The result obtained using this method represents the ideal flotation response of a given sample [44].

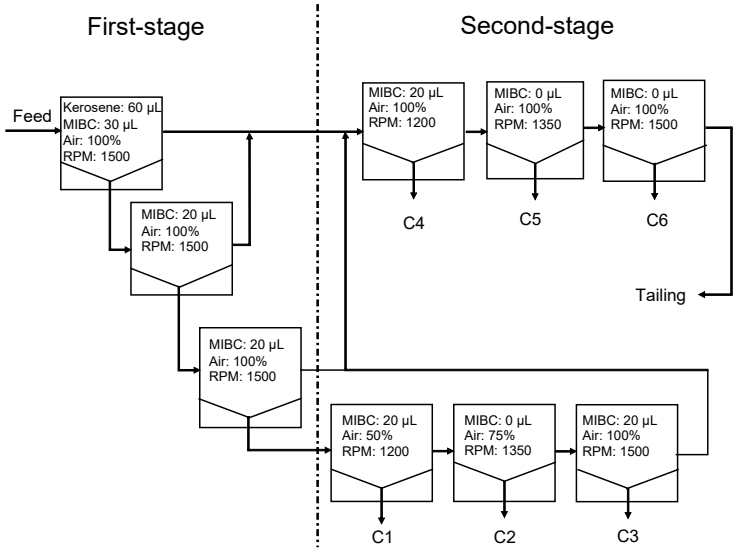

Figure 3-1. A schematics of a modified froth flotation procedure for separation of mixed fine materials from lithium-ion batteries.

Figure 3-1 shows a schematic representation of a modified experimental procedure used in this study, which consists of two stages of separation experiments. The first stage is to

separate floatable materials from non-floatable materials by minimizing the amount of entrained materials in froth layers. The first flotation experiment was carried out using 30 μL collector and 30 μL frother. Flotation continued until no visible particles appeared on the froth layers. Tailings from the first experiment were saved for the second stage experiment, while froth concentrate was re-pulped for the follow-up flotation experiment to clean non-floatable hydrophilic particles entrained in the froth layers. In the follow-up experiment, a small amount of frother (20 μL) was added to maintain a stable froth. The froth products from the second experiment were collected, while tailings from the first two flotation experiments were combined as the final tailing sample. This procedure was repeated for one or two additional times for fine or ultrafine particle samples when necessary to minimize the amount of entrained materials in froth concentrates.

The second stage of the modified procedure involves a segmentation of fine materials into components having various degrees of floatability. In this stage, froth product from the first stage of this procedure was re-pulped to obtain a 2L slurry as the feed. Flotation was initialized at an impeller speed of 1200 rpm and an aeration rate of approximately 50% of full range for 2 minutes. Flotation continued by increasing impeller speeds and/or aeration rates. Froth concentrates obtained at different operating conditions were collected, dried and sampled, and the leftover tailing was combined with those obtained in the first stage and thickened to obtain a 2-liter slurry.

The same experimental procedure was applied to the tailings. In this experiment, flotation was initialized at an impeller speed of 1200 rpm and an aeration rate of full range for 2 minutes. Flotation continued by increasing the aeration rate to 1350 rpm and 1500 rpm for 2 minutes, respectively. A constant froth height was kept over the course of the experiments by adding water. A total of three (3) froth concentrates combined with tailings were collected, dried and weighed. The chemical analysis of the samples was performed using the inductively coupled plasma optical emission spectrometry (ICP-OES) technique, which will be described in detail in the following paragraph.

3.2.3 Sample Characterization

Chemical analysis was performed using a Perkin Elmer Optima 7000DV ICP-OES system. Samples were prepared by digesting 10-100 mg solids in a mixture of hydrochloric acid (HCl) and hydrogen peroxide (H_2O_2) solution (HCl:H_2O_2 = 7:3 by volume) at a temperature of 80 ℃ for 15 minutes. The pregnant solutions were diluted with deionized (DI) water to obtain solutions having concentrations of the metal elements of interest in the range of 0.5–25.0 mg/L. Prior to the ICP analysis, sample solution was filtered using a membrane filter when necessary to remove suspended particles in liquids. The DI water was supplied from a Barnstead water purification system (Thermo Scientific). TGA studies were performed using a LECO TGA 701 instrument at a scanning rate of 1 ℃ min^{-1} at a temperature range of 25-800 ℃. The measurements were conducted at an air flowrate of 7 L/min. The TGA results were used to determine active material contents in samples. Both morphology and particle size of recycled fine battery powders were examined using a JEOL JSM-6400 Scanning Electron Microscope (SEM).

3.3 Results and Discussion

3.3.1 Single-material Flotation

Figure 3.2 presents the froth flotation results of pure graphite and lithium cobalt oxide powders in distilled water using 30 µL kerosene and 30 µL MIBC. Kerosene was added to increase hydrophobicity of graphite particles. In this testing, 20 grams of particles were added to 2L distilled water to obtain a slurry of 1% w/w solid concentration. The result is shown as recovery versus flotation time. As shown, over 98% of graphite particles were floated in 4 minutes after flotation commenced, while only 8% of lithium cobalt oxide particles were recovered in the froth concentrate. This result is not surprising in that graphite is naturally hydrophobic having a water contact angle of approximately 80° [40]. On the contrary, the lithium cobalt oxide ($LiCoO_2$) structure consists of CoO_2 slabs with layers of lithium in between [45]. When immersed in water, $LiCoO_2$ is easily hydrated, rendering the surface hydrophilic. Note that a tiny fraction of hydrophilic $LiCoO_2$ particles recovered in froth concentrates is attributed to particle entrainment [46]. The entrainment is proportional to water recovery, and entrainment is more pronounced with ultrafine particles [46, 47].

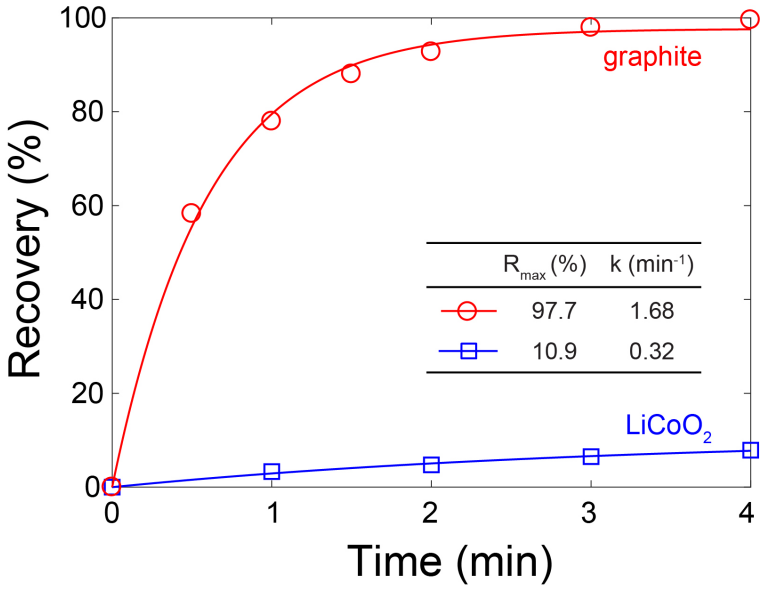

Figure 3-2. Laboratory froth flotation results of pure graphite and lithium cobalt oxide ($LiCoO_2$) at 1% w/w solid concentration.

It has been assumed that the separation of particles in froth layers from the suspension can be described using a first-order kinetic model as [48],

$$R = R_{max}\left(1 - \exp(-kt)\right) \tag{3.1}$$

where R_{max} is maximum recovery and k is rate constant. Both R_{max} and k values can be determined from experimental R versus t data using a linear least-squares regression. As

shown in Figure 1, the experimental data can be well represented by a model fit. The coefficient of determination, denoted R-squared, for two sets of experimental data are above 0.95, confirming that the experimental results are replicated by the first-order kinetic model. The R_{max} and k values obtained for graphite are 97.7% and 1.68min^{-1}, respectively, while those obtained for lithium cobalt oxide are 10.9% and 0.32 min^{-1}, respectively. As can be seen from Figure 3-2 and reflected by the R_{max} and k values, graphite powders were recovered by air bubbles in froth products, while cathode materials were selectively concentrated in tailings.

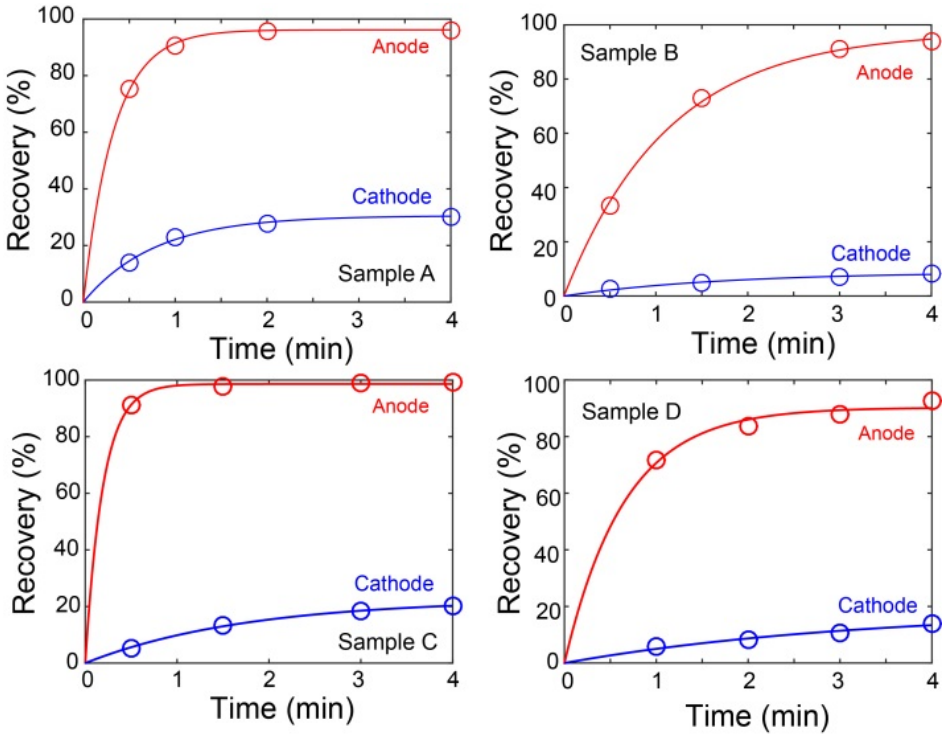

Figure 3-3. Froth flotation results of individual anode and cathode electrode materials liberated from four new lithium-ion batteries samples.

Table 3-1. Fitting parameters obtained from the model fit to the froth flotation result obtained with four new lithium-ion battery samples (A-D) as shown in Figure 3-3.

Samples	A		B		C		D	
	Anode	Cathode	Anode	Cathode	Anode	Cathode	Anode	Cathode
R_{max} (%)	96.18	30.51	97.56	8.842	98.61	22.56	90.25	18.80
k (min^{-1})	3.01	1.29	0.88	0.58	5.19	0.57	1.53	0.31

Froth flotation technique was extended to separate anode and cathode materials liberated from new lithium-ion batteries, and the results are shown in Figure 3-3. All new batteries surveyed in this study use graphite as the anode material and lithium metal oxide (*e.g.*, LCO, LMO, NCA) or lithium iron phosphate (LFP) as the cathode material. The top size of the feed was 210 μm, which is within the particle size range for effective separation process [49, 50]. As shown, anode materials liberated from all four samples floated well, with a total recovery of 92.7% or above in 3 minutes of flotation after aeration. On the contrary, cathode materials exhibited a low floatability, with the amount of floatable materials in the range of 8.1-31.0% for all four samples in 3 minutes of flotation. Also shown in Fig. 3 is the theoretical fit to the experimental data using Eq. (1) with the model parameters listed in Table 1. In general, the first-order kinetic model gave a reasonably good fit to the experimental data for all four samples surveyed. The present result shows that a separation of anode and cathode electrode materials from a mixture of fine battery materials can be achieved using the froth flotation process. Furthermore, there appears to be no discernible difference to the response of froth flotation for all four lithium-ion batteries surveyed in this study. This indicates that the froth flotation process might be versatile for any types of lithium-ion battery as long as graphite and lithium metal oxide are used as the anode and cathode materials, respectively.

Table 3-2. Fitting parameters obtained from the model fit to the flotation results of spent lithium-ion batteries samples (E-H) as shown in Figure 3-4.

Samples	E		F		G		H	
	Anode	Cathode	Anode	Cathode	Anode	Cathode	Anode	Cathode
R_{max} (%)	82.05	20.11	85.73	8.21	97.33	21.44	90.77	35.99
k (min^{-1})	2.31	0.75	2.05	2.06	3.10	0.79	2.65	0.78

It is worthy to mention that the recovery of "real" cathode materials is higher than that of "hypothetical" electrode materials. Fig. 3-3a, for example, shows that the recovery of cathode materials after 3 minutes of flotation was 27.1 %, which was substantially higher than that obtained with pure $LiCoO_2$. It is unlikely that a significant amount of cathode materials recovered by froth flotation was due to the entrainments in the froth layer, but instead originated from the hydrophobicity of liberated cathode materials. Cathode electrode is manufactured by coating a mixture of active cathode materials, conductive additives and binders (polyvinylidene fluoride, PVDF) on aluminum foils. Upon liberation, some cathode materials are covered by binders and conductive additives such as carbon blacks, rendering a fraction of electrode materials hydrophobic, resulting in a high recovery in froth concentrates. It should also be mentioned that the recovery of cathode materials was not consistent for all four batteries surveyed in this study, despite great care being taken to ensure the experimental procedures were exactly followed for

all experiments. Such a discrepancy might be attributed to the types and composition of binders and conductive additives in battery chemistry as well as manufacturing process.

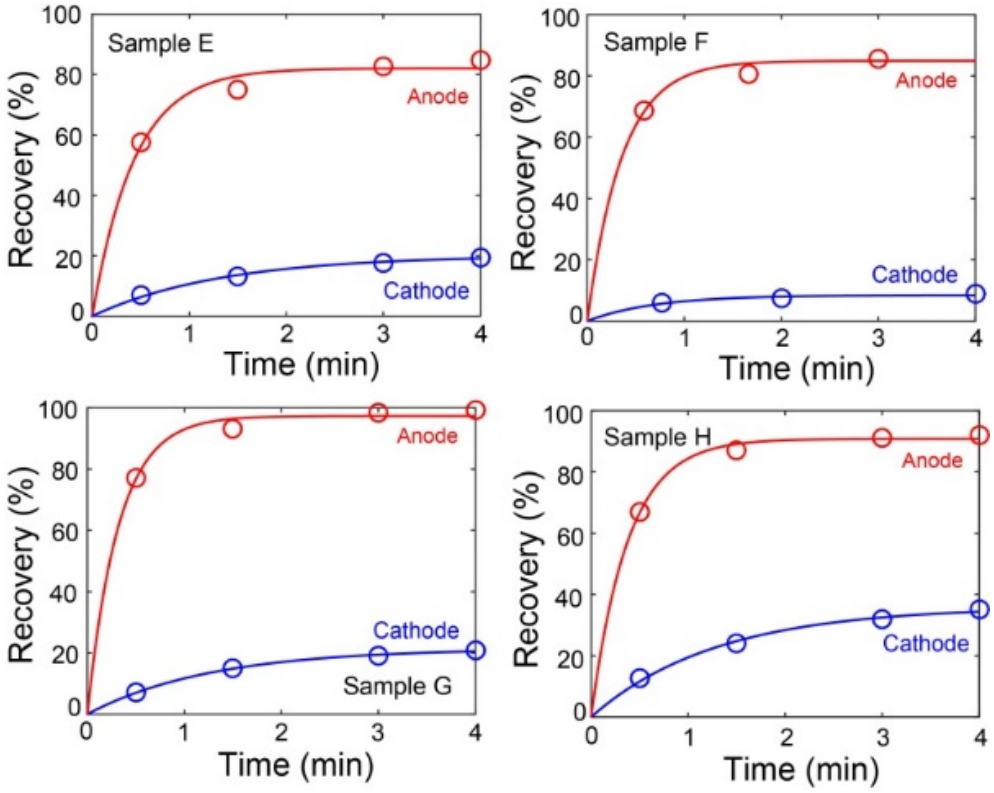

Figure 3-4. Froth flotation results of individual anode and cathode electrode materials liberated from four spent lithium-ion battery samples.

Froth flotation experiments were extended to spent lithium-ion batteries, and the results are shown in Fig. 3-4 and Table 3-2. Note that a fraction of electrode materials in spent batteries appeared to be less adhered on current conductors, which might be due to a weaker coating-to-foil adhesion by mechanical degradation [24]. In general, 80%-97% of anode materials were floated in 4 minutes after aeration commenced, while the fraction of floated cathode materials varied from 8.8% to 35.0% for all four samples surveyed. The present work seems to indicate that the hydrophobicity of anode materials weakens slowly after having reached their useful life cycle. While the hydrophobicity of those electrode materials weakened slightly, the extent of their material degradation is not clear and will be discussed in future.

To illustrate the role of binder and conducting additives, thermogravimetric analysis (TGA) were performed on both froth and tailing products. Figure 3-5 shows the results of a froth product after 30 seconds of flotation and a tailing using cathode materials liberated from spent lithium-ion battery cells as sample. The result is shown as weight and derivative weight loss as a function of temperature. The TGA curve of the tailing product shows a loss of weight started at a temperature of approximately 300 °C, signifying an onset of decomposition of binder and carbon additives under an air

atmosphere [51]. The peak of binder's decomposition occurred at a temperature of 498 ℃, which is consistent with the literature data [52, 53]. The total weight loss of the sample reached 4.5% at a temperature of 800 ℃.

The TGA curve of the froth concentrate exhibits a distinct response in weight loss to the temperature rise compared to the tailing product. As shown, the derivative weight loss curve of the froth product has a secondary peak at a temperature of 558 ℃, which might be indicative of conductive additives' decomposition. Clearly, those additives are hydrophobic and consequently they are floatable. The total weight loss of the froth product reached 13.1% at a temperature of 800℃.

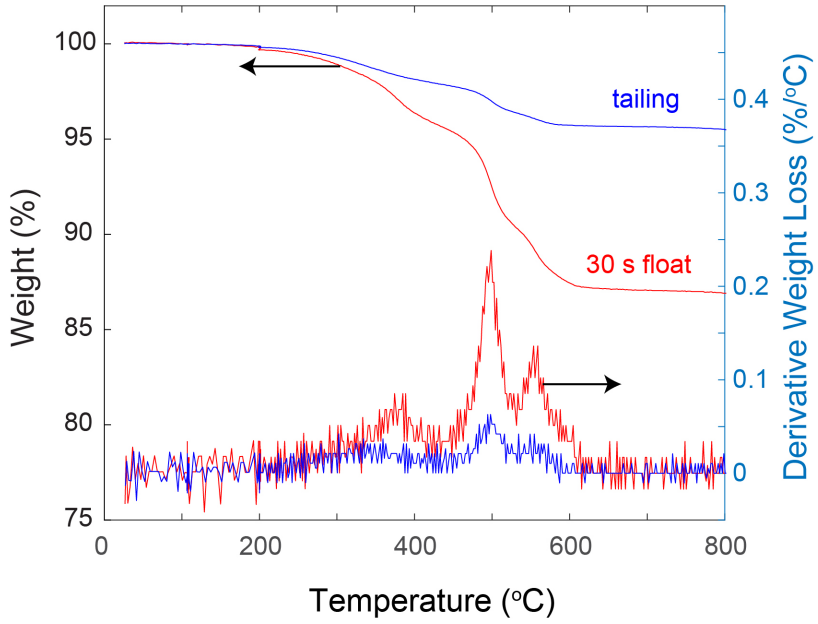

Figure 3-5. Thermogravimetric analysis of a froth concentrate after 30 seconds of flotation and a tailing product after 4 minutes of floatation.

Table 3-3 shows both froth flotation and TGA results obtained using the cathode coating materials liberated from spent lithium-ion battery cells. The active material content was determined from the total weight loss at a temperature of 800 ℃, at which both binders and additives were decomposed. As shown, the active material content in tailing and 30-second froth concentrate is reach 95.4% and 86.9%, respectively. The result confirms that both conductive additives and binders in liberated cathode materials are hydrophobic, causing liberated cathode materials being floated in froth products. It should also be mentioned that a majority of binders might be engulfed in coarse cathode materials [54], which explained that the active material content in tailing product remained at 95.4%.

Table 3-3. Weight and active material content of froth concentrates and tailing product.

Products	Weight (%)		Active Material (%)
	Individual	Cumulative	
Froth (0-0.5 min)	9.40	9.40	86.9
Froth (0.5-1.5 min)	8.02	17.42	89.9
Froth (1.5-4.0 min)	7.27	24.69	94.4
Tailing	75.31	100.00	95.4
Feed	-	-	94.1

3.3.2 Flotation of mixed materials

The aforementioned paragraphs verified that a froth flotation process can be used to separate cathode materials from anode materials in the fine fractions of shredded lithium-ion battery based on the difference in the surface hydrophobicity of the two constituents to be separated. Let us hypothetically assume that 100% of anode electrode materials are floatable while 20% of cathode electrode materials are floatable, a froth flotation process can produce a high purity of cathode electrode materials in final tailing. To verify the hypothesis, a modified procedure was used to evaluate the separability of an anode and cathode electrode material mixture *via* froth flotation. The modified procedure has been described in the experimental section.

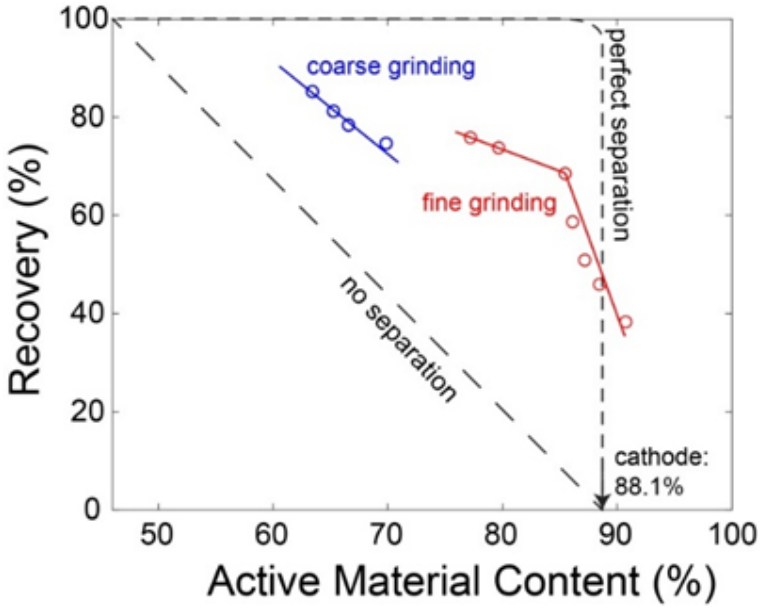

Figure 3-6. Recovery versus active material content curves at fine and coarse grinding obtained with spent lithium-ion batteries.

Figure 3-6 shows the recovery versus active material content at two different particle sizes. The result was obtained using 12 identical spent cylinder lithium-ion battery cells. A fine grinding was carried out by agitating slurries in a blender at a speed of 36000 rpm for 10 minutes. The mean particle sizes at coarse and fine grinding were estimated to be 60 and 18 μm, respectively, as determined from SEM images. As shown, the recovery *vs*. active material content curves at fine grinding exhibits a sharper inflection point and is significantly shifted to the right as compared to those obtained at coarse grinding. The result clearly suggests that fine grinding can produce a purer product than coarse grinding at the same recovery. For instance, at fine grinding, the active material content in tailings reaches 87.2% at a recovery of 51.6%. The coarse grinding, on the contrary, produces a tailing product with the active materials content of 69.9% at a recovery of 70.9%. Also shown in Fig. 6 are a hypothetical "no" separation curve and a near "perfect" separation curves for comparison. Both curves assume that composition of liberated cathode materials does not change upon the liberation. Table 3-4 shows the content of metal elements in tailings at fine and coarse finding. Clearly, the chemical analysis result is in good agreement with the active material content data.

Table 3-4. A comparison of cobalt (Co) and lithium (Li) concentrations and active material content of tailing product obtained at fine grinding and coarse grinding.

Grinding	Co (%)	Li (%)	Active Material (%)
coarse	36.10	4.47	69.9
fine	46.73	5.70	90.8

It should be mentioned that the low active material content in tailings obtained at a coarse grinding is attributed to the fact that a fraction (~20%) of anode materials were reported to the tailings. In this regard, a small fraction of anode powders is non-floatable, which may be attributed to surface oxidization in water. By reducing particle size using a fine grinding process, surface oxidized groups might be removed and new hydrophobic surfaces would be exposed so that graphite can be readily floatable again. Figure 3-7 shows the TGA curves of final tailing products at coarse and fine grinding, respectively. For tailing products at the fine grinding, there are two peaks occurred at a temperature of 380 ℃ and 558 ℃, which might be relevant to the thermal decomposition of poly(methyl methacrylate) (PMMA) binders and conductive additives [53] For tailings at the coarse grinding, however, there is an additional peak occurred at a temperature of 582 ℃. This represents the decomposition of anode materials used in the lithium-ion batteries. At a temperature of 800 ℃, the total weight loss of the tailings at coarse and fine grinding reached 9.2% and 30.1%, respectively.

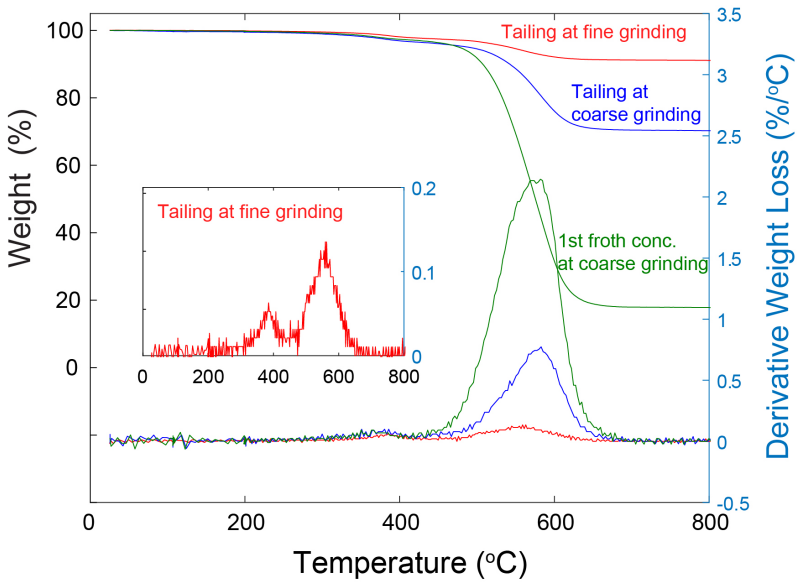

Figure 3-7. Thermogravimetric analysis of tailing products obtained at fine and coarse grindings as well as the 1st froth concentrate at coarse grinding.

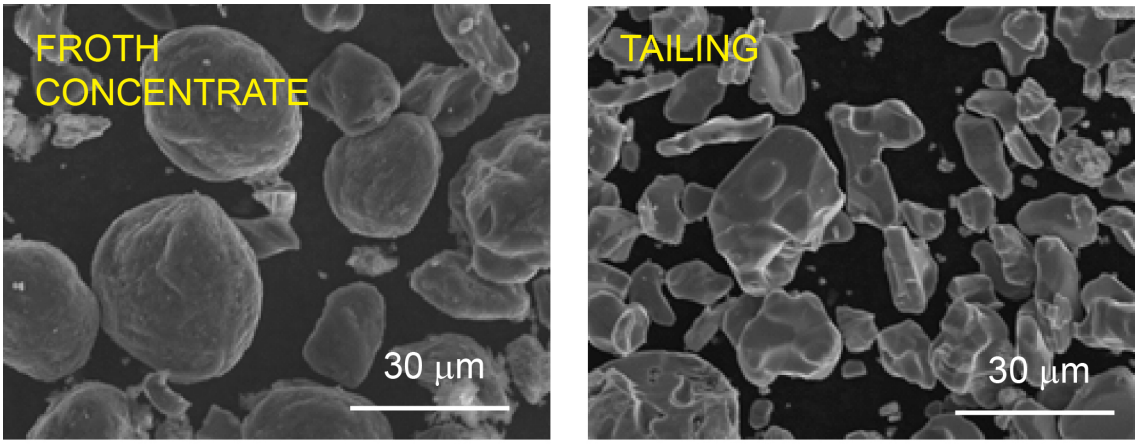

Figure 3-8. SEM photos of froth and tailing products at fine grinding.

Also shown in Figure 3-7 is the TGA curve of the first froth product at coarse grinding for comparison. The TGA curve shows that the peak temperature occurred at 582 ℃, confirming the presence of anode materials. The total mass loss reached 82.1% at 800 ℃. We anticipated that the froth product contains approximately 80% anode materials and 20% cathode materials.

Figure 3-8 shows a SEM photo of froth product and tailings at a fine grinding, respectively. The froth product is mainly graphite, with particle sizes of 16-25 μm. The tailing consists of pure lithium metal oxide particles of uniform size, in the range of 6-25 μm.

It is also notable to mention that the active material content in the tailing at fine grinding reaches 90.8% (Table 3-4), which is greater than the theoretical value of pure cathode material (88.1%). This is attributed to the rejection of all anode materials in froth products as well as some of conducting additives and hydrophobic binder [55]. In addition, graphite recovered from spent lithium-ion batteries might become a commodity for downstream applications [56]. In terms of graphite particle purity, froth concentrates contain 16% and 22% of active cathode electrode materials at 60 µm and 18 µm grinding sizes, respectively. Since it is difficult to liberate binders from the cathode materials mechanically, a further upgrading of graphite purity in the froth products would be very difficult. To do so, cathode materials could be selectively leached into liquid while retaining graphite as solids [30]. Alternatively, particles of different specific gravities could be separated *via* gravity separation methods [57, 58]. Therefore, we conclude based on this work that a froth flotation process is better suited for a production of pure cathode materials rather than a purification of anode materials.

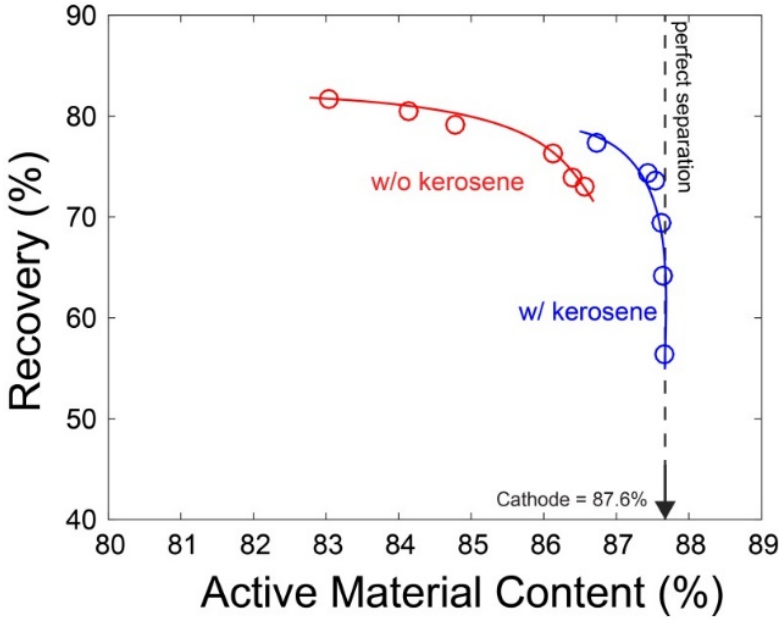

Figure 3-9. Recovery versus active material content curves obtained with and without the use of kerosene.

To ensure that tailings are free of anode materials (*i.e.* graphite), attention should be paid to ensure that graphite particles are rejected to froth concentrates. Figure 3-9 shows the recovery versus active material content with and without kerosene. The kerosene dosage is 100 µL, which is equivalent to 1 kg per metric tonne of fine battery materials. As shown, the recovery versus active material content curve exhibits a sharp inflection point regardless of the kerosene dosage. The recovery *vs*. active materials content data obtained without kerosene shows a comparable separation performance with those obtained at an excess kerosene dosage (100 µL). In terms of active material contents in final tailing

product, the use of kerosene increases the amount of active materials in tailings at an expense of the recovery. Figure 3-10 compares the TGA curves for the tailing products obtained with and without kerosene. As shown, the two curves split at a starting temperature of approximately 550 ℃, suggesting that there might be a small amount of anode materials left in tailing without kerosene. In addition, the overlaps of decomposition's peaks confirm that the two samples with and without kerosene contain same amount of binders and carbon additives. It is worthy to mention that both binders and conducting additives might be different between different lithium-ion batteries investigated in this study, and therefore we cannot compare decomposition peaks between different samples. Active material content in tailings at a 100 μL kerosene dosage reaches 87.67% while that obtained without kerosene is 86.56%. Thus, a control of collector dosage is critical if the objective of the flotation separation process is to recycle and purify cathode materials for making new batteries.

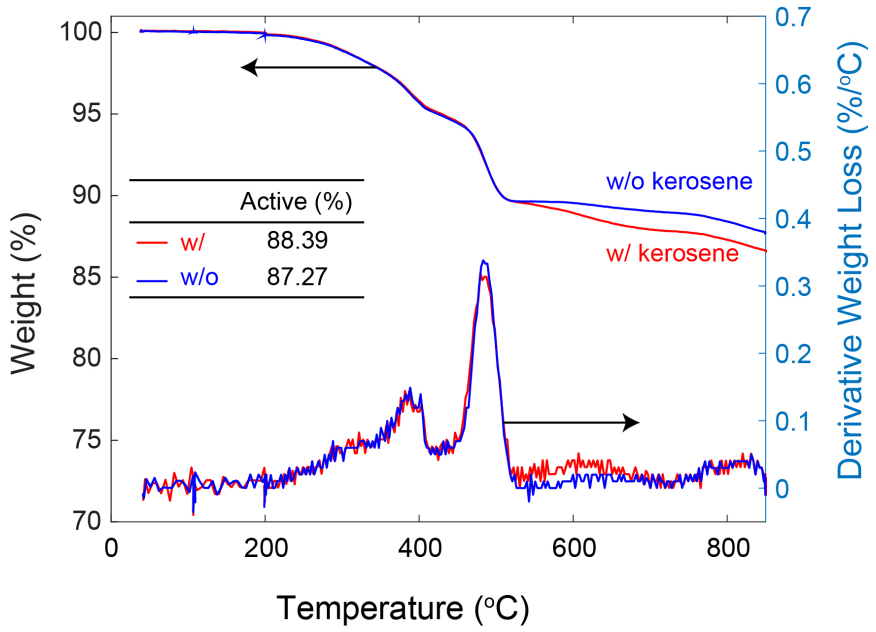

Figure 3-10. Thermogravtimetric analysis for tailing products obtained with and without the use of kerosene as the collector.

3.3.3 Direct-Recycle-Reuse (DR2) Process

The froth flotation technique exhibits many superior features over competing technologies in recycling valuable components and constituents from spent lithium-ion batteries. First, froth flotation is a physiochemical separation process that effectively preserves functional integrity of electrode materials during the recycling process [59]. As a result, active battery materials might be regenerated through a relithilization process and re-used in new batteries [24, 26]. Second, froth flotation serves as a beneficiation process, which has the potential to sort fine electrode materials by chemistry. Doing so increases energy efficiency in the downstream process while minimizing secondary waste to a great extent. For instance, the froth flotation process provides a metal-rich product

that can be used as high-value feedstock for the hydrometallurgical and pyrometallurgical processes. Lastly, beneficiation of fine battery materials using froth flotation is economically viable at a full-scale production. It was estimated that the operating cost is $4.40 per dry metric ton of fine battery materials based on industrial fine coal cleaning data [60]. This represents a remarkably low operating cost compared to the contained value in fine battery materials. In this regard, battery recycling *via* froth flotation is economically viable.

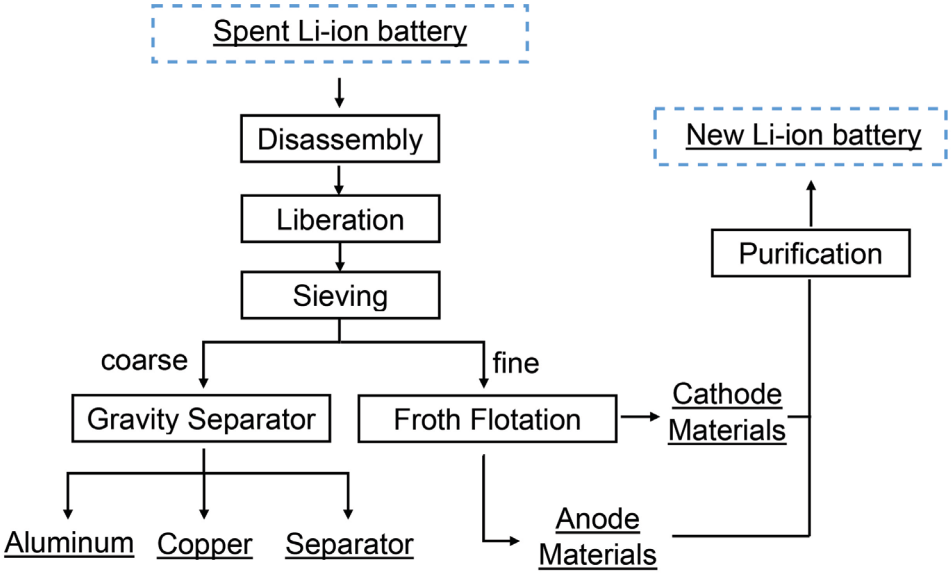

Figure 3-11. A schematic drawing of the Direct-Recycle-Reuse (DR2) Process. It is designed to produce cathode materials from spent lithium-ion batteries to close the loop of material use in new lithium-ion batteries.

On the basis of encouraging experimental result, a new Direct-Recycle-Reuse (DR2) process is proposed. Figure 3-11 shows a schematic representation of the DR2 process for producing pure cathode materials from spent lithium-ion batteries. In this process, lithium-ion batteries are shredded and crushed to pieces in inert gas. Upon a full liberation, solid components are sorted into a coarse fraction and a fine fraction by a screen. Coarse components, including casing, copper, aluminum, and plastic separator, are separated by a magnetic separator, a spiral classifier, and a gravity separator. In the fine fraction, active cathode materials can be recovered from fine fraction of shredded lithium-ion batteries using the froth flotation technique. The active cathode materials can be regenerated through re-lithithization and then used directly in manufacturing new lithium-ion batteries. The graphite particles leached from the metal cathode materials might be re-used in new batteries. The concept of the DR2 process follows the closed-loop model for lead-acid batteries, in which nearly all battery components are recycled and reused [3].

One major benefit of the DR2 process is that this process is applicable to any types of lithium-ion battery as long as they use graphite and lithium metal oxide as the anode and cathode electrode materials, respectively. Conventional hydrometallurgy and

pyrometallurgy processes will not be economically viable for lithium-ion batteries using $LiMn_2O_4$ or $LiFePO_4$ as the cathode chemistry, since the contained value in those cathode materials is very low. The DR2 process, however, preserves functional integrity of active electrode materials and consequently maximizes product values during the recycling process.

A possible concern with the DR2 process is the purity of cathode materials that might vary with feed samples and grinding conditions. There are three major sources of impurities, including ultrafine aluminum metal pieces, binders, and anode materials. Fine aluminum pieces can be dissolved in alkaline solutions. The binder might be re-dissolved in an organic solvent during new cathode electrode manufacturing. Future research should be directed towards the removal of a small amount of fine anode materials from the spent lithium-ion battery. One solution might be the development of novel chemical collectors for cycled graphite particles from the spent lithium-ion battery. It should be also noted that the densities of graphite particles and lithium cobalt oxide are 2.26 g/cm^3 and 4.9 g/cm^3, respectively. Thus, a gravity separation method based on differences in specific gravity between these particles has the potential to separate anode materials from cathode materials.

3.4 Summary and Conclusions

The separability of active anode and cathode materials from lithium-ion batteries was studied using the froth flotation technique. It was found that over 90% of anode materials were floatable after rinsing off electrolytes, while only 10-30% of liberated cathode materials were floatable using 2 kg/t kerosene as collector. The floatability of electrode materials exhibits comparable performance between brand new batteries and spent batteries with the exception that a few of spent batteries exhibit a slightly lower recovery (75-90%) for anode materials. The mechanism of partial floatability of cathode materials was examined using the thermogravimetric and chemical analysis. It was found that the partial floatability of cathode materials might be attributed to the coverage of hydrophobic binders and carbon additives on surfaces.

Experiments with mixed materials were performed using a modified procedure based on the release analysis method. The results were shown as recovery versus active material contents. It was found that for spent lithium-ion batteries, a fraction of graphite particles might be non-floatable, resulting in a tailing product of a lower grade. A finer grinding enables an exposure of fresh hydrophobic surfaces in water, resulting in an increase in purity of cathode materials in tailings. Kerosene was found to be an effective collector for increasing the hydrophobicity of anode materials, and consequently for increasing the grade of cathode materials in the tailings. The present result showed that a tailing product having 87.4% active materials can be obtained at a total recovery of 74.3%, demonstrating the effectiveness of the froth flotation process in producing pure cathode materials from spent batteries. Based on the present result, a novel Direct-Recycle-Reuse (DR2) system was proposed that has the potential to close the loop of material use in lithium-ion batteries.

3.5 Reference

1. Larcher, D. and J.M. Tarascon, *Towards greener and more sustainable batteries for electrical energy storage.* Nature Chemistry, 2014. **7**: p. 19-29.
2. Tarascon, J.M. and M. Armand, *Issues and challenges facing rechargeable lithium batteries.* Nature, 2001. **414**: p. 359-367.
3. Gaines, L., *The future of automotive lithium-ion battery recycling: Charting a sustainable course.* Sustainable Materials and Technologies, 2014. **1-2**: p. 2-7.
4. Richa, K., et al., *A future perspective on lithium-ion battery waste flows from electric vehicles.* Resources, Conservation and Recycling, 2014. **83**: p. 63-76.
5. Wang, Q., et al., *Thermal runaway caused fire and explosion of lithium ion battery.* Journal of Power Sources, 2012. **208**: p. 210-224.
6. Kang, D.H.P., M. Chen, and O.A. Ogunseitan, *Potential Environmental and Human Health Impacts of Rechargeable Lithium Batteries in Electronic Waste.* Environmental Science & Technology, 2013. **47**(10): p. 5495-5503.
7. Dunn, J.B., et al., *The significance of Li-ion batteries in electric vehicle life-cycle energy and emissions and recycling's role in its reduction.* Energy & Environmental Science, 2015. **8**(1): p. 158-168.
8. Dunn, J.B., et al., *Impact of Recycling on Cradle-to-Gate Energy Consumption and Greenhouse Gas Emissions of Automotive Lithium-Ion Batteries.* Environmental Science & Technology, 2012. **46**(22): p. 12704-12710.
9. Wang, X., et al., *Economic and environmental characterization of an evolving Li-ion battery waste stream.* Journal of Environmental Management, 2014. **135**: p. 126-134.
10. Bied-Charreton, B., *Closed loop recycling of lead/acid batteries.* Journal of Power Sources, 1993. **42**(1): p. 331-334.
11. Rydh, C.J. and M. Karlström, *Life cycle inventory of recycling portable nickel–cadmium batteries.* Resources, Conservation and Recycling, 2002. **34**(4): p. 289-309.
12. Schultmann, F., B. Engels, and O. Rentz, *Closed-Loop Supply Chains for Spent Batteries.* Interfaces, 2003. **33**(6): p. 57-71.
13. Zeng, X., J. Li, and L. Liu, *Solving spent lithium-ion battery problems in China: Opportunities and challenges.* Renewable and Sustainable Energy Reviews, 2015. **52**: p. 1759-1767.
14. Ordoñez, J., E.J. Gago, and A. Girard, *Processes and technologies for the recycling and recovery of spent lithium-ion batteries.* Renewable and Sustainable Energy Reviews, 2016. **60**: p. 195-205.
15. Xu, J., et al., *A review of processes and technologies for the recycling of lithium-ion secondary batteries.* Journal of Power Sources, 2008. **177**(2): p. 512-527.
16. Bernardes, A.M., D.C.R. Espinosa, and J.A.S. Tenório, *Recycling of batteries: a review of current processes and technologies.* Journal of Power Sources, 2004. **130**(1): p. 291-298.
17. Al-Thyabat, S., et al., *Adaptation of minerals processing operations for lithium-ion (LiBs) and nickel metal hydride (NiMH) batteries recycling: Critical review.* Minerals Engineering, 2013. **45**: p. 4-17.

18. Cui, J. and E. Forssberg, *Mechanical recycling of waste electric and electronic equipment: a review.* Journal of Hazardous Materials, 2003. **99**(3): p. 243-263.
19. Shin, S.M., et al., *Development of a metal recovery process from Li-ion battery wastes.* Hydrometallurgy, 2005. **79**(3): p. 172-181.
20. Bertuol, D.A., et al., *Application of spouted bed elutriation in the recycling of lithium ion batteries.* Journal of Power Sources, 2015. **275**(Supplement C): p. 627-632.
21. Wang, X., G. Gaustad, and C.W. Babbitt, *Targeting high value metals in lithium-ion battery recycling via shredding and size-based separation.* Waste Management, 2016. **51**: p. 204-213.
22. Tedjar, F. and J.-C. Foudraz, *Method for the mixed recycling of lithium-based anode batteries and cells*. 2010, Recupyl, Domene.
23. Wills, B.A. and J. Finch, *Wills' Mineral Processing Technology: An Introduction to the Practical Aspects of Ore Treatment and Mineral Recovery*. 2015: Elsevier Science.
24. Chen, J., et al., *Environmentally friendly recycling and effective repairing of cathode powders from spent LiFePO4 batteries.* Green Chemistry, 2016. **18**(8): p. 2500-2506.
25. Ganter, M.J., et al., *Cathode refunctionalization as a lithium ion battery recycling alternative.* Journal of Power Sources, 2014. **256**: p. 274-280.
26. Song, X., et al., *Direct regeneration of cathode materials from spent lithium iron phosphate batteries using a solid phase sintering method.* RSC Advances, 2017. **7**(8): p. 4783-4790.
27. Li, L., et al., *Recovery of metals from spent lithium-ion batteries with organic acids as leaching reagents and environmental assessment.* Journal of Power Sources, 2013. **233**: p. 180-189.
28. Li, L., et al., *Recovery of cobalt and lithium from spent lithium ion batteries using organic citric acid as leachant.* Journal of Hazardous Materials, 2010. **176**(1): p. 288-293.
29. Kepler, K.D., et al., *Process for recycling electrode materials from lithium-ion batteries* I. Farasis Energy, Editor. 2016.
30. Contestabile, M., S. Panero, and B. Scrosati, *A laboratory-scale lithium-ion battery recycling process.* Journal of Power Sources, 2001. **92**(1): p. 65-69.
31. Gao, W., et al., *Lithium Carbonate Recovery from Cathode Scrap of Spent Lithium-Ion Battery: A Closed-Loop Process.* Environmental Science & Technology, 2017. **51**(3): p. 1662-1669.
32. Dorella, G. and M.B. Mansur, *A study of the separation of cobalt from spent Li-ion battery residues.* Journal of Power Sources, 2007. **170**(1): p. 210-215.
33. Lee, C.K. and K.-I. Rhee, *Preparation of LiCoO2 from spent lithium-ion batteries.* Journal of Power Sources, 2002. **109**(1): p. 17-21.
34. Shin, E.J., et al., *A green recycling process designed for LiFePO4 cathode materials for Li-ion batteries.* Journal of Materials Chemistry A, 2015. **3**(21): p. 11493-11502.
35. Zou, H., et al., *A novel method to recycle mixed cathode materials for lithium ion batteries.* Green Chemistry, 2013. **15**(5): p. 1183-1191.

36. Gratz, E., et al., *A closed loop process for recycling spent lithium ion batteries.* Journal of Power Sources, 2014. **262**: p. 255-262.
37. Pan, L., S. Jung, and R.-H. Yoon, *A fundamental study on the role of collector in the kinetics of bubble-particle interaction.* International Journal of Mineral Processing, 2012(106-109): p. 37-41.
38. Pan, L., S. Jung, and R.H. Yoon, *Effect of hydrophobicity on the stability of the wetting films of water formed on gold surfaces.* Journal of Colloid and Interface Science, 2011. **361**(1): p. 321-330.
39. Paulson, O. and R.J. Pugh, *Flotation of Inherently Hydrophobic Particles in Aqueous Solutions of Inorganic Electrolytes.* Langmuir, 1996. **12**(20): p. 4808-4813.
40. Wakamatsu, T. and Y. Numata, *Flotation of graphite.* Minerals Engineering, 1991. **4**(7): p. 975-982.
41. Kim, Y., et al., *Recovery of LiCoO2 from wasted lithium ion batteries by using mineral processing technology.* Resources Processing, 2004. **51**(1): p. 3-7.
42. Smith, W.N. and S. Swoffer, *Recovery of lithium ion batteries*. 2013.
43. Dell, C.C., *Release analysis - a new tool for ore dressing research*, in *Recent development in mineral dressing* 1953, Institution of Mining and Metallurgy: London. p. 75-84.
44. Forrest, W.R., G.T. Adel, and R.H. Yoon, *Characterizing Coal Flotation Performance Using Release Analysis.* Coal Preparation, 1994. **14**(1-2): p. 13-27.
45. Shao-Horn, Y., et al., *Atomic resolution of lithium ions in LiCoO2.* Nature Materials, 2003. **2**: p. 464.
46. Trahar, W.J., *A rational interpretation of the role of particle size in flotation.* International Journal of Mineral Processing, 1981. **8**(4): p. 289-327.
47. Zheng, X., N.W. Johnson, and J.P. Franzidis, *Modelling of entrainment in industrial flotation cells: Water recovery and degree of entrainment.* Minerals Engineering, 2006. **19**(11): p. 1191-1203.
48. Xu, M., *Modified flotation rate constant and selectivity index.* Minerals Engineering, 1998. **11**(3): p. 271-278.
49. Trahar, W.J., *The selective flotation of galena from sphalerite with special reference to the effects of particle size.* International Journal of Mineral Processing, 1976. **3**(2): p. 151-166.
50. Gaudin, A.M., J.O. Groh, and H.B. Henderson, *Effect of particle size on flotation.* Am. Inst. Min. Metall. Eng., 1931. **414**: p. 3-23.
51. Hanisch, C., et al., *Recycling of lithium-ion batteries: a novel method to separate coating and foil of electrodes.* Journal of Cleaner Production, 2015. **108**: p. 301-311.
52. Tian, L.y., X.b. Huang, and X.z. Tang, *Study on morphology behavior of PVDF-based electrolytes.* Journal of Applied Polymer Science, 2004. **92**(6): p. 3839-3842.
53. Chiu, F.-C. and Y.-J. Chen, *Evaluation of thermal, mechanical, and electrical properties of PVDF/GNP binary and PVDF/PMMA/GNP ternary nanocomposites.* Composites Part A: Applied Science and Manufacturing, 2015. **68**: p. 62-71.

54. Zhang, X., et al., *Sustainable Recycling and Regeneration of Cathode Scraps from Industrial Production of Lithium-Ion Batteries.* ACS Sustainable Chemistry & Engineering, 2016. **4**(12): p. 7041-7049.
55. Pan, L. and R.-H. Yoon, *Measurement of hydrophobic forces in thin liquid films of water between bubbles and xanthate-treated gold surfaces.* Minerals Engineering, 2016. **98**: p. 240-250.
56. Pierson, H.O., *Handbook of Carbon, Graphite, Diamonds and Fullerenes* 1994: Noyes Publications.
57. Honaker, R.Q., *High capacity fine coal cleaning using an enhanced gravity concentrator.* Minerals Engineering, 1998. **11**(12): p. 1191-1199.
58. Falconer, A., *Gravity separation: old technique/new methods.* Physical Separation in Science and Engineering, 2003. **12**(1): p. 31-48.
59. Fuerstenau, M.C., G.J. Jameson, and R.-H. Yoon, *Froth flotation: a century of innovation*. 2007: SME.
60. Luttrell, G.H., *Coal Preparation*, in *Meeting Projected Coal Production Demands in the USA*. 2008. p. 106-143.

4 Effect of Solid Electrolyte Interphase on Anode and Cathode Materials Separation by Froth Flotation

4.1 Introduction

Recycling lithium-ion batteries (LIBs) is an essential component to develop sustainable energy storage solutions to combat the climate change.[1] Lately, this topic has attracted attention from academia, general public, media, as well as the governments across the globe for its social, environmental and economic benefits.[2, 3] Spent LIBs pose significant health, safety, and environmental risks.[4-6] Inappropriate management of spent LIBs may lead to severe fire and explosions.[7] Heavy metals and toxic electrolytes from Li-ion batteries may cause groundwater pollution.[8] On the other hand, LIBs contain significant amounts of valuable metals and other materials.[9-11] Recycling and reusing components from spent LIBs may enable a sustainable supply of raw materials that can be used in manufacturing and may lower the life-cycle cost of LIBs.[12, 13]

Past efforts have been devoted to recovering black mass from spent lithium-ion batteries using a conventional hammer milling process.[14, 15] The recovered black mass consists of electrode materials with trace amounts of impurities, including current collectors, separators, and casing.[16] Among them, the most valuable components are cathode materials, which contain lithium (Li), nickel (Ni), and cobalt (Co).

The recovery of metal values from the black mass has been investigated using both the pyrometallurgical and hydrometallurgical processes. The pyrometallurgical process smelts cathode active materials to metal alloys using reducing agents at a temperature of 800 – 1000°C, while leaving both lithium and other metals in slags.[17] Unfortunately, the pyrometallurgical process recovers transition metals only, and many of other battery components/elements, such as graphite and lithium, are either decomposed or wasted. The thermal decomposition of organic binder may generate toxic, fluorine-containing gas compounds that must be captured and treated.[18]

Hydrometallurgical routes for metal extraction have also been extensively investigated.[19-22] Metals in cathode materials are digested using inorganic acids (e.g., H_2SO_4 or HCl),[23, 24] organic acids,[25] ammonia,[26-28] and, more recently, deep eutectic solvents.[29] Generally, metals in these solutions are purified by precipitation and solvent extraction.[21, 30, 31] Valuable metals are then recovered in the form of pure metals, metal hydroxides, and metal sulfates.[14, 19, 30, 32] However, the hydrometallurgical process may damage anode materials during the leaching process, and, thus, may not be suitable for the upcycling of spent anode materials.

The third route for LIB recycling is direct recycling.[2, 33-35] The direct recycling process separates and recovers individual battery components from spent LIBs in the solid phase while preserving their functional integrity for new battery manufacturing. Direct recycling involves 1) a separation and purification of cathode active materials, and 2) a repair and rejuvenation of aged cathode active materials to their original electrochemical performance. Separating anode and cathode materials from the black mass is an essential component for the direct recycling process.

Froth flotation was introduced in the separation of anode and cathode materials from black mass.[34, 36] Graphite particles, used as the anode materials, are naturally hydrophobic, while metal oxides (cathode) are hydrophilic. Froth flotation process separates mixed materials based on the difference in surface hydrophobicity. Any changes to surface properties of the electrode materials may impact the degree of separation. For lightly degraded, spent Li-ion batteries, there were no significant changes in the surface properties of the electrode materials. Therefore, anode and cathode materials can be separated from each other by froth flotation using hydrocarbon oils as collectors. It was shown that the tailing product after the froth flotation consisted of 90% pure metal oxide and the recovery was approximately 80%.[37] The impurities present in the tailing products were PVDF binder and carbon additives from the cathode composites. However, for severely degraded cells, the degree of separation of aged anode and cathode materials seemed to be inferior to that obtained with lightly-degraded cells.[38]

Various strategies were developed to improve the performance of separation of the aged anode and cathode materials by froth flotation.[39] One of the strategies is thermal pyrolysis, i.e. a heating process at various gas environments, prior to the flotation separation. The process was originally developed to delaminate electrode materials from current collectors by decomposing PVDF binder. The decomposition of PVDF binder and carbon additives results in a weak binding between electrode composite layers and current collectors.[40, 41]

The degree of separation of the anode and cathode materials by froth flotation improves after a heating step.[38, 42] It was previously shown that a good separation between the anode and cathode materials was accomplished after a heating process in vacuum at 550°C. The tailing product consisted of 94.72% pure cathode active materials at a recovery rate of 83.75%.[43] The authors claimed that the improvement in separation was attributed to a removal of organic binder. Similar experiments were conducted under the N_2 environment at a temperature of 550°C.[38] However, the recovery rate of metal oxides in the tailing product was only 49.6%. In addition, ultrasonic cleaning, ball grinding, and cryogenic grinding pretreatments showed some benefits to the froth flotation process.[44, 45] It is anticipated that the solid electrolyte interphase (SEI) layers are present on the surface of the anode materials after cycling.[46-48] Unfortunately, very few efforts have been devoted to unfolding the mechanism involved in the impact of the SEI layers on the performance of the froth flotation separation process.

In this study, the flotation separation of aged anode and cathode materials from spent LIBs was systematically investigated by treating the black mass at different temperatures. Upon a pyrolysis treatment, the organic SEI layers on the surface of aged anode materials was decomposed. The bulk composition of the separated products was determined by thermogravimetric analysis (TGA) as well as scanning electron microscopy (SEM) coupled with energy-dispersive X-ray spectroscopy (EDX). Further information regarding surface characteristics and composition was obtained through contact angle measurements, X-ray photoelectron spectroscopy (XPS), and scanning transmission electron microscopy (STEM).

4.2 Experiment

4.2.1 Materials

Two types of 18650-type lithium-ion battery cells (Samsung 18650-26F and LG ABC21865) were used in this study. The spent battery cells were obtained by removing battery packs from used laptops. Deionized (DI) water was used in all experiments, and it was obtained from a Barnard water purification system (Thermo Fisher). The DI water had a resistance of above 18.1 megohm-cm. Figure 4-1 shows a procedure to prepare black mass from spent LIBs. Prior to disassembly, the cells were discharged to below 2.8 V at a C/10 rate to minimize fire and explosion risk. The discharged battery cells were opened using a rotary cutter under a fume hood. The outer casing was removed manually, and battery cores were unfolded manually to separate individual electrode layers. The electrode layers were rinsed with DI water for 3 to 4 times to remove excess electrolyte and solvents. Anode and cathode electrode sheets were cut into 2.5- × 2.5-cm (1 inch × 1 inch) pieces using a scissor. The cut pieces were placed in a commercial blender with DI water to prepare a slurry, and the slurry was mixed at 5000 RPM for 5-10 seconds to delaminate electrode materials from the current collectors. Since the electrode materials were much finer than individual current collectors, the electrode active powders were separated from current collectors by sieving using a 140-mesh screen. The undersized fraction consisted of electrode materials with less than 0.5% of current collector materials, which was confirmed with ICP analysis. The slurry was dewatered to remove organic solvent residues and vacuum filtered. The filter cake was rinsed three times. The anode and cathode powders were dried in an oven overnight at 105°C prior to the heating step.

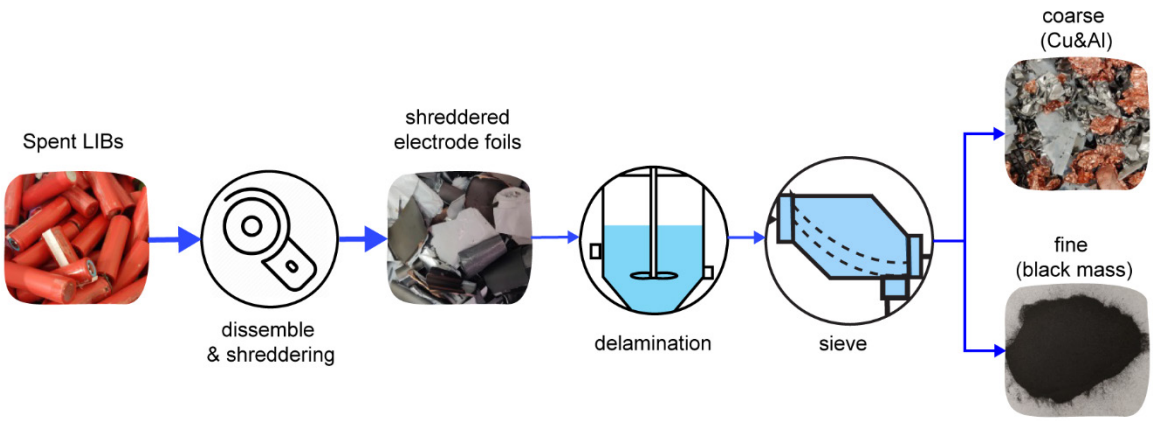

4.2.2 Thermal Pyrolysis

Thermal pyrolysis was conducted prior to the froth flotation process. A small quantity of black mass samples was placed in a ceramic crucible and transferred to a box furnace (Thermolyne FB1315M) for different time periods. The furnace was operated in air.

4.2.3 Froth flotation

Froth flotation experiments were conducted using a 1-L laboratory-scale Denver cell. Kerosene was used as the collector, and methyl isobutyl carbinol (MIBC) was used as the frother. The detailed experimental procedure can be found elsewhere.[34] Laboratory-scale froth flotation experiments were conducted using two protocols: 1) a modified release-analysis protocol,[49] and 2) a batch-kinetic protocol.[50] The release analysis protocol provided an ultimate measure of separability of the mixed materials by froth flotation. This procedure consisted of two stages. The first stage was to separate floatable materials from non-floatable materials while minimizing entrainments in the froth layers. This was accomplished by refloating froth concentrates 2-3 times. The second stage of the protocol was to separate floatable materials by different degrees of floatability. Since the total amount of the sample used in each experiment was less than 30 grams, the second stage of the protocol was not used in this work. In using the batch-kinetic protocol, successive samples of froth products were collected. A total of four to six froth concentrate samples were skimmed off at 0.5, 1, 2, 3, 4, and 6 minutes until no materials were floated on the froth layer. Both the froth and tailing products were dried overnight in the oven and weighted. The dried products were analyzed by SEM and TGA to obtain their chemical and material compositions.

4.2.4 Material Characterization

Thermogravimetric analyses (TGA) were conducted using a LECO TGA 701 thermogravimetric analyzer. The temperature was raised from room temperature to 800 ℃ at a rate of 1 ℃/min under an air flow rate of 7 L/min. Approximately 1 gram of each sample was used in the analysis.

Both the chemical composition and morphology of particles in the samples were determined using scanning electron microscopy (SEM) coupled with energy-dispersive X-ray spectroscopy (EDX). In determining chemical compositions, powder samples were placed on a carbon tape affixed to an aluminum pin stub. Excess powders were removed with canned air. Specimens were plasma coated with a 7-nm layer of platinum/palladium (Pt/Pd). Imaging and elemental mapping was performed in a Philips XL40 Environmental Scanning Electron Microscope (ESEM) at 15kV accelerating voltage under high-vacuum conditions. Images were obtained in a Back Scattered Electron (BSE) mode, and elemental mapping was conducted in a Secondary Electron (SE) mode.

The electron micrographs and EDX maps were obtained using a FEI Titan Themis aberration-corrected, scanning transmission electron microscope (STEM) operated at 200 KeV. The point resolution in the aberration-corrected mode was 0.08 nm. The microscope was fitted with a SuperXTM X-ray detector, which was a combination of 4 detectors for fast X-ray mapping in STEM mode. Nanometer resolution EDX maps were taken at an average beam current of 100 pA. The size of the maps was 512 × 512 pixels, and 50μs/pixel dwell time were used for collecting the signal. All maps were generated by summing over 10 frames. The drift correction during data collection and subsequent analysis were performed using Velox software.

4.2.5 Contact Angle Measurement

Surface hydrophobicity of the samples was determined by measuring water contact angles on a pressed powder plate using the sessile droplet technique. In using this method, powder samples were pressed into a thin plate by means of a hydraulic press using a 10-mm diameter dry pellet die. In making each plate, 0.07 grams of electrode powder were used. The pressed, thin plate was carefully placed on a stage of a customized, contact angle goniometer. A tiny droplet of water was placed on a plate using of a micro-syringe, and multiple side-view images were taken. From the images, the water contact angle was determined along the three-phase contact line. For hydrophilic powders, water slowly penetrated the cake caused cake fracking, and as a result, no contact angle data was obtained. In this study, at least three samples were evaluated, and average value was reported.

4.2.6 X-ray Photoelectron Spectroscopy (XPS)

The surface composition of the samples was characterized by XPS using PHI 5000 VersaProbe II system (Physical Electronics). The base pressure in the XPS chamber was $\sim 1 \times 10^{-8}$ torr. The X-ray source was operating at 25 W with monochromatic Al Kα radiation (hυ = 1486.6 eV), Ar+-ion and electron beam sample neutralization, and fixed analyzer transmission mode. The survey scans were acquired at 117.8eV. The high-resolution spectra of all samples were collected at a pass energy of 23.50 eV and electron escape angle of 45° to the sample plane. The spot size for X-ray beam was set to 100 μm. The Shirly background data were subtracted from all spectra. The reported binding energies were calibrated to adventitious carbon at a binding energy of 284.8 eV. The spectra were fitted to multiple Gaussian-Lorentz peaks by using the software package (Multipack) that Physical Electronics provided.

4.3 Results and Discussion

4.3.1 Thermal Pyrolysis

Figure 4-2 compares the SEM and EDX mapping (C, O, F, Co) images of the black mass with and without heating the black mass to a temperature of 400℃, 450℃ and 500℃ for 1 hour. As shown, without the heating treatment, there were agglomerates of cathode materials held together by PVDF binders. After a heating treatment at 400 ℃ for 1 hour (Fig. 4-2b), there were no significant changes in both the morphology and chemical composition of the black mass. At temperatures of 450 ℃ (Fig. 4-2c) and 500 ℃ Fig. 4-2d), the size of the electrode materials was significantly reduced. The presence of single cathode material was attributed to a decomposition of PVDF binders.

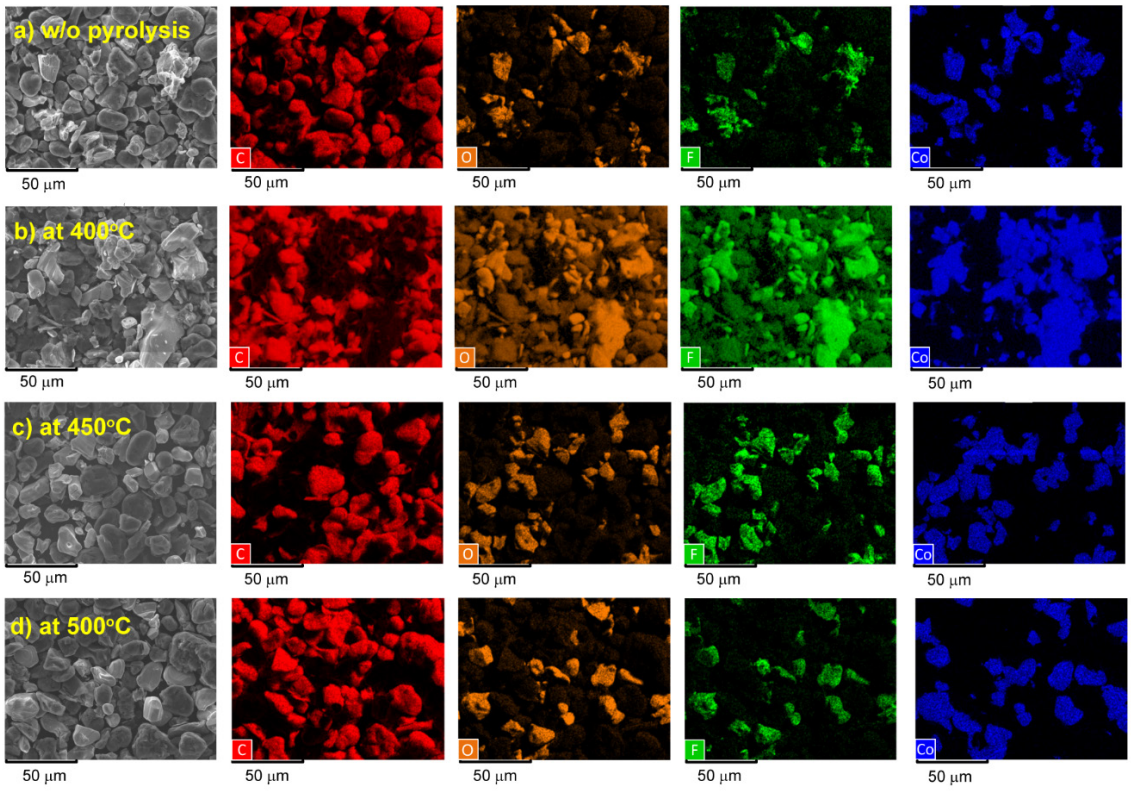

There was a trace amount (<1%) of fluorine detected on the surfaces of cathode particles after a pyrolysis process at 450 °C or above for 1 hour; the PVDF binders were now fully decomposed. The presence of fluorine was associated with metal fluoride on the surfaces of cathode materials due to the aging of Li-ion batteries [51], and/or a reaction of HF with cathode during the water-based recycling process. Nevertheless, the presence of fluorine-containing species does not significantly impact the hydrophilic nature of the cathode surface.

4.3.2 Froth flotation

4.3.2.1 Release Analysis

Figure 4-3 shows the flotation results with aged anode and cathode materials from spent LIBs with and without the pyrolysis pretreatment. The results are shown as the recovery *vs*. grade of the cathode active materials in the tailing. The separation performance of the anode and cathode materials improves as the recovery *vs*. grade points are shifted towards the top right-handed corner. For black mass without the heating step, the separation performance varied with the types of LIBs. For instance, one result showed that the flotation process produced 86.29% pure metal oxide at a recovery rate of 88.4%.

However, one result obtained with another LIB sample exhibited an inferior result, i.e., 55.11% recovery of oxides in the tailing product. The inconsistency in the separation performance was attributed to a non-uniformity of the surface properties of the electrode materials. An ability to restore the original surface properties of the electrode materials is critical to obtain a good separation of mixed electrode materials.

Also shown in Figure 4-3 are the separation results obtained after a pyrolysis treatment. It was found that the separation of aged anode and cathode materials was significantly improved after a heating step. For instance, at 500℃, the temperature at which PVDF binders were decomposed, the grade of metal oxide materials in the tailing product reached 98.50%, suggesting that almost all anode materials were reported to the froth product. The recovery of the metal oxide materials in the tailing increased from 75.97% after a 10-minute treatment to 99.78% after a 2-hr treatment.

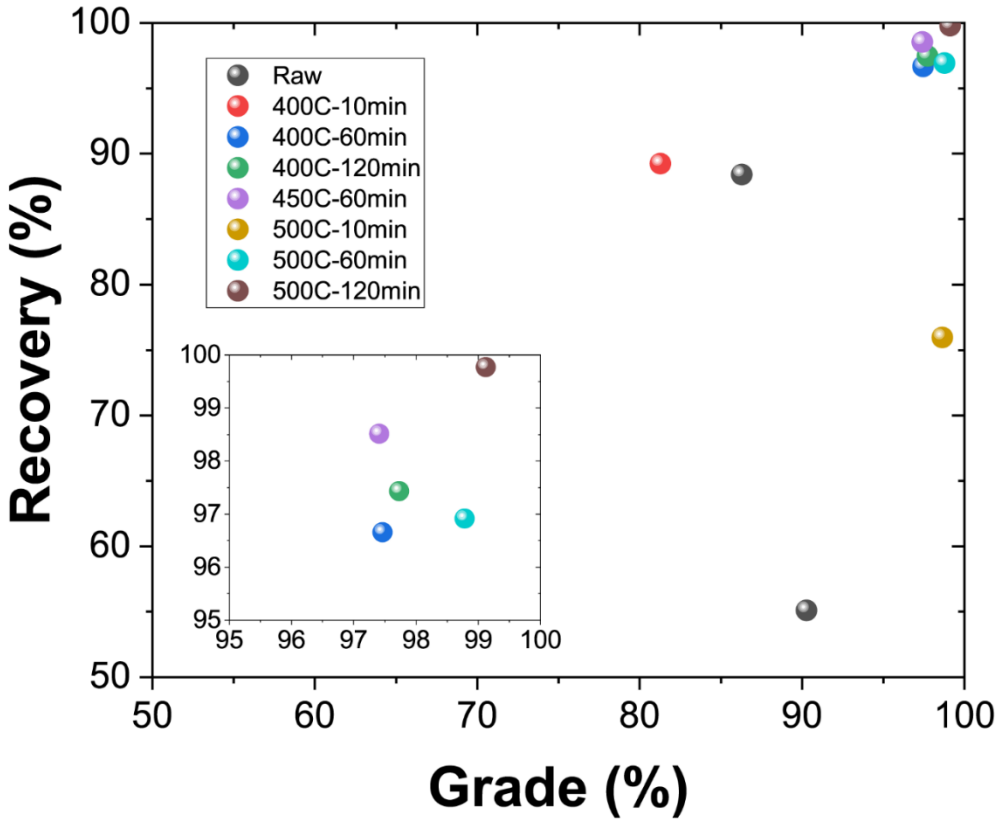

Figure 4-3. Recovery *vs*. grade of metal oxide materials in the tailing product after pyrolysis treatments at various temperatures and duration.

It is interesting to note that the result obtained after a pyrolysis treatment at 400℃ is comparable to that obtained at 450 and 500℃. The result shows that when the black mass was treated at 400ºC for two hours, the tailing product consisted of 97.73% pure metal oxide materials with all anode materials being rejected to the froth product This result was largely unexpected, since majority of the PVDF binder was still intact. Evidently,

there was an additional factor that contributed to the improvement of the anode/cathode separation by the froth flotation process, which was not previously revealed.

Table 4-1 shows the composition of both the froth and tailing products from the black mass with and without the pyrolysis treatment for 1 hour. Without the pyrolysis treatment, the floatable materials consisted of 78% graphite, 15.54% metal oxide and 6.48% PVDF binder and carbon additives combined. The tailing product consisted of 11.1% graphite, 2.61% PVDF binder and carbon additives combined, and 86.29% metal oxide. The presence of PVDF in the tailing product may be attributed to an encapsulation of PVDF binder in the cathode agglomerates. A significant improvement in the degree of separation of aged anode and cathode materials was also observed after a heating step at 400 ℃ for 1 hour. The tailing product consisted of 98.6% metal oxides and 1.4% PVDF and carbon additives combined. No anode material was found in the tailing product. On the other hand, the froth product consisted of 92% anode materials, 3.83% PVDF and carbon additive combined, and 4.3% metal oxides.

Table 4-1. Composition of froth and tailing products from spent black mass by froth flotation with and without pyrolysis treatment at different temperature.

Pre-treatment	Product	Composition (%)		
		Graphite	PVDF/C	Cathode
w/o pyrolysis	Froth	77.98%	6.48%	15.54%
	Tailing	11.1%	2.61%	86.29%
Pyrolysis at 400 ℃	Froth	91.89%	3.83%	4.28%
	Tailing	0%	1.38%	98.62%
Pyrolysis at 450 ℃	Froth	98.07%	-	1.93%
	Tailing	2.59%	-	97.41%
Pyrolysis at 500 ℃	Froth	96.08%	-	3.92%
	Tailing	0.34%	-	99.66%

Figure 4-4 shows SEM and EDX images of the froth and tailing products from the black mass without a pyrolysis treatment. Without the treatment, there were large cathode agglomerates (>50 µm) in the tailing product. The PVDF binder was encapsulated in the cathode agglomerates. In addition, there was a significant amount of anode materials present in the tailing product. In contrast, there were cathode materials and PVDF binder in the froth product. The presence of cathode materials in the froth product was attributed to the PVDF binder on the surface of the cathode particles.

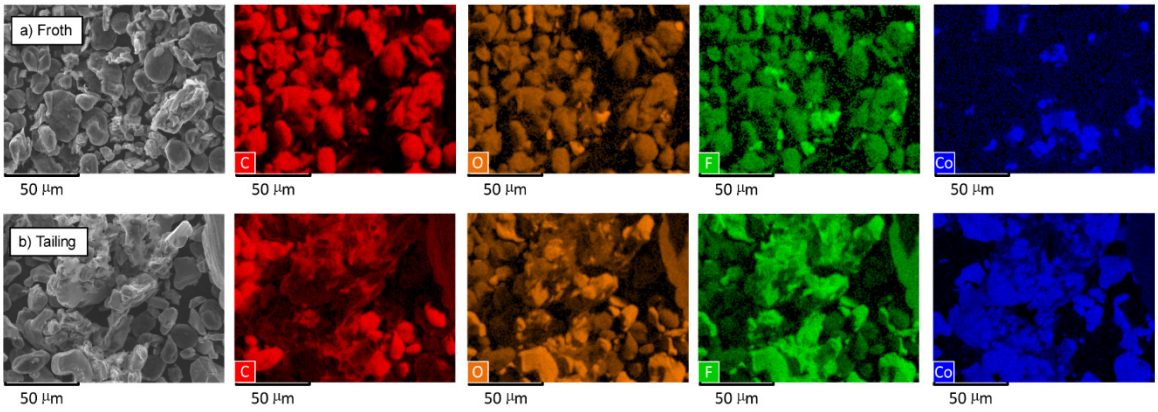

Figure 4-4. SEM/EDX images of froth and tailing products from black mass without a pyrolysis treatment.

Figure 4-5 show SEM and EDX images of both froth and tailing products from aged black mass after heating at 400 ℃ for 1 hour. There are large cathode agglomerates in the tailing product, possibly encapsulating some PVDF binders. The froth product contained a few cathode particles. Similar results were obtained after heating at 500 ℃ for 1 hour (Figure 4-6). There were single individual cathode particles in the tailing, suggesting that majority of PVDF decomposed.

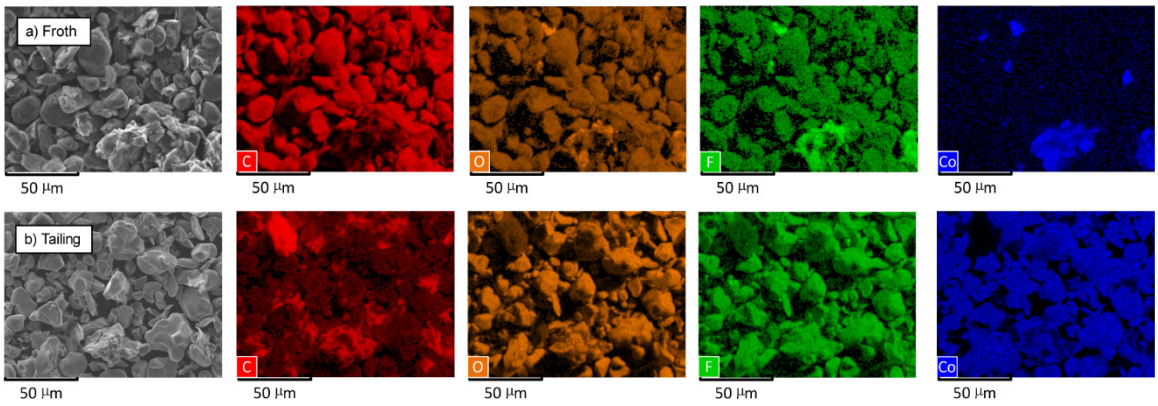

Figure 4-5. SEM/EDX images of a) a froth product and b) a tailing product from the aged black mass after a pyrolysis treatment at 400℃ for 1 hour.

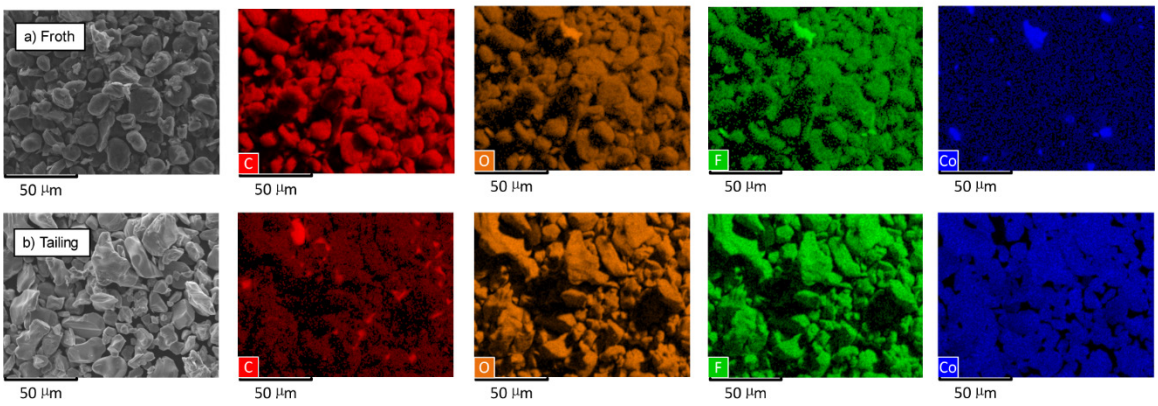

Figure 4-6. SEM/EDX images of a) a froth product and b) a tailing product from the aged black mass after a pyrolysis treatment at 500℃ for 1 hour.

4.3.2.2 Flotation Kinetics

To further illustrate the impact of heating temperature on the froth flotation separation of the aged anode and cathode materials, froth flotation experiments were conducted using the batch kinetic protocol. Figure 4-7a shows the cumulative percentage of PVDF and carbonaceous materials in the froth product as a function of the flotation time. Without a pyrolysis treatment, 55.48% of the impurities was removed after a 1-minute flotation time. After 6 minutes flotation time, the amount of impurities removed reached 75.06%. In comparison, after heating to 400℃ and 500℃, the amount of impurities removed was >90% after 1 minute and >97% after 4 minutes flotation times, demonstrating the effectiveness of froth flotation in removing hydrophobic materials.

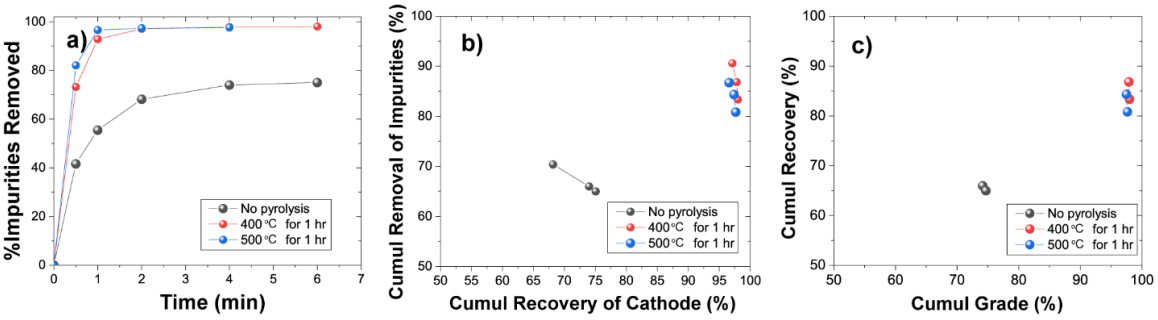

Figure 4-7. Froth flotation result with aged black mass sample using a batch kinetic procedure. a) Percentage of impurities removed by the froth flotation process vs. the flotation time; b) Cumulative removal of impurities vs. the cumulative recovery of cathode materials; c) Cumulative recovery of cathode vs. cumulative grade of cathode materials.

Figure 4-7b shows the cumulative recovery of cathode active materials versus the cumulative removal of impurities, and Figure 4-7c shows the cumulative recovery versus the cumulative grade of the cathode materials in the tailing product. Both performance curves shifted to the right after a heating step, suggesting that the separation performed better after heating. With one rougher stage, a tailing product was obtained that consisted of 96% cathode materials at a recovery rate of >90%. It should be noted that the separation results obtained after heating to 500℃ for 1 hour were slightly worse than those obtained after heating to 400℃. A better separation performance obtained at 400 ℃ may be attributed to a lower entrainment of fine particles in the froth layers and a higher surface hydrophobicity of the aged anode materials.

Contact angle measurements were conducted to better understand the change in surface hydrophobicity of both the anode and cathode materials after a pyrolysis treatment. The contact angle data obtained in this work were smaller than those reported in the literature in which polished flat surfaces were used.[52] This discrepancy was attributed to the surface roughness of the pressed cake.[53] The result (Table 4-2) shows that, without the pyrolysis treatment, the average contact angle of anode composites was 36.22°, while that of cathode composites was 54.67°. Upon heating at 400 ℃ for 1 hour, the contact angle on the anode surfaces was increased to 45.54º. The contact angles on the anode composite materials slightly decreased to 40º and 39º after heating at 450 and 500℃, respectively. The initial increase in the surface hydrophobicity of the aged anode may be attributed to the removal of hydrophilic layers on surfaces. At the temperatures of 450℃ and above, the PVDF binder decomposed, resulting in a decrease in the surface hydrophobicity.

On the contrary, the surface hydrophobicity of the cathode composite materials decreased monotonically with increasing the process temperature. For instance, without the heating step, the water contact angle on the cathode composite materials was 54º. After heating at 400℃ for 1 hour, the water contact angle decreased to 24º. No contact angles were measured with oxide materials obtained after heating at 450 ℃ and 500ºC for 1 hour. This was because the water penetrated into the cake by the capillary force immediately after a liquid drop was placed on the surface.

Table 4-2. Effect of temperature on the contact angle of anode and cathode composites with and without pyrolysis treatment for 1 hour.

Pre-treatment	Anode	Cathode
w/o pyrolysis	36.2º	54.6º
Pyrolysis at 400 ℃	45.5º	24.2º
Pyrolysis at 450 ℃	40.1º	-*
Pyrolysis at 500 ℃	39.0º	-*

4.3.3 Mechanisms and Discussion

To better understand the impact of the pyrolysis treatment on the surface composition of the aged anode materials, XPS experiments were performed on the aged anode materials from spent LIBs. Table 4-3 shows the atomic concentration of the aged anode materials from spent LIBs with and without a pyrolysis treatment. The XPS survey result shows that, without the pyrolysis treatment, carbon content on the surface of the aged anode materials was 85.40%, and the oxygen and fluorine contents were 12.52% and 1.83%, respectively. With the treatment, the carbon content increased to 88.95% at 400 ℃ and 95.20% at 500 ℃, while the oxygen content decreased to 8.39% at 400℃ and 4.31% at 500℃. The lower surface concentration of oxygen and higher carbon indicated an organic surface layer was removed by the heating process and the graphitic carbon was consequently exposed. The decrease in oxygen content contributed to an increased surface hydrophobicity of the anode materials.

Table 4-3. Elemental composition by atomic numbers on the surfaces of aged anode materials with and without the pyrolysis treatment determined by XPS.

Pre-treatment	C1s	O1s	F1s	P2p	Na1s
Without pyrolysis	85.40%	12.52%	1.83%	0.25%	0%
Pyrolysis at 400 ℃	88.95%	8.39%	0.99%	0.58%	1.09%
Pyrolysis at 500 ℃	95.20%	4.31%	0.28%	0.21%	0%

From Table 4-3, the fluorine content on anode surfaces decreased from 1.83% without the treatment to 0.99% and 0.28% after heating to 400 and 500 ℃, respectively. The decrease in the fluorine concentration with increasing the temperature was attributed to a decomposition of PVDF binder on the surface. The other trace elements, e.g. P and Na, found in the XPS data may be attributed to the presence of electrolyte residue and water-based binders, such as carboxymethyl cellulose and/or styrene-butadiene rubber.

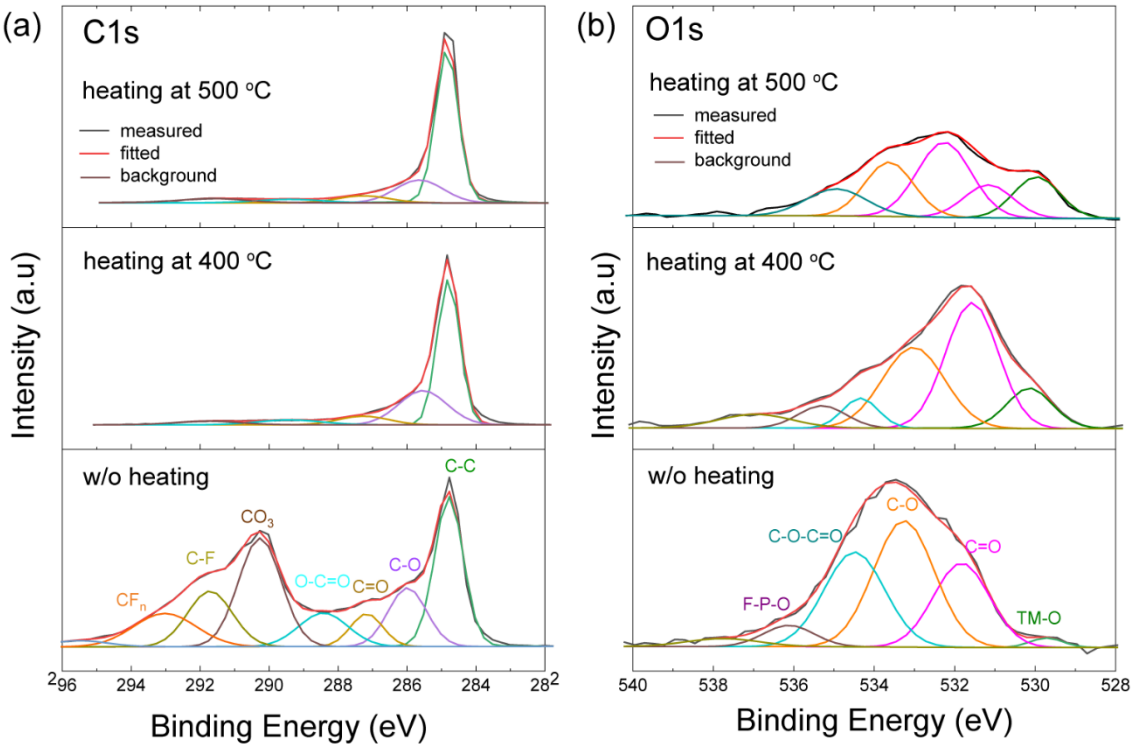

Figure 4-8. XPS spectra in C1s region and in O1s region of aged anode materials with and without pyrolysis processes. The spectra are from untreated, heating to 400 and to 500°C samples.

The detailed chemical composition of the aged anode materials was examined using high-resolution XPS. The C1s spectra (Fig. 4-8a) show a number of characteristic peaks present in the spent anode samples that were not treated thermally, which correspond to the carbons in the binder (CF_n, 294 eV, C-F, 292 eV), organic species on the anode surface (CO_3, 290 eV; O-C=O, 288 eV; C=O, 287.2 eV; C-O, 286 eV), and graphite (C-C, 284.2 eV). The organic species on the anode surface was most likely associated with solid electrolyte interphase (SEI) layer and was a result of cell cycling.[54] Upon heating at 500 °C, characteristic peaks associated with PVDF and the SEI layers disappeared, and only C-C bonds were seen on the anode surface. Note that all characteristic peaks associated with binder and SEI layers also disappeared after heating at 400°C, suggesting that this temperature effectively decompose the SEI layers and binder residues on surfaces. However, as seen from both the TGA and SEM data, there was still some binder entrained inside the cathode agglomerates; they did not completely decompose at this temperature.

The O1s spectra of the aged anode materials with and without the pyrolysis treatment are shown in Figure 4.8b. The characteristic peaks at 531.4 eV (e.g. C=O, C-OLi, RO-C=O), 532.2 eV (e.g. C-OH, C-O-C) and 533.7eV (e.g. C-O-C=O, P-O-P=O) were observed on the surfaces of aged anode materials without the treatment and are from the organic compounds in the SEI layers. With heating, the characteristic peaks for the aged anode materials changed. The peak intensities for the organic SEI species such as alcohol (C-

O), ether (C-O-C) and organic carbonates (C-O-C=O) decreased dramatically compared to those obtained without the heating step.

There may be trace amounts of transition metals (TMs) on the surface of anode materials, as seen in the XPS O1s spectra. This may be from the dissolution of TMs from the cathode and their deposition on the anode surface, which is quite common in NMC full cell systems.[55, 56] The formed inorganic TM-O compounds cannot be removed by heating.

Figure 4-9 shows a high angle annular dark field (HAADF) images of the aged anode materials at the surface with and without heating at 500 °C. Also shown in Figure 4-9 are the EDX data on the atomic fraction of carbon and oxygen from the bulk to the surface of the aged anode materials with and without a heating treatment. From the figure, the carbon content decreased while the oxygen content increased towards the surface of the aged anode materials that were not heated. After heating, the carbon content at the surface was >95% with less than 5% oxygen (within 20 nm below the surface). The difference in the carbon content at the surface contributed to the different flotation behaviors of the anode materials. The result is consistent with the previous findings.[57, 58].

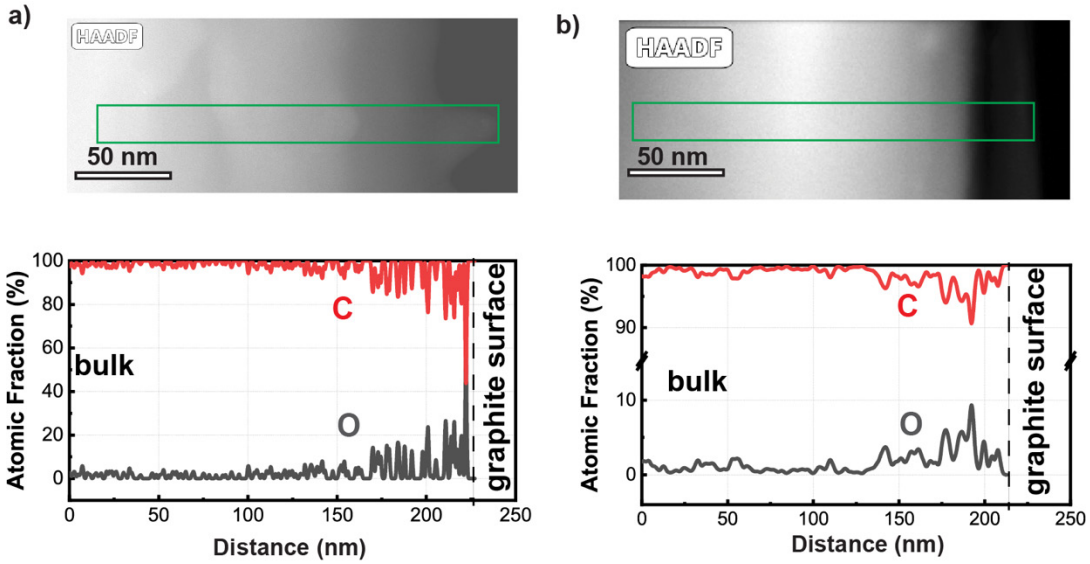

Figure 4-9. High angle annular dark field (HAADF) images and elemental analysis near the surface of the aged anode materials a) without and b) with a heating process at 500 °C.

In this study, we showed that not only the PVDF binder but also the SEI layers due to cycling impact how well the anode and cathode materials from spent Li-ion batteries can be separated. The SEI layers had a thickness of ~20 nm, consisted of oxygen-rich organic species, lowering the hydrophobicity of the anode materials and resulting in an unsuccessful separation of the aged anode and cathode materials. The pyrolysis process

removed the organic-rich SEI layers from the anode surface, restoring its original hydrophobicity. Now, the aged active materials can be separated easily.

Different strategies to remove the SEI layers on both the anode and cathode materials should be investigated in future. The removal of the SEI layers will be essential for the froth flotation process to be more efficiently used in a battery recycling application. With new types of binders and additives being developed and used in the LIBs, future work should be focused on developing other alternative technologies for separation of the anode and cathode materials.

4.4 Conclusion and Summary

The effect of thermal pyrolysis treatment on the froth flotation separation of aged anode and cathode materials from end-of-life Li-ion batteries was investigated using both modified release- analysis and batch-kinetic protocols. The results show that, after heating at temperatures of 450 ℃ and above, the performance of the froth flotation process was significantly improved due to a decomposition of the organic binder. The present result also showed that the separation performance after heating at 400 ℃ for an hour was comparable to the that obtained after heating at 500 ℃, which was contrary to the conventional wisdom that a complete removal of PVDF was necessary for a successful separation of aged anode and cathode materials.

The mechanism was examined using contact angle, XPS, and STEM analyses. The result showed that the water contact angle on the surface of the aged anode materials increased from 36^{o} without the heating to 45^{o} at 400 ℃ but decreased to 39-40^{o} at a higher temperature. Both XPS and STEM data showed that oxygen-rich, ~20 nm thick, SEI layers were present on the surfaces of the aged anode materials that were not heated. These SEI layers were removed at 400 ℃ or above for an hour, restoring their original hydrophobicity.

This work reveals for the first time the impact of the SEI layers on the separation of the aged anode and cathode materials by froth flotation from end-of-life LIBs. More specifically, the removal of the SEI layers on anode surfaces is essential to increase the grade of metal oxides in the tailing product, while the removal of PVDF binder may be necessary (but not mandatory) to achieve a high recovery. Technologies and strategies for removing organic SEI layers and PVDF binders are needed to achieve a good separation between battery materials in the future.

4.5 Reference

1. Ciez, R.E. and J.F. Whitacre, *Examining different recycling processes for lithium-ion batteries.* Nature Sustainability, 2019. **2**(2): p. 148-156.
2. Harper, G., et al., *Recycling lithium-ion batteries from electric vehicles.* Nature, 2019. **575**(7781): p. 75-86.
3. Gaines, L., *The future of automotive lithium-ion battery recycling: Charting a sustainable course.* Sustainable Materials and Technologies, 2014. **1-2**: p. 2-7.

4. Ellingsen, L.A.-W., et al., *Life Cycle Assessment of a Lithium-Ion Battery Vehicle Pack.* Journal of Industrial Ecology, 2014. **18**(1): p. 113-124.
5. Zeng, X., J. Li, and L. Liu, *Solving spent lithium-ion battery problems in China: Opportunities and challenges.* Renewable and Sustainable Energy Reviews, 2015. **52**: p. 1759-1767.
6. Xiao, J., J. Li, and Z. Xu, *Challenges to Future Development of Spent Lithium Ion Batteries Recovery from Environmental and Technological Perspectives.* Environmental Science & Technology, 2020. **54**(1): p. 9-25.
7. Feng, X., et al., *Thermal runaway mechanism of lithium ion battery for electric vehicles: A review.* Energy Storage Materials, 2018. **10**: p. 246-267.
8. Rahman, A., R. Afroz, and M. Safrin, *Recycling and Disposal of Lithium Battery: Economic and Environmental Approach.* IIUM Engineering Journal, 2017. **18**(2): p. 238-252.
9. Zheng, X., et al., *A Mini-Review on Metal Recycling from Spent Lithium Ion Batteries.* Engineering, 2018. **4**(3): p. 361-370.
10. Li, L., et al., *The Recycling of Spent Lithium-Ion Batteries: a Review of Current Processes and Technologies.* Electrochemical Energy Reviews, 2018. **1**(4): p. 461-482.
11. Olivetti, E.A., et al., *Lithium-Ion Battery Supply Chain Considerations: Analysis of Potential Bottlenecks in Critical Metals.* Joule, 2017. **1**(2): p. 229-243.
12. Richa, K., C.W. Babbitt, and G. Gaustad, *Eco-Efficiency Analysis of a Lithium-Ion Battery Waste Hierarchy Inspired by Circular Economy.* Journal of Industrial Ecology, 2017. **21**(3): p. 715-730.
13. Dunn, J.B., et al., *The significance of Li-ion batteries in electric vehicle life-cycle energy and emissions and recycling's role in its reduction.* Energy & Environmental Science, 2015. **8**(1): p. 158-168.
14. Gratz, E., et al., *A closed loop process for recycling spent lithium ion batteries.* Journal of Power Sources, 2014. **262**: p. 255-262.
15. da Costa, A.J., et al., *Beneficiation of cobalt, copper and aluminum from wasted lithium-ion batteries by mechanical processing.* International Journal of Mineral Processing, 2015. **145**: p. 77-82.
16. Zhang, T., et al., *Characteristics of wet and dry crushing methods in the recycling process of spent lithium-ion batteries.* Journal of Power Sources, 2013. **240**: p. 766-771.
17. Kwon, O.-s. and I. Sohn, *Fundamental thermokinetic study of a sustainable lithium-ion battery pyrometallurgical recycling process.* Resources, Conservation and Recycling, 2020. **158**: p. 104809.
18. Wang, M., et al., *A Facile, Environmentally Friendly, and Low-Temperature Approach for Decomposition of Polyvinylidene Fluoride from the Cathode Electrode of Spent Lithium-ion Batteries.* ACS Sustainable Chemistry & Engineering, 2019. **7**(15): p. 12799-12806.
19. Ferreira, D.A., et al., *Hydrometallurgical separation of aluminium, cobalt, copper and lithium from spent Li-ion batteries.* Journal of Power Sources, 2009. **187**(1): p. 238-246.

20. Chagnes, A. and B. Pospiech, *A brief review on hydrometallurgical technologies for recycling spent lithium-ion batteries.* Journal of Chemical Technology & Biotechnology, 2013. **88**(7): p. 1191-1199.
21. Chen, X., et al., *Hydrometallurgical recovery of metal values from sulfuric acid leaching liquor of spent lithium-ion batteries.* Waste Management, 2015. **38**: p. 349-356.
22. Yao, Y., et al., *Hydrometallurgical Processes for Recycling Spent Lithium-Ion Batteries: A Critical Review.* ACS Sustainable Chemistry & Engineering, 2018. **6**(11): p. 13611-13627.
23. Joulié, M., R. Laucournet, and E. Billy, *Hydrometallurgical process for the recovery of high value metals from spent lithium nickel cobalt aluminum oxide based lithium-ion batteries.* Journal of Power Sources, 2014. **247**: p. 551-555.
24. Meshram, P., B.D. Pandey, and T.R. Mankhand, *Hydrometallurgical processing of spent lithium ion batteries (LIBs) in the presence of a reducing agent with emphasis on kinetics of leaching.* Chemical Engineering Journal, 2015. **281**: p. 418-427.
25. Nayaka, G.P., et al., *Use of mild organic acid reagents to recover the Co and Li from spent Li-ion batteries.* Waste Management, 2016. **51**: p. 234-238.
26. Ku, H., et al., *Recycling of spent lithium-ion battery cathode materials by ammoniacal leaching.* Journal of Hazardous Materials, 2016. **313**: p. 138-146.
27. Zheng, X., et al., *Spent lithium-ion battery recycling – Reductive ammonia leaching of metals from cathode scrap by sodium sulphite.* Waste Management, 2017. **60**: p. 680-688.
28. Wang, H., et al., *Recovery of lithium, nickel, and cobalt from spent lithium-ion battery powders by selective ammonia leaching and an adsorption separation system.* ACS Sustainable Chemistry & Engineering, 2017. **5**(12): p. 11489-11495.
29. Tran, M.K., et al., *Deep eutectic solvents for cathode recycling of Li-ion batteries.* Nature Energy, 2019. **4**(4): p. 339-345.
30. Kang, J., et al., *Recovery of cobalt sulfate from spent lithium ion batteries by reductive leaching and solvent extraction with Cyanex 272.* Hydrometallurgy, 2010. **100**(3): p. 168-171.
31. Pranolo, Y., W. Zhang, and C.Y. Cheng, *Recovery of metals from spent lithium-ion battery leach solutions with a mixed solvent extractant system.* Hydrometallurgy, 2010. **102**(1): p. 37-42.
32. Lupi, C., M. Pasquali, and A. Dell'Era, *Nickel and cobalt recycling from lithium-ion batteries by electrochemical processes.* Waste Management, 2005. **25**(2): p. 215-220.
33. Gaines, L., *Lithium-ion battery recycling processes: Research towards a sustainable course.* Sustainable Materials and Technologies, 2018. **17**: p. e00068.
34. Zhan, R., Z. Oldenburg, and L. Pan, *Recovery of active cathode materials from lithium-ion batteries using froth flotation.* Sustainable Materials and Technologies, 2018. **17**: p. 1-9.
35. Shi, Y., G. Chen, and Z. Chen, *Effective regeneration of LiCoO 2 from spent lithium-ion batteries: a direct approach towards high-performance active particles.* Green Chemistry, 2018. **20**(4): p. 851-862.

36. Yu, J., et al., *A promising physical method for recovery of LiCoO2 and graphite from spent lithium-ion batteries: Grinding flotation.* Separation and Purification Technology, 2018. **190**: p. 45-52.
37. Shin, H., et al., *Electrochemical Performance of Recycled Cathode Active Materials Using Froth Flotation-based Separation Process.* Journal of The Electrochemical Society, 2020. **167**(2): p. 32-43.
38. Zhong, X., et al., *Pyrolysis and physical separation for the recovery of spent LiFePO4 batteries.* Waste Management, 2019. **89**: p. 83-93.
39. He, Y., et al., *Recovery of LiCoO2 and graphite from spent lithium-ion batteries by Fenton reagent-assisted flotation.* Journal of Cleaner Production, 2017. **143**: p. 319-325.
40. Yang, Y., et al., *Thermal treatment process for the recovery of valuable metals from spent lithium-ion batteries.* Hydrometallurgy, 2016. **165**: p. 390-396.
41. Hanisch, C., et al., *Recycling of lithium-ion batteries: a novel method to separate coating and foil of electrodes.* Journal of Cleaner Production, 2015. **108**(Part A): p. 301-311.
42. Wang, F., et al., *Recovery of valuable materials from spent lithium-ion batteries by mechanical separation and thermal treatment.* Journal of Cleaner Production, 2018. **185**: p. 646-652.
43. Zhang, G., et al., *Application of mechanical crushing combined with pyrolysis-enhanced flotation technology to recover graphite and LiCoO2 from spent lithium-ion batteries.* Journal of Cleaner Production, 2019. **231**: p. 1418-1427.
44. Liu, J., et al., *Recovery of LiCoO2 and graphite from spent lithium-ion batteries by cryogenic grinding and froth flotation.* Minerals Engineering, 2020. **148**: p. 106223.
45. Yu, J., et al., *Exploring the critical role of grinding modification on the flotation recovery of electrode materials from spent lithium ion batteries.* Journal of Cleaner Production, 2020. **274**: p. 123066.
46. Lu, M., H. Cheng, and Y. Yang, *A comparison of solid electrolyte interphase (SEI) on the artificial graphite anode of the aged and cycled commercial lithium ion cells.* Electrochimica Acta, 2008. **53**(9): p. 3539-3546.
47. An, S.J., et al., *The state of understanding of the lithium-ion-battery graphite solid electrolyte interphase (SEI) and its relationship to formation cycling.* Carbon, 2016. **105**: p. 52-76.
48. Heiskanen, S.K., J. Kim, and B.L. Lucht, *Generation and Evolution of the Solid Electrolyte Interphase of Lithium-Ion Batteries.* Joule, 2019. **3**(10): p. 2322-2333.
49. Dell, C., *An improved release analysis procedure for determining coal washability.* Journal of the Institute of Fuel, 1964. **37**: p. 149-150.
50. Xu, M., *Modified flotation rate constant and selectivity index.* Minerals Engineering, 1998. **11**(3): p. 271-278.
51. Li, D., et al., *Degradation mechanisms of C6/LiNi0.5Mn0.3Co0.2O2 Li-ion batteries unraveled by non-destructive and post-mortem methods.* Journal of Power Sources, 2019. **416**: p. 163-174.

52. Kozbial, A., et al., *Characterization of the Intrinsic Water Wettability of Graphite Using Contact Angle Measurements: Effect of Defects on Static and Dynamic Contact Angles.* Langmuir, 2017. **33**(4): p. 959-967.
53. Butt, H.-J., K. Graf, and M. Kappl, *Physics and Chemistry of Interfaces, 3rd Edition*. 2013, Weinheim, Germany: John Wiley & Sons. 161-163.
54. Wang, L., et al., *Identifying the components of the solid–electrolyte interphase in Li-ion batteries.* Nature Chemistry, 2019. **11**(9): p. 789-796.
55. Zhan, C., et al., *Dissolution, migration, and deposition of transition metal ions in Li-ion batteries exemplified by Mn-based cathodes – a critical review.* Energy & Environmental Science, 2018. **11**(2): p. 243-257.
56. Evertz, M., et al., *Unraveling transition metal dissolution of Li1.04Ni1/3Co1/3Mn1/3O2 (NCM 111) in lithium ion full cells by using the total reflection X-ray fluorescence technique.* Journal of Power Sources, 2016. **329**: p. 364-371.
57. Nie, M., et al., *Lithium Ion Battery Graphite Solid Electrolyte Interphase Revealed by Microscopy and Spectroscopy.* The Journal of Physical Chemistry C, 2013. **117**(3): p. 1257-1267.
58. Dollé, M., et al., *In situ TEM study of the interface carbon/electrolyte.* Journal of Power Sources, 2001. **97-98**: p. 104-106.

5 De-agglomeration of Cathode Composites and Its Purification by Flotation

5.1 Introduction

Li-ion batteries (LIBs) have become dominant energy storage devices for consumer electronics, electric vehicles (EVs), renewable energy storage, and grid applications. These LIBs have 3-12 years of lifetime depending on applications [1-3]. Once reaching their end of life, these batteries become hazardous materials in the waste stream and needs to be managed responsibly and environmentally [4, 5]. It is estimated that the amount of end-of-life (EOL) LIBs will rise as high as 160,000 metric tons per year by 2030 [6]. Recycling of LIBs not only keeps hazardous components from entering landfills [7-10], but also closes the loop of raw materials used in LIBs for resource conservation and long-term sustainability [11-15].

Recycling of LIBs might be cataloged into three different methods [16], namely pyro-metallurgy [17, 18], hydrometallurgy [19-23], and direct recycling process [24-26]. The pyrometallurgical process concentrates metal constituents such as cobalt and nickel in the molten phase, while other constituents such as aluminum and lithium in the slag phase. The metal alloys and slags are processed using hydrometallurgical methods to obtain pure metals or metal salts. The hydrometallurgical process first digests valuable metals within cathode active materials in acids [27, 28] and ammonia [29]. The valuable constituents in solutions such as cobalt and nickel are recovered in forms of metal sulfate [22, 30, 31], metal hydroxide [29, 32-34], or precursors [35-37] by chemical precipitation processes. The precursors are calcinated to synthesize cathode active materials [38].

Direct recycling is a third route for LIBs recycling. This method is designed to reuse cathode active materials from spent LIBs and/or manufacturing scraps in the manufacturing of new Li-ion batteries. This method has best economic and environmental benefits among the three recycling processes [39]. There are two steps involved: 1) recovery of electrode materials from LIBs, and 2) rejuvenation of recycled electrode materials. Much of previous efforts have been devoted to relithiation of spent cathode active materials [26, 40] using hydrothermal method [41, 42], electrochemical method [43], or direct calcination method [44]. All of these methods have been done at a laboratory scale by either peeling off electrode materials manually or dissolving binders in organic solvents.

The recovery of electrode materials from LIBs involves a delamination process and followed by a separation process. Various processes have been proposed to delaminate electrode composites from current collectors including ball milling [9, 45-47], impact milling [48-50], and cryogenic milling processes [13, 51, 52]. Since the delaminated electrode composite is much finer than the current collector, sieving can be used to separate electrode materials from other components [51]. A challenge is that these recycled cathode composite consists of 3-5% of carbon black and 3-5% polyvinylidene fluoride (PVDF) polymers. The presence of these impurities is detrimental to the follow-up rejuvenation process [53-55]. For instance, for the hydrothermal relithiation process to work, active materials react with lithium salt at a temperature of 180-220 ^{o}C followed by annealing at a temperature of 800 ^{o}C [56]. At this condition, both PVDF polymers and carbon additives might have been decomposed to CO_2 and HF [57], potentially causing a

change of surface properties of the electrode materials. Therefore, it is necessary to separate PVDF and carbon black from the cathode composite prior to the repairing and rejuvenation process.

Many processes have been developed to remove PVDF and/or carbon black from cathode composites [48, 58-60]. PVDF is an organic compound, and it is decomposed at a temperature of 500 ºC [61, 62]. An alternative method is a dissolution of PVDF binders in organic solvents, such as N-methyl pyrrolidone (NMP), dimethyl formamide (DMF), or dimethyl acetamide (DMAC) [59, 63]. The cathode active materials are then separated from slurries by filtration and/or centrifugation [64-66]. There are challenges associated with the use of solvents for the binder removal. First of all, solid-liquid separation might be difficult since a dissolution of PVDF molecules in organic solvents results in an increase in slurry viscosity [67]. Secondly, cleaning and drying of cathode active materials after solvent treatment might be costly and energy intensive, since some of the solvents evaporate at temperatures of above 100 ºC [68]. Last but not the least, most of solvents developed to date are not environmentally friendly.

The mechanical process provides an alternative solution for removing PVDF binders and carbon blacks from cathode composites. This process has been introduced for the purpose of delamination [69, 70] by means of agitation [71] and ultrasonication [49, 72]. The result from our past research showed that a fraction of PVDF binders might have been separated from cathode composites during the mechanical agitation process [73]. However, a detailed study on the de-agglomeration of individual components from the cathode composite has not yet been conducted, and the mechanisms involved are unknown.

In the present work, the mechanical de-agglomeration of PVDF from cathode composites has been investigated. The de-agglomeration performance is determined by separating mixed materials by their degree of surface hydrophobicity. The compositions are then determined using scanning electron microscopy coupled with X-ray energy-dispersive spectroscopy (SEM-EDS) as well as thermogravimetric analysis (TGA). The mechanism is examined by characterizing the surface compositions of cathode composites using X-ray photoelectron (XPS) spectroscopy. The results are compared between new LIBs and EOL LIBs.

5.2 Materials and Experiments

5.2.1 Materials

Both new and EOL Li-ion batteries are used as the samples. New battery cells are obtained from online vendors, and EOL battery cells are supplied by the University Information Technology office and industry partners. All experiments are carried out using de-ionized (DI) water, which was obtained from a Barnstead water purification system (Thermo Fisher). It has a resistance above 18.2 MΩ·cm.

5.2.2 Delamination

The battery cells are opened using a rotary tool to remove the stainless steel outer casing. As a safety precaution, all battery cells are discharged to a voltage below 0.5 V at a C/10 discharge rate prior to the dismantling process [74]. The battery cores are then unfolded to separate anode layers, cathode layers, plastic separators, and other components. The unfolding process is performed under a fume hood to evaporate volatile organic solvent residues.

The delamination process is carried out using a wet agitation process in a blender. For new LIBs, the electrode composite coatings remain on the surface of the current collector foils after the electrode layers are manually separated. To obtain the cathode composite, individual cathode sheets are mixed with water and agitated for 5-10 seconds. The processed slurry consists of a mixture of aluminum current collectors and cathode composites. A wet sieving method is used to separate cathode composites from current collectors. Coarse materials above the screen, which consist of both current collectors and non-delaminated cathode composites, are returned to the blender for delamination. This process is repeated until at least 85% of the cathode composite is delaminated and reclaimed. The impurity of current collector pieces in the reclaimed cathode composite is less than 0.3%.

For EOL LIBs, upon a manual separation of individual layers, cathode materials are adhered to both current collectors and separators. This is ascribed to a degradation of PVDF binders and a formation of an SEI layer, resulting in a weakened adhesion between electrode composite layers and current collectors. In this study, cathode composites on separator layers are manually scraped off in water, while those on current collectors are reclaimed using a wet delamination process as described above. In using this method, 5-20 seconds of agitation is sufficient to delaminate the electrode composite from the current collectors. The processed slurries are then sieved using a 70-mesh screen, rinsed with DI water three times, and filtered to obtain filter cakes. The recycled cathode composite consists of approximately 94% cathode active materials and 6% PVDF and carbon black. Fig. 8-1 shows the photos of battery components obtained from LIBs including anode current collectors (Cu foils), separators, cathode current collectors (Al foils), anode composites, and cathode composites.

5.2.3 De-agglomeration process

De-agglomeration process is carried out in a commercial blender, which provides ultrahigh shear forces as an industrial-scale disintegrator/mixer. In this experiment, approximately 50-100 grams of wet filter cakes are mixed with 1 L of DI water to prepare a slurry. The slurry is agitated at a tip speed of 90-100 m/s for various durations. The processed materials are analyzed for size and chemical compositions using scanning electron microscopy (SEM) coupled with X-ray energy-dispersive (EDS) spectroscopy as described in the following session [75].

A determination of its process performance is challenging using the SEM/EDS analysis. In this study, a new method of assessing performance is introduced by taking advantage

of the differences in surface hydrophobicity of individual components within cathode composites. Both PVDF and carbon black are hydrophobic [76, 77], while cathode active materials are naturally hydrophilic [48]. Upon the de-agglomeration process, the mixed materials are separated by the degree of different hydrophobicity using the froth flotation method. A perfect separation between PVDF/carbon and cathode active materials might be achieved if individual components are fully liberated.

In this study, separation experiments are carried out by froth flotation using a modified release analysis protocol [78, 79]. The release analysis protocol consists of two steps. The first step is to separate floatable materials from non-floatable materials by minimizing entrainments in froth layers. The second step involves a separation of floatable materials by the degree of surface hydrophobicity. Kerosene was used to enhance the hydrophobicity of PVDF and carbon black for a better separation performance.

5.2.4 Morphological and Surface Characterization

Both the chemical composition and morphology of the samples are determined using scanning electron microscopy (SEM) coupled with energy-dispersive X-ray spectroscopy (EDS). In determining chemical compositions, powder mounts are prepared by pressing aluminum pin stubs, with carbon tape affixed to their faces into the powdered specimens. Excess powder is removed with canned air. Specimens are plasma coated with a 7-nm layer of platinum/palladium (Pt/Pd). Imaging and elemental mapping is performed in a Philips XL40 Environmental Scanning Electron Microscope (ESEM) at 15kV accelerating voltage under high-vacuum conditions. Images are obtained in a Back Scattered Electron (BSE) mode, and elemental mapping is conducted through Secondary Electron (SE) mode.

The compositions of the separated samples are determined using the thermogravimetric analysis (TGA) method. TGA experiments are performed in a LECO TGA 701 instrument at a scanning rate of 1 °C min^{-1} at a temperature range of 25-600 °C. The measurements are conducted at an air flowrate of 7 L/min.

The surface elemental compositions of the samples are characterized using the X-ray photoelectron spectroscopy (XPS) in a PHI-5800 instrument. An Mg anode operated at 400W is used to generate X-rays ($h\nu$ = 1253.6 eV) and a hemispherical analyzer angled at 45 degrees from the sample is used to detect electrons from an analysis area with a nominal diameter of 800 μm. Survey spectra are collected with 187.85 eV pass energy. High resolution spectra are collected with 23.50 eV pass energy. The C1s, F1s, and O1s regions are collected. A neutralizer is used for charge compensation of the material. All regions are charge corrected with respect to aliphatic carbon at a binding energy of 284.8 eV.

5.3 Result and Discussion

5.3.1 Sample Characterization

Figure 5-1 shows the weight percentage of delaminated cathode composites at different size fractions, *i.e.*, -212+105 μm, -105+74 μm, -74+37 μm, and -37 μm. As shown, after the delamination process, 40.6% of materials are at a size range above 150 mesh (+105 μm). The ultrafine fraction (-37 μm) accounts for 14.2% of the total weight. Recognizing that the size of cathode active materials is on the order of 10 μm, and the majority of delaminated electrode materials are agglomerates bonded by PVDF binders.

The delaminated cathode composites were subjected to a de-agglomeration process. In this process, slurries containing the cathode composites were agitated for 5 minutes and 20 minutes, respectively. As shown in Fig. 5-1, the medium size of cathode composite is approximately 37 μm after a 5-min size reduction process with a top size of 105 μm. Upon a 20-minute de-agglomeration process, the size of the cathode composite is reduced to a top size of 37 μm, demonstrating an effectiveness in de-agglomerating cathode composites.

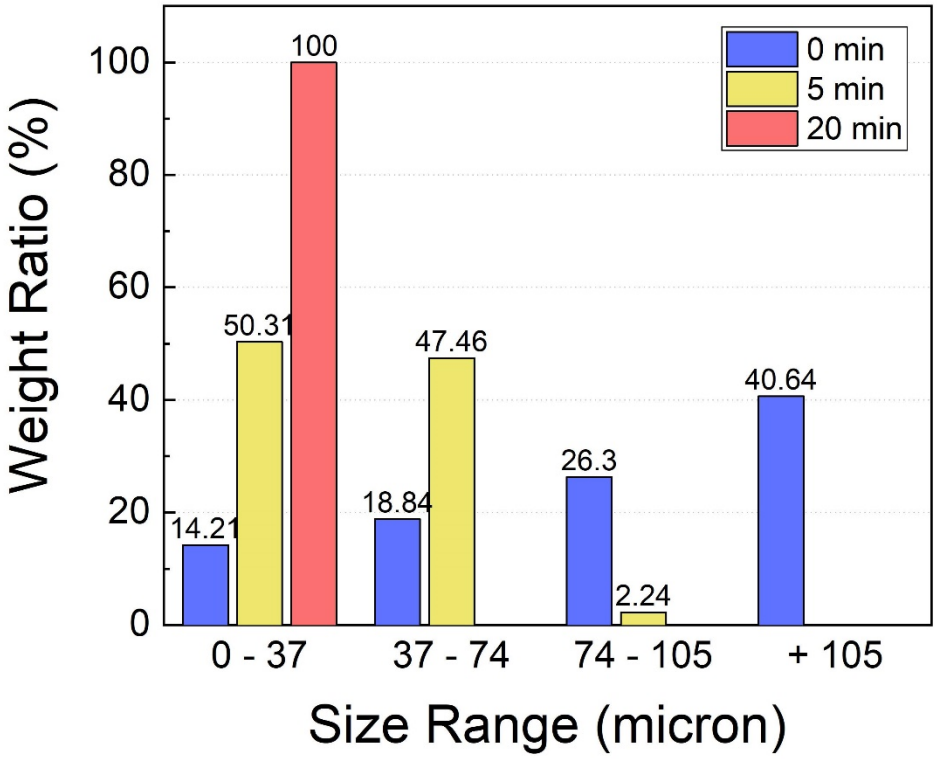

Figure 5-1. Size analysis of de-agglomerated cathode composites after a 0-min, 5-min, and 20-min mechanical de-agglomeration process.

Figure 5-2 compares the morphology and composition of the cathode composites with and without the de-agglomeration processes. Fig. 5-2a) and b) show both SEM as well as EDS elemental mapping images of samples without the de-agglomeration process at 37-

74 μm and 0-37 μm fractions, respectively. The result shows that, at the 37-74 μm fraction, individual cathode materials are engulfed by PVDF binders. At the 0-37 μm fraction, a fraction of cathode active materials is bonded with PVDF binders. In comparison, upon a 20-min de-agglomeration process, the delaminated samples are much more uniform and smaller than those obtained without the mechanical de-agglomeration process (Fig. 5-2c). The average size of the cathode composite after a 20-minute mechanical process is found to be 10 μm

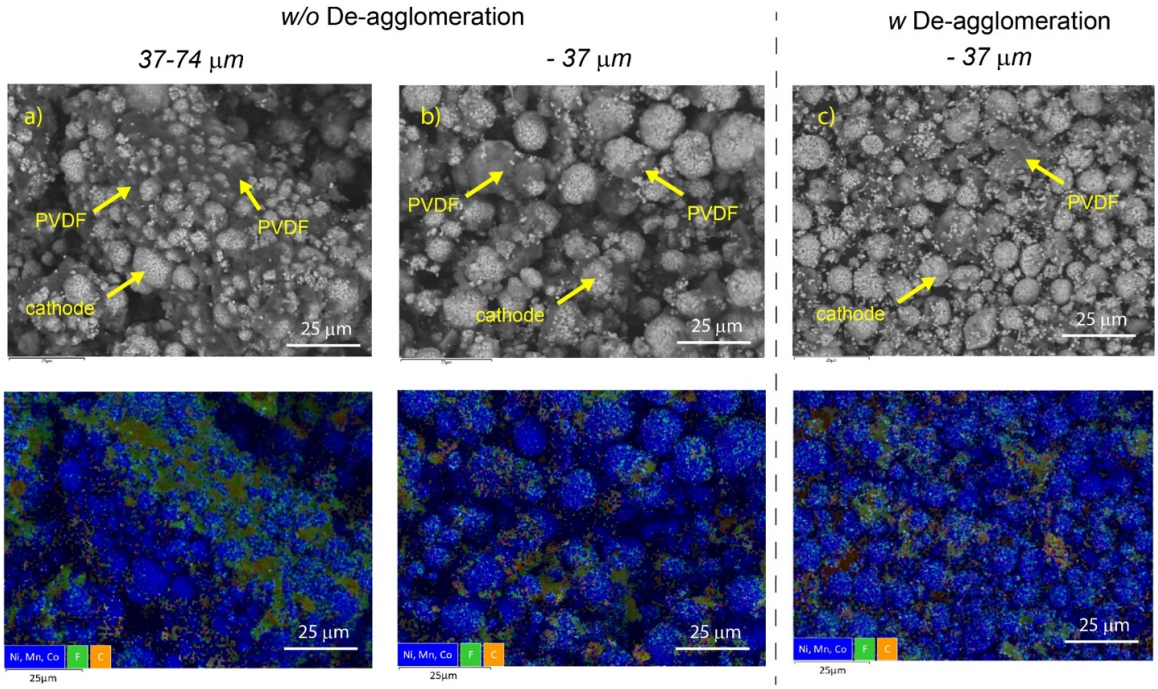

Figure 5-2. SEM and EDS elemental maps of cathode composites without a mechanical size reduction process at a) 37-74 μm and b) -37 μm size fractions; c) SEM and EDS elemental maps of cathode composite after a 20-minute de-agglomeration process.

There might be three mechanisms involved in the de-agglomeration process: 1) a breakage of intermolecular bonding between PVDF and cathode active materials, 2) a breakage of metallic bonds within cathode active materials, and 3) a breakage of covalent bonds within PVDF molecules. All three mechanisms result in the size reduction of the cathode composites. However,, the result obtained from the morphology and elemental mapping data is insufficient to quantify the process performance.

5.3.2 Characterization of de-agglomeration process

The process performance is quantified by the difference in material's composition between the froth concentrates and the tailing products. The cathode composites are separated by the difference in surface hydrophobicity using the froth flotation method. A modified release analysis protocol is used to separate mixed materials by the difference in surface hydrophobicity. Table 1 shows the result after a 0-min, 5-min, and 16-min de-

agglomeration process. The first froth concentrate (F1) consists of materials that are mostly hydrophobic, while the tailing product (T) consists of hydrophilic materials. The surface hydrophobicity is determined using the sessile drop technique by pressing powders into a plate using a hydraulic press. It has been shown that the first froth concentrate (F1) exhibits a water contact angle of approximately 70°. For the tailing products, water penetrates into the compressed plate with no water contact angle measured. The composition of the separated products is determined using thermogravimetric analysis (TGA). The cathode active material's content is determined from the remaining weight at a temperature of 600 ℃, at which both PVDF and carbon black are decomposed. The total weight loss at a temperature of 600 ℃ is referred to the total percentage of PVDF/C by weight in the sample.

Table 5-1. Weight and composition of separated cathode composites by surface hydrophobicity after a 0-min, 5-min and 16-min de-agglomeration process.

De-agglomeration	Product	Weight (g)	Weight (%)	Cathode (%)	PVDF/C (%)	%(PVDF/C)
0-minute	F1	1.50	6.22%	93.37%	6.54%	8.1%
	F2	1.00	4.15%	94.02%	5.98%	4.9%
	F3	3.61	14.97%	94.74%	5.26%	15.4%
	T	18.00	74.66%	95.12%	4.88%	71.6%
	Feed	24.11	100%	94.91%	5.08%	100%
5-minute	F1	5.93	25.42%	84.93%	15.07%	65.9%
	F2	1.00	4.29%	91.39%	8.61%	6.7%
	F3	0.81	3.47%	96.48%	3.52%	2.2%
	T	15.59	66.82%	97.82%	2.18%	25.2%
	Feed	23.33	100%	94.22%	5.78%	100%
16-minute	F1	4.61	16.13%	77.22%	22.78%	68.2%
	F2	1.17	4.09%	96.19%	3.81%	2.6%
	F3	0.76	2.66%	96.98%	3.02%	1.3%
	T	22.04	77.12%	98.06%	1.94%	27.9%
	Feed	28.58	100%	94.59%	5.41%	100%

A control experiment was first carried out with the cathode composites without a de-agglomeration process. As shown in Table 5-1, the F1, F2 and F3 products have cathode active material contents of 93.37%, 94.02%, and 94.74%, respectively, and the tailing product has 95.12% cathode active material. The weight percentages of the floatable materials in the F1-F3 products are 6.22%, 4.15%, and 14.97% by weight, respectively. The flotation of a small fraction of the cathode composites is ascribed to an exposure of PVDF and/or carbon on surfaces. Since the weight percentage corresponds to the percentage of PVDF/C in each separated product, there is no liberation of individual PVDF particles from the cathode composite.

Also shown in Table 5-1 are both the weight and composition of separated cathode composites after a 5-min and 16-min de-agglomeration process, respectively. After a 5-min de-agglomeration process, approximately 25% of the feed are floated in the first froth concentrate while 66.8% of the feed are left in the tailing product. The first froth concentrate consists of 84.93% cathode active materials, whereas the tailing product consists of 97.8% cathode active materials. The difference in the active material content between the first froth concentrate and the tailing product suggests that a partial segmentation of PVDF binders from the cathode composites is achieved after a 5-min de-agglomeration process, allowing a concentration of hydrophobic PVDF particles in the froth concentrate.

The result also shows that the de-agglomeration performance increases with increasing the duration of the de-agglomeration process. For instance, upon a 16-min de-agglomeration process, the content of PVDF/C in the froth product (F1) is increased to 22.78%, and the content of cathode active materials in the tailing product (T) is increased to 98.06%. Note that cathode active materials (~ 5.0 g/cm^3) are much denser than carbon black (1.7 g/cm^3) and PVDF (1.78 g/cm^3). In this regards, the froth concentrate contains equal sizes f cathode active materials as PVDF/carbon, which agrees well with the SEM result (Fig. 5-4a).

To quantitatively determine the composition of the separated products, thermogravimetric analyses (TGA) were performed. Fig. 5-3a shows the TGA result obtained with the first froth concentrate (F1) and the tailing product (T) without the de-agglomeration process. The result is shown as weight loss as well as a derivative of weight loss as a function of temperature. The TGA curves show two characteristic peaks at temperatures of 300-350 ℃ and 480-500 ℃. These two peaks are referred to the decomposition of PVDF binder and carbon black, respectively [80]. The first froth concentrate contains approximately 3% of carbon black, while the tailing contains 1.5% of carbon black only. However, both the froth concentrate and tailing products contain approximately 3.0% of PVDF binders. It is possible that a fraction (~33%) of carbon black particles from cathode composites has been liberated and selectively recovered in the froth concentrate.

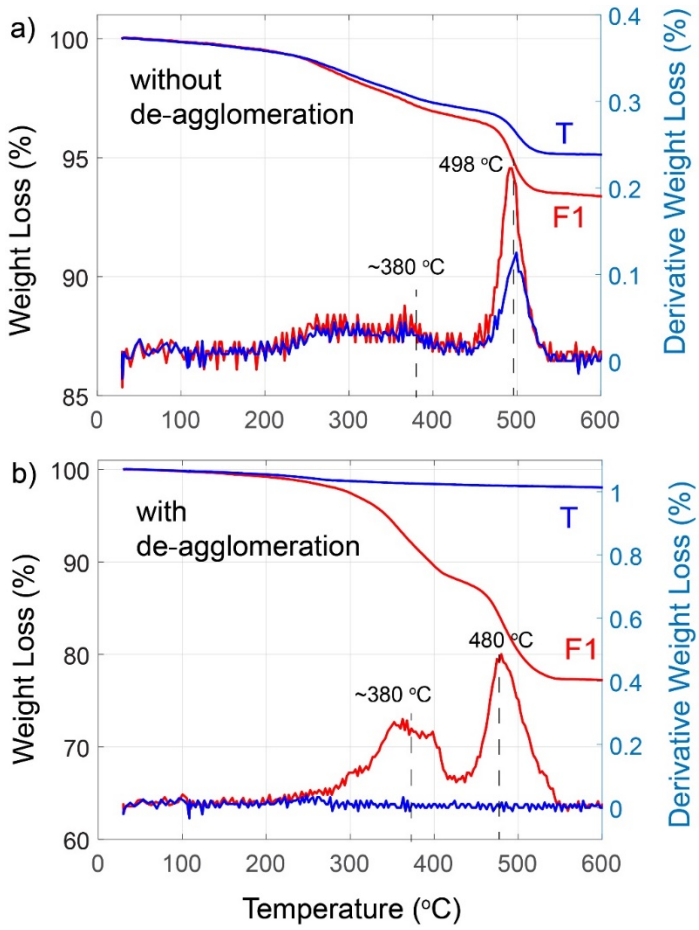

Figure 5-3. TGA result of the first froth concentrate (F1) and tailing products (T) of a) cathode composite without de-agglomeration and b) cathode composite after a 16-min de-agglomeration process.

Fig. 5-3b shows the TGA result after a 16-minute mechanical de-agglomeration process. From the weight loss curve, the first froth concentrate (F1) contains ~12% PVDF and ~10% carbon black, while the tailing product (T) contains less than 2% PVDF binders and carbon black combined. Note that the characteristic TGA peak of carbon black in the tailing product is shifted to a lower temperature (*i.e.* 480 °C), which might be associated to a smaller particle size after the de-agglomeration process.

Both morphology and surface chemical compositions of the separated products upon the de-agglomeration process are examined using scanning electron microscope coupled with energy-dispersive spectroscopy (SEM/EDS). Fig. 5-4a shows both SEM and EDS elemental mapping images of both the froth concentrate (F1) and tailing (T) products after a 16-minute de-agglomeration process. As shown, the first froth concentrate contains both PVDF binders and cathode active materials. Note that a fraction of PVDF binders are present as agglomerates, suggesting that PVDF binders are liberated from the cathode composite during the de-agglomeration process. These PVDF binder particles are

floated, and re-agglomerated when the slurry is dried in the oven. On the contrary, the tailing product contains negligible PVDF particles (Fig. 5-4a).

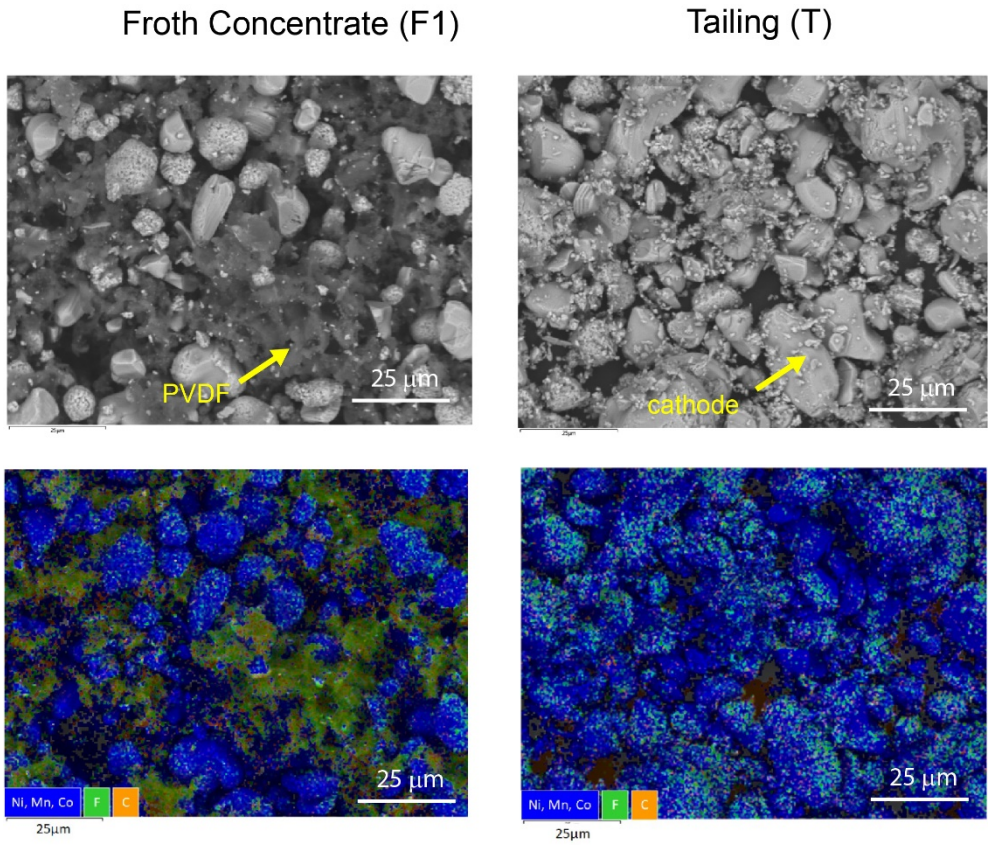

Figure 5-4. SEM/EDS images of both the first froth concentrate and tailing products after a 16-minute de-agglomeration process.

Note that fluorine (F) signals are detected on the surface of cathode active materials, as shown from the EDS elemental mapping image. Two possible sources are 1) a formation of metal fluoride during a water-based recycling process, and/or 2) fractures of PVDF binders left on the surfaces of cathode active materials. The EDS spectra of the tailing product shows that the fluorine content is less than 0.1% by weight, indicating that the fluorine signal is mainly attributed to a formation of surface species. In addition, a small fraction of the tailing product has a characteristic size of 1-5 µm. The presence of these micron-sized cathode active materials may be attributed to a breakdown of individual cathode active materials during the size reduction process.

5.3.3 Effect of Cycling

The performance of PVDF binders deteriorates when battery cells reach their end of life cycles [81]. The weakened performance is attributed to the expansion and contraction of electrode materials during the cycling. This partially contributes to a weakened contact between cathode composite layers and current collectors [81, 82]. Our hypothesis is that

the weakened bonding energy between PVDF and cathode active materials due to battery cycling benefits the de-agglomeration performance.

To validate this hypothesis, the de-agglomeration experiments were extended with end-of-life (EOL) LIBs. These spent LIBs cells were obtained from used laptop batteries. These EOL LIBs suffer capacity loss because of electrode disintegration [83-85], material deterioration [86-88], loss of free lithium [89-91], surface layer formation [92-94], and contact deterioration [95-97]. Table 5-2 shows the process performance result obtained with EOL LIBs. Without the de-agglomeration process, the first froth concentrate contains 88.04% active cathode materials while the tailing products contains 95.78% cathode active materials. The difference in active material content between the first froth concentrate and the tailing product is unexpected, in that a fraction of PVDF binders have already been segmented from the cathode composites even without the de-agglomeration process.

Table 5-2. Weight and compositions of separated cathode composite by surface hydrophobicity from end-of-life Li-ion batteries with and without the de-agglomeration process.

De-agglomeration	Product	Weight (g)	Weight (%)	Cathode (%)	PVDF/C (%)	%(PVDF/C)
0-minute	F1	1.46	7.66%	88.04%	11.96%	18.2%
	F2	0.5	2.62%	90.80%	9.20%	4.8%
	F3	0.5	2.62%	92.70%	7.30%	3.8%
	T	16.59	87.09%	95.78%	4.22%	73.1%
	Feed	19.05	100.00%	94.97%	5.03%	100%
5-minute	F1	1.15	4.32%	48.41%	51.59%	37.8%
	F2	0.16	0.60%	68.35%	31.65%	3.2%
	F3	0.32	1.20%	82.46%	17.54%	3.8%
	T	25	93.88%	96.57%	3.43%	55.2%
	Feed	26.63	100.00%	94.15%	5.85%	100%
16-minute	F1	1.21	3.03%	33.42%	66.58%	39.9%
	F2	0.76	1.90%	38.23%	61.77%	23.2%

F3	1.52	3.81%	91.66%	8.34%	6.3%
T	36.41	91.25%	98.30%	1.70%	30.6%
Feed	39.9	100.00%	94.94%	5.06%	100%

Also shown in Table 5-2 are the results obtained after 5-min and 16-min de-agglomeration processes. The result is consistent with those obtained with new LIBs, *i.e.* the de-agglomeration performance increases with process duration. For instance, with a 5-minute size reduction process, the active material content in the first froth concentrate is decreased to 48.41%, while the content of cathode active materials in the tailing product is increased to 96.57%. With a 16-minute size reduction process, the active material content in the first froth concentrate is reduced to 33.42%, and active cathode materials content in the tailing product is increased to 98.30%. Quantitative thermogravimetric analysis of both the froth and tailing products obtained with EOL LIBs can be found in Fig. 8-2.

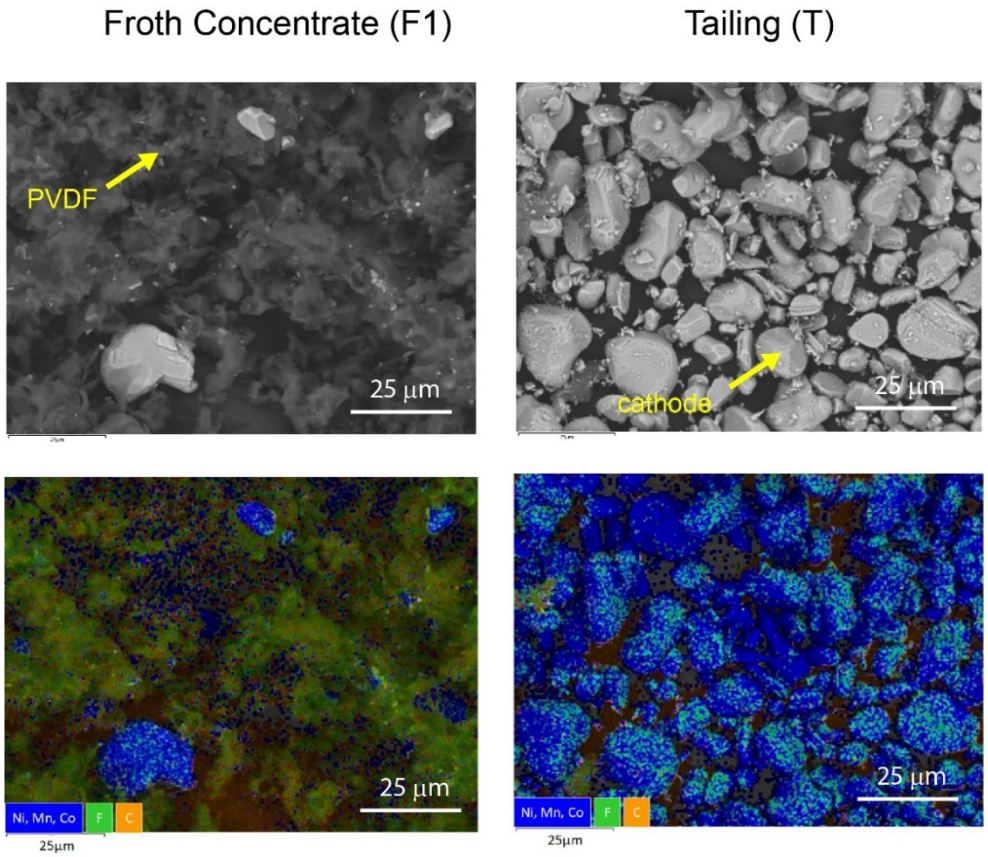

Figure 5-5. SEM/EDS images of the first froth concentrate and tailing products after a 16-minute de-agglomeration process

Fig. 5-5 shows SEM and EDS elemental mapping images of both the froth and tailing products after a 16-minute de-agglomeration process. The SEM image shows that the majority of the tailing product consists of cathode active materials. On the contrary, the majority of the first froth concentrate consists of PVDF binder and carbon. The fluorine peaks observed on the surface of cathode active materials in the tailing product might be metal fluoride species, which might be attributed to 1) a hydrolysis of electrolyte ($LiPF_6$) that forms HF and reacts with cathode active materials, 2) SEI layers on cycled cathode materials [98].

5.3.4 De-agglomeration Mechanism

To further examine the mechanism involved during the size reduction process, X-ray photoelectron spectroscopy (XPS) analysis was performed to determine surface composition and chemical states of both the froth and tailing products. Fig. 5-6 compares spectra in F1s XPS regions of both first froth concentrate and tailing products obtained with a) new LIBs and b) EOL LIBs after a 16-minute size reduction process. The F1s XPS spectra (Fig. 5-6a) show two characteristic peaks which correspond to the fluorine in the PVDF binders (C-F, 688.0 eV for tailing, 687.8 eV for froth) and the fluorine bonded to a metal (M-F, 685.2 eV for tailing, 685.3 eV for froth). This latter peak might correspond to the fluorine in LiF. As shown, the peaks that appeared in the F1s XPS spectrum of the tailing products are smaller (signals are multiplied by a factor of 10 for visual comparison of the binding energies) compared to the peaks in the F1s spectrum of the first froth concentrate. This result confirms that the majority of the fluorine-containing species (*e.g.,* PVDF) are in the froth product. The peak of M-F (685.2 eV or 685.3 eV) suggests a formation of surface species on cathode surfaces, which might be ascribed to a decomposition of $LiPF_6$ during the recycling process.

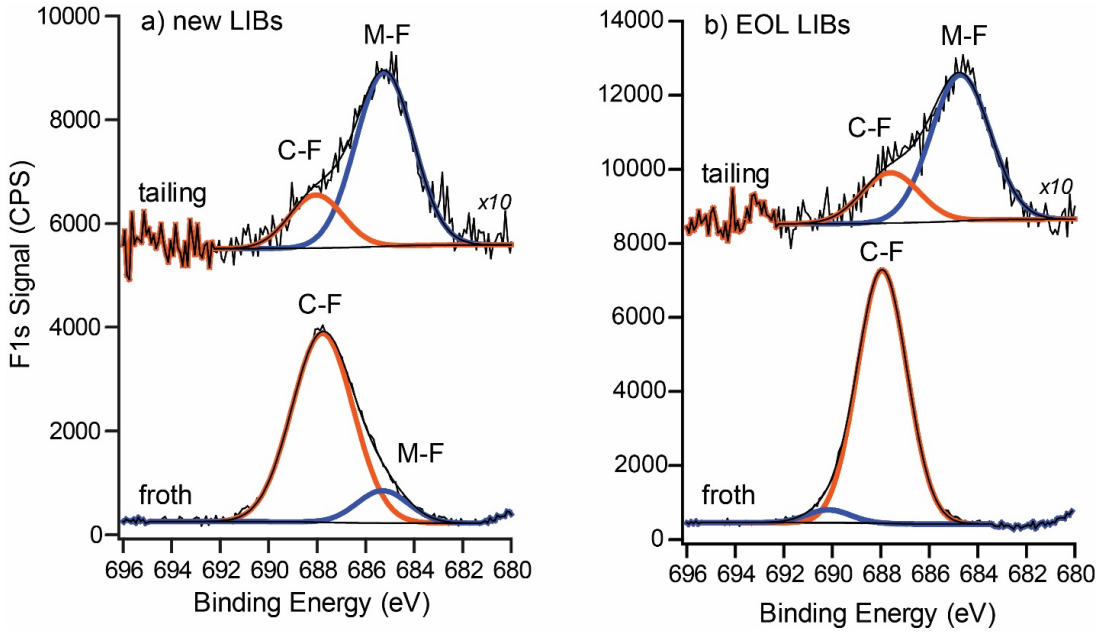

Figure 5-6. F1s spectra of froth and tailing products upon a 16-min de-agglomeration process with a) new Li-ion batteries and b) end-of-life (EOL) Li-ion batteries.

Also shown in Fig. 5-6 are the F1s spectra obtained from end-of-life (EOL) Li-ion batteries after a 16-min de-agglomeration process. The F1s XPS spectra of the froth product show one dominating characteristic peak which corresponds to the fluorine in the PVDF binders (C-F, 687.8 eV for froth). On the contrary, the tailing product exhibits negligible M-F and C-F signals in the F1s spectra due to the absence of fluorine-containing species in the tailing product. All evidences suggest that the de-agglomeration has been achieved by breaking intermolecular bonds between PVDF molecules and cathode active materials as well as covalent bonds within PVDF binders. The breakage of intermolecular and intramolecular bonds results in a de-agglomeration of the cathode composites.

A schematic drawing of the de-agglomeration of cathode composite during the mechanical de-agglomeration process can be found in Fig. 8-3 as well as in the graphical abstract section. The shear force overcomes intermolecular interaction between PVDF and cathode active materials and the intramolecular bond of PVDF molecules, enabling a liberation of PVDF binders from cathode composites. The mechanical size reduction might have contributed to a size reduction of a small fraction of cathode active materials, as manifested by the presence of ultrafine cathode active materials (size < 3 μm). This work offers a non-chemical and non-thermal method for liberating PVDF binders from cathode composite. Both PVDF binders and carbon additives can be separated from cathode active materials by the froth flotation method, which will be discussed in a separated communication.

5.4 Conclusion and Summary

De-agglomeration of PVDF binders from cathode composites of Li-ion batteries by a mechanical method has been demonstrated and investigated. It has been found that a high-shear mixing process reduces the size of the cathode composites. The process performance has been evaluated by separating the mixture by the degree of surface hydrophobicity using the froth flotation method. It has been found that no liberation occurred between PVDF and cathode active materials without the de-agglomeration process. The de-agglomeration of the cathode composites increases with increasing the duration of the mechanical size reduction process.

It has also been shown that de-agglomeration performance is enhanced with end-of-life Li-ion batteries compared to new Li-ion batteries. The results show that the majority of PVDF binders are present as individual particle after a de-agglomeration process. The improved performance is ascribed to a weakened bonding between PVDF and cathode active materials as well as within PVDF molecules after charging-discharging cycling. The XPS result shows that a breakage of both intramolecular and intermolecular bonds within the cathode composite governs the de-agglomeration process. This work offers a new non-chemical method for liberating PVDF binders from cathode composites, which can be integrated with the rejuvenation process for the direct recycling of Li-ion batteries in the future.

5.5 Reference

1. Wood, E., M. Alexander, and T.H. Bradley, *Investigation of battery end-of-life conditions for plug-in hybrid electric vehicles.* Journal of Power Sources, 2011. **196**(11): p. 5147-5154.
2. Sarre, G., P. Blanchard, and M. Broussely, *Aging of lithium-ion batteries.* Journal of power sources, 2004. **127**(1-2): p. 65-71.
3. Marano, V., et al. *Lithium-ion batteries life estimation for plug-in hybrid electric vehicles*. in *2009 IEEE vehicle power and propulsion conference*. 2009. IEEE.
4. Gaines, L., *The future of automotive lithium-ion battery recycling: Charting a sustainable course.* Sustainable Materials and Technologies, 2014. **1-2**: p. 2-7.
5. Bernardes, A.M., D.C.R. Espinosa, and J.A.S. Tenório, *Recycling of batteries: a review of current processes and technologies.* Journal of Power Sources, 2004. **130**(1): p. 291-298.
6. Richa, K., et al., *A future perspective on lithium-ion battery waste flows from electric vehicles.* Resources, Conservation and Recycling, 2014. **83**: p. 63-76.
7. Boyden, A., V.K. Soo, and M. Doolan, *The Environmental Impacts of Recycling Portable Lithium-Ion Batteries.* Procedia CIRP, 2016. **48**: p. 188-193.
8. Winslow, K.M., S.J. Laux, and T.G. Townsend, *A review on the growing concern and potential management strategies of waste lithium-ion batteries.* Resources, Conservation and Recycling, 2018. **129**: p. 263-277.
9. Li, L., et al., *Environmental friendly leaching reagent for cobalt and lithium recovery from spent lithium-ion batteries.* Waste Management, 2010. **30**(12): p. 2615-2621.
10. Richa, K., C.W. Babbitt, and G. Gaustad, *Eco-efficiency analysis of a lithium-ion battery waste hierarchy inspired by circular economy.* Journal of Industrial Ecology, 2017. **21**(3): p. 715-730.
11. Gao, W., et al., *Lithium Carbonate Recovery from Cathode Scrap of Spent Lithium-Ion Battery: A Closed-Loop Process.* Environmental Science & Technology, 2017. **51**(3): p. 1662-1669.
12. Zhang, X., et al., *A closed-loop process for recycling LiNi1/3Co1/3Mn1/3O2 from the cathode scraps of lithium-ion batteries: Process optimization and kinetics analysis.* Separation and Purification Technology, 2015. **150**: p. 186-195.
13. Gratz, E., et al., *A closed loop process for recycling spent lithium ion batteries.* Journal of Power Sources, 2014. **262**: p. 255-262.
14. Natarajan, S. and V. Aravindan, *Recycling Strategies for Spent Li-Ion Battery Mixed Cathodes.* ACS Energy Letters, 2018. **3**(9): p. 2101-2103.
15. Natarajan, S. and V. Aravindan, *Burgeoning Prospects of Spent Lithium-Ion Batteries in Multifarious Applications.* Advanced Energy Materials, 2018. **8**(33): p. 1802303.
16. Harper, G., et al., *Recycling lithium-ion batteries from electric vehicles.* Nature, 2019. **575**(7781): p. 75-86.
17. Li, J., G. Wang, and Z. Xu, *Environmentally-friendly oxygen-free roasting/wet magnetic separation technology for in situ recycling cobalt, lithium carbonate and graphite from spent LiCoO2/graphite lithium batteries.* Journal of Hazardous Materials, 2016. **302**: p. 97-104.

18. Xiao, J., J. Li, and Z. Xu, *Novel Approach for in Situ Recovery of Lithium Carbonate from Spent Lithium Ion Batteries Using Vacuum Metallurgy.* Environmental Science & Technology, 2017. **51**(20): p. 11960-11966.
19. Wang, H., et al., *Recovery of lithium, nickel, and cobalt from spent lithium-ion battery powders by selective ammonia leaching and an adsorption separation system.* ACS Sustainable Chemistry & Engineering, 2017. **5**(12): p. 11489-11495.
20. Ku, H., et al., *Recycling of spent lithium-ion battery cathode materials by ammoniacal leaching.* Journal of Hazardous Materials, 2016. **313**: p. 138-146.
21. Lee, C.K. and K.-I. Rhee, *Reductive leaching of cathodic active materials from lithium ion battery wastes.* Hydrometallurgy, 2003. **68**(1): p. 5-10.
22. Kang, J., et al., *Recovery of cobalt sulfate from spent lithium ion batteries by reductive leaching and solvent extraction with Cyanex 272.* Hydrometallurgy, 2010. **100**(3): p. 168-171.
23. Larouche, F., et al. *Recycling of Li-Ion and Li-Solid State Batteries: The Role of Hydrometallurgy:* . in *Proceedings of the First Global Conference on Extractive Metallurgy*. 2018.
24. Shi, Y., G. Chen, and Z. Chen, *Effective regeneration of LiCoO 2 from spent lithium-ion batteries: a direct approach towards high-performance active particles.* Green Chemistry, 2018. **20**(4): p. 851-862.
25. Wang, H. and J.F. Whitacre, *Direct Recycling of Aged LiMn2O4 Cathode Materials used in Aqueous Lithium-ion Batteries: Processes and Sensitivities.* Energy Technology, 2018. **6**(12): p. 2429-2437.
26. Li, X., et al., *Direct regeneration of recycled cathode material mixture from scrapped LiFePO4 batteries.* Journal of Power Sources, 2017. **345**: p. 78-84.
27. Vieceli, N., et al., *Hydrometallurgical recycling of lithium-ion batteries by reductive leaching with sodium metabisulphite.* Waste Management, 2018. **71**: p. 350-361.
28. Bahaloo-Horeh, N. and S.M. Mousavi, *Enhanced recovery of valuable metals from spent lithium-ion batteries through optimization of organic acids produced by Aspergillus niger.* Waste Management, 2017. **60**: p. 666-679.
29. Zheng, X., et al., *Spent lithium-ion battery recycling – Reductive ammonia leaching of metals from cathode scrap by sodium sulphite.* Waste Management, 2017. **60**: p. 680-688.
30. Nan, J., et al., *Recovery of metal values from a mixture of spent lithium-ion batteries and nickel-metal hydride batteries.* Hydrometallurgy, 2006. **84**(1): p. 75-80.
31. Nguyen, V.T., et al., *The separation and recovery of nickel and lithium from the sulfate leach liquor of spent lithium ion batteries using PC-88A.* Korean Chemical Engineering Research, 2015. **53**(2): p. 137-144.
32. Zou, H., et al., *A novel method to recycle mixed cathode materials for lithium ion batteries.* Green Chemistry, 2013. **15**(5): p. 1183-1191.
33. Nayaka, G.P., et al., *Recovery of valuable metal ions from the spent lithium-ion battery using aqueous mixture of mild organic acids as alternative to mineral acids.* Hydrometallurgy, 2015. **151**: p. 73-77.

34. Joulié, M., R. Laucournet, and E. Billy, *Hydrometallurgical process for the recovery of high value metals from spent lithium nickel cobalt aluminum oxide based lithium-ion batteries.* Journal of Power Sources, 2014. **247**: p. 551-555.
35. Dewulf, J., et al., *Recycling rechargeable lithium ion batteries: Critical analysis of natural resource savings.* Resources, Conservation and Recycling, 2010. **54**(4): p. 229-234.
36. Santana, I.L., et al., *Photocatalytic properties of Co3O4/LiCoO2 recycled from spent lithium-ion batteries using citric acid as leaching agent.* Materials Chemistry and Physics, 2017. **190**: p. 38-44.
37. Shin, E.J., et al., *A green recycling process designed for LiFePO 4 cathode materials for Li-ion batteries.* Journal of Materials Chemistry A, 2015. **3**(21): p. 11493-11502.
38. Jo, M., et al., *Effects of Residual Lithium in the precursors of Li[Ni1/3Co1/3Mn1/3]O2 on their lithium-ion battery performance.* Journal of Physics and Chemistry of Solids, 2018. **118**: p. 47-52.
39. Gaines, L., *Lithium-ion battery recycling processes: Research towards a sustainable course.* Sustainable Materials and Technologies, 2018. **17**: p. e00068.
40. Dai, Q., et al., *EverBatt: A Closed-loop Battery Recycling Cost and Environmental Impacts Model*. 2019, Argonne National Lab.(ANL), Argonne, IL (United States).
41. Zhang, X., et al., *Sustainable Recycling and Regeneration of Cathode Scraps from Industrial Production of Lithium-Ion Batteries.* ACS Sustainable Chemistry & Engineering, 2016. **4**(12): p. 7041-7049.
42. Shi, Y., et al., *Ambient-Pressure Relithiation of Degraded LixNi0.5Co0.2Mn0.3O2 (0 < x < 1) via Eutectic Solutions for Direct Regeneration of Lithium-Ion Battery Cathodes.* Advanced Energy Materials, 2019. **9**(20): p. 1900454.
43. Ganter, M.J., et al., *Cathode refunctionalization as a lithium ion battery recycling alternative.* Journal of Power Sources, 2014. **256**: p. 274-280.
44. Jiangping Chen, Q.L., Jishun Song, Dawei Song, Lianqi Zhang and Xianxing Shi, *Environmentally friendly recycling and effective repairing of cathode powders from spent LiFePO4 batteries.* Green Chemistry, 2016: p. 2500-2506.
45. Wang, M.-M., C.-C. Zhang, and F.-S. Zhang, *An environmental benign process for cobalt and lithium recovery from spent lithium-ion batteries by mechanochemical approach.* Waste Management, 2016. **51**: p. 239-244.
46. Guo, Y., et al., *Improved extraction of cobalt and lithium by reductive acid from spent lithium-ion batteries via mechanical activation process.* Journal of Materials Science, 2018. **53**(19): p. 13790-13800.
47. Zhang, X., et al., *A novel process for recycling and resynthesizing LiNi1/3Co1/3Mn1/3O2 from the cathode scraps intended for lithium-ion batteries.* Waste Management, 2014. **34**(9): p. 1715-1724.
48. He, Y., et al., *Recovery of LiCoO2 and graphite from spent lithium-ion batteries by Fenton reagent-assisted flotation.* Journal of Cleaner Production, 2017. **143**: p. 319-325.

49. Zhang, T., et al., *Characteristics of wet and dry crushing methods in the recycling process of spent lithium-ion batteries.* Journal of Power Sources, 2013. **240**: p. 766-771.
50. Yu, J., et al., *A promising physical method for recovery of LiCoO2 and graphite from spent lithium-ion batteries: Grinding flotation.* Separation and Purification Technology, 2018. **190**: p. 45-52.
51. Wang, X., G. Gaustad, and C.W. Babbitt, *Targeting high value metals in lithium-ion battery recycling via shredding and size-based separation.* Waste Management, 2016. **51**: p. 204-213.
52. Lee, C.K. and K.-I. Rhee, *Preparation of LiCoO2 from spent lithium-ion batteries.* Journal of Power Sources, 2002. **109**(1): p. 17-21.
53. Shui, J.-L., H.-H. Wang, and D.-J. Liu, *Degradation and revival of Li–O2 battery cathode.* Electrochemistry Communications, 2013. **34**: p. 45-47.
54. Sloop, S.E. and R. Parker, *System and method for processing an end-of-life or reduced performance energy storage and/or conversion device using a supercritical fluid*. 2011, Google Patents.
55. Ramoni, M.O. and H.-C. Zhang, *End-of-life (EOL) issues and options for electric vehicle batteries.* Clean Technologies and Environmental Policy, 2013. **15**(6): p. 881-891.
56. Shi, Y., G. Chen, and Z.J.G.C. Chen, *Effective regeneration of LiCoO 2 from spent lithium-ion batteries: a direct approach towards high-performance active particles.* 2018. **20**(4): p. 851-862.
57. Zeng, X., J. Li, and L. Liu, *Solving spent lithium-ion battery problems in China: Opportunities and challenges.* Renewable and Sustainable Energy Reviews, 2015. **52**: p. 1759-1767.
58. Nie, H., et al., *LiCoO 2: recycling from spent batteries and regeneration with solid state synthesis.* Green Chemistry, 2015. **17**(2): p. 1276-1280.
59. Contestabile, M., S. Panero, and B. Scrosati, *A laboratory-scale lithium-ion battery recycling process.* Journal of Power Sources, 2001. **92**(1): p. 65-69.
60. Zhang, G., et al., *Application of mechanical crushing combined with pyrolysis-enhanced flotation technology to recover graphite and LiCoO2 from spent lithium-ion batteries.* Journal of Cleaner Production, 2019. **231**: p. 1418-1427.
61. Yamaki, J.-i., et al., *Thermal stability of graphite anode with electrolyte in lithium-ion cells.* Solid State Ionics, 2002. **148**(3): p. 241-245.
62. Kim, Y.W., et al., *Single-step synthesis of proton conducting poly(vinylidene fluoride) (PVDF) graft copolymer electrolytes.* European Polymer Journal, 2008. **44**(3): p. 932-939.
63. Zhang, X., et al., *An overview on the processes and technologies for recycling cathodic active materials from spent lithium-ion batteries.* Journal of Material Cycles and Waste Management, 2013. **15**(4): p. 420-430.
64. Zhou, X., et al. *Recycling of electrode materials from spent lithium-ion batteries*. in *2010 4th International Conference on Bioinformatics and Biomedical Engineering*. 2010. IEEE.

65. Song, X., et al., *Direct regeneration of cathode materials from spent lithium iron phosphate batteries using a solid phase sintering method.* Rsc Advances, 2017. **7**(8): p. 4783-4790.
66. Ordoñez, J., E.J. Gago, and A. Girard, *Processes and technologies for the recycling and recovery of spent lithium-ion batteries.* Renewable and Sustainable Energy Reviews, 2016. **60**: p. 195-205.
67. Sun, A.C., et al., *A study of thermodynamics and kinetics pertinent to formation of PVDF membranes by phase inversion.* Desalination, 2013. **309**: p. 156-164.
68. Kim, K.M., et al., *Effect of evaporation temperature on the crystalline properties of solution-cast films of poly(vinylidene fluoride)s.* Korean Journal of Chemical Engineering, 2003. **20**(5): p. 934-941.
69. Xiao, J., J. Li, and Z. Xu, *Recycling metals from lithium ion battery by mechanical separation and vacuum metallurgy.* Journal of Hazardous Materials, 2017. **338**: p. 124-131.
70. Bertuol, D.A., et al., *Application of spouted bed elutriation in the recycling of lithium ion batteries.* Journal of Power Sources, 2015. **275**: p. 627-632.
71. Zhang, T., et al., *Chemical and process mineralogical characterizations of spent lithium-ion batteries: An approach by multi-analytical techniques.* Waste Management, 2014. **34**(6): p. 1051-1058.
72. He, L.-P., et al., *Recovery of cathode materials and Al from spent lithium-ion batteries by ultrasonic cleaning.* Waste Management, 2015. **46**: p. 523-528.
73. Zhan, R., et al., *Recovery of active cathode materials from lithium-ion batteries using froth flotation.* 2018: p. e00062.
74. Perea, A., et al., *State of charge influence on thermal reactions and abuse tests in commercial lithium-ion cells.* Journal of Power Sources, 2018. **399**: p. 392-397.
75. Waldmann, T., et al., *Temperature dependent ageing mechanisms in Lithium-ion batteries – A Post-Mortem study.* Journal of Power Sources, 2014. **262**: p. 129-135.
76. Wang, X.L., et al., *Micro-porous layer with composite carbon black for PEM fuel cells.* Electrochimica Acta, 2006. **51**(23): p. 4909-4915.
77. Kuo, C.-Y., et al., *Fabrication of a high hydrophobic PVDF membrane via nonsolvent induced phase separation.* Desalination, 2008. **233**(1): p. 40-47.
78. Dell, C., *Release analysis, a new tool for ore dressing research*, in *Recent Developments in Mineral Dressing*. 1953, London DIM.
79. Forrest, W.R., G.T. Adel, and R.H. Yoon, *Characterizing Coal Flotation Performance Using Release Analysis.* Coal Preparation, 1994. **14**(1-2): p. 13-27.
80. Hanisch, C., et al., *Recycling of lithium-ion batteries: a novel method to separate coating and foil of electrodes.* Journal of Cleaner Production, 2015. **108**: p. 301-311.
81. Vetter, J., et al., *Ageing mechanisms in lithium-ion batteries.* Journal of Power Sources, 2005. **147**(1): p. 269-281.
82. Grillet, A.M., et al., *Conductivity degradation of polyvinylidene fluoride composite binder during cycling: Measurements and simulations for lithium-ion batteries.* Journal of The Electrochemical Society, 2016. **163**(9): p. A1859-A1871.

83. Kim, H., et al., *The Insertion Mechanism of Lithium into Mg2Si Anode Material for Li-Ion Batteries.* Journal of the Electrochemical Society, 1999. **146**(12): p. 4401-4405.
84. Ulus, A., et al., *Tin alloy-graphite composite anode for lithium-ion batteries.* Journal of The Electrochemical Society, 2002. **149**(5): p. A635-A643.
85. Hassoun, J., S. Panero, and B. Scrosati, *Electrodeposited Ni–Sn intermetallic electrodes for advanced lithium ion batteries.* Journal of Power Sources, 2006. **160**(2): p. 1336-1341.
86. Köhler, J., et al., *LiV3O8: characterization as anode material for an aqueous rechargeable Li-ion battery system.* Electrochimica Acta, 2000. **46**(1): p. 59-65.
87. Itou, Y. and Y. Ukyo, *Performance of LiNiCoO2 materials for advanced lithium-ion batteries.* Journal of Power Sources, 2005. **146**(1): p. 39-44.
88. Väyrynen, A. and J. Salminen, *Lithium ion battery production.* The Journal of Chemical Thermodynamics, 2012. **46**: p. 80-85.
89. Zhang, Q. and R.E. White, *Capacity fade analysis of a lithium ion cell.* Journal of Power Sources, 2008. **179**(2): p. 793-798.
90. Agubra, V. and J. Fergus, *Lithium ion battery anode aging mechanisms.* Materials, 2013. **6**(4): p. 1310-1325.
91. Ramasamy, R.P., J.-W. Lee, and B.N. Popov, *Simulation of capacity loss in carbon electrode for lithium-ion cells during storage.* Journal of Power Sources, 2007. **166**(1): p. 266-272.
92. Shim, J., et al., *Electrochemical analysis for cycle performance and capacity fading of a lithium-ion battery cycled at elevated temperature.* Journal of Power Sources, 2002. **112**(1): p. 222-230.
93. Zhang, Y., C.-Y. Wang, and X. Tang, *Cycling degradation of an automotive LiFePO4 lithium-ion battery.* Journal of Power Sources, 2011. **196**(3): p. 1513-1520.
94. Yang, L., M. Takahashi, and B. Wang, *A study on capacity fading of lithium-ion battery with manganese spinel positive electrode during cycling.* Electrochimica Acta, 2006. **51**(16): p. 3228-3234.
95. Liu, D., et al., *On the stress characteristics of graphite anode in commercial pouch lithium-ion battery.* Journal of Power Sources, 2013. **232**: p. 29-33.
96. Watanabe, S., et al., *Capacity fade of LiAlyNi1−x−yCoxO2 cathode for lithium-ion batteries during accelerated calendar and cycle life tests (surface analysis of LiAlyNi1−x−yCoxO2 cathode after cycle tests in restricted depth of discharge ranges).* Journal of Power Sources, 2014. **258**: p. 210-217.
97. Lee, R.-C., et al., *Synthesis of high-performance MnOx/carbon composite as lithium-ion battery anode by a facile co-precipitation method: Effects of oxygen stoichiometry and carbon morphology.* Journal of Power Sources, 2014. **253**: p. 373-380.
98. Joshi, T., et al., *Effects of dissolved transition metals on the electrochemical performance and SEI growth in lithium-ion batteries.* Journal of the electrochemical society, 2014. **161**(12): p. A1915-A1921.

6 Separation of Lithium Metal Oxide and Graphite using Film flow Enhanced Gravity Separation

6.1 Introduction

Lithium-ion (Li-ion) batteries, commercialized in 1990 by Sony, have become the state-of-the-art technology for energy storage due to high energy density and long cycling life [1-3]. Once the batteries reach the end of their life, it is necessary to recycle them [4]. Battery recycling is an integrated part of environmental stewardship for energy storage and electric vehicle (EV) businesses. Currently, in many countries, battery recycling is mandatory. The Li-ion batteries contain hazardous and flammable materials, and thermal runaway may result in fires and explosions [4, 5]. Li-ion batteries contain ~50% by weight of critical and strategic minerals including lithium, nickel, cobalt, manganese, and graphite [6, 7]. The separation and upcycling of individual battery components from Li-ion batteries is essential to achieve its sustainability [4, 8].

Recycling of Li-ion batteries is designed to close the loop of materials used in Li-ion batteries [9]. Both pyrometallurgical and hydrometallurgical processes are designed to recover valuable metals, such as cobalt and nickel. Direct recycling separates and recovers both the anode and cathode active materials from Li-ion batteries without digesting the active materials in liquids or smelting them into alloys [4]. In using the direct recycling process, battery cells are dissembled and crushed into individual battery components. The solvent within Li-ion batteries evaporates quickly at room temperature due to its high vapor pressure, which leave behind the solid residues that contain electrode sheets. Size separation and gravity separation are used to separate various battery components [10-12]. Once the active materials are delaminated from current collectors, the fine fraction consists of different types of anode and cathode active materials, while the coarse fraction consists of current collectors, *e.g.* Cu and Al, and separators. Graphite is commonly used as the anode active material, while lithium-containing metal oxides, *e.g.* lithium nickel manganese cobalt oxide (NMC), are used as the cathode active material. The recycled active materials may be relithiated prior to their re-use in new batteries [13-18]. Nevertheless, separation of the anode and cathode active materials from Li-ion batteries is preferred prior to the follow-up direct recycling and chemical refining processes.

Prior R&D efforts were devoted to the froth flotation method [19-21]. Froth flotation separates the mixed materials by takin advantage of the difference in the surface hydrophobicity of the two materials. Graphite is hydrophobic, while lithium metal oxide is hydrophilic. Air bubbles carry hydrophobic graphite particles to the froth layers, leaving hydrophilic metal oxide materials in the slurry [19]. Separation occurs when particle-loaded froth flows into the launder. For lightly used EV batteries, anode active materials remain hydrophobic, and therefore, all anode materials are floated with kerosene as the collector. A satisfactory separation between the anode and cathode active materials is achieved [22]. For severely degraded Li-ion batteries, electrolyte degradation results in a formation of oxygen-rich surface electrolyte interphase (SEI) layer, rendering the surface hydrophilic [23]. In addition, the exposure of both PVDF binders and carbon additives may result in an unfavorable flotation of cathode materials. It has been shown that the separation of anode and cathode active materials from end-of-life Li-ion batteries improves after a thermal treatment process [20, 21]. The thermal

treatment process effectively removes the SEI layers, rendering the surface of the anode active materials hydrophobic [20]. Alternatively, an improvement in the froth flotation separation has been achieved using a fine grinding that exposed the fresh surface of the aged anode active materials [24].

Gravity separation between the anode and cathode active materials has also been previously investigated [25, 26]. Various heavy liquids were used to separate the anode active materials from cathode active materials [25, 26]. Cathode active materials, *e.g.* lithium cobalt oxides (LCO) and lithium nickel-manganese-cobalt oxides ($LiNi_xMn_yCo_zO_2$, x+y+z=1), have densities of 4.5-5.0 g/cm^3, while the density of graphite is 2.26 g/cm^3. Therefore, heavy liquids having densities in the range of 2.26-4.50 g/cm^3 enable a separation between the two mixed materials, such as diiodomethane, bromoform, sodium polytungstate (SPT), lithium metatungstate (LMT) [27]. However, these heavy liquids are viscous, and thereby limit a wide range of industrial applications. In addition, organic heavy liquids are toxic, and the recycling of these heavy liquids is challenging [28]. Alternatively, enhanced gravity separation technologies, such as Multi Gravity Mozley Separator (MGS), Falcon, Knelson, and Kelsey Jig, have been developed over the decades to separate ultrafine particles [29, 30]. Separation of the anode and cathode active materials from Li-ion batteries were studied using the Falcon SB concentrator operating at 10-150 G forces [31]. The result has shown limited success [32]. To date, no satisfactory separation performance has been achieved using the gravity separation methods.

Both the anode and cathode active materials used in Li-ion batteries have particle sizes of 5-20 microns. The Falcon ultrafine (UF) concentrator is one of enhanced gravity separation technologies that has been demonstrated previously to separate ultrafine particles [33]. This concentrator is used commercially for concentrating platinum group metals (PGM), gold, and silver from an ultrafine ore feed [34-36]. In this study, the separation of two battery materials using the Falcon UF concentrator is evaluated with a blended mixture of pristine graphite and lithium nickel-manganese-cobalt oxide as the sample. The effect of feed mass, solid composition, G forces, and feed composition are systematically evaluated. The results are analyzed to determine two key metrics, namely, the separation index (SI), and the cumulative grade of NMC in the concentrate. Based on the result from the single-stage experiment, multiple stages of the separation experiments are evaluated. In addition, separation between anode and cathode materials from spent Li-ion batteries was evaluated by the enhanced gravity separation method. Comparison has been conducted with feed mass w/ and w/o thermal treatment.

6.2 Materials and Methods

6.2.1 Materials

Pristine lithium nickel manganese cobalt oxide ($LiNi_{0.33}Mn_{0.33}Co_{0.33}O_2$, NMC111) was obtained from Toda America, and pristine graphite (SLC1520P) powders were obtained from Superior Graphite. De-ionized (DI) water, with a resistance of 17.9-18.2 MΩ·cm, was obtained from a Barnard water purification system (Thermo Fisher). Lithium

metatungstate (LMT), with a specific density of 2.95, was obtained from LMT Liquid Inc and was used as received.

Individual spent Li-ion batteries were removed from used Laptop battery packs. They were discharged to 2.8V at C/10 rate and hold at 2.8 V for at least 24 hours, prior to the dismantling process for the safety caution. The battery cells were opened using a rotary tool to remove the stainless-steel outer casing, dismantling process carried out in fume hood to avoid inhalation of volatile organics. The battery cores were unfolded to separate anode layers, cathode layers, plastic separators, and other components manually. The delamination process is carried out using a wet agitation process in a 1-L commercial blender. 5-20 seconds of agitation is sufficient to delaminate the electrode composite from the current collectors. The processed slurries are then sieved using 70- and 140-mesh screens, materials above screen got re-blended to reduce particle size and re-screened until most of black mass recovered. Under size materials rinsed with DI water three times to wash off excess electrolytes and organics, then filtered to obtain filter cakes. Electrode mixture dried in force air oven overnight at 90 ℃. The black mass samples were heat treated at temperatures of 250, 300, 350, 400 ℃ for 1 hr. Black mass without thermal treatment compared as blank group.

6.2.2 Separation Mechanism

Figure 6-1 shows a schematic drawing of the Falcon UF concentrator used in this study. The Falcon UF concentrator is a conical smooth bowl with a slight reduction in diameter at the outlet to create a retention zone [37]. The UF concentrator has a depth of 105 mm (4.13 inches) and an inner diameter of 100 mm (4.00 inches). The bowl rotates up to 4,800 RPM, creating a centrifugal force in the range of 50G - 300G. The UF concentrator consists of two sections including 1) a migration zone and 2) a retention zone [37]. At the migration zone, under the centrifugal force, the slurry forms a thin liquid film with particles preferentially concentrated along the wall of the bowl, creating strong interlayer shears. Due to the difference in particle settling velocity enhanced by centrifugal force, fine heavy particles arrive at the wall prior to coarse light ones. As the slurry continues to feed into the bowl, more particles compact at the wall of the rotating bowl. Small denser particles across the interlayers and move into its inner wall, pushing coarser and lighter particles out of the bed. These lighter and coarser particles are flushed with the overflow stream [38]. Particles at the retention zone are collected manually in the laboratory setting, and may be recovered with a flushing water in the commercial operation.

6.2.3 Experimental Procedure

In this study, separation of the pristine NMC and graphite powders was conducted using Falcon L40 ultrafine (UF) bowl. The two materials were mixed with DI water at different weight ratios to prepare a slurry. The slurry was agitated using an overhead agitator (Caframo) to ensure that the two materials were mixed. In a nominal operation, a slurry was fed through a center feed tube of the rotating concentrator. The feed rate was approximately 3.0 L/min. The rotation ceased when the slurry was no longer flushed into the overflow stream. Materials inside the concentrator were sampled, collected, and dried in an oven at 100 ℃ overnight. All samples were weighted, and a fraction of these

samples were analyzed using the thermogravimetric analysis (TGA) to determine materials' composition.

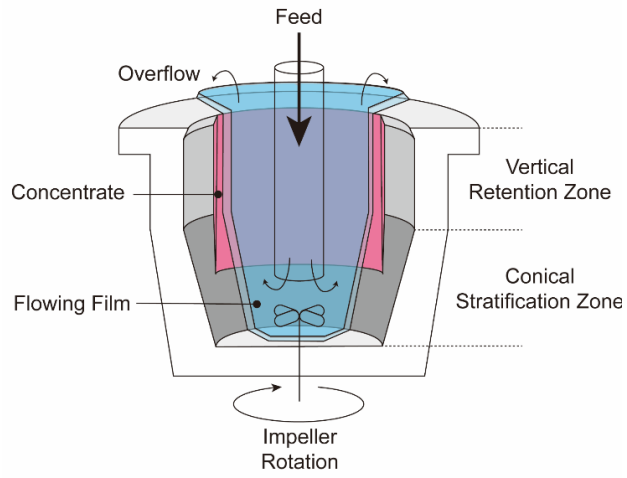

Figure 6-1. A schematic cross section of the Falcon L40 ultrafine (UF) concentrator after Refs [33, 39].

6.2.4 Data Analysis

Two experimental procedures were used to evaluate the separation performance. In the first method, materials collected inside the bowl were used as the concentrate product, while the overflow slurry was treated as the tailing product. The separation index (SI) is defined as the recovery of graphite (R_c) in the concentrate subtracted from the recovery of NMC (R_{NMC}) in the concentrate, as $SI = R_{NMC} - R_c$. The SI value equal to 1 suggests a perfection separation between the two materials, and the SI equal to 0 means that no separation between the two materials. In using the second method, materials collected at the different vertical sections within the concentrator were sampled and analyzed. Materials collected below a given cut-off position were used as the concentrate product, while the materials collected above the cut-off position within the concentrator were combined with the overflow product, and used as the tailing product. Both the SI values as well as the cumulative recovery and grade of NMC in the concentrated product were determined at different cut-off positions.

6.2.5 Characterization

Material compositions of the samples were analyzed by thermogravimetric analysis (TGA) using a thermogravimetric analyzer (TGA701, LECO). The chamber temperature rose from room temperature to 800 ℃ with at 1 ℃/min rate. The measurements were conducted at an air flow of 7 L/min. The remaining mass percentage of the sample at 800 ℃ was the mass percentage of NMC in the sample, while the percentage of the weight loss was the percentage of graphite in the sample. For black mass obtained from spent LIBs, weight loss between 25 and 400 ℃ is considered as PVDF and organic layers from particle surface, 400 – 800 ℃ weight loss is attributed to graphite burn off, the remained mass is cathode material. Both the chemical composition and morphology of samples

were determined using scanning electron microscopy (SEM) coupled with energy-dispersive X-ray spectroscopy (EDX). Imaging and elemental mapping was performed in a Philips XL40 environmental scanning electron microscope (ESEM) at 15kV accelerating voltage in high vacuum. Images were obtained under back scattered electron (BSE) mode.

6.3 Results

6.3.1 Material Characterization

Figure 6-2a) shows particle size distribution (PSD) by volume of both the pristine NMC111 and graphite materials. The mean particle sizes of the pristine NMC and graphite materials were 9.23 and 18.22 µm, respectively. As shown, graphite particles were slightly bigger than NMC111 powders. Figure 6-2b) shows an image of a mixture of pristine NMC111 and graphite in the LMT solution in 2 days after mixing. Graphite powders floated to the top of the LMT solution while NMC111 sunk to the bottom, confirming the difference in specific densities between the two materials. Figure 6-3c shows SEM/EDX images of the pristine NMC111 and graphite materials. Both particles were spherical. The result confirmed that graphite particles were slightly larger than that of NMC111.

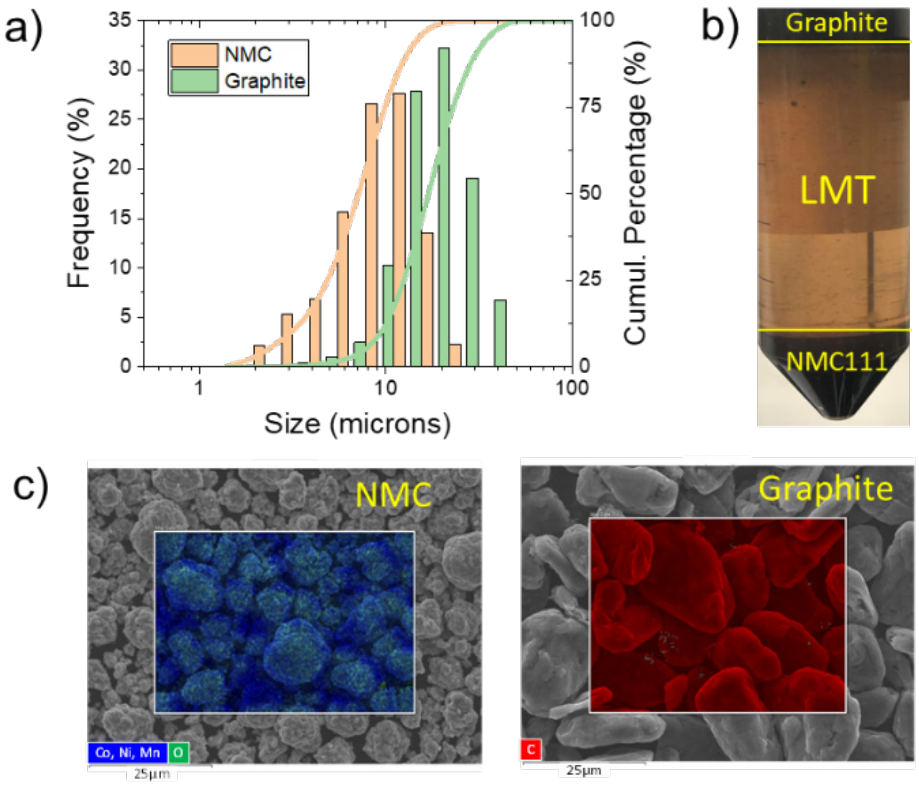

Figure 6-2. Characteristics of the NMC and graphite samples used in this study. a) Particle size distribution of pristine graphite and MC111 materials, b) a photo of a mixture of pristine graphite and NMC111 materials in lithium metatungstate (LMT) solutions of a specific density of 2.95, and c) SEM images of pristine NMC111 and graphite materials.

6.3.2 Effect of operational variables

Table 6-1 shows both the yield and compositions of both the concentrate and tailing products after one pass in the Falcon UF concentrator. Materials collected within the bowl were the concentrate product, while the overflow slurry were the tailing product. The UF concentrator operated at 163 g-force (60 Hz). A 6-liter slurry consisted of 180 grams of NMC111 and 120 grams of graphite was fed to the concentrator. The results showed that 67% of the dry mass was collected within the concentrator, and the remaining 33% of the dry mass was rejected to the tailing product. The concentrate product consisted of 86.48% of NMC and 13.52% of graphite by weight, while the tailing product consisted of 87.75% of graphite and 12.25% of NMC by weight. The yield (or recovery) of NMC in the concentrate product reached 93.78%, while the yield of graphite in the concentrate product was 24.76%. The separation index (SI) was determined to be 69.02%. A good separation performance was achieved after one pass in the UF concentrator.

Table 6-1. Separation between the NMC and graphite materials in a 5% solid slurry after one pass in a Falcon UF concentrator operating at 163 G.

Product	Mass (g)	Yield (%)	Composition		Distribution (%)	
			NMC (%)	C (%)	NMC (%)	C (%)
Concentrate	201.55	67.18 %	86.48%	13.52%	93.78%	24.76%
Tailing	94.32	32.82 %	12.25%	87.75%	6.22%	75.34%
Feed	295.87	100.00 %	62.82%	37.18%	100.00%	100.00%

Figure 6-3 shows the effect of feed mass on the separation between the NMC and graphite with experimental data shown in Table 6-2. These results were obtained with 100 to 600 grams of 5 wt. % slurries having an NMC:C ratio of 60:40 by weight. The gravity separation operated at 163 G force. The yield of the concentrate decreased with increasing the feed mass monotonically, as shown in Figure 6-3a. Figure 6-3b shows the percentage of NMC in both the concentrate and tailing products at different feed masses. It was shown that the grade of NMC in the concentrate increased with increasing the feed mass. For instance, the grade of NMC in the concentrate increased from 65.46% at 100 grams of the dry feed to 90.82% at 600 grams of the dry feed. The percentage of NMC in the tailing product decreased from 20.40% at 100 grams of feed to 11.25% at 400 grams

of feed, but was increased to 18.23% at 600 grams of dry feed. This result showed that 500-600 grams of feed mass might be desirable to achieve a higher grade of NMC in the concentrate.

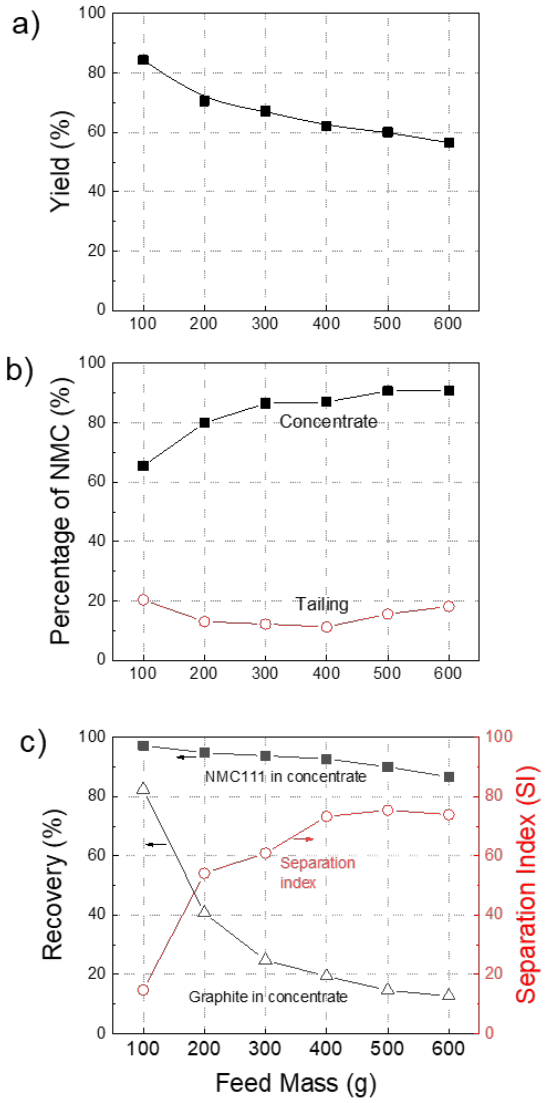

Figure 6-3. Effect of feed mass on the separation between the NMC and graphite. a) yield of the concentrate, b) percentages of NMC in the concentrate and in the tailing products, c) recovery of NMC111 in the concentrate and tailing products as well as the separation index.

Table 6-2. Effect of feed mass on the separation between the NMC and graphite in the concentrate and tailing products.

Feed mass (g)	Mass of Conc (g)	Yield of Conc (%)	R_{NMC} in Conc	R_C in Conc	Separation index	%NMC in Conc	%NMC in Tail
100 g	84.35 g	84.35%	97.20%	82.43%	14.77%	65.46%	20.40%
200 g	141.11 g	70.55 %	94.82%	40.69%	54.13%	79.96%	13.10%
300 g	201.55 g	67.18 %	93.78%	24.76%	60.92%	86.48%	12.25%
400 g	264.04 g	62.12 %	92.69%	19.39%	73.30%	86.98%	11.25%
500 g	303.75 g	60.09 %	90.03%	14.66%	75.38%	90.70%	15.64%
600 g	337.37 g	56.48 %	86.61%	12.71%	73.90%	90.82%	18.23%

Figure 6-3c shows the recovery of both the NMC and graphite in the concentrate product, respectively, at different feed masses. At 100 grams of the dry feed, despite the recovery of the NMC in the concentrate was 97.20%, the recovery of graphite in the concentrate was 82.43%. In this regard, the separation index was only 14.77%, suggesting a poor separation between the NMC and graphite materials. When the feed mass was increased, the recovery of the NMC materials in the concentrate dropped slightly with increasing the feed mass. On the other hand, the recovery of graphite in the concentrate dropped significantly with increasing the feed mass. For instance, the recovery of graphite in the concentrate dropped from 82.43% at 100 grams of feed mass to 12.71% at 600 grams of feed mass. As a consequence, the separation index (SI) increased with increasing the feed mass and reached a plateau of 75.38% at 500 grams of feed mass. The separation index (SI) dropped slightly to 73.90% at 600 grams of dry feed due to a lower yield (86.61%) of NMC in the concentrate product. The lower separation performance at the higher feed mass may be attributed to an overloading of the feed in the concentrator.

Figure 6-4 shows the effect of G forces on the separation between the NMC and graphite. The feed was a 5 wt. % slurry with 400 grams of the dry feed having a 3:2 NMC-to-graphite ratio by weight. The experiments were conducted at different G forces in the range of 41 G – 290 G. The yield of the NMC in the concentrate increased with increasing G force, and reached a plateau at 113 G force or higher, while the yield of graphite in the concentrate product decreased with increasing the G force. For instance, at 41-72 G force, the yield of the NMC in the concentrate product was 73.94%, while the yield of graphite in the concentrate product was 21.13%. This resulted in a separation index of 52.80%. The separation index improved with increasing the G forces and reached a plateau of 76-78% at 113 – 290 G force. It was found that that the G force had a minimal impact on the separation performance at 113 G force or higher.

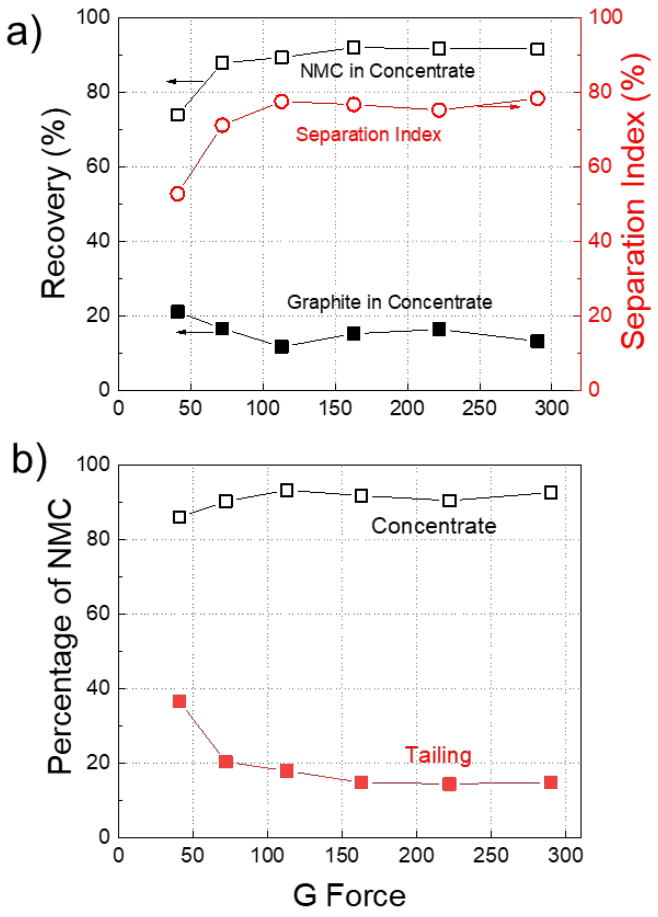

Figure 6-4. Effect of G force on the separation between the NMC and graphite. a) recovery of NMC and graphite in the concentrate as well as the separation index at different G forces; b) percentage of NMC in both the concentrate and tailing products.

Figure 6-4b shows the grade of NMC in both the concentrate and tailing products. The percentage of the NMC materials in the concentrate increased with increasing the G force, while the percentage of NMC in the tailing product decreased with increasing the G force. The percentage of NMC in the concentrate product reached 91-93% at 113-290 G force after one pass in the UF concentrator. On the contrary, the grade of NMC in the tailing product decreased from 36.61% at 41 G force to 14.49-14.88% at 163-290 G force.

Figure 6-5 shows the effect of solid concentration on the separation between the NMC and graphite. The feed was 300 grams and 400 grams of a blended mixture having a 60:40 NMC-to-graphite ratio by weight. The solid concentration in the slurry ranged from 2.5% to 20%. For both 300 and 400 grams of feed mass, the recovery of NMC in the concentrate product increased with increasing the solid concentrations. And, the recovery of graphite in the concentrate product increased with increasing the solid concentration. At 15% solid concentration or higher, there was a substantial increase in

the recovery of graphite in the concentrate product compared to that obtained at 10% solid concentration or less.

Figure 6-5b shows the separation index at different solid concentrations. The separation index (SI) increased with increasing the solid concentrations, and reached a plateau at 10% solid concentration. At 15% solid concentration or higher, the separation index dropped by 5%-10%. As shown, with 300 grams of dry feed, the optimum separation index was 76.12%. With 400 grams of dry feed, the optimum separation index was 79.14%. At low solid concentration, i.e., a dilute slurry, heavy particles were easily flushed with the slurry into the overflow stream, resulting in a decrease in recovery of the NMC in the concentrate product. At high solid concentration, graphite particles trapped between interlayers within the particle bed, resulting in a poor separation between the graphite and NMC.

In addition, solid concentration was found to be important to the grade of NMC in both the concentrate and tailing products. The result (Figure 6-5c) showed that the percentage of NMC in the concentrate product was relatively the same at 10% solid concentration or less. However, as the solid concentration increased, the percentage of NMC in the tailing product was decreased. As shown, with 300 grams of the dry feed, the grade of NMC in the tailing product was decreased from 17.8% at 2.5% solid concentration to 11.3% at 10% solid concentration.

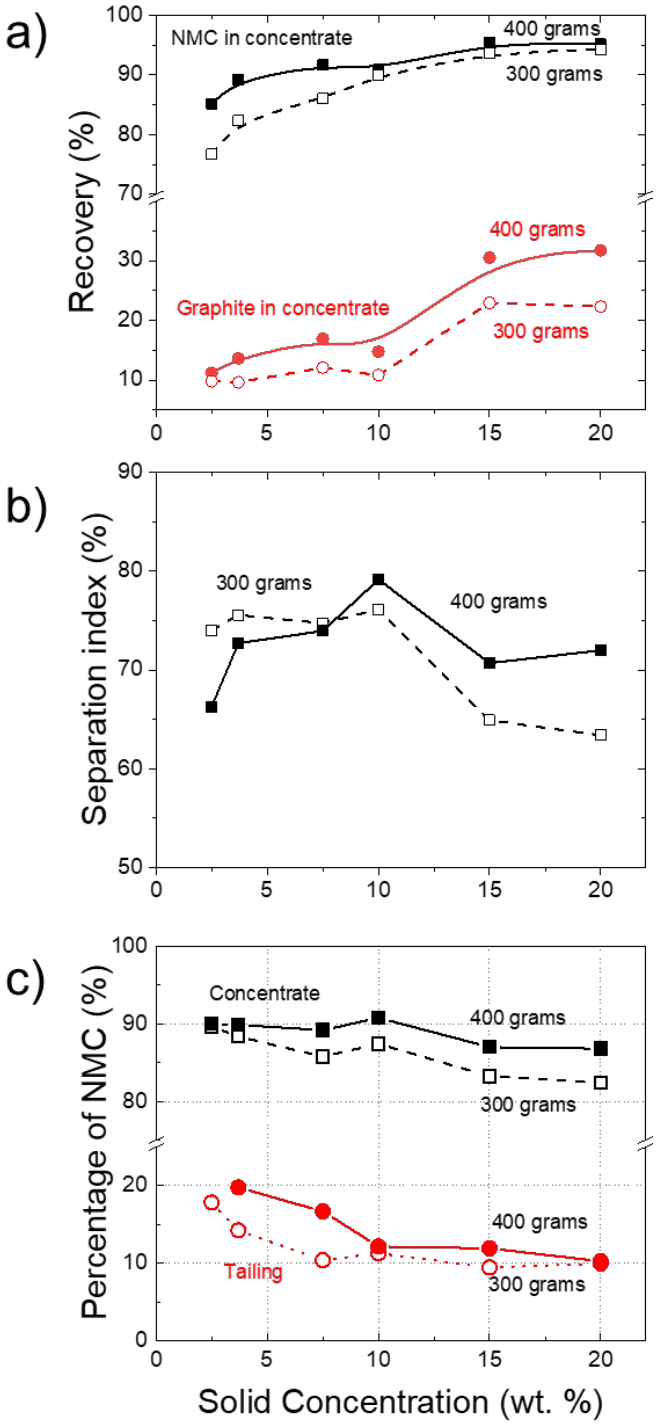

Figure 6-5. Effect of solid concentration on the separation between the NMC and graphite with 300 grams and 400 grams of dry feed mass. a) recovery of NMC and graphite materials in the concentrate product, b) separation index, and c) percentage of NMC in the concentrate and tailing products.

6.3.3 Effect of Cut-off position

To better understand the distribution of the NMC and graphite materials inside the concentrator, materials collected at different vertical sections along the inner wall of the concentrator bowl were characterized. Each section has a depth of 15 mm. Figure 6-6a shows a schematic cross section of the Falcon ultrafine (UF) bowl. The lowest section is labelled as section #1, while the upper section is labelled as section #7. Table 6-3 shows the result obtained with 300 grams of dry feed in a 5 wt. % slurry. The concentrator operated at 163 G force. The heavier NMC materials were concentrated at the lower section of the wall. As the slurry flow upward, more graphite particles were retained at the upper sections of the concentrator. For instance, the percentage of NMC at section 4 was 94.28% and the percentage of NMC was decreased to 61.84% at section 5, 41.52% at section 6, and 45.46% at section 7. Also shown in Table 6-4 is the distribution of NMC and graphite at each section within the concentrator. Over 80% of the NMC materials were concentrated at the lower sections (1-5) of the concentrator, while 75.24% of the graphite powders were reported to the overflow product and ~20% of the graphite powders were collected at the upper section within the UF concentration. Less than 7% of the NMC materials were collected at the overflow product.

Table 6-3. Distribution of NMC and graphite within the Falcon UF concentrator.

Position	Location (mm)	Mass in dry g)	Weight (%)	%NMC (%)	Distribution of NMC (%)	Distribution of Graphite (%)
Tail	-	94.32	31.88%	12.25%	6.22%	75.24%
7	90-105	5.90	1.99%	45.46%	1.44%	2.93%
6	75-90	15.78	5.33%	41.52%	3.52%	8.39%
5	60-75	27.81	9.40%	61.84%	9.25%	9.65%
4	45-60	42.46	14.35%	94.28%	21.53%	2.21%
3	30-45	39.67	13.41%	99.21%	21.18%	0.28%
2	15-30	43.67	14.76%	99.23%	23.32%	0.31%
1	0-15	26.27	8.88%	95.79%	13.54%	1.00%
Total		295.87	100.00%	62.87%	100%	100%

Table 6-4 shows the effect of cut-off positions on both the recovery and grade of the NMC in the concentrate product as well as the percentage of NMC in the tailing product.

Materials collected below the cut-off position were treated as the concentrate product, while the materials collected above the cut-off position mixed with the overflow product were treated as the tailing product. The result showed that the cumulative yield of both the NMC and graphite in the concentrate product increased with increasing cut-off positions. For instance, at a cut-off position of 4, the cumulative yield of the NMC in the concentrate product reached 79.56% and that of graphite in the concentrate product reached 3.8%. As a result, the separation index at the cut-off position of 4 was 75.76%. At the cut-off position of 6, the cumulative yield of both the NMC and graphite in the concentrate were increased to 92.34% and 21.84%, respectively. The separation index (SI) was found to be increasing with increasing the cut-off positions. The separation index was increased from 12.53% at a cut-off position of 1 to 75.76% at a cut-off position of 4, and then decreased to 69.02% at a cut-off position of 7. The optimum separation index occurred at the cut-off position of 4.

Table 6-4. Cumulative Result of the Separation Performance between graphite and oxides minerals.

Cut-off position	Cumulative Recovery of NMC (%)	Cumulative Yield of Graphite (%)	Separation Index (%)	Cumulative Grade of NMC (%)
7	93.78%	24.76%	69.02%	86.48%
6	92.34%	21.84%	70.50%	87.72%
5	88.81%	13.45%	75.36%	91.77%
4	79.56%	3.80%	75.76%	97.25%
3	58.03%	1.59%	56.44%	98.40%
2	36.85%	1.31%	35.54%	97.94%
1	13.54%	1.00%	12.53%	95.79%

Also shown in Table 6-4 is the cumulative grade of NMC in the concentrate product at different cut-off positions. The cumulative grade of the NMC in the concentrate product was found to be increasing with increasing the cut-off position, and reaching a plateau, and then decreasing with raising the cut-off position. The optimum cumulative grade of NMC in the concentrate product was 98.40% at a cut-off position of 3, at which the cumulative yield of NMC in the concentrate product was 58.03%. At a cumulative grade of NMC in the concentrate product of 91.77%, the cumulative recovery was increased to 88.81%. Note that the separation index is more relevant to the rougher stage, in which an optimum separation between the NMC and graphite is needed. The cumulative grade of NMC in the concentrate product may be more relevant to the cleaner stage, in which the

grade of the NMC materials in the concentrate product is important. The present result shows that the cut-off position is vital to achieve an optimum separation performance and ensure that the product grade meets the product specifications.

To further demonstrate the effect of feed mass on the separation between the NMC and graphite, detailed analyses on the separation between the NMC and graphite at different feed masses were conducted. Figure 6-6b shows the yield of concentrate at different positions within the concentrator. As shown, at 200 grams of dry feed or lesser, most of the materials were concentrated at the position 3-5. When the feed mass was increased, more materials were accumulated at the lower sections of the concentrator. Figure 6-6c shows the percentage of the NMC in each section of the concentrator. As shown, the percentage of NMC at each section of the concentrator decreased with raising the position. The percentage of the NMC was increased with increasing the feed mass, and reached the plateau at 500-600 grams of the feed. Figure 6-6d shows the distribution of NMC within the concentrator at different feed mass. Less than 10% in total of the NMC materials were concentrated at the upper section of the concentrator. Majority of the NMC materials were distributed at the section #5 or below.

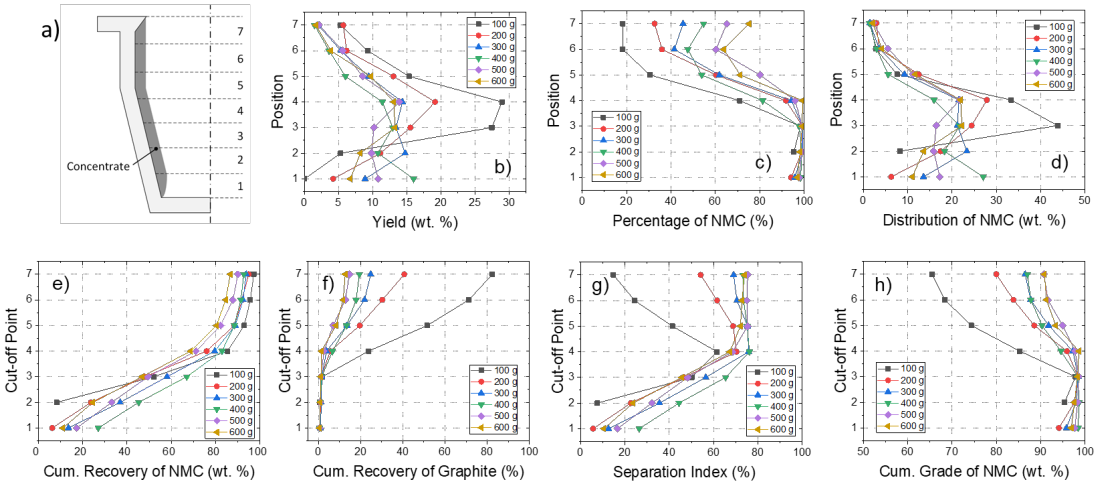

Figure 6-6. Distribution of materials within the Falcon UF concentrator and the effect of cut-off positions on the separation performance at different feed mass. a) a schematic cross section of the UF concentrator and materials collected within the concentrator were separated into seven fractions vertically; b) yield of concentrates at each position; c) percentage of NMC in each section; d) distribution of NMC within the concentrator; e) effect of cut-off position on the cumulative recovery of NMC in the concentrate product; f) effect of cut-off position on the cumulative recovery of graphite in the concentrate product; g) effect of cut-off position on the separation index, h) effect of cut-off position on the cumulative grade of NMC.

Figure 6-6e and 6-6f shows the cumulative recovery of the NMC and graphite in the concentrate product as a function of cut-off positions, respectively. As expected, the cumulative recovery of the NMC increased with increasing the cut-off position. The

optimum cumulative recovery of NMC were obtained at 300 grams or 400 grams of the feed. At a lower feed mass, most of graphite and NMC were retained within the bowl. At a higher feed mass, the cumulative recovery of the NMC in the concentrate product was slightly reduced, which might be attributed to an overloading of the materials within the concentrator. Likewise, the cumulative recovery of the graphite in the concentrate products was increased with increasing the cut-off positions. The cumulative recovery of graphite in the concentrate decreased with increasing the feed mass from 100 grams to 600 grams. Figure 6-6g shows the separation index as a function of the cut-off positions. The separation index varied with the feed mass. At the feed mass of 300 grams or below, the separation index increased and then decreased with increasing the cut-off position. The optimum separation index occurred at a cut-off position of 4. At the feed mass of 400 grams or above, the separation index was increased and then remained consistently with increasing the cut-off position. Figure 6-6h shows the cumulative grade of the NMC in the concentrate product as a function of cut-off positions. The cumulative grade of NMC in the concentrate product increased and then decreased with increasing the cut-off position. The high feed mass resulted in a higher cumulative grade of oxides. Nevertheless, at 500-600 grams of the dry feed, the cumulative grade of NMC in the concentrate product was above 90% at any cut-off positions.

Table 6-5 shows the cut-off position where the SI and the cumulative grade of NMC in the concentrate reached the optimum at different feed mass. The SI peaked at position 4 at the feed mass of 400 grams or less. At the feed mass of 500 and 600 grams, the peak position occurred at position 7. However, the maximum SI dropped from 76.16% at 400 grams, to 75.4% with 500 grams of feed and 73.9% at 600 grams of dry feed, respectively. The optimum cut-off position where the cumulative grade of NMC in the concentrate product was found to be position 3-4, and the optimum cut-off position was insensitive to the amount of the feed mass.

The present result provides an optimum operating condition for the follow-up multi-stage separation experiments. To maximize both the throughput and separation performance, the separation experiments were preferred to operate with 300-500 grams of the dry feed. Materials collected inside the concentrator were used as the concentrate product, while the overflow product was used as the tailing product. To maximize the percentage of NMC in the concentrate product, the cut-off position should be position 4 or 5.

Table 6-5. Optimum cut-off position that maximizes the separation index and cumulative grade of NMC in the concentrate product.

Feed mass	Max Separation Index	Max Cumulative Grade
100 g	4	3
200 g	4	3

300 g	4	3
400 g	4	2
500 g	7	3
600 g	7	4

6.3.4 Effect of Feed Composition

Effect of feed composition on the separation performance was examined. The 60:40 NMC-to-graphite ratio by weight is a typical ratio for the black mass from Li-ion batteries. After one pass in the Falcon UF concentrator, the tailing product contained 10-30% of NMC materials which are needed to be recovered to maximize the total recovery. Figure 6-7 shows the separation result obtained with the feed that consisted of 20% by weight of graphite and 80% by weight of NMC. The concentrator operated at 163 G force. It was found that the recovery of NMC in the concentrate product decreased slightly with increasing the feed mass and the solid concentration in the slurry have minor impacts on the recovery of NMC in the concentrate product. However, the recovery of graphite in the concentrate was decreased at a more rapid rate with increasing the feed mass. For instance, at 100 grams of feed mass, the recovery of graphite in the concentrate product at 5% solid concentration reached 71.60%. The graphite recovery in the concentrate product was decreased to 25.65% and 15.32% at 300 grams and 500 grams of the feed mass, respectively. The result also showed that the recovery of graphite in the concentrate at 10% solid concentration was higher than those obtained at 5% solid concentration. As a consequence, the separation index was increased with increasing the feed mass from 100 grams to 400 grams and decreased at the feed mass of 500 grams or above (Figure 6-7b). With 400 grams of the feed mass, the separation index (SI) reached an optimum of 67.75% at 400 grams of the feed. The effect of solid concentration on the gravity separation between the NMC and graphite was also examined (Figure 6-7b). It was shown that the higher solid concentration (10% by weight) lowers the separation performance slightly.

Figure 6-8 shows the effect of solid concentration and feed mass on the percentage of NMC in both the concentrate and the tailing products. It is desirable to have a low percentage of NMC in the tailing product to ensure a maximum recovery of NMC. The result showed the percentage of NMC in the tailing product was in the range of 3% and 5%, while the percentage of NMC in the concentrate product was in the range of 38-47% for 300 grams of the feed mass, and 47-53% for 400 grams of the feed mass. The percentage of NMC in the concentrate product increased with increasing the feed mass. The result shows that the 5% solid concentration works best in maximizing the grade of NMC in the concentrate product and minimizing the grade of NMC in the tailing product.

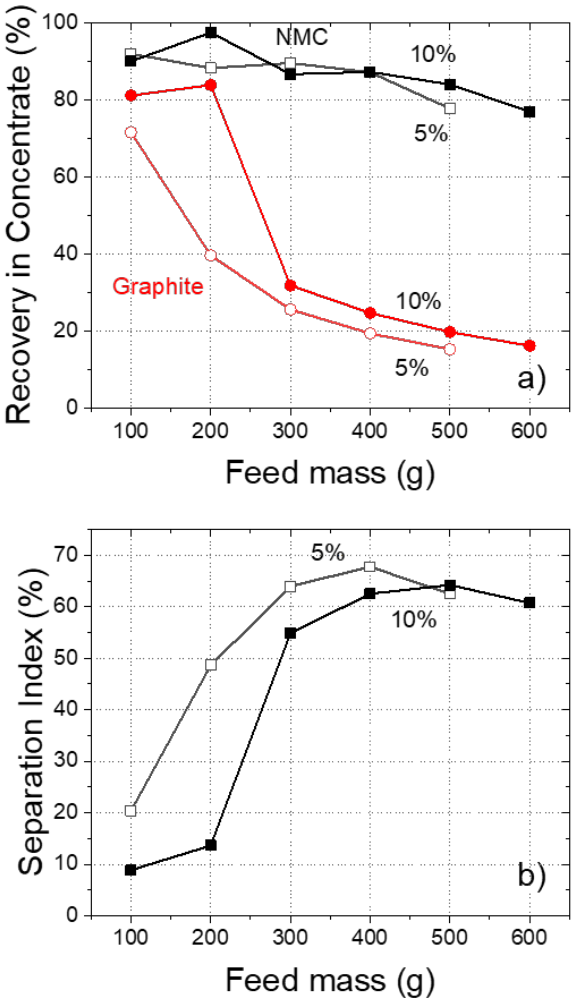

Figure 6-7. Effect of feed mass and solid concentration on a) recovery of NMC and graphite in the concentrate product, b) separation index between the NMC and graphite from a blended feed with 20:80 NMC-to-graphite ratio by weight.

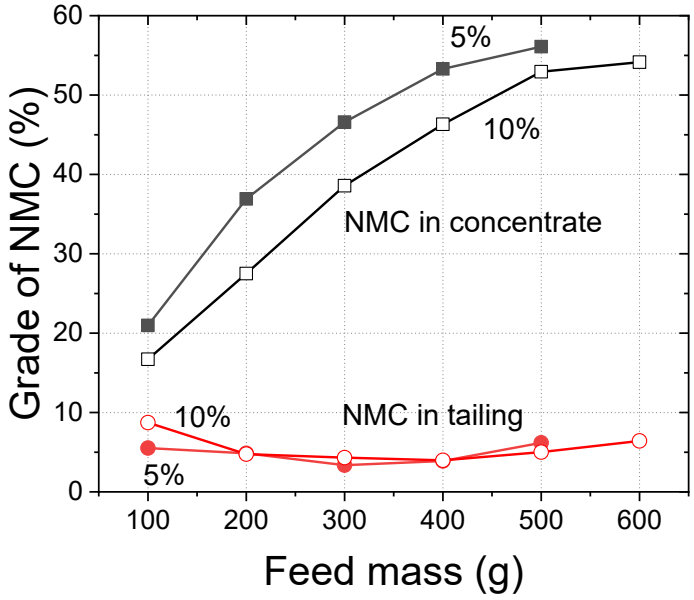

Figure 6-8. Effect of feed mass and solid concentration on the grade of NMC in the concentrate and tailing products from a blended feed with 20:80 NMC-to-graphite ratio by weight.

6.3.5 Multistage Separation

To evaluate the separation performance between the NMC and graphite after multiple stages of Falcon UF gravity separation, multistage of gravity separation experiments were conducted. Figure 6-8 shows a schematic drawing of a flowsheet that was used to separate a mixture of pristine NMC and graphite materials. The flow sheet consisted of a rougher stage, two cleaner stages and two scavenger stages. In the rougher stage, the feed was spitted into two circuits in parallel with 300 grams of the dry feed in each run. The rougher stage operated at 300 G force. Materials collected within the concentrator from the two parallel runs were combined and mixed with DI water to prepare a 5% solid slurry, and fed into a cleaner stage. The cleaner stage operated at 300 G force. The materials at the cut-off position of 5 were mix with DI water to prepare a 5% solid slurry. The slurry was then fed into a second cleaner stage. The materials collected at a cut-off position of 5 were used as the final concentrate product. Both the overflow product and cake materials collected above the cut-off position from both the first and stage cleaner stages were combined into one middling product. The overflow products after the rougher stage was dewatered by filtration and combined. The filter cake was mixed with 6L of the process water to prepare a slurry with 5% solids by weight, and fed into the first scavenger cycle. The overflow product from the first scavenger cycle were dewatered and mixed with 4L of the process water to prepare a slurry and fed to a second scavenger cycle. The overflow product was used as the final tailing product. Both the concentrate products from both the first and the second scavenger cycles were combined and reported as the middling product.

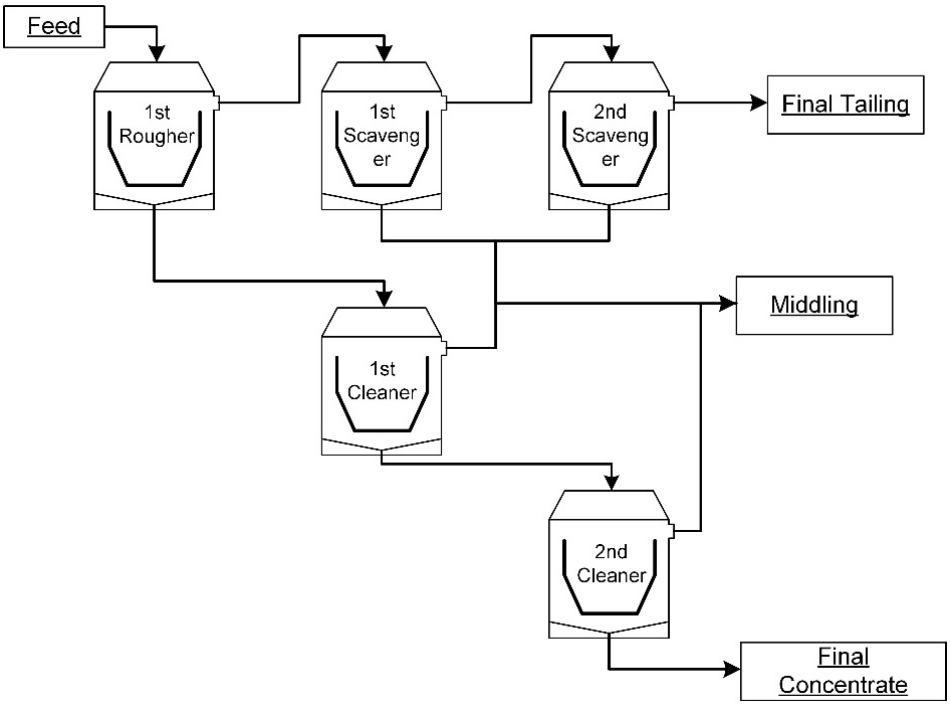

Figure 6-9. A schematic drawing of a gravity separation circuit that was used to separate a mixture of pristine NMC and graphite powders.

Table 6-6 shows the multistage separation experiment result. The feed consisted of approximately 60% by weight of NMC and 40 % by weight of graphite. After one rougher stage, the concentrate product consisted of 87-90% of NMC and 10-13% of graphite. The tailing product consisted of 18-20% of NMC by weight and 80-82% by weight of graphite. A reasonable separation between the NMC and the graphite was accomplished after one pass in the UF gravity separation. The concentrate product from the rougher stage was fed into two cleaner stages in series. After the first cleaner stage, the percentage of NMC in the concentrate product was raised to 96.95%. The percentage of NMC was further raised to 99.02% after the second cleaner stage. The tailing product from the rougher cycle was fed into two scavenger cycles. The percentage of NMC in the tailing products was lowered to 3.88 % and 0.35%, respectively after two scavenger cycles in sequence. The final tailing product contained 0.35% of NMC and 99.7% of graphite. Figure 6-10 shows the SEM images of both the final concentrate and tailing products. The result showed that the concentrate product consisted of NMC materials, and the tailing product consisted of graphite materials. The middling product can be fed back into the rougher cycle and being reprocessed. The circuit design will be conducted to meet the design requirement (product purity) and minimize the amount of the intermediate products in the circulation.

Table 6-6. Materials' composition of separated products after each stage of the Falcon UF separation.

Process	NMC in Feed (%)	NMC in Concentrate (%)	NMC in Tailing (%)
1st Rougher - Run1	62.94%	89.94%	19.69%
1st Rougher - Run2	60.78%	87.79%	17.91%
1st Cleaner	88.11%	98.38%	64.31%
2nd Cleaner	98.66%	99.40%	95.07%
1st Scavenger	19.46%	45.35%	3.88%
2nd Scavenger	2.94%	6.63%	0.35%

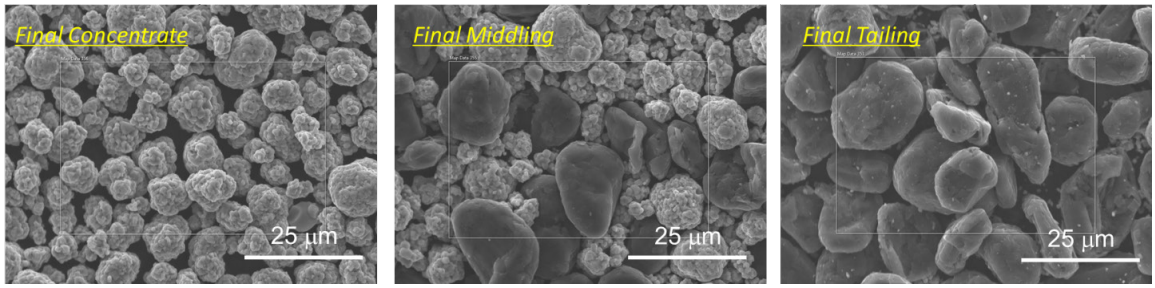

Figure 6-10. SEM image of the concentrate product after the second cleaner cycle and the final tailing product after the second scavenger cycles, and the combined middling products from the process.

6.3.6 Black Mass from Spent Li-ion Batteries

Figure 6-11 shows the black mass obtained from spent LIBs under thermal treatment of different temperatures for 1 h each with 500 magnifications: raw black mass, 250 ℃, 300 ℃, 350 ℃, 400 ℃. It is noticeable that with 70- and 140-mesh screening, most of the powders are individual particles, while some cathode agglomerates were found as well. Particle size distribution by volume on raw black mass has also been conducted, the 50^{th} and 95^{th} percentiles are 23.27 and 86.79 µm, respectively. One interesting finding is that average particle size of individual graphite is larger than that of individual cathode powder.

As shown in figure 6-11 a-c, with thermal treatment temperature among 250 and 300 ℃, cathode agglomerates can still be found among the black mass mixture. However, with increased temperatures of 350 and 400 ℃ shown in figure 6-11 d and 6-11 e, no agglomerate was found. Also, the structure of individual particles remain the same after

elevated temperatures, all powders settled as single particles. This means with 350 and 400 ℃ thermal treatment for 1 h, PVDF was completely burnt off, individual anode and cathode electrode powders reclaimed. Another interesting finding is cathode powder found at 350 ℃ are more shinny than the one found at 400 ℃, this is possibly due to the SEI layer burnt off with increased thermal temperature. Similar phenomena were found in chapter 4 as well.

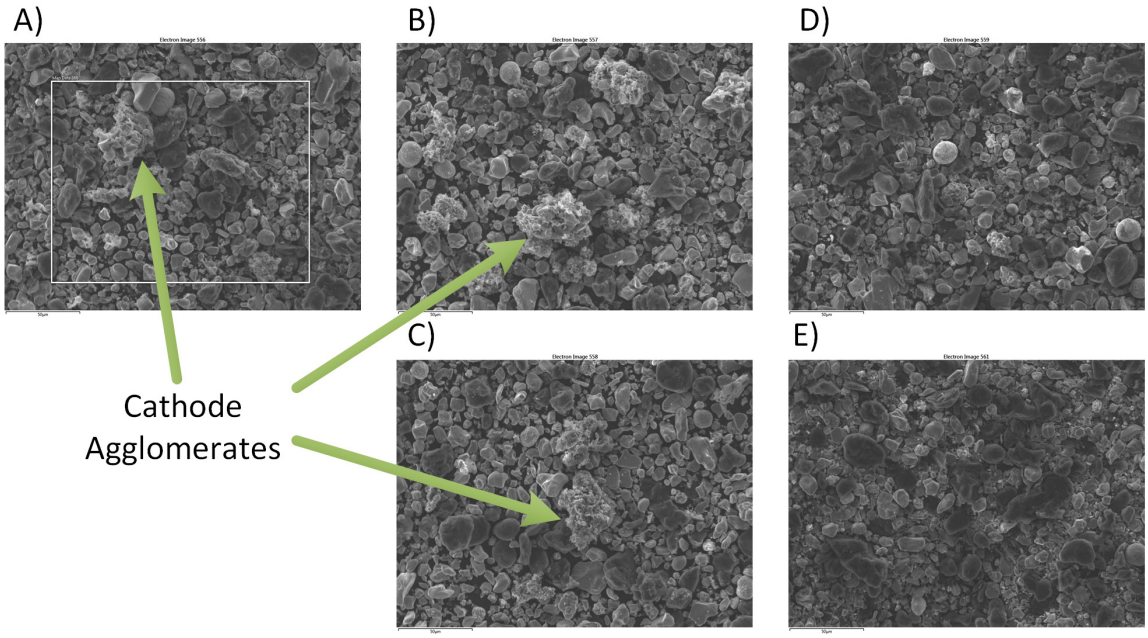

Figure 6-11. Black mass obtained from spent LIBs under different thermal treatment temperatures: A) raw black mass; B) 250 ℃; C) 300 ℃; D) 350 ℃; E) 400 ℃.

Multistage separations have been conducted with feed of raw black mass and 400 ℃ treated black mass using two stages of centrifugal gravity separation, flow sheet is the same as proposed in figure 6-9. Total of 800 grams of materials fed to two parallel roughers, low COP selected for rougher to maximize cathode grade in concentrate. To generate high grade products, high COP and low COP selected for scavenger and cleaner, respectively. Figure 6-12 shows the separation performances using recovery versus grade for anode in tailing and cathode in concentrate to evaluate experiments with and without thermal treatment. Rougher stages were first compared to understand the separation performance with only one run of gravity separator. 61% and 79% of cathode recovered at concentrate with over 93% and 94% grade for raw and pyrolyzed black mass, while 92% and 90% of anode recovered with 50% and 64% grade, respectively. It is interesting to find that only with rougher operation, over 93% grade of cathode can be reclaimed in concentrate, while anode material collected with high recovery numbers but low grade. For pyrolyzed sample, cathode grade got further improved from 98.88% to 99.11% with decreased recovery from 69.79% to 65.60% using 1 pass and 2 passes of cleaner. Even for the raw black mass, its grade in concentrate got improved from 97.765 to 98.35% with additional cleaners as well, yet the recovery decreased to 48.89% and 42.90%.

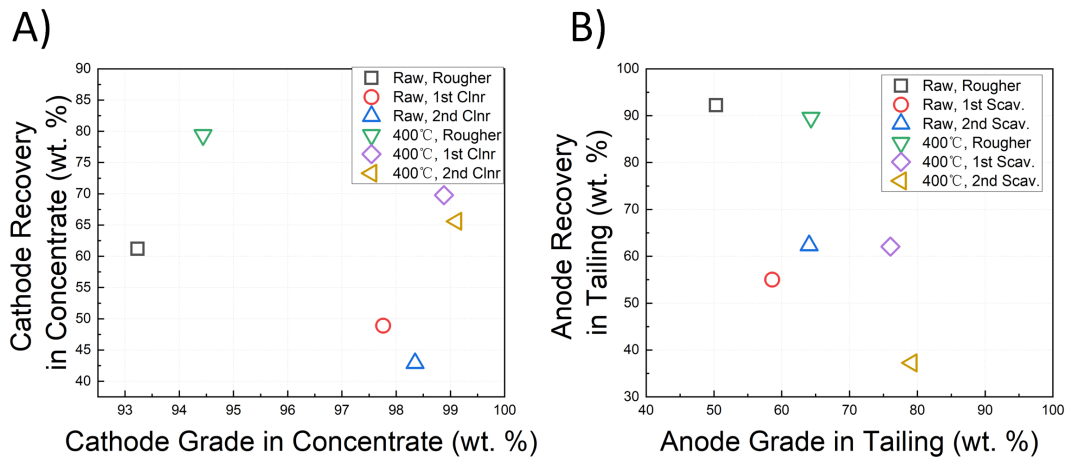

Figure 6-12. Recovery versus grade of electrode materials obtain for with and without thermal treatment black mass multistage operations. A) Comparison of cathode recovery and grade in concentrate; B) Comparison of anode recovery and grade in tailing.

To compare these results with data from multistage using pristine materials discussed above, cathode separation performances in concentrate were almost the same. Pyrolyzed and pristine multistage operations can achieve both over 98% of cathode obtain with recovery over 69% for 1 cleaner, and over 99.0% grade with 65% recovery with 2 cleaners. This inspiring finding suggests that pristine experiment is fully capable of guiding real black mass gravity separation obtained from spent LIBs, similar method applied to raw black mass as well with minimal decrease in cathode grade and recovery. Also, it is confirmed that thermal treatment at 400 °C can generate individual electrode materials that comparable with the pristine powders.

However, anode separation performance is way worse than pristine experiment, especially in grade of graphite. Even with thermal treatment, grade of anode in tailing increased from 64%, to 76% and 79% with additional scavenger stages. Its recovery decreased from 90%, to 62% and 37%, which is similar with pristine experiment. To explain this result, morphology of final tailing product with raw black mass is investigated and shown in figure 6-13a, while its final concentrate is shown in figure 6-13b. In tailing product, more amorphous binder is found, some agglomerated with electrode materials, others are just attached onto particle surface. Due to lower density of PVDF, majority of them is collected in the final tailing, this explains low anode grade in tailing for raw black mass experiment. After thermal treatment, 400 °C might broke down some cathode particles into smaller ones (- 5 µm), they reported to tailing product due to too fine of size and lower tailing's anode grade. Those cathode particles might come from long charging-discharging cycles of spent LIBs, which can be rarely found in pristine cathode. Nevertheless, despite of poor anode separation, grade and recovery of cathode materials from spent LIBs are satisfactory, pristine electrode materials separation can guide the separation process using black mass from real cells.

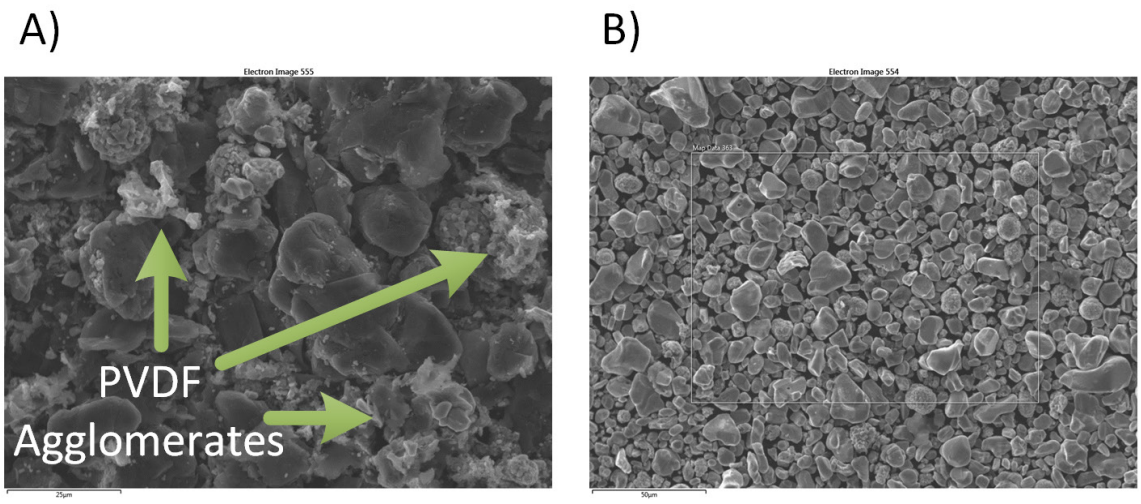

Figure 6-13. Comparisons of final A) tailing and B) concentrate product from multistage separation with raw black mass as feed material.

6.4 Discussion

The present work introduces a new method of separating electrode active materials used in Li-ion batteries. The gravity separation method takes advantage of the differences in the specific densities between the two materials being separated. NMC in water has a specific density of 4.5-5.0, while graphite has a specific density of 2.26. The difference in the specific densities enables a separation between the two materials. One method of separating these two materials is through the use of heavy liquids with densities between 2.26 g/cm^3 and 4.5 g/cm^3, such as diiodomethane, bromoform, and water-based sodium/lithium polytungstate [40]. As shown in Figure 6-2b, graphite floats on the surface of the LMT solution while the NMC powders sink to the bottom (Figure 2b), resulting in a separation between the two materials. However, heavy liquids are expensive, and the process is slow since many of these heavy liquids are viscous [41].

Gravity separation technologies have been used for decades and are commonly used in the mining and aggregate industries. Gravity separation operates in dry and wet slurries. Various gravity separation technologies have been developed to separate particles at different size ranges [42]. Mineral jig is commonly used to separate coarse particles [43]. For particles having sizes ranged between 100 µm and 1 mm, the spiral, sluice, Reichert cone, teeter-bed separator, shaking table, and reflux classifier are used to separate mixed materials in a slurry [44-46]. For ultrafine powders, enhanced gravity separation technologies have been developed. These technologies include the multigravity mozley separator (MGS), Falcon separator, and Knelson separator [47-49]. All these technologies operate under centrifugal forces.

Particle sizes of the electrode active materials are vital to the choice of a viable gravity separation technology. Crushing of spent Li-ion batteries results in a segmentation of individual battery components [50]. The fine fraction of the crushed materials, also

known as black mass, consists of anode active materials and cathode active materials. Particle size of the black mass was below 50 microns. Therefore, the Falcon UF and MGS might work well for separating the two mixed electrode active materials. The present result demonstrates that the use of the Falcon Ultrafine (UF) separator enables a good separation between the NMC and graphite. Compared with the froth flotation process, gravity separation is less sensitive to cycling, since the specific densities of the electrode active materials do not change upon the cycling. Enhanced gravity separation has the potential to replace the froth flotation technique as a separation method for the direct recycling process.

6.5 Conclusions

Separation between the pristine graphite and NMC materials was evaluated using the Falcon Ultrafine (UF) concentrator. A series of experiments were conducted to study the effect of G forces, solid concentration, feed mass, and feed composition on the separation performance. The weight and composition of the separated products were analyzed to determine the separation indices, which were then used as a metric for the separation performance. The result showed that both the feed mass the solid concentration impacted the separation performance significantly, with an optimum performance obtained at 400 grams of dry feed and 5-10% solid concentration. In addition, it was shown that the separation performance improved with increasing the G force. At 113 G force or higher, the separation performance was less sensitive to the G force. The present result also showed that the feed composition impacted the separation performance. For a feed having 20% of NMC111 and 80% of graphite by weight, the optimum separation was obtained at 5% solid concentration and 400 grams of dry feed mass. The percentage of NMC in the tailing product after one pass in the UF concentrate was lowered to 3.89%. A multistage separation experiment was conducted using 400 grams of the feed consisting of 60% NMC111 by weight. A final concentrate product consisted of 99% NMC111, and a final tailing product consisted of 99% of graphite. Similar result was found for cathode in concentrate with black mass feed obtain from spent LIBs, with and without thermal treatment, cathode grades in final concentrate can achieve over 98% after multistage operation. This result shows promise in separating electrode active materials from spent li-ion batteries using gravity separation method.

6.6 Reference

1. Armand, M. and J.M. Tarascon, *Building better batteries.* Nature, 2008. **451**(7179): p. 652-657.
2. Larcher, D. and J.M. Tarascon, *Towards greener and more sustainable batteries for electrical energy storage.* Nature Chemistry, 2014. **7**: p. 19-29.
3. Tarascon, J.M. and M. Armand, *Issues and challenges facing rechargeable lithium batteries.* Nature, 2001. **414**: p. 359-367.
4. Harper, G., et al., *Recycling lithium-ion batteries from electric vehicles.* Nature, 2019. **575**(7781): p. 75-86.
5. Gaines, L., K. Richa, and J. Spangenberger, *Key issues for Li-ion battery recycling.* MRS Energy & Sustainability, 2018. **5**: p. E14.

6. Olivetti, E.A., et al., *Lithium-Ion Battery Supply Chain Considerations: Analysis of Potential Bottlenecks in Critical Metals.* Joule, 2017. **1**(2): p. 229-243.
7. Xu, C., et al., *Future material demand for automotive lithium-based batteries.* Communications Materials, 2020. **1**(1): p. 99.
8. Gaines, L., *Lithium-ion battery recycling processes: Research towards a sustainable course.* Sustainable Materials and Technologies, 2018. **17**: p. e00068.
9. Ciez, R.E. and J.F. Whitacre, *Examining different recycling processes for lithium-ion batteries.* Nature Sustainability, 2019. **2**(2): p. 148-156.
10. Bertuol, D.A., et al., *Application of spouted bed elutriation in the recycling of lithium ion batteries.* Journal of Power Sources, 2015. **275**: p. 627-632.
11. Bi, H., et al., *Pneumatic separation and recycling of anode and cathode materials from spent lithium iron phosphate batteries.* Waste Management & Research, 2019. **37**(4): p. 374-385.
12. Zhong, X., et al., *Pneumatic separation for crushed spent lithium-ion batteries.* Waste Management, 2020. **118**: p. 331-340.
13. Shi, Y., G. Chen, and Z. Chen, *Effective regeneration of LiCoO2 from spent lithium-ion batteries: a direct approach towards high-performance active particles.* Green Chemistry, 2018. **20**(4): p. 851-862.
14. Sloop, S.E., et al., *Cathode healing methods for recycling of lithium-ion batteries.* Sustainable Materials and Technologies, 2019. **22**.
15. Shi, Y., et al., *Ambient-Pressure Relithiation of Degraded LixNi0.5Co0.2Mn0.3O2 (0 < x < 1) via Eutectic Solutions for Direct Regeneration of Lithium-Ion Battery Cathodes.* Advanced Energy Materials, 2019. **9**(20).
16. Chen, J., et al., *Environmentally friendly recycling and effective repairing of cathode powders from spent LiFePO4 batteries.* Green Chemistry, 2016. **18**(8): p. 2500-2506.
17. Zhang, X., et al., *Sustainable Recycling and Regeneration of Cathode Scraps from Industrial Production of Lithium-Ion Batteries.* ACS Sustainable Chemistry & Engineering, 2016. **4**(12): p. 7041-7049.
18. Nie, H., et al., *LiCoO2: recycling from spent batteries and regeneration with solid state synthesis.* Green Chemistry, 2015. **17**(2): p. 1276-1280.
19. Zhan, R., Z. Oldenburg, and L. Pan, *Recovery of Active Cathode Materials from Lithium-ion Batteries using Froth Flotation.* Sustainable Materials and Technologies, 2018: p. submitted.
20. Zhan, R., et al., *Significance of a Solid Electrolyte Interphase on Separation of Anode and Cathode Materials from Spent Li-Ion Batteries by Froth Flotation.* ACS Sustainable Chemistry & Engineering, 2021. **9**(1): p. 531-540.
21. Zhang, G., et al., *Removal of Organics by Pyrolysis for Enhancing Liberation and Flotation Behavior of Electrode Materials Derived from Spent Lithium-Ion Batteries.* ACS Sustainable Chemistry & Engineering, 2020. **8**(5): p. 2205-2214.
22. Shin, H., et al., *Electrochemical Performance of Recycled Cathode Active Materials Using Froth Flotation-based Separation Process.* Journal of The Electrochemical Society, 2020. **167**(2): p. 020504.

23. An, S.J., et al., *The state of understanding of the lithium-ion-battery graphite solid electrolyte interphase (SEI) and its relationship to formation cycling.* Carbon, 2016. **105**: p. 52-76.
24. Liu, J., et al., *Recovery of LiCoO2 and graphite from spent lithium-ion batteries by cryogenic grinding and froth flotation.* Minerals Engineering, 2020. **148**: p. 106223.
25. Al-Shammari, H. and S. Farhad, *Regeneration of Cathode Mixture Active Materials Obtained from Recycled Lithium Ion Batteries*. 2020, SAE Technical Paper.
26. Kepler, K.D., et al., *Processing for recycling electrode materials from lithium-ion batteries*. 2016: US.
27. Munsterman, D. and S. Kerstholt, *Sodium polytungstate, a new non-toxic alternative to bromoform in heavy liquid separation.* Review of Palaeobotany and Palynology, 1996. **91**(1): p. 417-422.
28. Callahan, J., *A nontoxic heavy liquid and inexpensive filters for separation of mineral grains.* Journal of Sedimentary Research, 1987. **57**(4): p. 765-766.
29. Roy, S., *Recovery improvement of fine iron ore particles by multi gravity separation.* The Open Mineral Processing Journal, 2009. **2**(14): p. 17-30.
30. Kroll-Rabotin, J.-S., F. Bourgeois, and É. Climent, *Physical analysis and modeling of the Falcon concentrator for beneficiation of ultrafine particles.* International Journal of Mineral Processing, 2013. **121**: p. 39-50.
31. Zhang, Y., et al., *Application of Falcon centrifuge in the recycling of electrode materials from spent lithium ion batteries.* Journal of Cleaner Production, 2018. **202**: p. 736-747.
32. Zhu, X.-n., et al., *Pre-concentration of graphite and LiCoO2 in spent lithium-ion batteries using enhanced gravity concentrator.* Physicochemical Problems of Mineral Processing, 2018. **54**(2): p. 293-299.
33. Dehaine, Q., et al., *Experimental investigation into the kinetics of Falcon UF concentration: Implications for fluid dynamic-based modelling.* Separation and Purification Technology, 2019. **215**: p. 590-601.
34. Adams, M.D., *Summary of gold plants and processes*, in *Developments in Mineral Processing*, M.D. Adams and B.A. Wills, Editors. 2005, Elsevier. p. 994-1013.
35. Coetzee, L.L., et al., *Modern gold deportments and its application to industry.* Minerals Engineering, 2011. **24**(6): p. 565-575.
36. Gül, A., et al., *Beneficiation of the gold bearing ore by gravity and flotation.* International Journal of Minerals, Metallurgy, and Materials, 2012. **19**(2): p. 106-110.
37. McAlister, S.A. and K.C. Armstrong. *Development of the Falcon Concentrator*. in *SME Annual Meeting*. 1998. Orlando, Florida: Society for Mining, Metallurgy, and Exploration.
38. Kroll-Rabotin, J.-S., É. Climent, and F. Bourgeois, *Beneficiation of concentrated ultrafine suspensions with a Falcon UF concentrator.* Canadian Institute of Mining Journal, 2011. **2**(4): p. 189-198.

39. Filippov, L.O., Q. Dehaine, and I.V. Filippova, *Rare earths (La, Ce, Nd) and rare metals (Sn, Nb, W) as by-products of kaolin production – Part 3: Processing of fines using gravity and flotation.* Minerals Engineering, 2016. **95**: p. 96-106.
40. Gregory, M.R. and K.A. Johnston, *A nontoxic substitute for hazardous heavy liquids—aqueous sodium polytungstate (3Na2WO4.9WO3.H2O) solution (Note).* New Zealand Journal of Geology and Geophysics, 1987. **30**(3): p. 317-320.
41. Boente, C., et al., *Soil washing optimization by means of attributive analysis: Case study for the removal of potentially toxic elements from soil contaminated with pyrite ash.* Journal of Cleaner Production, 2017. **142**: p. 2693-2699.
42. Das, A. and B. Sarkar, *Advanced Gravity Concentration of Fine Particles: A Review.* Mineral Processing and Extractive Metallurgy Review, 2018. **39**(6): p. 359-394.
43. Chatterjee, A., *Role of particle size in mineral processing at Tata Steel.* International Journal of Mineral Processing, 1998. **53**(1): p. 1-14.
44. Mishra, B.K. and A. Tripathy, *A preliminary study of particle separation in spiral concentrators using DEM.* International Journal of Mineral Processing, 2010. **94**(3): p. 192-195.
45. Noble, A. and G.H. Luttrell, *A review of state-of-the-art processing operations in coal preparation.* International Journal of Mining Science and Technology, 2015. **25**(4): p. 511-521.
46. Falconer, A., *Gravity separation: old technique/new methods.* Physical separation in science and engineering, 1970. **12**.
47. Çiçek, T. and I. Cöcen, *Applicability of Mozley multigravity separator (MGS) to fine chromite tailings of Turkish chromite concentrating plants.* Minerals Engineering, 2002. **15**(1): p. 91-93.
48. Kroll-Rabotin, J.-S., F. Bourgeois, and É. Climent, *Experimental validation of a fluid dynamics based model of the UF Falcon concentrator in the ultrafine range.* Separation and Purification Technology, 2012. **92**: p. 129-135.
49. Uslu, T., E. Sahinoglu, and M. Yavuz, *Desulphurization and deashing of oxidized fine coal by Knelson concentrator.* Fuel Processing Technology, 2012. **101**: p. 94-100.
50. Zhang, T., et al., *Characteristics of wet and dry crushing methods in the recycling process of spent lithium-ion batteries.* Journal of Power Sources, 2013. **240**: p. 766-771.

7 Circuit Design and Separation of Anode and Cathode Active Materials using Enhanced Gravity Separation

7.1 Background

Lithium-ion batteries (LIBs) are becoming more and more essential in consumer market as energy storage devices. It serves for portable electronics in daily life like laptops and power tools, grid-scale battery storage, and most importantly, electric vehicles (EVs). Comparing to other rechargeable batteries, LIBs have advantages including high energy density, low self-discharge, minimal memory effect [1-3]. With the EVs' emerging markets in US and all over the world, productions of LIBs have grown significantly. It is expected that global LIB demand will increase from 408 GWh in 2025 and 1,293 GWh in 2030 [4] to satisfies surged sales of EVs while it helps to reach decarbonize transportations and to improve air quality. However, it is vital to point out that LIB has an average lifetime of 2 – 10 years [5-7]. Upon reaching end-of-life (EOL) stage, replacement is required, retired LIBs need to be managed properly to enter waste stream [8, 9]. Currently, if the retired LIBs still function well and have not structure damage, they are normally collected and packed for reuse purposes as power storage [10, 11]. For the batteries already damaged or can no longer be used again, decent disposal procedure is required to prevent thermal runaway and environmental pollutions [12, 13]. Cathode materials are weighted ~ 50 % in LIBs, which composited by valuable lithium metal oxides (cobalt, nickel, manganese) [14, 15], unit prices for them are ~ $48/kg for LCO and ~ $30/kg for NMC materials, their raw materials' value drop to $38/kg and ~$18/kg, respectively [16]. After reaching EOL, there is no material loss within the batteries, transition metals can still be reclaimed to re-supply back to the market. With the distinct structure and function integrity maintained, upcycled cathode materials have potential to be used for new battery manufacturing. Hench, recycling activity is generally accepted for proper disposal of retried LIBs.

LIB recycling activities are aiming to separate and concentrate anode and cathode electrode materials from black mass [17]. Popular methods include pyrometallurgy, hydrometallurgy, and physical separation. Pyrometallurgy is high temperature smelting reduction process to obtain metal alloys [18, 19]. However, toxic gases generations are challenging sustainable operations, loss of lithium metal in slag is also irreversible [8, 20]. High energy cost and less retrieved materials makes pyrometallurgy method less viable for industrial scale process. Hydrometallurgy applies leaching method to dissolve metal fractions for subsequent separation and concentration, typical leaching agents are organic acids, inorganic acids, and ammonia-ammonium salt systems [21-23]. It can achieve high recoveries and grades of individual recycled metals, yet the prices are high for leaching chemicals [24, 25]. Also, treatments for waste gases and water are required as well. Physical methods have promising results on recovering electrode materials without damaging or interfering their function integrities potentially while preserving their distinct structures. In comparison, recycled products from hydro- and pyro-metallurgy require more processes [26] to be supplied back into LIB market, these would also increase their production costs. Currently, physical separation methods contain size separation [27], froth flotation [28], electrostatic separation [29], gravity separation [30], etc. Size separation have LIBs shredded or milled before screen sieving, large particles like copper and aluminum foils can be removed first while black mass are concentrated in finer size fractions (normally below 200 or 100 microns) [31, 32]. PVDF and CMC

binders are agglomerating electrode particles into irregular composites at this size range, other process is required for subsequent separation. Froth flotation separates electrode materials by their different surface hydrophobicities, it is normally a reverse flotation because its less valuable product is more floatable. Graphite is relatively hydrophobic and will be carried to froth layer by rising air bubbles, hydrophilic cathode materials are remained in water phase and collected as tailing products [33, 34].Electrostatic separation aims to separate materials by magnetic differences, one application is to remove Cu and Al pieces to minimize impurities from cathode powders [27, 29]. Also, it helps to separate magnetic cathode material such as LFP (Lithium Ferrous Phosphate) from other components [35]. Gravity separation can remove lighter impurities such as plastic membrane from black mass or separate electrode sheets from each other, by exploiting their density differences [30, 36]. If the purity of recycled cathode active materials from the black mass is above 99%, the recycled cathode active materials may be directly recycled into new battery applications after appropriate rejuvenation, re-lithiation, and proper treatments [37, 38].

In this research, we proposed a modified circuit design for both multistage and locked cycle operations through centrifugal gravity separation method to separate and concentrate pristine anode and cathode electrode materials. Investigation of application of centrifugal gravity separation has been conducted previously [39], yet the separation result and product purification were not competitive among physical separation methods. This study starts with detailed investigations on stages including rougher, scavenger, and cleaner for estimations on multistage experiments. Effects of feed mass and material ratios are surveyed, separation index, grades and recoveries of electrode materials are compared. With the understanding of operation performances on different stages and their optimized working conditions, multistage operation have been conducted while effect of passes on scavenger and cleaner, effect of cut-off point (COP) on rougher are fully discussed to achieve higher grades of graphite in final tailing and cathode in final concentrate.

7.2 Materials and Experiments

7.2.1 Materials

Pristine graphite (SLC1520P) powders obtained from Superior Graphite. Pristine lithium nickel manganese cobalt oxide ($LiNi_{0.33}Mn_{0.33}Co_{0.33}O_2$) powders obtained from Toda America. De-ionized (DI) water obtained from a Barnard water purification system (Thermo Fisher), with resistance of 17.9 – 18.2 MΩ · cm. 25mmol Lithium hydroxide (LiOH) solution is prepared by dissolving LiOH crystals into water at room temperature with assistance of magnetic agitator.

7.2.2 Experimental Procedure

Falcon L40 enhanced gravity concentrator with Ultra-Fine (UF) bowl was used to separate graphite and lithium nickel manganese cobalt oxide (NMC) powders from a mixture. Feed materials are prepared by mixing pristine graphite and cathode powders with DI water under different materials ratios, Caframo constant-torque brushless mixer

used for agitation with rate of 1,000 RPM for 10 mins to acquire suspension slurries. Learning from the last chapter, weight percentages for graphite and NMC are 40% and 60% for rougher single stage, multistage, and locked cycle experiments, this cathode-to-anode ratio represent the mass of the active materials within the Li-ion batteries. Anode/cathode ratios are 85/15 and 65/35 for scavenger single stage, 15/85 and 5/95 for cleaner singles stage for predictions on multistage and locked cycle experiments. Solid concentrations are 5% for all single stages and start with 5% for multistage experiment. First cycle of locked cycle experiment begins with 5% for rougher, scavenger, and cleaner, then water usages are fixed for following cycles. Centrifugal 'G Force' are set at 163, 290, and 222 for rougher, scavenger, and cleaner stages, respectively. Agitation turned on using control panel, suspension slurry being fed into gravity separator steadily through feeding tube, dense and large particles are being concentrated within the bowl, light and small particles are being rejected from the bowl and collected as overflow products. After each batch, tailing is pressure filtered, materials from bowl and tailing are sampled. Samples and final products are dried in forced air oven at 95℃ overnight before characterizations, materials are weighted before and after drying.

7.2.3 Characterization

Thermogravimetric analysis (TGA) conducted using a LECO TGA 701, temperature rises from 25℃ to 800℃ with a step rate of 1℃/min, air flow rate is 7L/min. Percentage of cathode material is the remained material after thermal treatment, while graphite burnt off at range of 500 – 700℃. FEI Philips XL 40 Environmental Scanning Microscope (E-SEM) used for investigation of materials' morphology, and energy dispersive spectrometer (EDS) analysis.

7.3 Results and Discussions

7.3.1 Single stage separation

Figure 7-1 shows a schematic drawing of a direct recycling process composed of centrifugal gravity separation. The Li-ion batteries are dismantled first, electrolyte and organic solvents are rinsed off. Electrode active materials from the electrode sheets are detached from current collectors by thermal process or solvent treating process. Once the binders used in Li-ion batteries are removed, a mixture of anode and cathode active materials were obtained from Li-ion batteries, where centrifugal gravity separation applied to separate cathode from anode materials.

Single-stage experiments were conducted to study the impact of operation conditions on separation performance. In this study, separation of pristine anode and cathode materials using the Falcon UF separator have been studied. The effect of feed mass, feed ratio, and cut-off point was studied. Optimal operation condition was 400 grams of total dry feed, 5 – 10% solid concentration, with 113 or higher of G Force. It is expected that the feed masses and material ratios are changing among different stages and cycles, which could in turn affect the separation performances. Thus, single stage centrifugal separation experiments conducted in this study firstly to deeper understand their relationships.

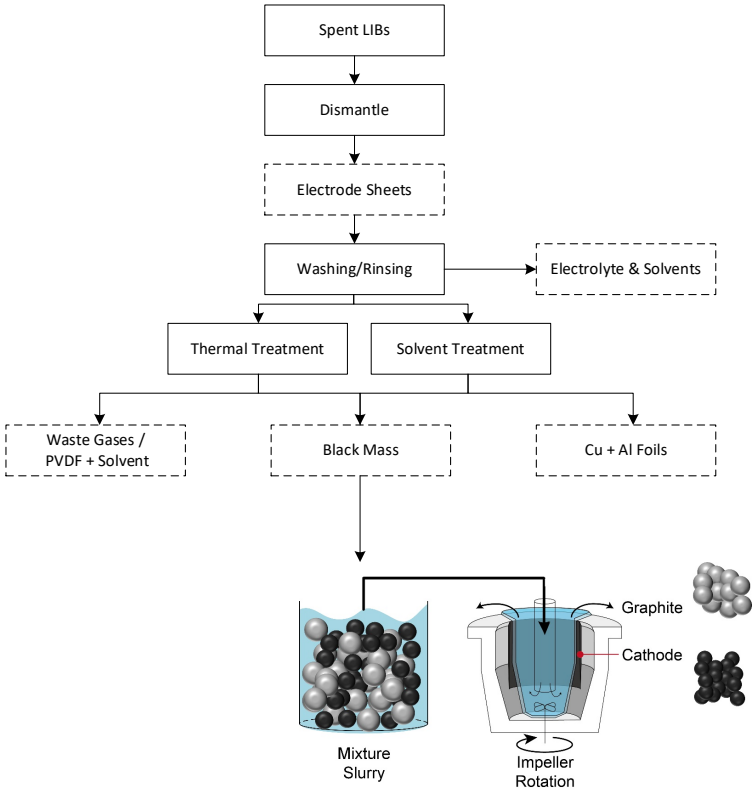

Figure 7-1. Schematic drawing of proposed direct recycling method contained centrifugal gravity separation.

In this work, in the typical method, the high cut-off-position is where the overflow product is treated as the tailing product while the materials collected within the concentrator bowl. For the low-cut-off position, materials collected at 3-cm below the top edge of the concentrator bowl were treated as the concentrate product, and materials collected at the top fraction (within 3-cm below the concentrator bowl) were combined with the overflow products, and treated as the tailing product. Figure 7-2a shows the cathode grades in tailings and concentrates at different feed masses ranging from 300 to 800 grams. The feed consisted of 60% NMC111 and 40% graphite by weight. The separation experiments were conducted at a solid load of 5%, DI water was used. The effect of two cut-off positions on separation performance was investigated. Since the NMC111 (= 5.1 kg/cm3) is much heavier than graphite (= 2.2 kg/cm^3), the concentrate product is enriched with NMC111, while the tailing products are enriched with graphite. As shown in fig. 7-2a, at feed mass of 300 and 400 grams with high COP, the tailing product consisted of ~ 8% of NMC111 and ~ 92% of graphite, while the concentrate product consisted of 77% and 92% of NMC111, respectively. When the dry feed mass was increased from 400 grams to 800 grams, the percentage of NMC111 in the tailing product was increased to 26% and 34% at 500 grams and 800 grams of dry feed mass. The percentage of NMC111 in the concentrate product was increased from 77% at 300 grams of the dry feed mass to 92% at 800 grams of feed masses. Similar trend was found with low COP, with cathode grades higher in both concentrate and tailing products, the

difference is introduced by categorization of top concentrate product. The present result showed that the percentage of NMC111 in both the concentrate and tailing products increased with increasing the feed mass. It was found that the saturated concentrate bed was around 300 grams of the dry materials regardless of the feed mass. When the feed mass was increased, denser and smaller NMC111 particles penetrate into the inside of the concentrate bed while the lighter graphite particles were replaced and rejected to the tailing product. When the feed mass was increased to 400 g or above, the percentage of NMC111 in the tailing product reached a plateau, meaning exchanging of particles on concentrate surface has reached equilibrium. With the feed mass was further increased, the NMC111 materials cannot be retained by the concentrate bed and are reporting to the overflow products. The result confirms that a significant increase in the percentage of NMC111 in the tailing product at 500 grams of feed mass, and their steady rise between 500 and 800 grams.

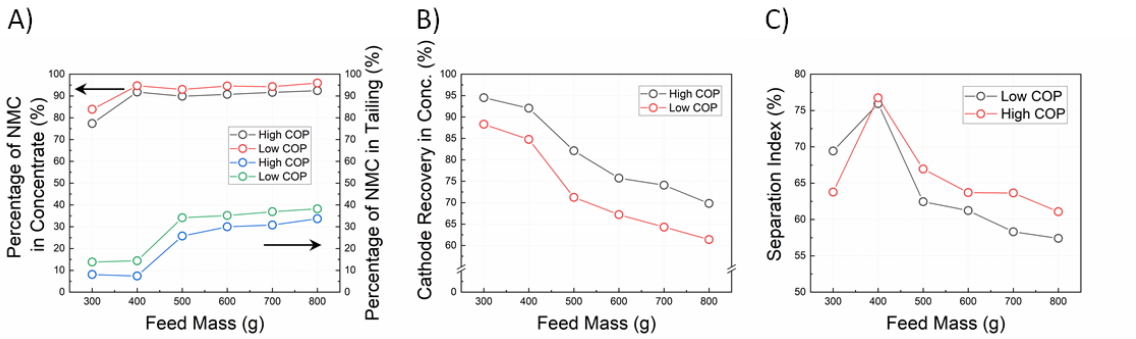

Figure 7-2. Rougher stage separation performance with 300 – 800 grams of feed mass. A) Grade of cathode in concentrate and tailing; B) Recovery of cathode in concentrate; C) Separation Index.

Figure 7-2b shows the NMC111 recovery in concentrate products at different feed masses for rougher operations. It starts from 88.3% for low COP and 94.5% for high COP, both curves decrease regularly with increase feed mass, end at recoveries of 61.4% and 69.8%, respectively. Combining both grade and recoveries of cathode materials, feed mass of 400 grams is desirable for rougher operation for it yields high cathode grade in concentrate, low cathode grade in tailing, and relatively high recovery cathode in concentrate. Figure 7-2c shows the separation index at different feed mass. The separation index is defined as the recovery of NMC111 in the concentrate product minus the recovery of graphite in concentrate product. The more the separation index closer to 1, the better the separation is. When the separation index is zero, no separation is occurred. The result showed that the separation performed the best at 400 grams of feed mass in dry, ~ 76% SI were achieved for both high and low COP. With feed mass between 500 and 800 grams, SI number gradually decreases from 67% and 62% to 61% and 57% for high and low COP, respectively.

As shown in the paragraphs above, after one pass in the rougher stage, the tailing product consisted of 10-35% of NMC111 depending on the feed mass, a further stage of the

separation process may be needed to reclaim more valuable materials from these low NMC111 mixtures. Hence, scavenger is designed to recover NMC111 that was lost in the tailing product in the rougher stage. The tailing product from the scavenger stage should consist of 95% of graphite by weight or above, while the concentrate is blend of anode and cathode materials. Beyond the feed mass and COP selections, the effect of different NMC-graphite ratio in the feed was also investigated.

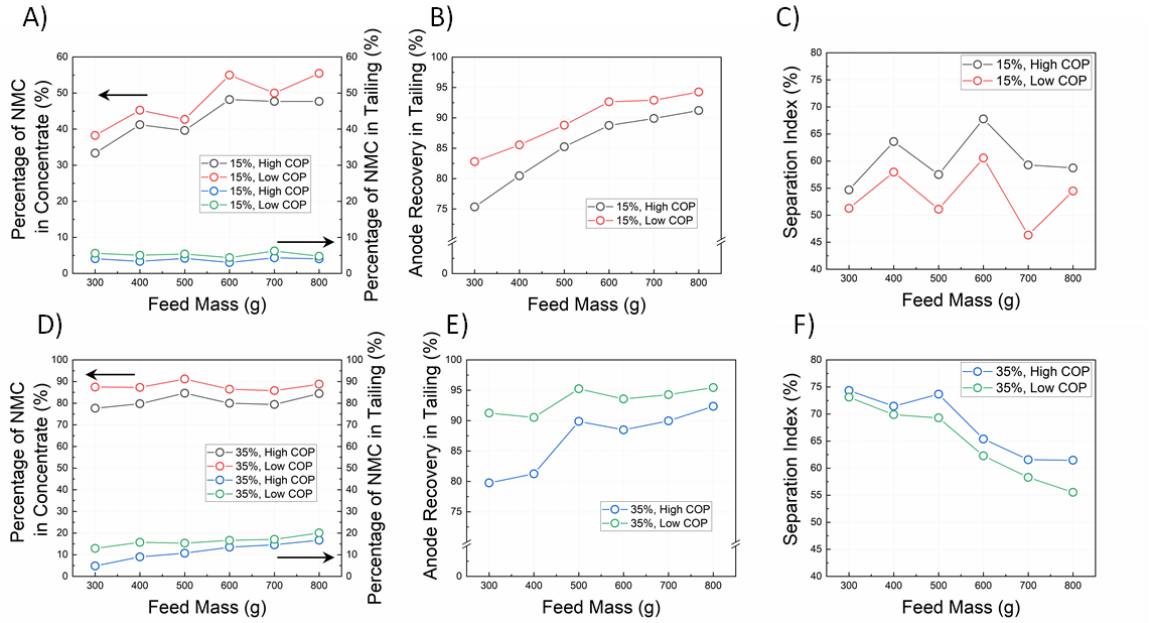

Figure 7-3. Scavenger stage separation performance with 300 – 800 grams of feed mass. 15 wt.% cathode in feed: A) Grade of cathode in concentrate and tailing; B) Recovery of anode in tailing; C) Separation Index. 35 wt.% cathode in feed: D) Grade of cathode in concentrate and tailing; E) Recovery of anode in tailing; F) Separation Index.

Two feeds with different ratios of NMC111 were used in this study. NMC111 grade of 15% (85/15 anode/cathode weight ratio) and NMC grade of 35% (65/35 anode/cathode weight ratio) are selected as feed materials because they are usually the lower and upper levels found in scavenger feeds. Figure 7-3a shows the percentage of NMC in both the concentrate and tailing products at different feed masses, effect of COP was studied. The result showed that the percentage of NMC in the concentrate product increased gradually with increased feed mass, which ranged from 33% to 48%. The separation index result (Figure 7-3c) was insensitive to the feed mass, they were fluctuated between 55% and 65%. At the same time, the percentage of NMC in the tailing remained low at 5% despite of feed mass. This result suggests that the concentrate bed within the bowl has not been saturated, the continuous feeding allows an exchange of heavy and light particles on the surface of the concentrator bowl. As a consequence, the more and more anode materials got recovered in tailing with increasing the feed mass. The present result suggested that at feed mass of 800 grams, 15% cathode grade in feed is still not enough to saturate the concentrate bed, light materials are still preferred to stay in concentration in bowl rather than being rejected to tailings. The effect of cut-off points on the separation between

NMC111 and graphite was also examined. High COP started with lower cathode grade as 33.4%, and then stabilized at 47.7% at 800 grams feed. Low COP started with 38.3% and ended with 55.5%. However, cathode grades in tailing remain stable with increasing feed mass, which were at the range of 3 – 6% for both COP selections.

Figure 7-3d shows the percentage of NMC111 in the concentrate and tailing products versus feed mass with two COPs under feed mass consisting of 35% NMC111 by weight. Contrarily, both cathode grades in concentrate were at higher plateaus starting from feed mass of 300 grams, while cathode grades in tailing were increasing gradually with increased feed mass. With high COP, cathode grades in concentrate were between 77.7% and 84.5%, low COP has higher range between 85.8% and 91.2%. Their corresponding cathode grades in tailing were from 4.8% to 16.7% and 12.9% to 20.1%, respectively. Comparing results with feed consisting of 15% and 35% NMC111 by weight in the feed, both cathode grades in tailings and concentrates are higher in 35% than in 15%. This tells that higher cathode grade to scavenger feed yields higher cathode grade in both separation products. Secondly, with 35% cathode grade feed, scavenger bowl already reaches saturation at 300-400 grams of feed mass, excess heavy fraction (i.e., NMC111) were collected in the overflow product. Figure 7-3f showed its separation index, different from scavenger with feed of 15% NMC111, increased heavy content in feed yield a decrease of SI with increased feed mass. It started with 74% and 73% and ended with 61% and 56% for high and low COPs, respectively. This further confirmed saturation of concentrate bed has been achieved at 300-400 grams of feed mass.

All anode recoveries increase with increased feed mass as can found in figure 7-3b and 7-3e, low COP and higher cathode grade in feed gives higher anode recovery in tailing products. This is because more materials are selected for tailings and more graphite powders are able to overflow rather than trapped in bed with increased cathode grade in feed. For example, high COP with 15% cathode content feed yielded anode recovery in tailing from 82.5% to 92.5% with increased feed mass, while this range fell between 91% and 94%. To conclude scavenger single stages, for multistage and first few runs of locked cycle experiments, with steady cathode grades in tailings, feed mass should be increased to obtain higher grade graphite materials. After several runs, it is essential to reduce feed mass to lower cathode lost in tailing products for locked cycle experiment. Moreover, in order to acquire high graphite grade in tailing from scavenger, it is likely that subsequent pass of scavenger is needed.

For cleaner stage, a further upgrade on the percentage of NMC111 in the concentrate products is desired, which is over 99% purity of NMC111. In this study, the effect of cut-off position is very important. whose function is to purify the grade of cathode in final products. Figure 7-4a shows the percentage of NMC111 in the concentrate and tailing products with high and low COPs for the feed consisted of 85% by weight of NMC111. The result showed that the percentage of NMC111 in the concentrate product remained at 96% using the high COP. Switching to low COP, the percentage of NMC111 in the concentrate product reached over 98.9% at any feed masses ranging from 300 to 800 grams of the dry feed. The percentage of NMC in the tailing product increased with

increasing feed mass. This is because more NMC powders were rejected from the concentrator bowl into the overflow product stream.

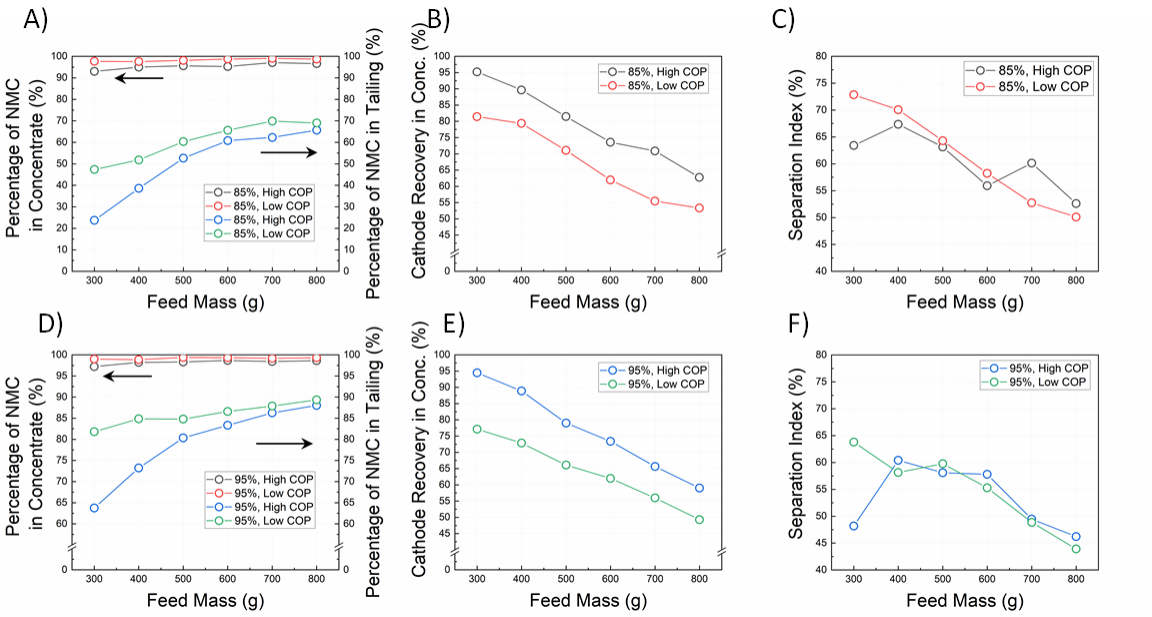

Figure 7-4. Scavenger stage separation performance with 300 – 800 grams of feed mass. 85 wt.% cathode in feed: A) Grade of cathode in concentrate and tailing; B) Recovery of cathode in concentrate; C) Separation Index. 95 wt.% cathode in feed: D) Grade of cathode in concentrate and tailing; E) Recovery of cathode in concentrate; F) Separation Index.

Also shown in Figure 7-4 d-f is the results with the feed consisting of 95% of NMC111 by weight. This is to show how additional purification step can further increase the percentage of NMC111 in the concentrate product. The result (Figure 7-4d) revealed that the percentage of NMC111 in the concentrate product was increased by 1–4 %, over 99% of NMC111 in the concentrate product can be obtained for low COP at any feed masses ranging from 300 grams to 800 grams of dry feed. Attributed to over saturation of concentration bed within the bowl at the high feed loading, the percentage of NMC111 in the tailing product increased with increasing the feed mass. Consequently, by using the low COP, the percentage of NMC111 in the tailing product increased from 80% at 300 grams of dry feed to 89% at 800 grams of the dry feed. This results in an increased rejection of NMC111 into the overflow product stream.

Figure 7-4b and 4e show the recovery of NMC111 in the concentrate product at different feed mass. The recovery rate of NMC111 in the concentrate product decreased with increasing the feed load, it was found that the lower cathode content in the feed and low COP gives higher recovery despite of cathode ratio in feed mass. Separation Index were compared in figure 7-4c and 7-4f, all SI decreased with increasing feed mass from 400 to 800 grams of feed mass. However, sharp drops at 300 grams feed mass found for both high COP despite of NMC content in feed, this is due to 300 grams of dry mass feed is at

the edge of bed saturation, majority of materials retained in the bowl while minimal products got collected from tailing, the differences of electrode material recoveries got minimized.

The results obtained from single stage illustrates that using multistage of purification and separation processes, the concentrate product may contained 99% of NMC111, while the tailing product in the scavenger cycle may contain 99% of graphite product. Validation using different circuit designs can be found in the following paragraphs.

7.3.2 Circuit Design

As described above, the effect of feed ratios on the separation performance using the enhanced gravity separation was examined. Figure 7-5 shows the effect of circuit design on the separation performance between anode and cathode active materials. A total of five circuit designs were evaluated and shown in figure 7-5 a-e, and effect of the cut-off points on the separation performance were examined, detailed anode and cathode recovery vs. grade plots in tailings and concentrates are compared in figure 7-5f and 7-5g. Figure 7-5a shows an operation with two parallel rougher process, each fed by 400 grams of dry mass with 60/40 cathode/anode ratios as discussed previously. Solid concentrations were fixed at 5 wt. %, low COP selected, black squares found in figure 7-5f and 7-5g are its separation results. ~ 92% of graphite recovered in tailing with grade of 73%, while 80% of cathode recovered with grade of 94%. With only one rougher pass, relatively high grade cathode and relatively high recovery of graphite have been achieved. To further understand the potential of separation abilities, more circuit designs are innovated.

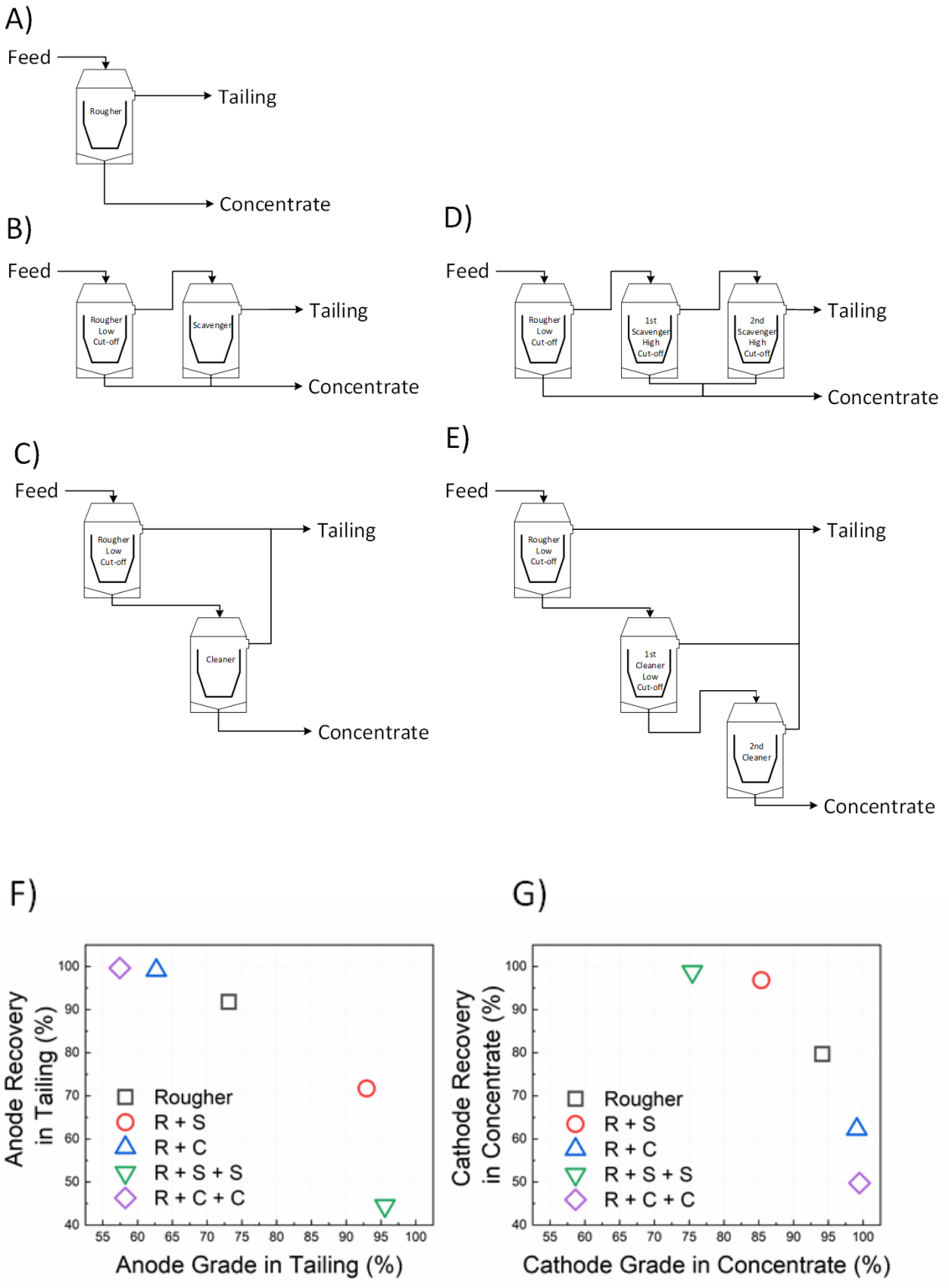

Figure 7-5. Circuit designs and their corresponding separation performances. Circuit designs: A) Rougher; B) Rougher + scavenger; C) Rougher + cleaner; D) Rougher + two

passes of scavenger; E) Rougher + two passes of cleaner. Separation performances: F) Recovery versus grade of anode materials in tailing; G) Recovery versus grade of cathode materials in concentrate.

Figure 7-5b and figure 7-5c are circuit designs for rougher with one more stage of scavenger (R + S) and cleaner (R + C), respectively. They are both designed to further purify anode and cathode electrode materials, in other words, higher grades of electrode materials are expected with inevitably lower recoveries. For R + S (figure 7-5b), tailing product from rougher fed into one pass of scavenger with feed mass of 367.8 grams. High COP selected for scavenger to improve graphite grade in tailing, remain materials collected as concentrate product, red circle in figure 7-5f and 7-5g shows its separation performance. Graphite grade got improved from 73% to 93%, with 20% of recovery lost. Similarly, R + C shown in figure 7-5c is rougher plus one pass of cleaner, where concentrate product from rougher fed to cleaner with 411.34 grams of dry mass. Low COP selected for cleaner, concentrate product contained cathode material over 99.1% with 62% recovery, while the rest combined as tailing. Both anode and cathode materials achieve over 93% grades with ~20% recovery lost, two passes of scavenger and cleaner have been proposed to obtain further purified materials. Figure 7-5d shows circuit design of R + S + S, where tailing product from first scavenger got re-cleaned with one more pass of scavenger, while the rest combined as concentrate. Figure 7-5f shows the design of rougher plus two stages of cleaner, concentrate product of 1st cleaner got re-cleaned as well. Graphite grade of 95.6% obtained with recovery of 44.5%, while cathode grade of 99.5% achieved with 49.8% recovery. This circuit analysis proves the viability to obtain high grades of materials through multistage cleaner and scavenger designs.

7.3.3 Multistage Operation

Figure 7-6 shows the flow charts using a combined multistage operation. The solid percentage of the feed was maintained at 5% for each stage, and the results using multistage operations are shown in Table 1 with different COP selection. Total of three products obtain, they are: tailing, middling, and concentrate. This is different from circuit designs which only contained two products each, only one high grade product can be achieved between graphite and NMC111, while the rest one is black mass mixture. In this case, middling is added to ensure high grade products can be achieved in tailing and concentrate. Combinations of COP selections are also compared to understand its impacts on final products' grades, table 3 shows all eight sets of selections and cathode compositions for corresponding products. Plus symbol is for high COP, minus symbol is for low COP.

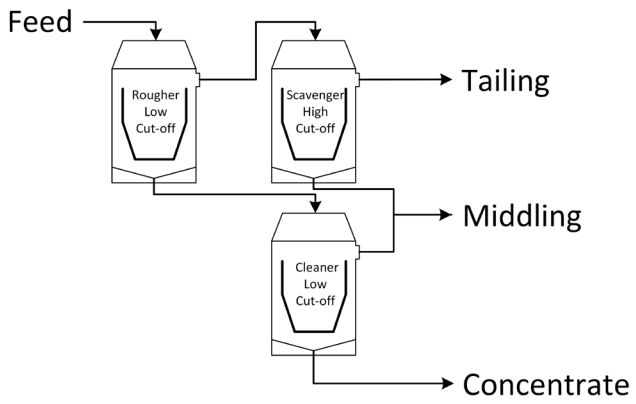

Figure 7-6. Multistage operation with one pass of scavenger and cleaner.

Table 7-1. Cathode grade in tailing, middling, and concentrate with different selections of cutoff point combinations after multistage operation with one pass scavenger and cleaner.

Operation Stages			**NMC Percentages in Products (%)**		
R	S	C	Tailing	Middling	Concentrate
+	+	+	3.88%	45.33%	96.95%
+	-	+	6.53%	17.29%	96.95%
+	+	-	3.88%	56.05%	98.38%
+	-	-	6.53%	29.84%	98.38%
-	+	+	7.06%	59.75%	97.60%
-	-	+	10.60%	64.20%	97.60%
-	+	-	7.06%	66.79%	99.10%
-	-	-	10.60%	71.05%	99.10%

For rougher stage, low COP yields higher grades in all three final products despites of combination from scavenger and cleaner. This can be explained as low COP yields less cathode with higher grade reported to rougher concentrate, while more cathode is lost and collected in rougher tailing. For example, with both high COPs for scavenger and cleaner, switch from high COP to low COP in rougher incurred cathode grades in tailing, middling, and concentrate increased from 3.88%, 45.33%, and 96.95%, to 7.06%, 59.75%, and 97.60%, respectively. For scavenger stage, high COP generates tailing with

higher grade of graphite, while the change in middling is dependent more on rougher COP selection: with high COP rougher, high COP scavenger yields lower graphite grade in middling; with low COP rougher, high COP scavenger yields higher graphite grade in middling. Similarly, with low COP for cleaner, higher grade of cathode can be obtained. For example, with low COP on rougher, cathode grade in concentrate got improved from 97.60% to 99.10% by switching cleaner COP. It is noticeable that maximum grades of anode in tailing and cathode in concentrate were not achieved under same condition, this means one more pass on both scavenger and cleaner might be necessary to achieve high grade materials simultaneously. Also, it is found that cathode grade in concentrate is easier to achieve over 99% than graphite in tailing. Instead of using low COP in rougher to further maximize the cathode grade that's already high enough after one cleaner, it is worthwhile to test high COP rougher for subsequent multistage operation.

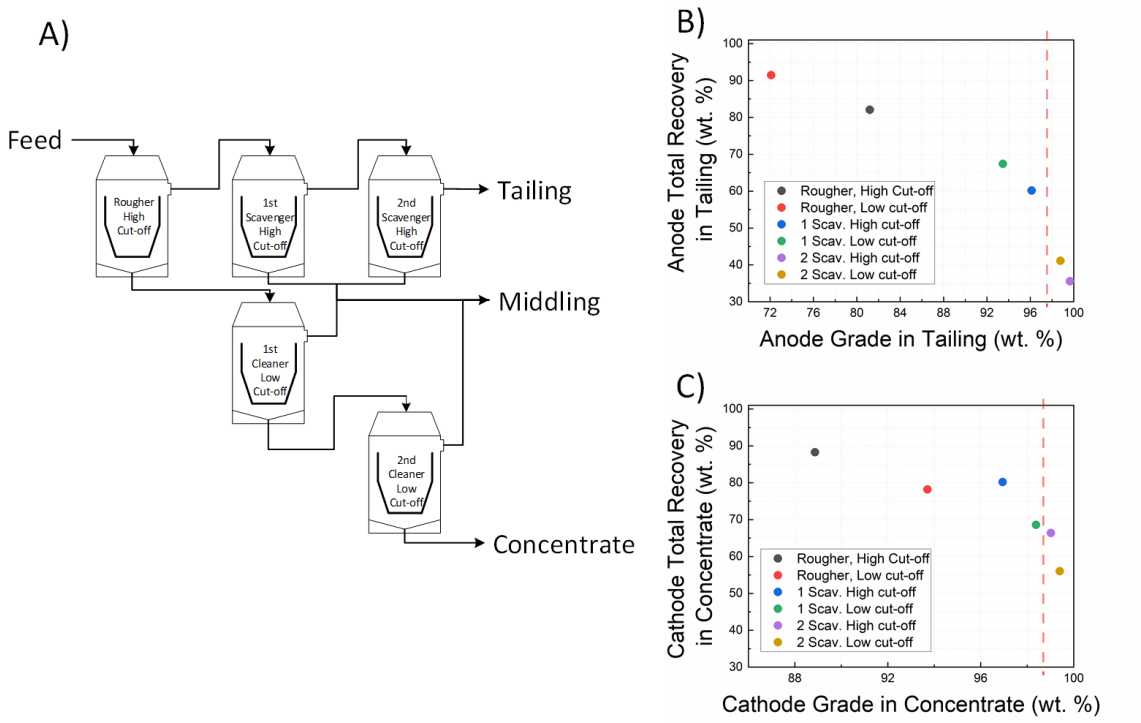

Figure 7-7. A) Multistage operation with two passes of scavenger and cleaner, high COP selected for rougher. B) Recovery versus grade of anode materials in tailing for different operations; C) Recovery versus grade of cathode materials in concentrate for different operations.

Figure 7-7a shows the optimized multistage operation for separating of anode and cathode materials using centrifugal gravity separation. The results are shown in figure 7-7b and 7-7c as the overall recovery vs. the grade of single components in the tailing and concentrate products. Rougher performance is compared first, it does not have any middling product, black and red dots represent results for its high and low COPs, respectively. With low COP, 78.2% of cathode is recovered in concentrate with grade of 93.7%, 91.5% of graphite collected in tailing with grade of 72.1%. Cathode grade is

already improved significantly from 60% with just one stage of rougher. With high COP for rougher, cathode grade drops to 88.9% while its recovery rises to 88.3%, yet graphite's grade builds up to 81.2% with decreased recovery of 82.1%. High COP is selected for rougher as discussed above for the following process.

After rougher stage, about 307.6 and 490.5 grams of materials with 18.8% and 88.9% cathode contents fed to scavenger and cleaner, respectively. Results of them also shown in figure 7-7b and 7-7c, for cleaner with low and high COP, grade of cathode in concentrate can reach 98.4% with 68.6% of recovery and 97.0% grade with 80.2% recovery. In tailing product, 60.2% and 67.4% of graphite recoveries obtained for high and low COP, with graphite grades of 96.1% and 93.5%, respectively. Thus, high COP is selected for scavenger, low COP is selected for cleaner to acquire higher grade electrode materials. This is corresponded with circuit design result.

With one or two cleaner stages, the grade of NMC111 in the concentrate product was increased from 88.9% with one rougher stage, to 98.4% and 99.4% after one and two additional cleaner stages. However, the recovery of NMC111 in the concentrate products were decreased from 88.3% with one rougher stage to 56.0% with two additional scavenger stages. With two scavenger passes, the percentage of graphite in the tail product was increased from 81.2% in rougher, to 96.1% and 99.7% with one and two scavenger passes. Its recovery decreases from 82.1%, to 60.2% and 35.6%, correspondingly. To better understand the COP selection for rougher, table 2 listed to compare grades and recoveries of NMC111 and graphite in final products after multistage of two passes. Graphite grade in tailing got improved significantly from 95.58% to 99.65% with 9.5% of recovery lost. Cathode grade only got decreased by 0.11% while 6.7% more of cathode retained in concentrate. Due to cathode materials is more valuable from black mass mixture, high COP rougher really benefits the final products.

7.4 Conclusion and Summary

In this study, multistage centrifugal gravity separation has been investigated on separation of anode and cathode electrode materials. Rougher, scavenger, and cleaner stages were studied individually on effect of cut-off point, effect of material ratio, effect of feed mass. Material distribution and separation performances are compared by recovery and grade analysis, and separation index. With G force of 60 Hz, feed solid concentration of 5 wt.%, feed weight ratio for cathode/anode: 60/40, best separation for rougher occurred at 400 grams of feed mass. Cathode grade in concentrate exceed 90% with recovery over 73%. Scavenger conducted with feed weight ratio of cathode/anode as 35/65 and 15/85 under G force of 70 Hz, and 5 wt.% feed. Generally, low cathode grade (<20%) found in tailing while cathode grade in concentrate increases with increased feed mass. Cleaner stage conducted with feed weight ratio of cathode/anode as 85/15 and 95/5, G force of 80 Hz, 5 wt.% feed. Cathode grade in tailing increases with increased feed mass, cathode grade in concentrate remained over 90%. The insensitivities of cathode grades to feed mass in scavenger and cleaner stages is attributed to saturation status of concentrate bed.

Circuit design was investigated to realize processing routes of high grades materials. With low COP rougher, over 99% of cathode and 95% of graphite were achieved using two passes of cleaner and scavenger, respectively. Multistage with one pass of scavenger and cleaner conducted to investigate the COP selections for each stage. High COP selected for scavenger and low COP selected for cleaner to produce higher grades of materials, COP of rougher switched from low to high to acquire higher grade graphite in tailing. Beside tailing and concentrate, remained materials collected as middling. Multistage of two passes on scavenger and cleaner also conducted to finally obtain high grade of graphite in tailing and cathode in concentrate, 99.40% grade of NMC111 reclaimed with 55.99% recovery, while 99.65% grade of graphite collected with 35.56% recovery.

7.5 Reference

1. Armand, M. and J.M. Tarascon, *Building better batteries.* Nature, 2008. **451**(7179): p. 652-657.
2. Tarascon, J.M. and M. Armand, *Issues and challenges facing rechargeable lithium batteries.* Nature, 2001. **414**: p. 359-367.
3. Larcher, D. and J.M. Tarascon, *Towards greener and more sustainable batteries for electrical energy storage.* Nature Chemistry, 2014. **7**: p. 19-29.
4. Curry, C., *Lithium-ion battery costs and market.* Bloomberg New Energy Finance, 2017. **5**: p. 4-6.
5. Marano, V., et al. *Lithium-ion batteries life estimation for plug-in hybrid electric vehicles*. in *2009 IEEE vehicle power and propulsion conference*. 2009. IEEE.
6. Sarre, G., P. Blanchard, and M. Broussely, *Aging of lithium-ion batteries.* Journal of power sources, 2004. **127**(1-2): p. 65-71.
7. Wood, E., M. Alexander, and T.H. Bradley, *Investigation of battery end-of-life conditions for plug-in hybrid electric vehicles.* Journal of Power Sources, 2011. **196**(11): p. 5147-5154.
8. Gaines, L., *The future of automotive lithium-ion battery recycling: Charting a sustainable course.* Sustainable Materials and Technologies, 2014. **1-2**: p. 2-7.
9. Bernardes, A.M., D.C.R. Espinosa, and J.A.S. Tenório, *Recycling of batteries: a review of current processes and technologies.* Journal of Power Sources, 2004. **130**(1): p. 291-298.
10. Liao, Q., et al., *Performance assessment and classification of retired lithium ion battery from electric vehicles for energy storage.* International Journal of Hydrogen Energy, 2017. **42**(30): p. 18817-18823.
11. Li, S., et al., *Optimization between the PV and the Retired EV Battery for the Residential Microgrid Application.* Energy Procedia, 2015. **75**: p. 1138-1146.
12. Wang, Q., et al., *Thermal runaway caused fire and explosion of lithium ion battery.* Journal of Power Sources, 2012. **208**: p. 210-224.
13. Ordoñez, J., E.J. Gago, and A. Girard, *Processes and technologies for the recycling and recovery of spent lithium-ion batteries.* Renewable and Sustainable Energy Reviews, 2016. **60**: p. 195-205.
14. Olivetti, E.A., et al., *Lithium-Ion Battery Supply Chain Considerations: Analysis of Potential Bottlenecks in Critical Metals.* Joule, 2017. **1**(2): p. 229-243.

15. Xu, C., et al., *Future material demand for automotive lithium-based batteries.* Communications Materials, 2020. **1**(1): p. 99.
16. Gaines, L., et al., *Direct Recycling R&D at the ReCell Center.* Recycling, 2021. **6**(2): p. 31.
17. Gaines, L., *Lithium-ion battery recycling processes: Research towards a sustainable course.* Sustainable Materials and Technologies, 2018. **17**: p. e00068.
18. Yun, L., et al., *Metallurgical and mechanical methods for recycling of lithium-ion battery pack for electric vehicles.* Resources, Conservation and Recycling, 2018. **136**: p. 198-208.
19. Chen, M., et al., *Recycling End-of-Life Electric Vehicle Lithium-Ion Batteries.* Joule, 2019. **3**(11): p. 2622-2646.
20. Chen, Y., et al., *Toxicity Identification and Evolution Mechanism of Thermolysis-Driven Gas Emissions from Cathodes of Spent Lithium-Ion Batteries.* ACS Sustainable Chemistry & Engineering, 2019. **7**(22): p. 18228-18235.
21. Joulié, M., R. Laucournet, and E. Billy, *Hydrometallurgical process for the recovery of high value metals from spent lithium nickel cobalt aluminum oxide based lithium-ion batteries.* Journal of Power Sources, 2014. **247**: p. 551-555.
22. Zheng, Y., et al., *Leaching Procedure and Kinetic Studies of Cobalt in Cathode Materials from Spent Lithium Ion Batteries using Organic Citric acid as Leachant.* International Journal of Environmental Research, 2016. **10**(1): p. 159-168.
23. Meng, X. and K.N. Han, *The Principles and Applications of Ammonia Leaching of Metals—A Review.* Mineral Processing and Extractive Metallurgy Review, 1996. **16**(1): p. 23-61.
24. An, L., *Recycling of Spent Lithium-Ion Batteries.* Processing Methods and Environmental Impacts, 2019.
25. Yao, Y., et al., *Hydrometallurgical Processes for Recycling Spent Lithium-Ion Batteries: A Critical Review.* ACS Sustainable Chemistry & Engineering, 2018. **6**(11): p. 13611-13627.
26. Yao, L., et al., *Recycling and synthesis of LiNi1/3Co1/3Mn1/3O2 from waste lithium ion batteries using d,l-malic acid.* RSC Advances, 2016. **6**(22): p. 17947-17954.
27. Zhang, T., et al., *Chemical and process mineralogical characterizations of spent lithium-ion batteries: An approach by multi-analytical techniques.* Waste Management, 2014. **34**(6): p. 1051-1058.
28. Zhan, R., Z. Oldenburg, and L. Pan, *Recovery of active cathode materials from lithium-ion batteries using froth flotation.* Sustainable Materials and Technologies, 2018. **17**: p. e00062.
29. Silveira, A.V.M., et al., *Recovery of valuable materials from spent lithium ion batteries using electrostatic separation.* International Journal of Mineral Processing, 2017. **169**: p. 91-98.
30. Zhong, X., et al., *Pneumatic separation for crushed spent lithium-ion batteries.* Waste Management, 2020. **118**: p. 331-340.
31. Shin, S.M., et al., *Development of a metal recovery process from Li-ion battery wastes.* Hydrometallurgy, 2005. **79**(3): p. 172-181.

32. Kang, J., et al., *Recovery of cobalt sulfate from spent lithium ion batteries by reductive leaching and solvent extraction with Cyanex 272.* Hydrometallurgy, 2010. **100**(3): p. 168-171.
33. Yu, J., et al., *A promising physical method for recovery of LiCoO2 and graphite from spent lithium-ion batteries: Grinding flotation.* Separation and Purification Technology, 2018. **190**: p. 45-52.
34. Yu, J., et al., *Exploring the critical role of grinding modification on the flotation recovery of electrode materials from spent lithium ion batteries.* Journal of Cleaner Production, 2020. **274**: p. 123066.
35. Bi, H., et al., *A new model of trajectory in eddy current separation for recovering spent lithium iron phosphate batteries.* Waste Management, 2019. **100**: p. 1-9.
36. Barik, S.P., G. Prabaharan, and B. Kumar, *An innovative approach to recover the metal values from spent lithium-ion batteries.* Waste Management, 2016. **51**: p. 222-226.
37. Lee, J., et al., *Kinetic Rejuvenation of Li-Rich Li-Ion Battery Cathodes upon Oxygen Redox.* ACS Applied Energy Materials, 2020. **3**(8): p. 7931-7943.
38. Yang, T., et al., *An Effective Relithiation Process for Recycling Lithium-Ion Battery Cathode Materials.* Advanced Sustainable Systems, 2020. **4**(1): p. 1900088.
39. Zhang, Y., et al., *Application of Falcon centrifuge in the recycling of electrode materials from spent lithium ion batteries.* Journal of Cleaner Production, 2018. **202**: p. 736-747.

8 Conclusion and Future Work

8.1 Conclusions

In this work, physical separation methods of froth flotation and enhanced gravity separation have been detailed investigated to separate anode and cathode electrode materials with various of material sources. High grades of electrode materials recovered after separations, with remained distinct structures, they preserve potential for direct recycling application.

Forth flotation separate the particles with different surface hydrophobicity. Anode materials (graphite) are relatively hydrophobic, while cathode materials (lithium metal oxides) are generally hydrophilic. After flotation, anode material is expected to concentrate in froth product, cathode material remained in slurry and collected as tailing product. Flotation of anode and cathode conducted first using black mass from new and spent LIBs, it was found that over 90% of anode floated after electrolyte rinse off, while 10-30% liberated cathode floated with addition of collector. Flotability of particles are comparable between new and spent LIBs, while recovery of anode materials decreased by 5 – 15 % for spent cells. Through thermogravimetric analysis (TGA), it is possible that surface hydrophobic layer such as PVDF binder and carbon additives render the hydrophilicity of cathode materials. To improve the flotability of anode materials, fine grinding and addition of kerosene as collector applied to further purify tailing product. With modified procedure, 87.4% grade of cathode recovered with recovery of 74.3% in tailing, remained impurities in tailing are PVDF and carbon additives that agglomerated with cathode powder.

To remove the surface layers of anode and cathode electrode materials, thermal treatment with 300, 400, and 500 ℃ have been conducted in air atmosphere, subsequent froth flotation was systematically investigated. Under thermal treatment with 400 ℃ and above, both SEI layers on anode surface and PVDF binder on cathode surface were burnt off, original hydrophobicity of particles regained. Removal of surface has been testified by contact angle measurement, XPS, and STEM analysis. Contact angle increased for thermally treated anode and decreased for treated cathode, XPS shows amounts of surface layer related compounds got significantly decreased after pyrolysis for both anode and cathode powders, STEM shows the decrease of SEI layer on anode surface. Over 99% grades of lithium metal oxide and over 98% of graphite were obtained after flotation.

Deagglomeration pretreatment on cathode composites carried out to liberate individual cathode particles and carbon additives from PVDF binder and improve purify of cathode in tailing product after froth flotation. High shear agitation is a mechanical method to deagglomerate raw cathode material from spent LIB, 16 mins of agitation in room temperature with 0.05 g/L is sufficient to achieve good de-agglomeration. Individual cathode particles regained their surface hydrophilicity and concentrated in tailing product with over 98% grade after modified flotation process, PVDF and carbon additives reported to froth product. XPS result shows that a breakage of both intramolecular and intermolecular bonds within the cathode composite governs the de-agglomeration process.

Enhanced gravity separation first conducted using pristine graphite + NMC111 materials. Effects of G Force, solid concentration, and feed ratio on the separation performance have been studied through a series of experiment. It was found that both feed mass and solid concentration impact the separation performance significantly, optimal condition is with 400 grams of feed at 5 – 10 wt. %. At 60 Hz or higher, separation performance is insensitive to G Force. Multistage operation conducted with pristine anode and cathode materials, black mass from spent LIBs with and without thermal treatment. It is found that over 99% grade of anode and cathode can be achieved for pristine operation. Thermal treatment can improve the cathode grade from 98% to 99% in final concentrate with feed of black mass mixture from spent LIBs, their cathode recoveries are also comparable with pristine experiment. However, due to the existence of binder and generation of small cathode particles after thermal treatment, grade of anode got significantly reduced in final tailing product. The result indicates that pristine multistage experiment can be used for guidance for real electrode material separation.

Enhanced gravity separation has been further investigated on circuit design for multistage operation, addition of passes on scavenger and cleaner have also been studied. Individual stages of rougher, scavenger, and cleaner have been detailed compared of anode and cathode separation performance in tailing and concentrate with respect of feed mass and material ratio. Optimized condition of rougher is 60 Hz G force, 400 grams of feed material, 5 wt. % of feed. For scavenger and cleaner, cathode/anode ratios of 15/85, 35/65, and 85/15, 95/5 have been compared. Circuit designs are compared to realize the processing routes of obtaining high grade materials, grades of anode and cathode can exceed 95% in tailing and concentrate with two passes of scavenger and cleaner, respectively. Discussion of COP in rougher also compared. Final optimized multistage operation can obtain 99% grades of electrode materials for both anode and cathode.

8.2 Proposed flow sheet for lithium-ion battery recycling

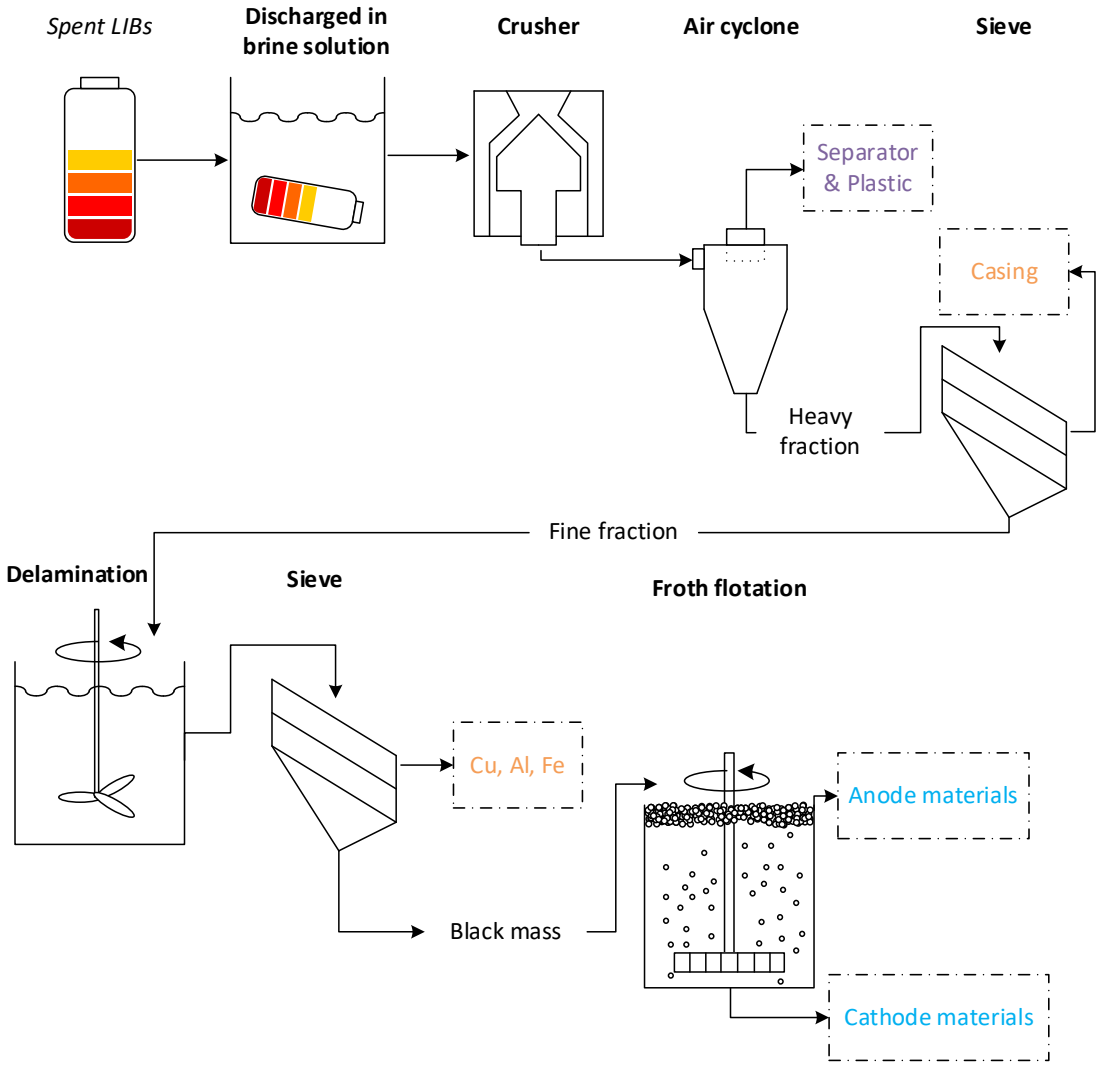

Figure 8-1. Proposed recycling and separation flow sheet for spent Lithium-ion batteries from cell discharging to electrode materials purification.

Based on the introduction of physical pretreatments and discussions of physical separations, a processing flow chart of spent lithium-ion batteries proposed in figure 8-1. It is designed for future massive and scale-up processing of spent LIBs with various feed stock. final products include fractions of separator and plastics, stainless-steel casing, copper and aluminum metal foils, anode materials, and cathode materials. It starts from discharging of cells by immersion in brine solution to dry out excess energy, potential short-circuit or thermal runaway hazards during the crushing are minimized. Then cells are crushed to open, stainless-steel casing and inner materials got down-sized. Light fraction like plastic separator membrane and other plastics are removed by air cyclone separator due to their low densities, while the crashed casings are removed by screening

due to much larger particle size. Subsequent delamination process is conducted using high shear agitation to liberate cathode and anode materials from aluminum and copper foils. Particle sizes of both metal foils and electrode composites reduced through agitation, separation of them realized through another size screening with smaller openings. Concentrated black mass fed to froth flotation for separation, hydrophilic cathode materials collected in sink product, graphite collected in froth product.

8.3 Future work

Direct recycling of upcycled materials from both flotation and gravity separation deserved to be further investigated. Both processes are water-based, both morphology and surface chemistry analysis shown no structure change after separation processes, meaning recycled materials still preserve distinct construction for electrochemistry application. Further rejuvenation and modification steps on materials might be necessary to improve its cycling performance in new batteries. For example, relithiation could re-supply lithium ions that might loss during the water-based separation process. Thermal treatment might help to solve the material cracks due from cycling effects and to burn off organic impurities from electrode surface.

A comprehensive processing route need is required for scale up ideas of both froth flotation and gravity separation. More work needs to be focused on optimizing the pretreatment process: dissembling, dismantling, material classification and separation. Current recycling process, especially in lab operation, only focused on reclaimed black mass powders, yet the total material recovery from the cell is always neglected. To make the recycling process economically viable, detailed material flow and design of individual step is necessary.

A Appendix

A.1 De-agglomeration of Cathode Composites and Its Purification by Flotation

Fig. 8-1 shows photos of battery components obtained from LIBs including anode current collectors (Cu foils), separators, cathode current collector (Al foils), anode composite, and cathode composite. The cathode composites were obtained by delaminating coatings from Al current collector using the delamination method as described above. The top size of the delaminated cathode composites was 212 μm.

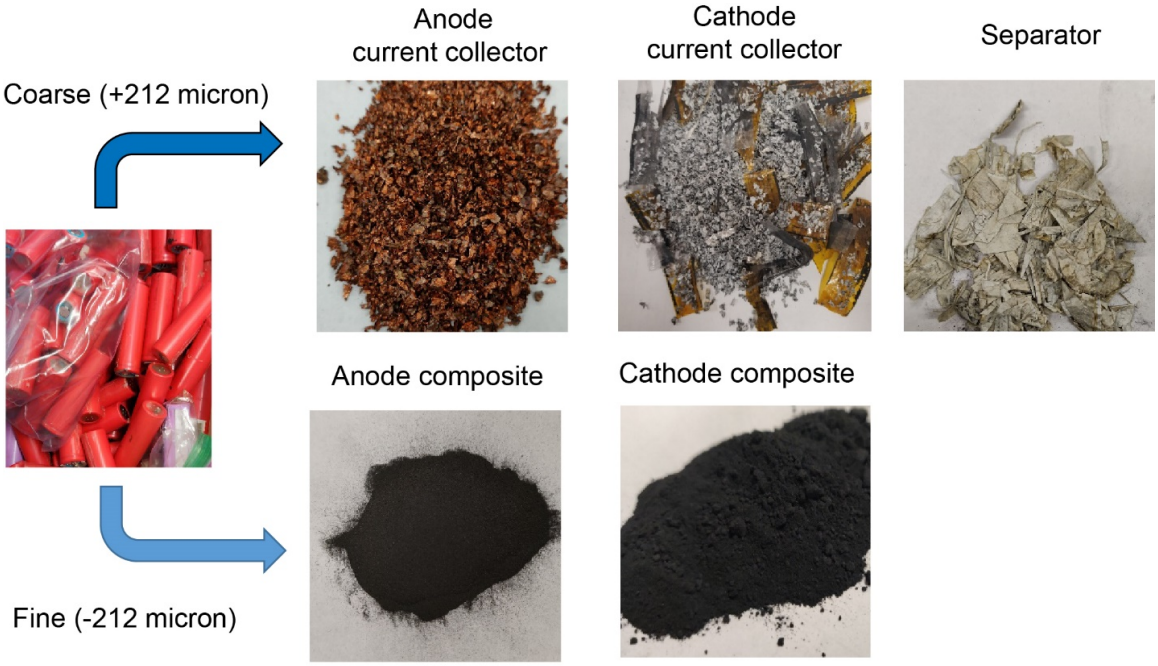

Figure 8-2. Photos of a variety of coarse and fine battery components obtained from Li-ion battery.

Fig. 8-2 shows the TGA results of both the froth and tailing products with and without 16-minute size reduction process. There are two characteristic peaks for the froth products at temperatures of approximately 379 ℃ and 490 ℃, which are referred to a decomposition of PVDF binders and carbon, respectively. Both characteristic peaks observed in the froth products were negligible in the tailing products after a 16-minute de-agglomeration process.

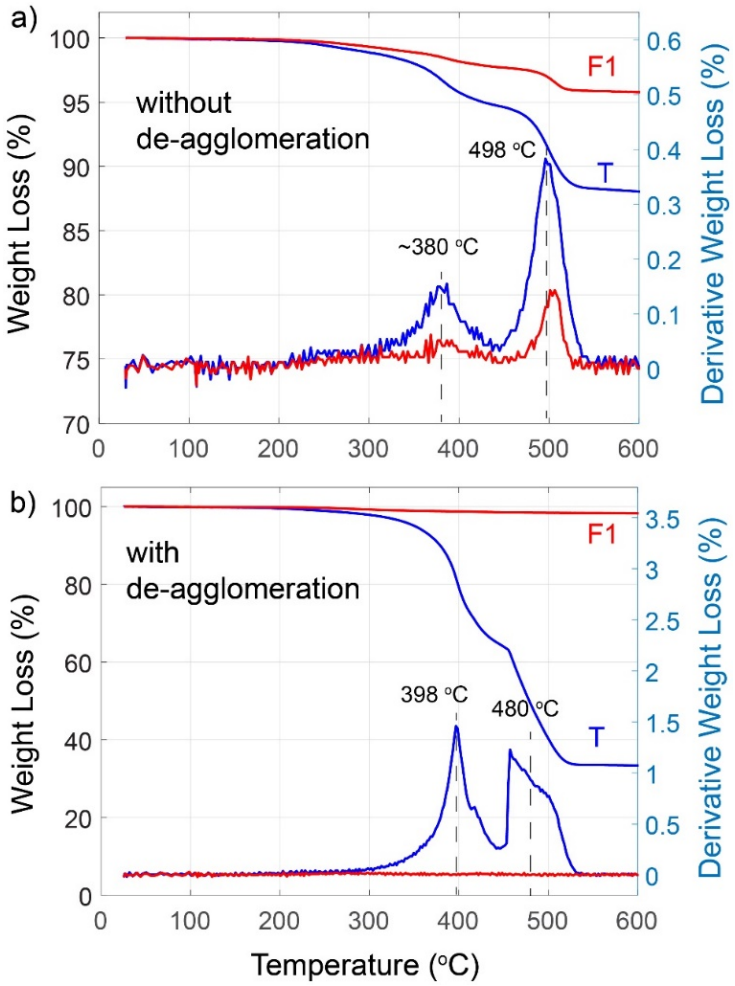

Figure 8-3. A comparison of TGA result of the froth and tailing products obtained with EOL LIBs with and without 16-minute high-shear de-agglomeration process.

Fig. 8-3 shows a schematic drawing of the de-agglomeration of cathode composite during the mechanical high-shear de-agglomeration process. The shear force overcomes both intermolecular and intramolecular bonds within the cathode composite, enabling a liberation of PVDF binders from cathode composites. The mechanical size reduction might also contribute to a size reduction of cathode active materials, as manifested by a small fraction of ultrafine cathode active materials (size < 3 μm).

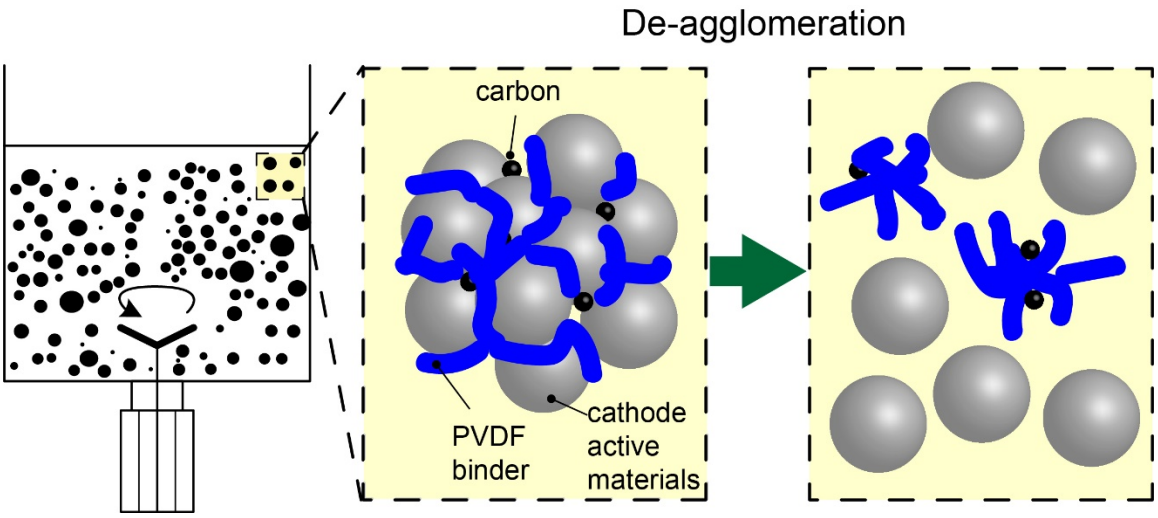

Figure 8-4. A schematic diagram of the mechanisms involved in de-agglomeration of cathode composite during the mechanical size reduction process.

B Copyright documentation

B.1 Figure 2-2a permission

ELSEVIER LICENSE
TERMS AND CONDITIONS

Sep 03, 2021

This Agreement between Michigan Technological University -- Ruiting Zhan ("You") and Elsevier ("Elsevier") consists of your license details and the terms and conditions provided by Elsevier and Copyright Clearance Center.

License Number	5141681168030
License date	Sep 03, 2021
Licensed Content Publisher	Elsevier
Licensed Content Publication	Waste Management
Licensed Content Title	Challenging the concept of electrochemical discharge using salt solutions for lithium-ion batteries recycling
Licensed Content Author	Severi Ojanen,Mari Lundström,Annukka Santasalo-Aarnio,Rodrigo Serna-Guerrero
Licensed Content Date	Jun 1, 2018
Licensed Content Volume	76
Licensed Content Issue	n/a
Licensed Content Pages	8

Start Page	242
End Page	249
Type of Use	reuse in a thesis/dissertation
Portion	figures/tables/illustrations
Number of figures/tables/illustrations	1
Format	both print and electronic
Are you the author of this Elsevier article?	No
Will you be translating?	No
Title	Lithium-ion battery recycling using mineral processing methods
Institution name	Michigan Technological University
Expected presentation date	Sep 2021
Portions	figure 2
Requestor Location	Michigan Technological University 1400 Townsend Dr. HOUGHTON, MI 49931 United States Attn: Michigan Technological University
Publisher Tax ID	98-0397604

B.2 Figure 2-2b permission

ELSEVIER LICENSE
TERMS AND CONDITIONS

Sep 03, 2021

This Agreement between Michigan Technological University -- Ruiting Zhan ("You") and Elsevier ("Elsevier") consists of your license details and the terms and conditions provided by Elsevier and Copyright Clearance Center.

License Number	5141700234016
License date	Sep 03, 2021
Licensed Content Publisher	Elsevier
Licensed Content Publication	Journal of Cleaner Production
Licensed Content Title	A cleaner approach to the discharge process of spent lithium ion batteries in different solutions
Licensed Content Author	Jiefeng Xiao,Jie Guo,Lu Zhan,Zhenming Xu
Licensed Content Date	May 10, 2020
Licensed Content Volume	255
Licensed Content Issue	n/a
Licensed Content Pages	1
Start Page	120064

End Page	0
Type of Use	reuse in a thesis/dissertation
Portion	figures/tables/illustrations
Number of figures/tables/illustrations	1
Format	both print and electronic
Are you the author of this Elsevier article?	No
Will you be translating?	No
Title	Lithium-ion battery recycling using mineral processing methods
Institution name	Michigan Technological University
Expected presentation date	Sep 2021
Portions	Figure 7
Requestor Location	Michigan Technological University 1400 Townsend Dr. HOUGHTON, MI 49931 United States Attn: Michigan Technological University
Publisher Tax ID	98-0397604
Total	0.00 USD

B.3 Figure 2-4a permission

ELSEVIER LICENSE
TERMS AND CONDITIONS

Sep 03, 2021

This Agreement between Michigan Technological University -- Ruiting Zhan ("You") and Elsevier ("Elsevier") consists of your license details and the terms and conditions provided by Elsevier and Copyright Clearance Center.

License Number	5141701152588
License date	Sep 03, 2021
Licensed Content Publisher	Elsevier
Licensed Content Publication	Waste Management
Licensed Content Title	Targeting high value metals in lithium-ion battery recycling via shredding and size-based separation
Licensed Content Author	Xue Wang,Gabrielle Gaustad,Callie W. Babbitt
Licensed Content Date	May 1, 2016
Licensed Content Volume	51
Licensed Content Issue	n/a
Licensed Content Pages	10
Start Page	204

End Page	213
Type of Use	reuse in a thesis/dissertation
Portion	figures/tables/illustrations
Number of figures/tables/illustrations	1
Format	both print and electronic
Are you the author of this Elsevier article?	No
Will you be translating?	No
Title	Lithium-ion battery recycling using mineral processing methods
Institution name	Michigan Technological University
Expected presentation date	Sep 2021
Portions	Figure 2
Requestor Location	Michigan Technological University 1400 Townsend Dr. HOUGHTON, MI 49931 United States Attn: Michigan Technological University
Publisher Tax ID	98-0397604
Total	0.00 USD

B.4 Figure 2-4c permission

ELSEVIER LICENSE
TERMS AND CONDITIONS

Sep 03, 2021

This Agreement between Michigan Technological University -- Ruiting Zhan ("You") and Elsevier ("Elsevier") consists of your license details and the terms and conditions provided by Elsevier and Copyright Clearance Center.

License Number	5141701322151
License date	Sep 03, 2021
Licensed Content Publisher	Elsevier
Licensed Content Publication	Journal of Power Sources
Licensed Content Title	Characteristics of wet and dry crushing methods in the recycling process of spent lithium-ion batteries
Licensed Content Author	Tao Zhang,Yaqun He,Linhan Ge,Rusan Fu,Xia Zhang,Yajun Huang
Licensed Content Date	Oct 15, 2013
Licensed Content Volume	240
Licensed Content Issue	n/a
Licensed Content Pages	6
Start Page	766

End Page	771
Type of Use	reuse in a thesis/dissertation
Portion	figures/tables/illustrations
Number of figures/tables/illustrations	1
Format	both print and electronic
Are you the author of this Elsevier article?	No
Will you be translating?	No
Title	Lithium-ion battery recycling using mineral processing methods
Institution name	Michigan Technological University
Expected presentation date	Sep 2021
Portions	Figure 1
Requestor Location	Michigan Technological University 1400 Townsend Dr. HOUGHTON, MI 49931 United States Attn: Michigan Technological University
Publisher Tax ID	98-0397604

B.5 Figure 2-5 permission

ELSEVIER LICENSE
TERMS AND CONDITIONS

Sep 03, 2021

This Agreement between Michigan Technological University -- Ruiting Zhan ("You") and Elsevier ("Elsevier") consists of your license details and the terms and conditions provided by Elsevier and Copyright Clearance Center.

License Number	5141710035644
License date	Sep 03, 2021
Licensed Content Publisher	Elsevier
Licensed Content Publication	Journal of Cleaner Production
Licensed Content Title	Recovering lithium cobalt oxide, aluminium, and copper from spent lithium-ion battery via attrition scrubbing
Licensed Content Author	Samuel D. Widijatmoko,Gu Fu,Zheng Wang,Philip Hall
Licensed Content Date	Jul 1, 2020
Licensed Content Volume	260
Licensed Content Issue	n/a
Licensed Content Pages	1

Start Page	120869
End Page	0
Type of Use	reuse in a thesis/dissertation
Portion	figures/tables/illustrations
Number of figures/tables/illustrations	2
Format	both print and electronic
Are you the author of this Elsevier article?	No
Will you be translating?	No
Title	Lithium-ion battery recycling using mineral processing methods
Institution name	Michigan Technological University
Expected presentation date	Sep 2021
Portions	Figure 2 and Figure 4
Requestor Location	Michigan Technological University 1400 Townsend Dr. HOUGHTON, MI 49931 United States Attn: Michigan Technological University
Publisher Tax ID	98-0397604

B.6 Figure 2-6 permission

ELSEVIER LICENSE
TERMS AND CONDITIONS

Sep 04, 2021

This Agreement between Michigan Technological University -- Ruiting Zhan ("You") and Elsevier ("Elsevier") consists of your license details and the terms and conditions provided by Elsevier and Copyright Clearance Center.

License Number	5141710889160
License date	Sep 04, 2021
Licensed Content Publisher	Elsevier
Licensed Content Publication	Sustainable Materials and Technologies
Licensed Content Title	Selective liberation in dry milled spent lithium-ion batteries
Licensed Content Author	Samuel D. Widijatmoko,Fu Gu,Zheng Wang,Philip Hall
Licensed Content Date	Apr 1, 2020
Licensed Content Volume	23
Licensed Content Issue	n/a
Licensed Content Pages	1
Start Page	e00134

End Page	0
Type of Use	reuse in a thesis/dissertation
Portion	figures/tables/illustrations
Number of figures/tables/illustrations	1
Format	both print and electronic
Are you the author of this Elsevier article?	No
Will you be translating?	No
Title	Lithium-ion battery recycling using mineral processing methods
Institution name	Michigan Technological University
Expected presentation date	Sep 2021
Portions	Table 4
Requestor Location	Michigan Technological University 1400 Townsend Dr. HOUGHTON, MI 49931 United States Attn: Michigan Technological University
Publisher Tax ID	98-0397604
Total	0.00 USD

B.7 Figure 2-7 permission

Efficient Separation of Aluminum Foil and Cathode Materials from Spent Lithium-Ion Batteries Using a Low-Temperature Molten Salt

Author: Mengmeng Wang, Quanyin Tan, Lili Liu, et al

Publication: ACS Sustainable Chemistry & Engineering

Publisher: American Chemical Society

Date: May 1, 2019

B.8 Figure 2-8 permission

ELSEVIER LICENSE
TERMS AND CONDITIONS

Sep 04, 2021

This Agreement between Michigan Technological University -- Ruiting Zhan ("You") and Elsevier ("Elsevier") consists of your license details and the terms and conditions provided by Elsevier and Copyright Clearance Center.

License Number	5141720195243
License date	Sep 04, 2021
Licensed Content Publisher	Elsevier
Licensed Content Publication	Hydrometallurgy
Licensed Content Title	Thermal treatment process for the recovery of valuable metals from spent lithium-ion batteries
Licensed Content Author	Yue Yang,Guoyong Huang,Shengming Xu,Yinghe He,Xin Liu
Licensed Content Date	Oct 1, 2016
Licensed Content Volume	165
Licensed Content Issue	n/a
Licensed Content Pages	7
Start Page	390

End Page	396
Type of Use	reuse in a thesis/dissertation
Portion	figures/tables/illustrations
Number of figures/tables/illustrations	2
Format	both print and electronic
Are you the author of this Elsevier article?	No
Will you be translating?	No
Title	Lithium-ion battery recycling using mineral processing methods
Institution name	Michigan Technological University
Expected presentation date	Sep 2021
Portions	Figure 3 and Figure 8
Requestor Location	Michigan Technological University 1400 Townsend Dr. HOUGHTON, MI 49931 United States Attn: Michigan Technological University
Publisher Tax ID	98-0397604

B.9 Figure 2-9 permission

ELSEVIER LICENSE
TERMS AND CONDITIONS

Sep 04, 2021

This Agreement between Michigan Technological University -- Ruiting Zhan ("You") and Elsevier ("Elsevier") consists of your license details and the terms and conditions provided by Elsevier and Copyright Clearance Center.

License Number	5141720373313
License date	Sep 04, 2021
Licensed Content Publisher	Elsevier
Licensed Content Publication	Journal of Hazardous Materials
Licensed Content Title	Vacuum pyrolysis and hydrometallurgical process for the recovery of valuable metals from spent lithium-ion batteries
Licensed Content Author	Liang Sun,Keqiang Qiu
Licensed Content Date	Oct 30, 2011
Licensed Content Volume	194
Licensed Content Issue	n/a
Licensed Content Pages	7
Start Page	378

End Page	384
Type of Use	reuse in a thesis/dissertation
Portion	figures/tables/illustrations
Number of figures/tables/illustrations	1
Format	both print and electronic
Are you the author of this Elsevier article?	No
Will you be translating?	No
Title	Lithium-ion battery recycling using mineral processing methods
Institution name	Michigan Technological University
Expected presentation date	Sep 2021
Portions	Figure 4
Requestor Location	Michigan Technological University 1400 Townsend Dr. HOUGHTON, MI 49931 United States Attn: Michigan Technological University
Publisher Tax ID	98-0397604

B.10 Figure 2-10a permission

ELSEVIER LICENSE
TERMS AND CONDITIONS

Sep 04, 2021

This Agreement between Michigan Technological University -- Ruiting Zhan ("You") and Elsevier ("Elsevier") consists of your license details and the terms and conditions provided by Elsevier and Copyright Clearance Center.

License Number	5141720596745
License date	Sep 04, 2021
Licensed Content Publisher	Elsevier
Licensed Content Publication	Sustainable Materials and Technologies
Licensed Content Title	A review of physical processes used in the safe recycling of lithium ion batteries
Licensed Content Author	Roberto Sommerville,James Shaw-Stewart,Vannessa Goodship,Neil Rowson,Emma Kendrick
Licensed Content Date	Sep 1, 2020
Licensed Content Volume	25
Licensed Content Issue	n/a
Licensed Content Pages	1

Start Page	e00197
End Page	0
Type of Use	reuse in a thesis/dissertation
Portion	figures/tables/illustrations
Number of figures/tables/illustrations	1
Format	both print and electronic
Are you the author of this Elsevier article?	No
Will you be translating?	No
Title	Lithium-ion battery recycling using mineral processing methods
Institution name	Michigan Technological University
Expected presentation date	Sep 2021
Portions	Figure 6
Requestor Location	Michigan Technological University 1400 Townsend Dr. HOUGHTON, MI 49931 United States Attn: Michigan Technological University
Publisher Tax ID	98-0397604

B.11 Figure 2-10b permission

ELSEVIER LICENSE
TERMS AND CONDITIONS

Sep 04, 2021

This Agreement between Michigan Technological University -- Ruiting Zhan ("You") and Elsevier ("Elsevier") consists of your license details and the terms and conditions provided by Elsevier and Copyright Clearance Center.

License Number	5141720782612
License date	Sep 04, 2021
Licensed Content Publisher	Elsevier
Licensed Content Publication	Waste Management
Licensed Content Title	Pneumatic separation for crushed spent lithium-ion batteries
Licensed Content Author	Xuehu Zhong,Wei Liu,Junwei Han,Fen Jiao,Hailing Zhu,Wenqing Qin
Licensed Content Date	Dec 1, 2020
Licensed Content Volume	118
Licensed Content Issue	n/a
Licensed Content Pages	10
Start Page	331

End Page	340
Type of Use	reuse in a thesis/dissertation
Portion	figures/tables/illustrations
Number of figures/tables/illustrations	1
Format	both print and electronic
Are you the author of this Elsevier article?	No
Will you be translating?	No
Title	Lithium-ion battery recycling using mineral processing methods
Institution name	Michigan Technological University
Expected presentation date	Sep 2021
Portions	Figure 1
Requestor Location	Michigan Technological University 1400 Townsend Dr. HOUGHTON, MI 49931 United States Attn: Michigan Technological University
Publisher Tax ID	98-0397604
Total	0.00 USD

B.12 Figure 2-10c permission

ELSEVIER LICENSE
TERMS AND CONDITIONS

Sep 04, 2021

This Agreement between Michigan Technological University -- Ruiting Zhan ("You") and Elsevier ("Elsevier") consists of your license details and the terms and conditions provided by Elsevier and Copyright Clearance Center.

License Number	5141721130608
License date	Sep 04, 2021
Licensed Content Publisher	Elsevier
Licensed Content Publication	Waste Management
Licensed Content Title	A novel pulsated pneumatic separation with variable-diameter structure and its application in the recycling spent lithium-ion batteries
Licensed Content Author	Xueshuai Zhu,Chenyu Zhang,Ping Feng,Xizu Yang,Xiaojuan Yang
Licensed Content Date	Jul 15, 2021
Licensed Content Volume	131
Licensed Content Issue	n/a
Licensed Content Pages	11

Start Page	20
End Page	30
Type of Use	reuse in a thesis/dissertation
Portion	figures/tables/illustrations
Quantity	1
Number of figures/tables/illustrations	1
Format	both print and electronic
Are you the author of this Elsevier article?	No
Will you be translating?	No
Title	Lithium-ion battery recycling using mineral processing methods
Institution name	Michigan Technological University
Expected presentation date	Sep 2021
Portions	Graphical abstract
Requestor Location	Michigan Technological University 1400 Townsend Dr. HOUGHTON, MI 49931 United States Attn: Michigan Technological University

B.13 Figure 2-11 permission

ELSEVIER LICENSE
TERMS AND CONDITIONS

Sep 04, 2021

This Agreement between Michigan Technological University -- Ruiting Zhan ("You") and Elsevier ("Elsevier") consists of your license details and the terms and conditions provided by Elsevier and Copyright Clearance Center.

License Number	5141721323660
License date	Sep 04, 2021
Licensed Content Publisher	Elsevier
Licensed Content Publication	Waste Management
Licensed Content Title	A new model of trajectory in eddy current separation for recovering spent lithium iron phosphate batteries
Licensed Content Author	Haijun Bi,Huabing Zhu,Lei Zu,Yuxuan Bai,Song Gao,Yong Gao
Licensed Content Date	Dec 1, 2019
Licensed Content Volume	100
Licensed Content Issue	n/a
Licensed Content Pages	9

Start Page	1
End Page	9
Type of Use	reuse in a thesis/dissertation
Portion	figures/tables/illustrations
Number of figures/tables/illustrations	1
Format	both print and electronic
Are you the author of this Elsevier article?	No
Will you be translating?	No
Title	Lithium-ion battery recycling using mineral processing methods
Institution name	Michigan Technological University
Expected presentation date	Sep 2021
Portions	Figure 1(c)
Requestor Location	Michigan Technological University 1400 Townsend Dr. HOUGHTON, MI 49931 United States Attn: Michigan Technological University
Publisher Tax ID	98-0397604

B.14 Figure 2-12 permission

ELSEVIER LICENSE
TERMS AND CONDITIONS

Sep 04, 2021

This Agreement between Michigan Technological University -- Ruiting Zhan ("You") and Elsevier ("Elsevier") consists of your license details and the terms and conditions provided by Elsevier and Copyright Clearance Center.

License Number	5141721499952
License date	Sep 04, 2021
Licensed Content Publisher	Elsevier
Licensed Content Publication	Journal of Cleaner Production
Licensed Content Title	Recovering lithium cobalt oxide, aluminium, and copper from spent lithium-ion battery via attrition scrubbing
Licensed Content Author	Samuel D. Widijatmoko,Gu Fu,Zheng Wang,Philip Hall
Licensed Content Date	Jul 1, 2020
Licensed Content Volume	260
Licensed Content Issue	n/a
Licensed Content Pages	1

B.15 Figure 2-13c permission

ELSEVIER LICENSE
TERMS AND CONDITIONS

Sep 04, 2021

This Agreement between Michigan Technological University -- Ruiting Zhan ("You") and Elsevier ("Elsevier") consists of your license details and the terms and conditions provided by Elsevier and Copyright Clearance Center.

License Number	5141730190154
License date	Sep 04, 2021
Licensed Content Publisher	Elsevier
Licensed Content Publication	Minerals Engineering
Licensed Content Title	Recovery of LiCoO2 and graphite from spent lithium-ion batteries by cryogenic grinding and froth flotation
Licensed Content Author	Jiangshan Liu,Haifeng Wang,Tingting Hu,Xuejie Bai,Shuai Wang,Weining Xie,Juan Hao,Yaqun He
Licensed Content Date	Mar 15, 2020
Licensed Content Volume	148
Licensed Content Issue	n/a
Licensed Content Pages	1

Start Page	120869
End Page	0
Type of Use	reuse in a thesis/dissertation
Portion	figures/tables/illustrations
Number of figures/tables/illustrations	1
Format	both print and electronic
Are you the author of this Elsevier article?	No
Will you be translating?	No
Title	Lithium-ion battery recycling using mineral processing methods
Institution name	Michigan Technological University
Expected presentation date	Sep 2021
Portions	Figure 10
Requestor Location	Michigan Technological University 1400 Townsend Dr. HOUGHTON, MI 49931 United States Attn: Michigan Technological University
Publisher Tax ID	98-0397604

B.16 Figure 2-14a permission

ACS Publications
Most Trusted. Most Cited. Most Read.

Alkali Metal Salt Catalyzed Carbothermic Reduction for Sustainable Recovery of LiCoO2: Accurately Controlled Reduction and Efficient Water Leaching

Author: Wenqiang Wang, Yu Han, Tao Zhang, et al
Publication: ACS Sustainable Chemistry & Engineering
Publisher: American Chemical Society
Date: Oct 1, 2019

B.17 Figure 2-14b permission

ELSEVIER LICENSE
TERMS AND CONDITIONS

Sep 04, 2021

This Agreement between Michigan Technological University -- Ruiting Zhan ("You") and Elsevier ("Elsevier") consists of your license details and the terms and conditions provided by Elsevier and Copyright Clearance Center.

License Number	5141730481762
License date	Sep 04, 2021
Licensed Content Publisher	Elsevier
Licensed Content Publication	Journal of Cleaner Production
Licensed Content Title	Coupling reactions and collapsing model in the roasting process of recycling metals from LiCoO2 batteries
Licensed Content Author	JiaKai Mao,Jia Li,Zhengming Xu
Licensed Content Date	Dec 20, 2018
Licensed Content Volume	205
Licensed Content Issue	n/a
Licensed Content Pages	7
Start Page	923

End Page	929
Type of Use	reuse in a thesis/dissertation
Portion	figures/tables/illustrations
Number of figures/tables/illustrations	1
Format	both print and electronic
Are you the author of this Elsevier article?	No
Will you be translating?	No
Title	Lithium-ion battery recycling using mineral processing methods
Institution name	Michigan Technological University
Expected presentation date	Sep 2021
Portions	Graphical Abstract
Requestor Location	Michigan Technological University 1400 Townsend Dr. HOUGHTON, MI 49931 United States Attn: Michigan Technological University
Publisher Tax ID	98-0397604